University of Windsor
Scholarship at UWindsor

Electronic Theses and Dissertations

2016

Interlocked Molecules and Materials with an Imidazole Core

Nasim Farahani
University of Windsor

Follow this and additional works at: http://scholar.uwindsor.ca/etd

Recommended Citation
Farahani, Nasim, "Interlocked Molecules and Materials with an Imidazole Core" (2016). *Electronic Theses and Dissertations.* Paper 5819.

This online database contains the full-text of PhD dissertations and Masters' theses of University of Windsor students from 1954 forward. These documents are made available for personal study and research purposes only, in accordance with the Canadian Copyright Act and the Creative Commons license—CC BY-NC-ND (Attribution, Non-Commercial, No Derivative Works). Under this license, works must always be attributed to the copyright holder (original author), cannot be used for any commercial purposes, and may not be altered. Any other use would require the permission of the copyright holder. Students may inquire about withdrawing their dissertation and/or thesis from this database. For additional inquiries, please contact the repository administrator via email (scholarship@uwindsor.ca) or by telephone at 519-253-3000ext. 3208.

Interlocked Molecules and Materials with an Imidazole Core

By

Nasim Farahani

A Dissertation
Submitted to the Faculty of Graduate Studies
Through the Department of Chemistry and Biochemistry
In Partial Fulfillment of the Requirements for
The Degree of Doctor of Philosophy at the
University of Windsor

Windsor, Ontario, Canada
2016

© 2016 Nasim Farahani

Interlocked Molecules and Materials with an Imidazole Core

by

Nasim Farahani

APPROVED BY:

_____

J. Tiburcio, External Examiner
CINVESTAV

_____

E. Maeva
Department of Physics

_____

S. A. Johnson
Department of Chemistry and Biochemistry

_____

T. B. Carmichael
Department of Chemistry and Biochemistry

_____

S. J. Loeb, Advisor
Department of Chemistry and Biochemistry

September 9, 2016

DECLARATION OF CO-AUTHORSHIP / PREVIOUS PUBLICATIONS

I. Co-Authorship Declaration

I hereby declare that this dissertation incorporates material that is a result of joint research, as follows; Chapter two (2) contains results pulished in the article (N. Farahani, K. Zhu, N. Noujeim and S.J. Loeb, "[2]Pseudorotaxane formation between rigid Y-shaped 2,4,5-triphenylimidazolium axles and [24]crown-8 ether wheels, *Organic and Biomolecular Chemistry*, **2014**, *27*(12), 4824). It contains joint research with K. Zhu, N. Noujeim and S.J. Loeb. I performed the synthetic experiments with assistance from K. Zhu. I collected and analyzed the NMR spectra and single-crystal X-ray diffraction (SCXRD) data with assistance from S.J. Loeb. I have permission from the publishing company to use this work in my dissertation. Chapter three (3) contains results pulished in the article (N. Farahani, K. Zhu, and S.J. Loeb, Rigid, Bistable Molecular Shuttles Combining T-shaped Benzimidazolium and Y-shaped Imidazolium Recognition Sites, *ChemPhysChem*, **2016**, *12*(17), 1875) and is a joint research with K. Zhu and S.J. Loeb. I performed the synthetic experiments with assistance from K. Zhu. I collected and analyzed the NMR spectra and single-crystal X-ray diffraction (SCXRD) data with assistance from S.J. Loeb. I have permission from the publishing company to use this work in my dissertation. Chapter four (4) contains results pulished in the article (N. Farahani, K. Zhu, C.A. O'Keefe, R.W. Schurko, and S.J. Loeb, Thermally Driven Dynamics of a Rotaxane Wheel about an Imidazolium Axle inside a Metal-Organic Framework, *ChemPlusChem*, **2016**, *8*(81), 836) and is a joint research with K. Zhu and S.J. Loeb and also contains an outcome of a collaboration with C.A. O'Keefe under the supervision of R.W. Schurko. I performed the synthetic experiments with assistance from K. Zhu. I collected and analyzed the PXRD, thermal gravimetric analysis, NMR and single-crystal X-ray diffraction (SCXRD) data with assistance from S.J. Loeb. C.A. O'Keefe collected and analyzed the SSNMR data. R.W. Schurko supervised all SSNMR data collection, analysis, and interpretation. I have

permission from the publishing company to use this work in my dissertation. Chapter five (5) is unpublished; it contains joint research with K. Zhu and S.J. Loeb and is the outcome of a collaboration with C.A. O'Keefe under the supervision of R.W. Schurko. I performed the synthetic experiments with assistance from K. Zhu. I collected and analyzed the PXRD, TGA, SEM, NMR and SCXRD data with assistance from S.J. Loeb. C.A. O'Keefe collected and analyzed the SSNMR data. R.W. Schurko supervised all SSNMR data collection, analysis, and interpretation. Chapter six (6) is also unpublished; it contains joint research with K. Zhu and S.J. Loeb. I performed the synthetic experiments with assistance from K. Zhu. I collected and analyzed the PXRD, TGA, SEM, NMR, BET data with assistance from S.J. Loeb.

I am aware of the University of Windsor Senate Policy on Authorship, and I certify that I have properly acknowledged the contribution of other researchers to my dissertation and have obtained written permission from each of the co-author(s) to include the above material(s) in my dissertation.

I certify that, with the above qualification, this dissertation, and the research to which it refers, is the product of my own work.

II. Declaration of Previous Publication

This dissertation includes 3 original papers that have been previously published in peer reviewed journals, as follows:

Dissertation Chapter	Publication title/full citation	Publication status
Chapter 2	"[2]Pseudorotaxane formation between rigid Y-shaped 2,4,5-triphenylimidazolium axles and [24]crown-8 ether wheels" (N. Farahani, K. Zhu, N. Noujeim and S.J. Loeb, *Organic and Biomolecular Chemistry*, **2014**, *27*(12), 4824).	*Published*
Chapter 3	"Rigid, Bistable Molecular Shuttles Combining T-shaped Benzimidazolium and Y-shaped Imidazolium Recognition Sites" (N. Farahani, K. Zhu, and S.J. Loeb, *ChemPhysChem*, **2016**, *12*(17), 1875).	*Published*
Chapter 4	"Thermally Driven Dynamics of a Rotaxane Wheel about an Imidazolium Axle inside a Metal-Organic Framework" (N. Farahani, K. Zhu, C.A. O'Keefe, R.W. Schurko, and S.J. Loeb, *ChemPlusChem*, **2016**, *8*(81), 836).	*Published*

I certify that I have obtained written permission from the copyright owner(s) to include the above published material(s) in my dissertation. I certify that the above material describes work completed during my registration as a graduate student at the University of Windsor.

I declare that, to the best of my knowledge, my dissertation does not infringe upon anyone's copyright nor violate any proprietary rights, and that any ideas, techniques, quotations, or any other material from the work of other people included in my dissertation, published or otherwise, are fully acknowledged in accordance with the standard referencing practices. Furthermore, to the extent that I have included copyrighted material that surpasses the bounds of fair dealing within the meaning of the Canada Copyright Act, I certify that I have

obtained written permission from the copyright owner(s) to include such material(s) in my dissertation.

I declare that this is a true copy of my dissertation, including any final revisions, as approved by my dissertation committee and the Graduate Studies office, and that this dissertation has not been submitted for a higher degree to any other University or Institution.

ABSTRACT

This dissertation is focused on designing new recognition motifs to develop mechanically interlocked molecules (MIM) and transferring the dynamics properties of these MIMs into crystalline metal-organic frameworks (MOFs). **Chapter 1** gives an introduction to rotaxanes, their application as molecular machines and their incorporation into MOFs. It also describes some recent success in creating [2]rotaxane-based MOFs that show rotational and translational motion.

Chapter 2 describes the design of a new templating motif for the formation of [2]pseudorotaxanes in which rigid, Y-shaped axles with an imidazolium core and aromatic substituents at the 2-, 4- and 5-positions interact with [24]crown-8 ether wheels ([24]crown-8 and dibenzo[24]crown-8). The Y-shape of the axle had a significant effect, raising the association between axle and wheel compared to those found for simple imidazolium or benzimidazolium derivatives.

In **chapter 3**, the Y-shaped 2,4,5-triphenylimidazolium recognition site was combined with the T-shaped 2,4,7-triphenylbenzimidazolium site to develop a rigid bistable [2]rotaxane molecular shuttle. Studies on the molecular shuttling in both the neutral and di-cationic states demonstrated the position of a 24-membered crown ether macrocycle can be controlled by acid-base chemistry.

In **chapter 4**, a new MIM linker was developed by using ring-closing metathesis (Grubbs I) which allowed clipping of a [24]crown-6 ether (**24C6**) wheel around an axle containing both Y-shaped di-phenyl-imidazole and *iso*phthalic acid groups. It was successfully incorporated into a Zn-based MOF, **UWDM-5**. VT ^{2}H SSNMR studies showed that the macrocyclic ring of **UWDM-5** undergoes rapid, thermally driven rotation about the axle inside the pores of the MOF at temperatures above 150 ^{o}C.

In **chapter 5**, a new MIM linker was made by using ring-closing metathesis to clip a [24]crown-6 ether (**24C6**) wheel around an axle containing bis(imidazolium) recognition site. A robust MOF material, **UWDM-6**, was constructed using this linker and Zr(IV) ions. VT ^{2}H SSNMR Studies on the dynamic motion of the macrocyclic ring in the neutral, di-cationic and Li-doped version of **UWDM-6** demonstrated the overall motion of the macrocycle inside the MOF is not significantly affected by protonation or Li^{+} chelation of the bis(imidazole).

In **Chapter 6**, two Zr-based MOFs, **UWCM-1** and **UWCM-2** were synthesized using the bis(imidazole) [2]rotaxane linker containing unreduced **24C6** wheel and naked bis(imidazole) linker, respectively. Subsequent ring removal of **UWCM-1** by post-synthetic modification utilizing Hoveyda-Grubbs II catalyst generated a MOF with a different topology which is identical to **UWCM-2**. Indeed, ring removal of **UWCM-1** leads to structural transformation of the MOF while the Zr clusters still remain intact.

DEDICATION

To my love, Esmaeil,

To my parents, Hassan and Houri,

To my brother, Navid.

I could not have done it without your unconditional love and constant support.

ACKNOWLEDGEMENTS

I would like to express my deepest gratitude to my advisor, Prof. Stephen J. Loeb, for his relentless guidance, caring and patience. He has constantly challenged me to push my intellectual limits and think on different fundamental limits. I would like to thank Dr. Kelong Zhu whom have been always had his door open to listen, advise and enduring question after question. I would also like to thank the rest of my committee members: Dr. Tricia B. Carmichael, Dr. Sam Johnson, and Dr. Elena Maeva for their guidance. I must thank Dr. Jorge Tiburcio at CINVESTAV for taking the responsibility as the external reviewer of my dissertation. I would also like to appreciate a number of people that made possible the successful completion of the adventure that was my dissertation:

Dr. Rob Schurko and his graduate student Chris O'keefe for all their help in the collection and analysis and modeling of all solid state NMR studies

Dr. Nick Vukotic for all his help and advice with X-ray diffraction studies

Dr. Giorgio Baggi for his help with association constant measurements which are presented in chapter 5 of this dissertation

Ms. Sharon Lackie for her expertise on various materials data collection techniques

Dr. Matt Revington, Dr. Janeen Auld and Mr. Joe Lichaa for all their helps and advice with analytical instruments

Any one in chemistry and biochemistry department: in particular, Dr. Yashi, Ghazaleh, Alex, Pablo, Mike, Christin, Emilyn for helping me in different ways.

Last, but certainly not least, I would like to thank Ginny Loeb for all of her kindness and caring.

I owe many thanks to my family for their patience, guidance, support and belief in me. Finally, thank you to my lovely husband, Esmaeil, for his unwavering love.

TABLE OF CONTENTS

LIST OF TABLES

LIST OF FIGURES

LIST OF SCHEMES

LIST OF ABBREVIATIONS/SYMBOLS

24C6	[24]crown-6
δ	Chemical Shift
Å	Angstrom
ATP	Adenosine Tri-Phosphate
B24C6	Benzo[24]crown-6
BDC	1,4-benzenedicarboxylic acid
BET	Brunauer-Emmett-Teller
BPE	Bis(pyridinium)ethane
CB[6]	Cucurbit[6]uril
$CHCl_3$	Chloroform
CP	Coordination Polymers
CT	Charge Transfer
D_2O	Deuterated Water
DB24C8	DiBenzo[24]crown-8
DCE	Dichloroethane
DCM	Dichloromethane
DCM-d_2	Deuterated Methylenechloride
DEF	Diethylformamide
DMF	Dimethylformamide
DMSO	Dimethylsulfoxide
DMSO-d_6	Deuterated Dimethylsulfoxide
EDG	Electron Donating Group
ESI-ToF	Electrospray Ionization – Time of Flight
EtOH	Ethanol

EXSY	Exchange Spectroscopy
EWG	Electron Withdrawing Group
FML	Fast-Motion Limit
HR-MS	High Resolution Mass Spectrometry
Hz	Hertz
ICP-MS	Inductively Coupled Plasma Mass Spectrometry
ICT	Intramolecular charge transfer
IMR	Intermediate-Motion Regime
FT-IR	Fourier Transform Infrared
HMBC	Heteronuclear Multiple-Bond Correlation
K	Kelvins
Ka	Association Constant
kJ/mol	Kilojoules per Mole
MeCN	Acetonitrile
MeCN-d_3	Deuterated Acetonitrile
$MeNO_2$	Nitromethane
MeOH	Methanol
MIM	Mechanically Interlocked Molecule
MOF	Metal-Organic Framework
MORF	Metal-Organic Rotaxane Framework
MP	Melting Point
MSNP	Mechanized Silica Nanoparticle
MW	Molecular Weight
NMR	Nuclear Magnetic Resonance
NOESY	Nuclear Overhauser Effect Specroscopy

OTf	Trifluoromethanesulfonate
ppm	Parts per Million
PRF	Polyrotaxane Framework
PSM	Post-Synthetic Modification
PTFE	Polytetrafluoroethylene
PXRD	Powder X-ray Diffraction
RCM	Ring-Closing Metathesis
RCP	Rotaxane Coordination Polymer
SBU	Secondary Binding Unit
SEM	Scanning Electron Microscopy
SML	Slow-Motion Limit
SPC	Soft Porous Crystal
TBAPy	1,3,6,8-tetrakis(*p*-benzoicacid)pyrene
TCPP	Tetra(4-carboxy)-phenyl-porphyrin
TGA	Thermogravimetric Analysis
THF	Tetrahydrofuran
TLC	Thin Layer Chromatography
UV-VIS	Ultraviolet-Visible Spectroscopy
UWCM	University of Windsor Crystalline Material
UWDM	University of Windsor Dynamic Material
VT	Variable Temperature

CHAPTER 1

1.1 Mechanically Interlocked Molecules

Mechanically interlocked molecules (MIMs) are molecules with constituent components that are not directly connected but are held together because of their topology; similar to keys on a key chain loop. Although all the interactions between interlocked components are non-covalent forces, the components cannot be separated without breaking a covalent bond in one of them.[1] Examples of mechanically interlocked molecular architectures include catenanes, rotaxanes, molecular knots, and molecular Borromean rings (Fig 1.1).

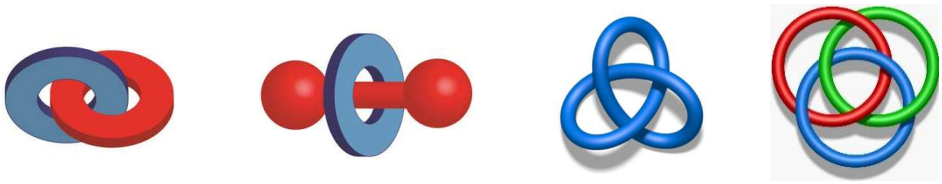

Catenane Rotaxane Trefoil knot Borromean ring

Figure 1.1 - Cartoon representation of some mechanically interlocked topologies: (a) a [2]rotaxane; (b) a [2]catenane; (c) a trefoil knot; (d) Borromean rings.

Although primary research into MIM architectures was mainly focused on their design and synthesis, the discovery of the first catenated DNA in the mitochondria of human cells, in 1967,[2] opened a new paradigm for the field of "biochemical topology".[3] Up until now, many examples of such structures have been discovered in biological systems such as cystine knots, cyclotides and a variety of peptides.[4] Indeed, the importance of topology in biological systems has played a significant role in the discovery of approaches to artificial interlocked compounds.

MIMs have attracted many researchers' attention mainly because they have different properties from their constituent components and thus can be used to develop molecular machines by manipulating the relative position of the components. Catenanes and rotaxanes are two major types of MIMs which have shown remarkable potential as molecular machines and switches.[5] Such assemblies can be synthesized efficiently through a combination of supramolecular, coordinative and traditional covalent interactions.[6]

1.1.1 [2]Pseudorotaxane

A [2]pseudorotaxane is an interpenetrated molecule consisting of a macrocyclic wheel that encircles a linear axle and forms a stable host-guest pair. The name "rotaxane" is derived from the Latin words for "wheel" and "axle". "Pseudo" means false, so "pseudorotaxane" without bulky groups at the end of the axle means false rotaxane. Based on the standard nomenclature, the number of components of a pseudorotaxane appears in a square bracket before the term.[7] For example, Fig. 1.2 shows a [2]pseudorotaxane comprised from a linear axle and a macrocyclic wheel.

Figure 1.2. Cartoon representation of a [2]pseudorotaxane complex in equilibrium with its components. Reprinted with permission from ref 7e.

A pseudorotaxane is a supramolecular complex but not a compound because it is always in equilibrium with its components in solution. Generally, the interpenetrated components of pseudorotaxanes are held together thermodynamically by non-covalent interactions including donor/acceptor forces, metal/ligand coordination, hydrogen bonding, π–π stacking, solvophobic repulsion, and/or electrostatic forces. For

[2]pseudorotaxanes, the larger association constant is due to stronger non-covalent interactions occurring between the two components.[8]

1.1.2 [2]Rotaxanes

A [2]rotaxane is a mechanically interlocked molecule composed of a dumbbell-shaped axle and macrocyclic ring. Unlike [2]pseudorotaxanes, a [2]rotaxane is not in equilibrium with its components due to capping of the ends of the linear axle with bulky groups which prevents dissociation.

[2]Rotaxanes can be prepared by a variety of approaches such as capping, clipping, slipping and active metal template.[9] Among the proposed methodologies, capping and clipping are the most common synthetic methods. In capping, the primary step is generation of a [2]pseudorotaxane precursor due to interaction of a linear axle and a macrocyclic ring. Then, the [2]pseudorotaxane is converted to a permanently interlocked [2]rotaxane by end-capping of the linear axle with two bulky stopper groups which prevent the wheel from dethreading.[10] In clipping, a precursor is formed due to interaction of a dumbbell-shaped axle with an open chain pre-macrocycle. Then, the precursor undergoes a ring closing reaction around the axle to form a [2]rotaxane[11] (Figure 1.3).

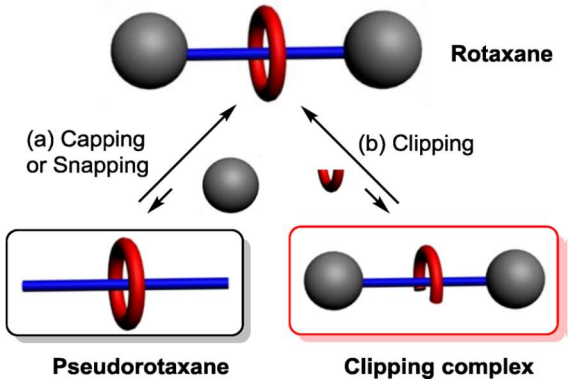

Figure 1.3. Cartoon representation of [2]rotaxane synthesis via (a) capping (b) clipping method. Reprinted with permission from ref 9d.

In general, synthesis of [2]rotaxanes is challenging mainly due to the mechanical nature of the interactions between host and guest molecules which demands proper arrangement of two free molecules in space. Therefore, one of the key steps to develop new MIMs is discovery of new templating pairs of axles and wheels for the formation of [2]pseudorotaxanes and study of their interactions. Although, it was found that the efficient interaction between electron-rich macrocyclic wheels and electron-poor (charged) axles could allow for the development of a wide variety of [2]pseudorotaxane complexes, there are only a few of them that are efficient at threading and at the same time allow for easy structural modification.[12] Indeed, there are still only a handful of these assemblies that are potentially useful for applications in molecular machines and switches.[9d, 13]

1.2 Molecular Machines

The word "machine" is referred to an apparatus consisting of several parts that can perform a useful task using a mechanical movement. Thus, a molecular machine is an assembly of distinct molecules that can produce a mechanical function in response to specific stimuli. Molecular machines can be divided into various categories such as "motors", "switches" and "tweezers". [14]

The fast growth of the field is undoubtedly corresponded to the discovery and the study of various biological systems performing as machines. In biological systems, molecular machines are vital as they can accomplish complex biological process. Numerous types of biological molecular machines composed of macromolecules, e.g., nucleic acids and proteins, are involved in a vast variety of chemical and mechanical functions essential for living activities.[15] One of the most typical examples is ATP synthase, a rotary motor that has a vital role in production of ATP.[16] It provides the required energy for the formation of ATP via proton pumping across membranes. ATP synthesis is one of the most important processes in our body as it is responsible for transporting chemical energy within cells for metabolism.

Hence, extensive use of biological molecular machines has been inspiring many scientists in supramolecular chemistry to create artificial molecular machines using multicomponent systems. Although, the use of supramolecular architectures in molecular machines is challenging due to difficulty in controlling mobility of the components, progress in the field of molecular machines is still accelerating. The boost in the interest for molecular machines was primarily because of the discovery of approaches to synthesize mechanically interlocked structures (e.g. catenanes and rotaxanes), and controlling their dynamic properties. Having control over the position and orientation of one molecular component relative to another can give machine-like properties to mechanically interlocked and interpenetrated molecules. Controlled motion can be achieved by manipulating non-covalent interactions that can be reached by various external stimuli, such as acid/base, anion, cation, heat, solvent polarity, photochemistry, and electrochemistry.[17] For [2]pseudorotaxanes, the main mechanical motion is threading and dethreading of the interpenetrated components.[18] In addition, a few examples have shown that the wheels also can undergo the shuttling motion on the unstoppered linear axle.[19] For [2]rotaxanes, two types of motions are involved (Fig. 1.4).[9d] They can undergo rotational motion[20] of the wheel relative to the axle or shuttling motion[21] of the wheel along the axle.

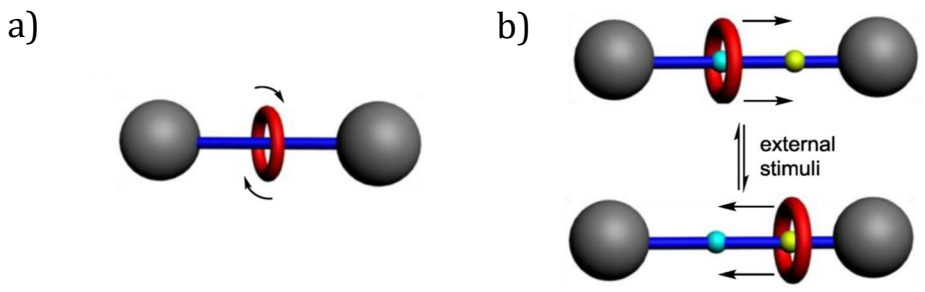

Figure 1.4. Cartoon representation of two types of molecular motion in [2]rotaxanes: (a) rotation and (b) shuttling. Reprinted with permission from ref 9d.

Since the dynamic properties of [2]pseudorotaxanes and [2]rotaxanes were detected, new strategies have been investigated to manipulate their mechanical motion under the influence of external stimuli. Thus, stimuli-responsive [2]pseudorotaxanes and [2]rotaxanes can be promising candidates for the development of molecular devices and molecular switches.[13c]

1.2.1 Controlling Threading and Dethreading

A [2]pseudorotaxane can easily undergo reversible threading/dethreading in solution as the linear axle does not have bulky end groups and it is always in equilibrium with the free molecular components. This reversible nature of threading and dethreading of the linear axle through the ring has been shown to be controlled by solvent[22] and/or temperature[23], or other suitable external inputs.[24]

In general, it has been shown that solvent polarity can affect the driving forces such as hydrogen bonding and π-stacking interactions. Solvation interactions are also competing with the complexation between host and guest species in solution.[24] As an example, [2]pseudorotaxane formation between **DB24C8** and dialkylammonium salts was shown to have the highest association constant in non-polar solvents due to the lack of competition from the solvent for the hydrogen bonding, whereas the complexation is negligible in DMSO[22]. Beside solvent, temperature also can have profound effect on the threading process not only from its association constant, but also from the threading-dethreading rate.[23, 8d] Temperature can alter the binding strength between the components. Thus, solvent polarity and temperature are simple external inputs widely used to tune the association process.

Furthermore, control over association and dissociation of a [2]pseudorotaxane can be achieved by several environmental stimuli including chemical (such as pH, anion and cation), photochemical and electrochemical, or other control methods.[24] For example, it is

well-known that the [2]pseudorotaxane formation between **DB24C8** and secondary ammonium salts could be chemically controlled by pH. For electron-rich **DB24C8** and an electron-poor axle with two terminal donor groups (N,N-dimethylamino) and an inner acceptor group ((bis(pyridinium))ethane (**BPE**), the association constant of the relevant [2]pseudorotaxane is increased dramatically by addition of a Lewis acid.[25] The thread is an organic D–π-A–π-D chromophore with an intense orange colour that turns colorless upon protonation due to elimination of intramolecular charge transfer (ICT). However, addition of **DB24C8** to a solution containing the thread, leads to a color change from colorless to pale-yellow as a result of weak charge-transfer interactions between **BPE** unit and **DB24C8** (Scheme 1.1).

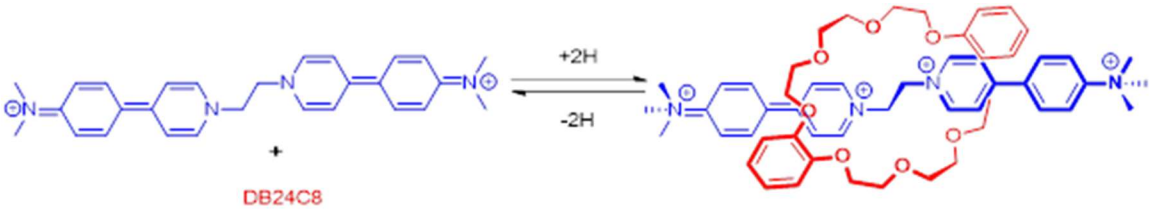

Scheme 1.1. A representation of the threading/unthreading process of a [2]pseudorotaxne by using acid and base.[25]

Another example of the stimulus-induced association/disassociation mobility of pseudorotaxanes is based on the use of an external electron-transfer photosensitizer.[26] In this system, a [2]pseudorotaxane is formed between a linear guest containing an electron-rich dioxynaphthalene unit and a cyclophane host containing an electron-poor 4,4'-bipyridinium unit (Scheme 1.2).

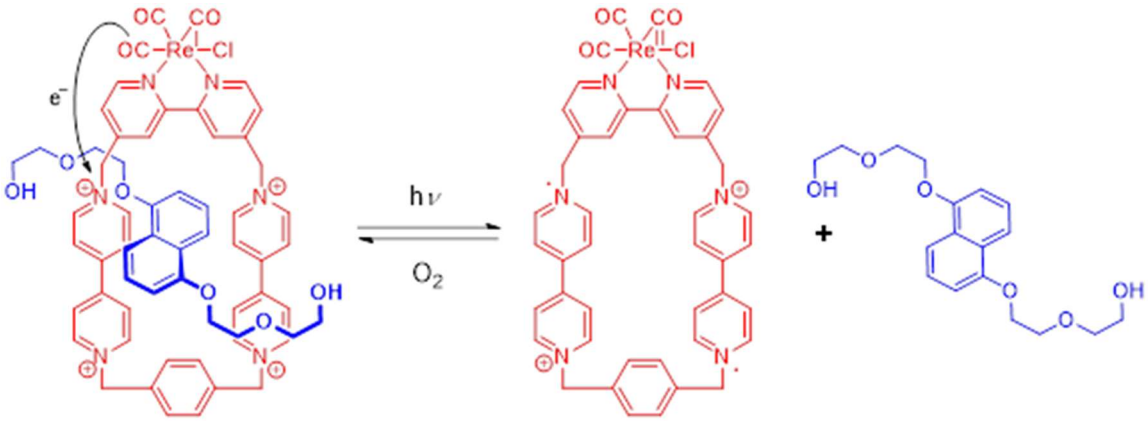

Scheme 1.2. A representation of the light-induced dissociation of a [2]pseudorotaxane incorporating the photosensitizing moiety in the macrocyclic wheel.[26]

Besides electron-acceptor motifs, the cyclophane comprises a 2,2'- bipyridine coordinating ligand which is coordinated to $[Re(CO)_3Cl]$ (a metal-based photosensitizer) to create a $[Re(CO)_3(cyclophane)Cl]^{4+}$ component. Upon mixing of the cyclophane wheel and linear axle, the emission band related to the thread (at λ_{max} = 345 nm) is quenched and a new absorption band (at λ_{max} = 497 nm) related to charge transfer (CT) transitions appears. This observation strongly suggests non-covalent interactions between the host and guest pairs. On the other hand, non-covalent interactions between the axle and the wheel can be reduced through light irradiation of the $[Re(CO)_3(cyclophane)Cl]^{4+}$ moiety of the [2]pseudorotaxane resulting in the transfer of one electron from the Re center to one of the 4,4'-bipyridinium units in the cyclophane component. Later, disassembly of the complex can happen in the presence of large amount of a sacrificial reducing agent. Additionally, the [2]pseudorotaxane can be recreated through reoxidization of the reduced 4,4'-bipyridinium unit in the presence of oxygen in the irradiated solution.

1.2.2 Controlling Rotational Motion

A method to extract a mechanical task from [2]rotaxanes would be to control the rotational mobility of the macrocyclic wheel around the dumbbell-shaped axle. The rate of

the macrocyclic rotation is intensely dependent on the strength of the non-covalent interactions between the two components, which must be broken and rebuilt during the movement of the macrocycle. Thus, increase in the intra-complex interactions can enhance the energy barrier to the rotational motion of the wheel. Studies have shown that the rate of rotational motion can be manipulated via temperature, solvent, chemical moieties, electric field strength and light.[27] These systems represent a blueprint toward the eventual construction of rotary molecular devices.

In an effort to investigate methods of controlling the rotational motion of the wheel around the thread in [2]rotaxanes, Leigh, Zerbetto, and co-workers demonstrated the rotational motion of the macrocyclic wheel around a fumaramide axle that can be addressed and to some extent controlled by alternating-current (ac) electric field.[28] The interpenetrated components of the their [2]rotaxane consist of a linear fumaramide axle with bulky stoppers and macrocycle with two isophthalamide groups which are held together by strong NH…O hydrogen bonds. The trans-olefin on the thread makes oxygen atoms accessible to form hydrogen bonding interactions with both sites of the macrocycle. Later, it was indicated that the relative motion within the amide-base [2]rotaxanes can also be manipulated by photochemical isomerization.[29] The consequence of isomerizing fumaramide (*trans* form) to the corresponding maleamide (*cis* form) [2]rotaxanes is that the amide groups of the axle are reorganized in positions such that they can form two hydrogen bonds with only one site of the wheel (Fig. 1.5a). The variable temperature (VT) ^{1}H NMR spectroscopy was used to determine the dynamic properties of both isomers in non-polar solvents (fig. 1.5b). As shown in Fig. 1.5b, the fumaramide system undergoes slow exchange on the NMR timescale wherein separate sets of peaks for both axial and equatorial H_E protons are observed at lowest temperature (223 K) corresponding to a macrocycle spinning rate of $\approx 1\ s^{-1}$ whereas coalescence of these protons occurs at 273 K. In contrast,

^{1}H NMR spectrum of the maleamide system exhibits only an averaged signal of H_{E1} and H_{E2} even at 223 K due to the rapid rotation of the macrocyclic ring around the axle (rate > 1.2 x 10^6). Hence, the *cis* form of this [2]rotaxanes undergoes much faster rotation due to a decreased barrier to rotational motion.

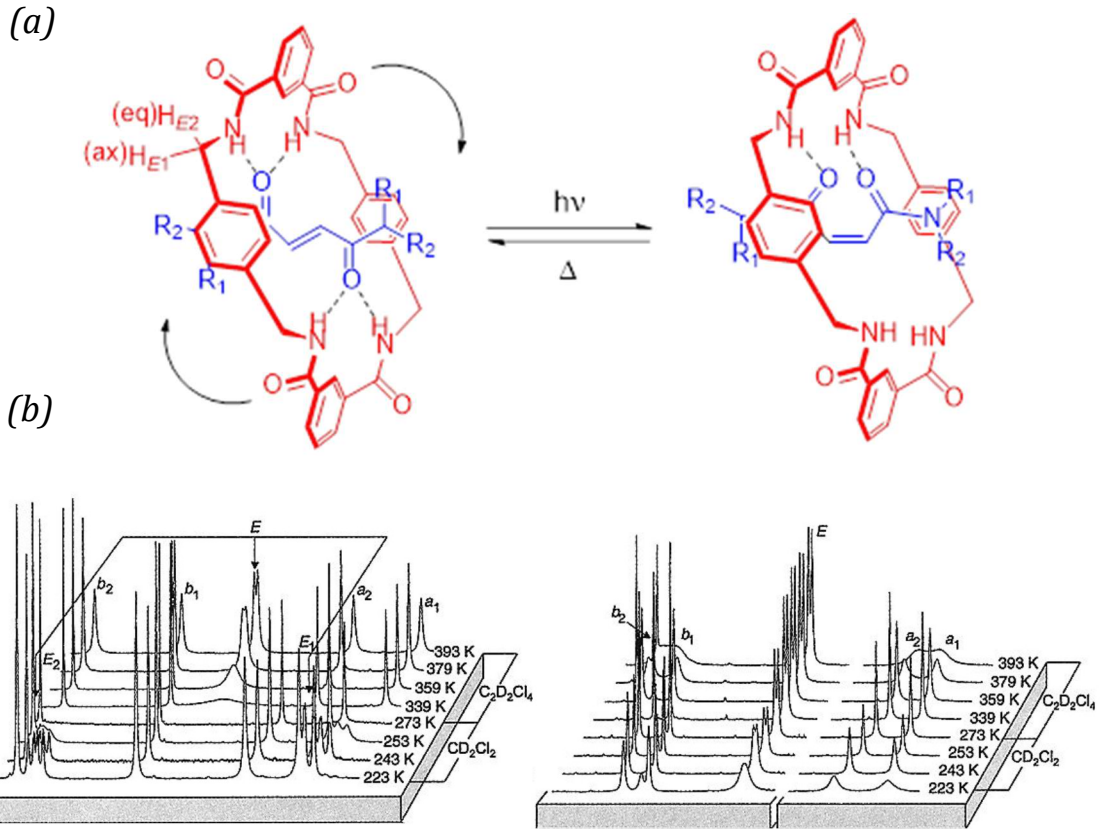

Figure 1.5. (a) A schematic representation of photo-isomarization of the [2]rotaxane (b) VT ^{1}H NMR spectra (400 MHz) of trans form (left) and cis form (right) of the [2]rotaxane in CD_2Cl_2 at 223-273 K and $C_2D_2Cl_4$ at 339-393 K. Reprinted with permission from ref 29.

In addition to photoisomerization-dependent disruption of hydrogen bonding in [2]rotaxanes, it has been also reported that non-covalent interactions can be controlled by change in the solvent and in turn the rate of rotation can be influenced.[30] For instance, as depicted by ^{1}H NMR studies on the motion of the fumaramide [2]rotaxane systems, addition

of 5% D_2O in the solvent significantly accelerates the mechanical motion of the macrocycle which results in coalescence at lower temperature. It is interesting to note that other polar solvents (i.e. alcohol, nitromethane) have much weaker effect. Thus, the function of water as a lubricant facilitates rearrangement of the wheel via formation of 3-D hydrogen bonding networks.

1.2.3 Molecular Shuttle

Translation is another type of motion that can be displayed by [2]rotaxanes. [2]Rotaxane molecular shuttles comprise a dumbbell shaped axle with two recognition sites and an encircled macrocyclic wheel that can undergo translation between the two sites.

A [2]rotaxane is referred as a degenerate molecular shuttle if the axle comprises two equivalent recognition sites with equal binding affinities for the wheel in which the wheel spends the same amounts of time at both stations.[31] However, a bistable [2]rotaxane molecular shuttle is created if there are two distinct recognition sites on the axle that have different binding affinities.[32] Bistable [2]rotaxanes can have two translational co-conformations with different molecular geometries depending on the position of the macrocyclic wheel relative to the axle. The population of the translational isomers mainly depends on the relative strengths of the non-covalent interactions between the wheel and the two sites. In such systems, the wheel spends the majority of its time around the most efficient site until an external stimulus changes the relative affinity of the wheel for the site, thereby causing the shuttling of the wheel to the other site. Accordingly, such [2]rotaxanes with two different recognition sites are considered as potential basics for molecular machinery, since there is the possibility of controlling the relative positioning of the interlocked components.

The shuttling mobility of rotaxanes first was reported in 1991 by Stoddart and co-workers.[33] A [2]rotaxane molecular shuttle was formed via interaction of a tetracationic

cyclophane ring and polyether thread with two hydroquinol recognition sites that is terminated at the ends by bulky triisopropylsilyl groups (Scheme 1.3). ^{1}H NMR studies of the [2]rotaxane in acetone-d_6 indicated the electron poor ring moves back and forth between two identical hydroquinol stations along the dumbbell-like axle with $\Delta G_c^{\ddagger}$ value of ca. 13 kcal mol^{-1}. This original work revealed that MIMs could be developed to imitate the mechanical motion of macroscopic switches and machines, and can be considered the archetype for the creation of various supramolecular assemblies with higher degree of complexity such as bistable molecular shuttles and other molecular switches.

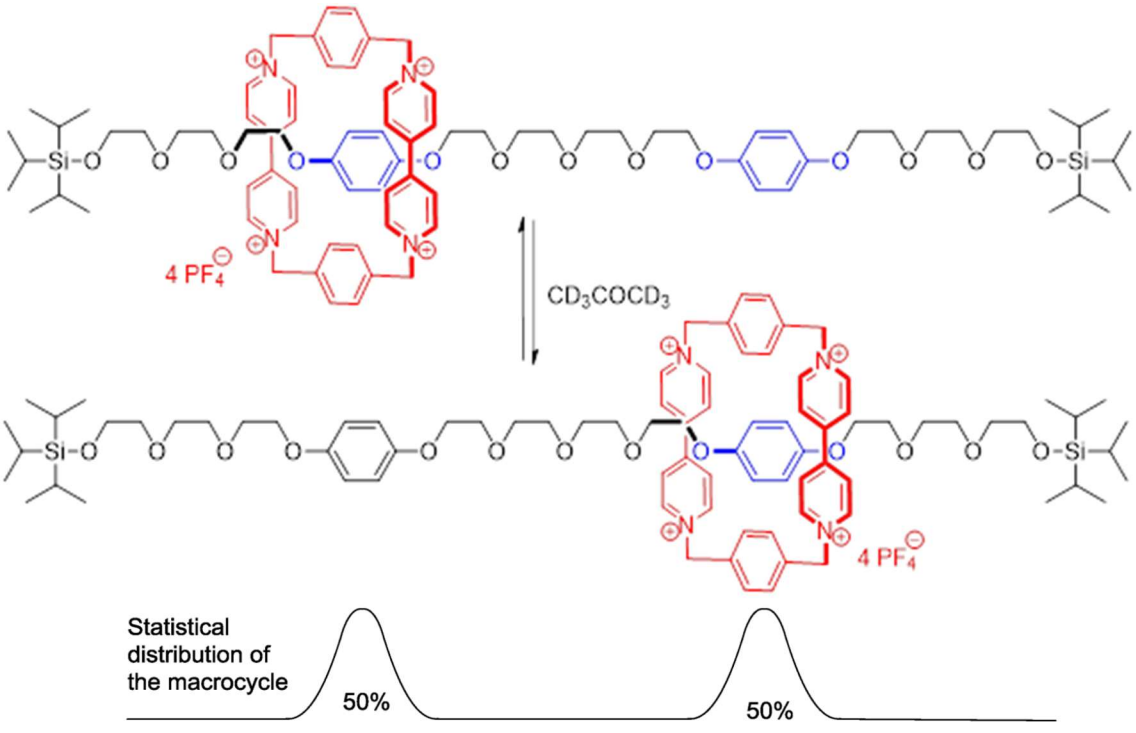

Scheme 1.3. A prototype molecular shuttle with a cyclophane ring shuttles between two identical hydroquinol sites in acetone-d_6. [33]

Besides [2]rotaxane molecular shuttles, there exists a few examples in the literature that show shuttling of the wheel along the bistable axle in [2]pseudorotaxanes.[34] Studies on switchable pseudorotaxanes are essential for the development of more practical MIM-based molecular machines and switches. In 2000, Kim and co-workers reported the first

fluorescent, reversible molecular switch based on a [2]pseudorotaxane that is formed using cucurbit[6]uril (**CB[6]**) wheel and fluorenyltriamine axle (Scheme 1.4).[35] Upon protonation of all of the nitrogen atoms on the axle, a competition is established between two recognition sites, which is dominated by the protonated diaminohexane station due to stronger non-covalent interactions between the wheel and the site. However, when the aniline nitrogen is deprotonated (pKa = 6.7), **CB[6]** migrated to the diaminobutane site because **CB[6]** has less binding affinity for the monoprotonated diaminohexane. The deprotonation process is accompanied with color change from yellow to violet and decrease in the fluorescence intensity. Thus, the switching of the wheel from one site to the other is simply detected by monitoring the color change and fluorescence with high sensitivity. The switching process could be manipulated several times by sequential addition of acid and base.

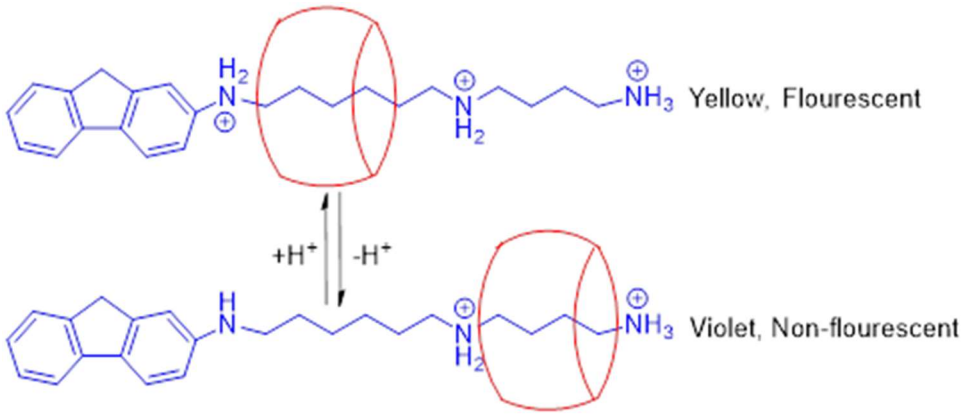

Scheme 1.4. The first fluorescent [2]pseudorotaxane-based molecular switch formed using cucurbituril[6] wheel and fluorenyltriamine axle.[35]

To date, almost all known [2]rotaxane molecular shuttles have large and flexible structures and operate efficiently in solution where they are widely dispersed.[36] In order to have better control over their switching or machine-like features, they could be transferred and organized into solid state materials with enough void spaces. However, these types of flexible structures are less efficient when incorporated into solid state

wherein the size, positional orientation, and rigidity of the MIM components are important factors.[37] To incorporate these nanoscale switches into highly-organized and condensed materials, assemblies with rigid axles and linear tracks as building blocks would be most desired. For this purpose, in 2012, Loeb and co-workers designed the first new MIM template between rigid T-shaped 2,4,7-triphenyl-substituted benzimidazolium axles and 24-membered crown ether wheels (Scheme 1.5).[38]

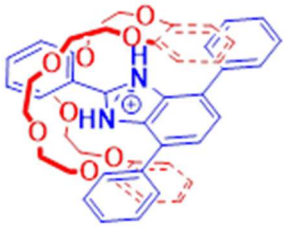

Scheme 1.5. A prototype [2]pseudorotaxane between rigid T-shaped 2,4,7-triphenyl-substituted benzimidazolium axles and 24-membered crown ether wheels.[38]

They used the T-shaped templating motif for construction of H-shaped, degenerate [2]rotaxane molecular shuttles with a rigid backbone.[39] The presence of two equivalent benzimidazole recognition sites on the rigid axle allows the [2]rotaxane to adopt three possible forms i.e. neutral, monocation and dication using acid-base chemistry. Each of these forms displays a different structure with different rate of shuttling. The neutral form of the molecular shuttle shows extremely rapid shuttling (4.3×10^6 s^{-1}, CD_2Cl_2) between two identical binding stations. Whereas adding one equivalent of acid produces the monocationic [2]rotaxane in which the crown ether resides at the charged site with stronger interactions, thereby the rate of shuttling is negligible (0.0 s^{-1}, CD_2Cl_2). However, when the [2]rotaxane is diprotonated, the wheel undergoes shuttling between two identical sites but at a much lower rate (8.4×10^{-3} s^{-1}, CD_2Cl_2) due to stronger interactions between the charged sites and crown ether wheel. Moreover, addition of an equivalent of Li^+ to the neutral

[2]rotaxane significantly decelerates the rapid shuttling of neutral form to an intermediate (5.1 s^{-1}, CD_2Cl_2). Indeed, Li^+ functions as a brake via intramolecular ferrying between the recognition sites. Scheme 1.6 indicates that four states of the H-shaped [2]rotaxane molecular shuttle can be reversibly interconverted.

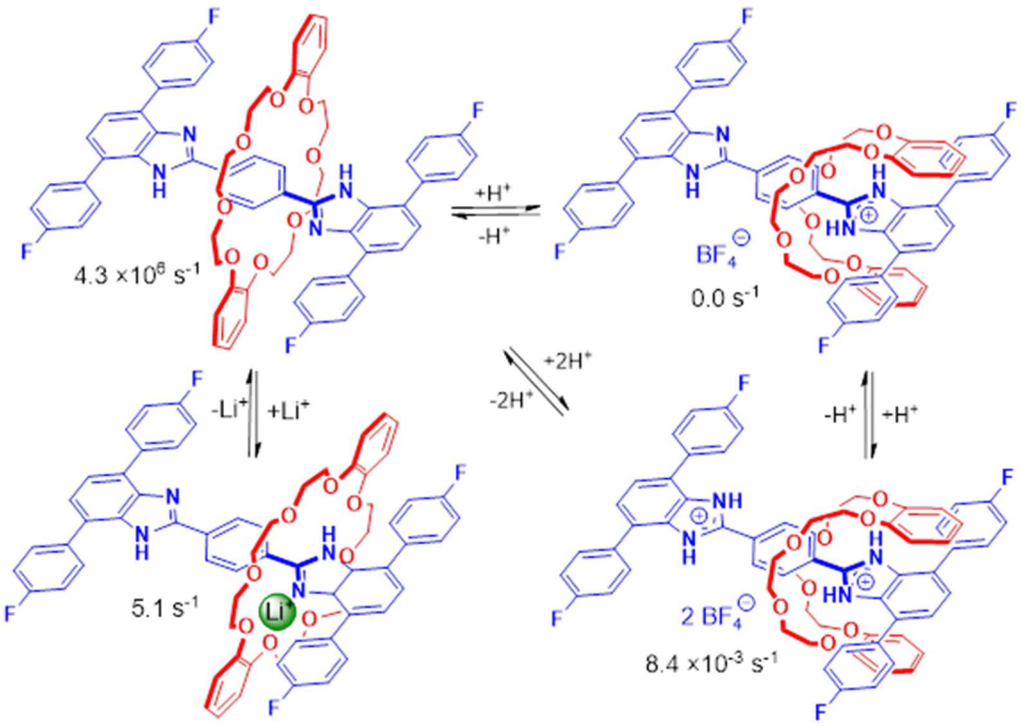

Scheme 1.6. Representation of reversible conversion between four states of a new compact and rigid, H-shaped [2]rotaxane molecular shuttle.[39]

1.2.4 Applications

In Nature, various operations and reactions happen in parallel. To make sure that these reactions and their outcome do not obstruct each other, these processes must be thoroughly controlled and switched on and off when needed. Reaching similar control over synthetic reactions could be valuable for affecting both the rate and product of the reactions. To this end, several artificial molecular machines have been reported using [2]rotaxane molecular shuttles to control the reactions through switching on and off catalytic activity

which have been inspired by enzymes.[40] In 2013, Leigh et al. intrigued by ribosomal protein synthesis, designed the first small molecule artificial molecular machine capable of peptide synthesis in a sequence-specific manner. The machine is based on a [2]rotaxane architecture, a macrocyclic ring with a catalytic arm encircled around an axle containing sequence of amino acid stations.[13b, 41] The catalytic arm of the wheel picks up amino acids sequentially from the strand and converts them to a sequence of peptides through native chemical ligation (NCL) (Fig. 1.6). Thus, in some aspects, the role of strand is analogue to mRNA in the ribosomal system. The steric hindrance of the loaded amino acid group allows the sequential reaction because it does not allow the ring passing over the barrier unit before the reaction of ring and amino acid has taken place. However, after cleavage of the amino acid from the strand, the ring can freely pass over the station. Moreover, the rigid axle of the [2]rotaxane minimizes the possibility of the catalytic arm facing an out of sequence amino acid.

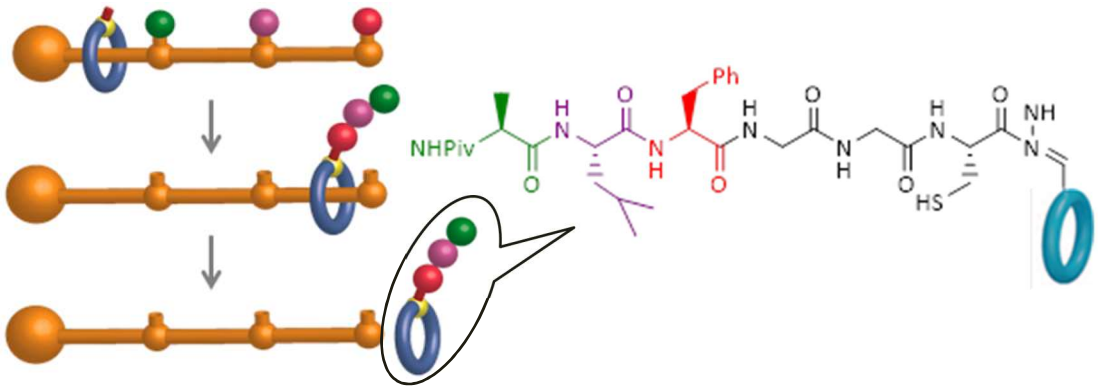

Figure 1.6. Cartoon representation of sequence-specific peptide synthesis by using a [2]rotaxane. Reprinted with permission from ref 13b.

Although there are molecular machines that function with efficiency in solution and have potential applications as molecular logic gates and sensors, they are less practical in the solid state where molecules are arranged in an orderly manner. If these tiny devices

could be organized on surfaces, interfaces and polymer matrixes with electronic, mechanical, or biological applications, controlling the properties and function of materials at macroscopic level would be very much closer to realization.[42] Hence, in recent years, controlled drug release through nanovalves, molecular electronics, artificial molecular muscles and information storage using solid-state molecular machines have been the subject of research in this field.[43]

Some very sophisticated examples in the literature have shown that interlocked architectures such as [2]pseudorotaxanes and bistable [2]rotaxanes on the surface of mesoporous silica nanoparticles (Si-MPs) can operate as nanovalves for controlled release of guest molecules under specific conditions.[44] Indeed, the relative positions of interlocked components is determinative to either restrict or allow access to the pores in materials. These porous mechanized silica nanoparticles (MSNPs) have great potential for drug and gene delivery applications because of their unique responsiveness and high stability. Fig. 1.10 shows [2]pseudorotaxane-based MSNPs that can be reversibly opened or closed under control and at the same time act as nanovalves to encapsulate or release guest molecules.[43a] The [2]pseudorotaxanes based on a linear thread with a secondary dialkylammonium unit and dibenzo[24]crown-8 are attached to the silica surface of the MSNPs such that the gates remain closed when **DB24C8** rings encircle the dialkylammonium ions due to primarily $[N\text{-}H\ldots O]^+$ hydrogen bonds. On the other hand, deprotonating the dialkylammonium units with a base or competitive binding of the **DB24C8** rings with fluorodialkylammonium or metal ions opens the gates due to elimination of non-covalent interactions between the rings and threads and so the rings dethread, allowing the guest molecules to be released (Fig. 1.7).

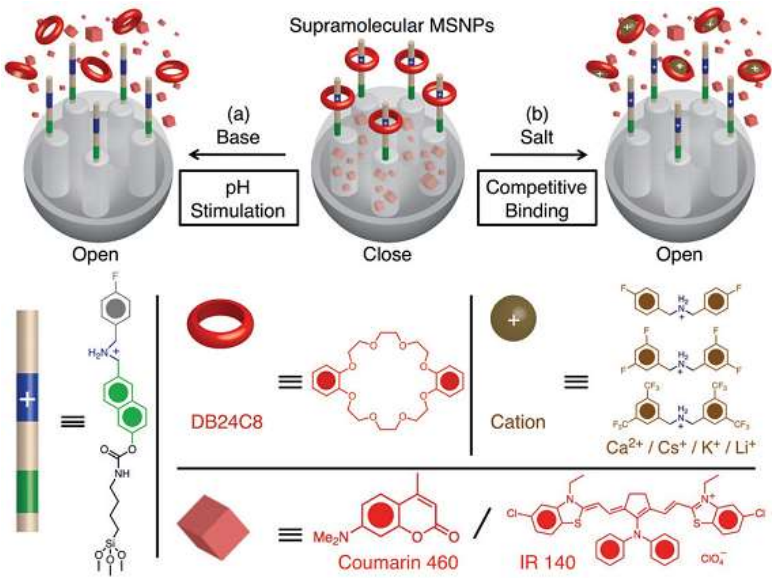

*Figure 1.7. A [2]pseudorotaxane-based MSNP acts as a nanovalve to encapsulate or release guest molecules. The guest molecules can be released by breaking the hydrogen-bonds between the secondary dialkylammonium sites and the **DB24C8** wheels using (a) addition of a base or (b) competitive binding of the **DB24C8** rings with fluorodialkylammonium or metal ions. Reprinted with permission from ref 44.*

Additionally, the ability to simply manipulate the mechanical, optical and interfacial properties of surfaces in a controlled and reversible manner would be extremely useful in development of technologically valuable devices. This challenge can be addressed by incorporating molecular machines such as [2]rotaxane molecular shuttles into devices that leads to stimuli-responsive modification of surfaces. To date, a number of molecular-machine-based materials where the interlocked components influence the properties of surfaces have been reported.[45] One relevant example is discussed below.

Leigh et al designed a photoresponsive system using a [2]rotaxane molecular shuttle with fluoroalkane region and *E* olefins physisorbed onto a gold surface by a thiol linker.[46] Irradiation with ultraviolet light (240–400 nm) isomerizes 50% of the *E* olefins to *Z* causing movement of the macrocycle from *Z* olefins to fluoroalkane region which leaves a more polarophilic surface (Fig. 1.8a). As contact angles of both polar and apolar liquids are

highly sensitive to small variations in the concentrations of fluoroalkane groups, this system was used to yield a surface with switchable wettability features. It was demonstrated that a small drop of diiodomethane (CH_2I_2) could be moved up on the [2]rotaxane-terminated surface with a 12° incline after irradiation with light which is associated with co-conformational change of the [2]rotaxane. Illumination of the right-hand side of the droplet and its neighboring surface that is accompanied with decrease in the *E/Z* ratio of the shuttles makes the surface less polarophobic. Thus, a pressure gradient inside the droplet is created due to decrease in the contact angle at the right-hand side. This phenomenon causes moving up and spreading of the droplet along the surface (Fig. 1.8b). Approximately 50% of the absorbed light energy is transformed into gravitational potential energy of the droplet. The above model of macroscopic control of molecular motion on the surface emphasizes on the significance of this research area for technological applications.

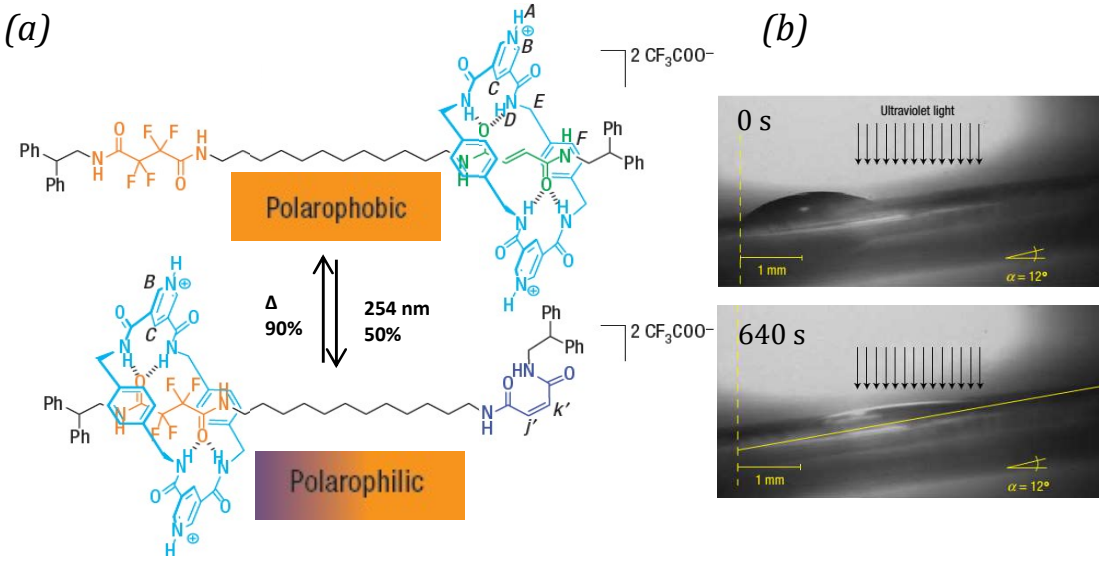

Figure 1.8. (a)A light-deriven [2]rotaxane molecular switch with fluoroalkane group used to affect the surface properties (b) lateral photos before and after light irradiation indicating transport of a small CH_2I_2 drop on a [2]rotaxane-terminated Au substrate up a 12° incline. Reprinted with permission from ref 46.

1.3 Metal Organic Framework

Metal-organic frameworks (MOFs), a subclass of coordination polymers (CP), are materials containing metal ions linked to organic ligands by strong bonds, which form one-, two-, or three-periodic architectures.[47] MOFs are architecturally robust crystalline structures with permanent porosity. These aspects have made them unique among other CPs and ideal materials for a wide range of applications such as gas adsorption and storage, chemical separations, molecular sensing, magnetism**,** heterogeneous catalysis and drug delivery.[48] A major progress in the field of MOF chemistry emerged in 1995 when the synthesis, single crystal X-ray structure, and gas sorption properties of the first robust and highly porous MOF, **MOF-5**, were published.[49] This prototype material contains non-interpenetrated lattices in a primitive cubic topology in which 1,4-benzenedicarboxylate (BDC^{2-}) units are linked by $Zn_4O(CO_2)_6$ clusters (Fig. 1.9). In the field of solid state chemistry, MOFs have attracted great interest in recent years since the versatile node and linker design of the crystalline lattice allows incorporation of a variety of functional groups.

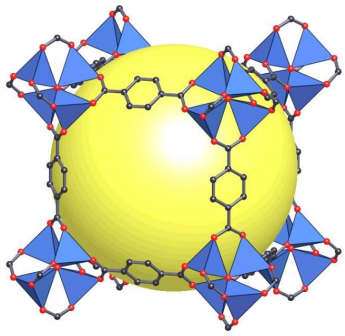

Figure 1.9. *Structure of the first robust and highly porous MOF,* ***MOF-5.*** *Reprinted with permission from ref 49.*

1.4 Metal Organic Frameworks with Interlocked Components

Pores of metal-organic frameworks (MOFs) provide a higher level of molecular organization and coherency which makes them a potential platform for the incorporation

and function of MIMs.[12c,50] It is worthy to note that the motivation for making MIM ligands (e.g. rotaxanes, catenanes) and their incorporation into coordination polymers was to introduce the effect of soft, dynamic molecular components of MIMs into the properties (e.g. magnetic, optical, mechanical) of the resulting materials.[51] These types of MIM-based materials have been called by several terms such as metal-organic rotaxane framework (MORF),[52] rotaxane coordination polymer (RCP)[53] or polyrotaxane framework (PRF).[7e]

In such materials, only weaker non-covalent bonds are broken and remade reversibly during a dynamic process and the relative movement of soft components will not affect the covalent bonds in the MOF backbone. Therefore, the term "robust dynamics" as introduced by Stoddart and Yaghi would be suitable since pairing the dynamics of interlocked components with the robust architecture of MOFs will produce dynamic materials that are still robust and rigid. These attributes allow for the potential incorporation and function of sophisticated molecular switches and molecular machines in the solid state in a controlled manner. Among metal-based materials, only stable 3-periodic MOFs are ideal candidates for the incorporation of MIMs because they provide the porosity crucial to create free volume such that the MIMs are able to undergo uninhibited dynamics (i.e., rotation, translational or co-conformational changes).[54]

In 2002, the first examples of MIM-based coordination polymers were reported by K. Kim.[55] As shown in Scheme 1.7, a series [2]pseudorotaxanes linkers with large association constants were prepared by threading cucurbit[6]uril wheels with pyridine-terminated spermine axles **1-3.**

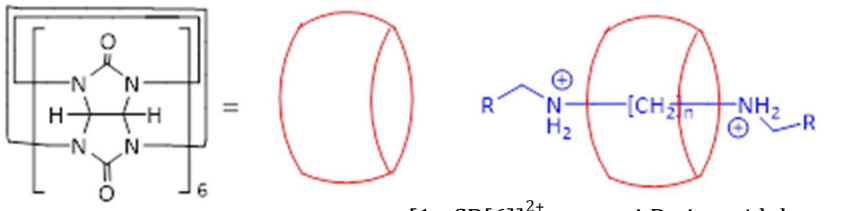

$[1\subset CB[6]]^{2+}$ n=4 R=4-pyridyl
$[2\subset CB[6]]^{2+}$ n=4 R=3-pyridyl
$[3\subset CB[6]]^{2+}$ n=5 R=3-pyridyl
$[4\subset CB[6]]^{2+}$ n=4 R=3-benzonitrile

*Scheme 1.7. Schematic representation of a series of [2]pseudorotaxane linkers with protonated diaminoalkane axles 1^{2+}–4^{2+} and **CB[6]** wheels.[55b]*

The reaction of [**1⊂CB[6]**]$^{2+}$ and silver tosylate developed a one-dimensional (1-D) **CP-1** such that a linear chain polymer is formed due to coordination of two [2]pseudorotaxane units to one Ag(I) ion in a *trans* geometry (Fig. 1.10a). The reaction of [**2⊂CB[6]**]$^{2+}$ and cobalt tosylate produced zigzag-shaped 1-D **CP-2** in which Co(II) nodes are in an octahedral geometry and two pyridyl groups are coordinated to each metal center in a cis arrangement (Fig. 1.10b). The combination of [**3⊂CB[6]**]$^{2+}$ with longer axle and silver nitrate gave helical 1D **CP-3** in which each Ag(I) is coordinated by two terminal pyridyl groups in a linear way (Fig. 1.10c).

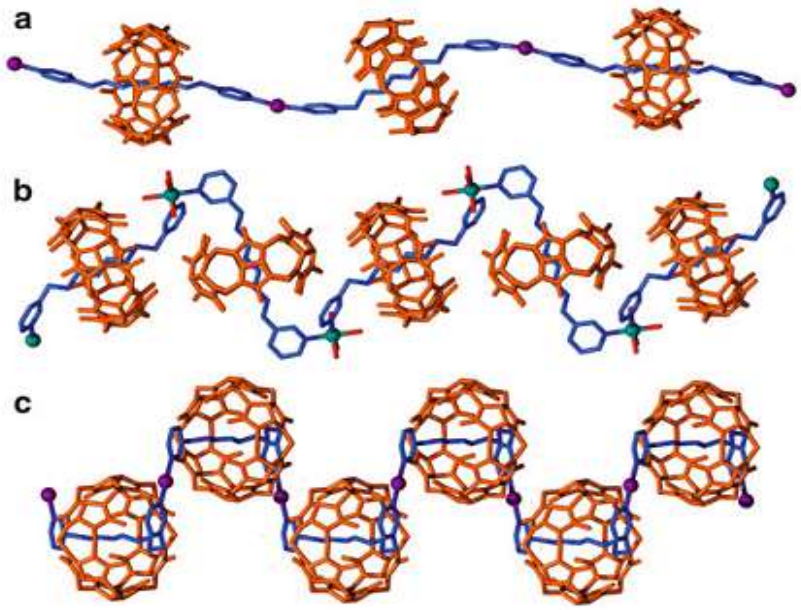

*Figure 1.10. Ball-stick representation of single x-ray crystal structure of (a) linear-shaped **CP-1** with [**1**⊂**CB[6]**]$^{2+}$ linkers Ag(I) nodes; (b) zigzag-shaped **CP-2** with [**2**⊂**CB[6]**]$^{2+}$ and Co(II) nodes; (c) helical-shaped **CP-3** with [**3**⊂**CB[6]**]$^{2+}$ and Ag(I) nodes. Reprinted with permission from ref 55b.*

As described above, the reaction of cobalt tosylate with [**2**⊂**CB[6]**]$^{2+}$ produces a 1-D CP. However, combining the same linker with an aqueous solution of copper nitrate yielded a non-interpenetrated two-periodic coordination polymer, **CP-4** in which each copper ion is coordinated by four equatorial pyridyl groups and one axial water molecule in a distorted square pyramidal geometry (Fig. 1.11a). Moreover, [**1**⊂**CB**[**6**]]$^{2+}$ linker can also produce a 2-D network, **CP-5**, under the same reaction procedure as **CP-1** by switching metal salt to silver nitrate. The framework consisting of hexagons with Ag(I) ions at the corners that each metal centre is coordinated by three pyridyl groups and one nitrate in a disordered tetrahedral geometry. The successful construction of 2-D polyrotaxanes suggested the possibility of construction of 3-D polyrotaxanes using similar approaches. It was found that the reaction of [**4**⊂**CB[6]**]$^{2+}$ with $Tb(NO_3)_3$ under hydrothermal condition gives 3-D **CP-6** (Fig. 1.11b).

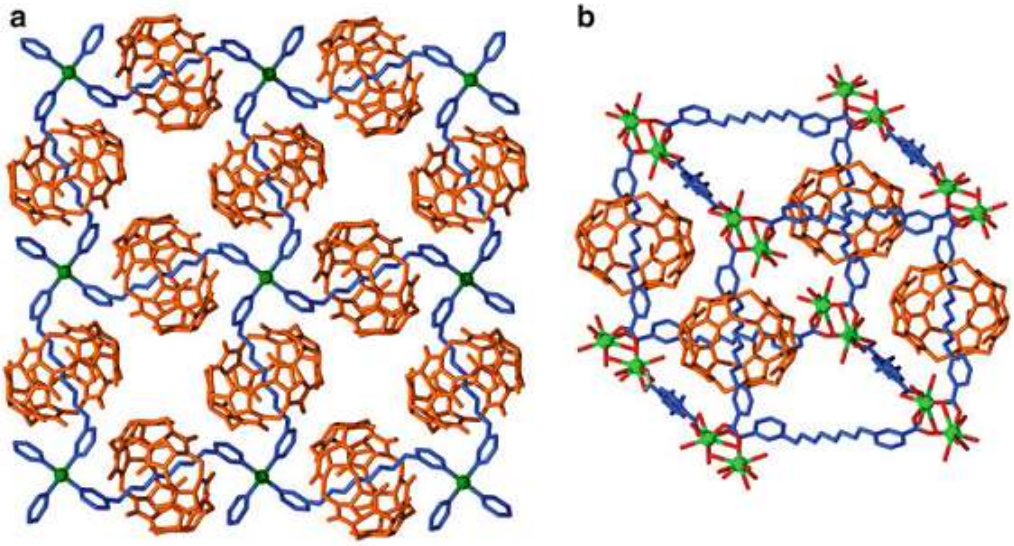

*Figure 1.11. Ball-stick representation of single x-ray crystal structure of (a) two-periodic square-grid shaped **CP-4** with [**2**⊂**CB[6]**]$^{2+}$ linkers and Cu(II) nodes. (b) three-periodic **CP-6** with [**4**⊂**CB[6]**]$^{2+}$ and binuclear Tb(III) nodes. Reprinted with permission from ref 55b.*

During the reaction, the terminal cyano groups on the [**4**⊂**CB[6]**]$^{2+}$ linkers are converted to carboxylate groups which combined with Tb^{+3} ions to produce a 3-D framework. **CP-6** consists of binuclear Tb(III) nodes that behave as a six-connected node and are coordinated by six carboxylate groups.

The above examples demonstrated that there are numerous ways to incorporate rotaxanes into interesting 1-, 2-, and 3-periodic structures. Although, a large variety of 1-, 2- and 3- periodic coordination polymers with rotaxanes have been prepared and characterized, none of these solid-state materials exhibited any actual dynamics (i.e. rotation or translation) related to the interlocked components. The next section describes some recent success in creating [2]rotaxane-based MOFs that do show the rotational and translational motion of their soft macrocyclic components by a thermal stimulus without any hindrance of the rigid material framework.

1.4.1 Dynamic and Controlled Motion in the Solid State

In 2012, Loeb and co-workers published a prototype MOF material containing [2]rotaxanes as a linker that exhibit dynamic motion of its macrocyclic ring inside this solid-state material.[56] For this purpose, a compact and rigid [2]rotaxane was designed using an axle containing two 3,5- benzene-dicarboxylic acid groups and a benzylanilinium recognition site that facilitates the ring-closing metathesis of a 24-membered crown ether, **24C6**. The recognition site is simply deprotonated to yield a neutral [2]rotaxane with only a single NH···O hydrogen bonding interaction between axle and wheel (Scheme 1.8).

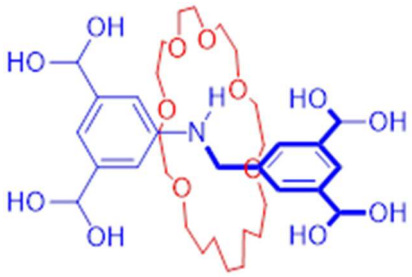

*Scheme 1.8. A neutral tetra-carboxylic acid [2]rotaxane linker designed to exhibit rotational motion of the **24C6** macrocycle.*[56]

The solvothermal reaction of the designated MIM linker and $Cu(NO_3)_2.3H_2O$ in a 3:2:2 mixture of dimethylformamide(DMF)/EtOH/H_2O at 65 °C for 48 h produced a robust 3-D Cu-based MOF, **UWDM-1** (University of Windsor Dynamic Material). **UWDM-1** consists of binuclear Cu(II) paddlewheel clusters coordinated by a tetra-carboxylate MIM molecule and two water molecules to form a non-interpenetrated porous framework with a rare β-phase of nbo topology (Fig. 1.12). There is 11% void space in the structure and these pores are filled by free water molecules. Activation of the solid results in removal of both free and coordinated water molecules which provides the void space necessary for the macrocyclic ring to undergo the rotational motion without perturbation of neighboring components. A

variable temperature (VT) ^{2}H SSNMR experiment was performed on the ^{2}H-labelled **UWDM-1** to determine the dynamic nature of macrocyclic ring inside the activated material.

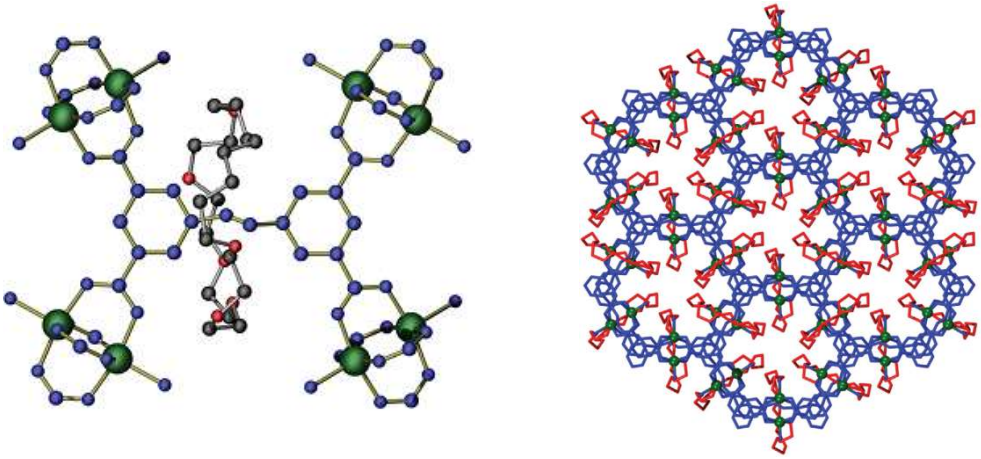

*Figure 1.12. The single X-ray structure of **UWDM-1** indicating (a) the basic repeated unit showing the MIM is coordinated to four Cu(II) paddlewheel clusters (b) a view down the c-axis showing the open channels in which rings are clearly separated from each other. Reprinted with permission from ref 56.*

Experimental and simulated VT ^{2}H SSNMR spectra are depicted in Fig. 1.13. Analysis of the ^{2}H powder patterns supported the postulate that the soft and flexible macrocyclic component is able to rotate rapidly about the rigid framework. The mobility of the ring increases with increase in temperature wherein at temperatures > 100 °C it undergoes independent rotation about the NH_2-CH_2 group with the rate > 10 MHz. the motion also can be quenched by decreasing the temperature or by addition of water to lock the ring by OH_2…O hydrogen bonding interactions. Furthermore, in order to identify the effect of ring size on the rotational dynamics, **UWDM-1** was synthesized with various sized macrocycles i.e. **22C6** and **B24C6** under the same synthetic conditions.[57] ^{2}H SSNMR studies of the resulting materials demonstrated both macrocycles undergo quite different degrees of motion from **24C6** inside the **UWDM-1**. However, all **UWDM-1** series form a similar topology.

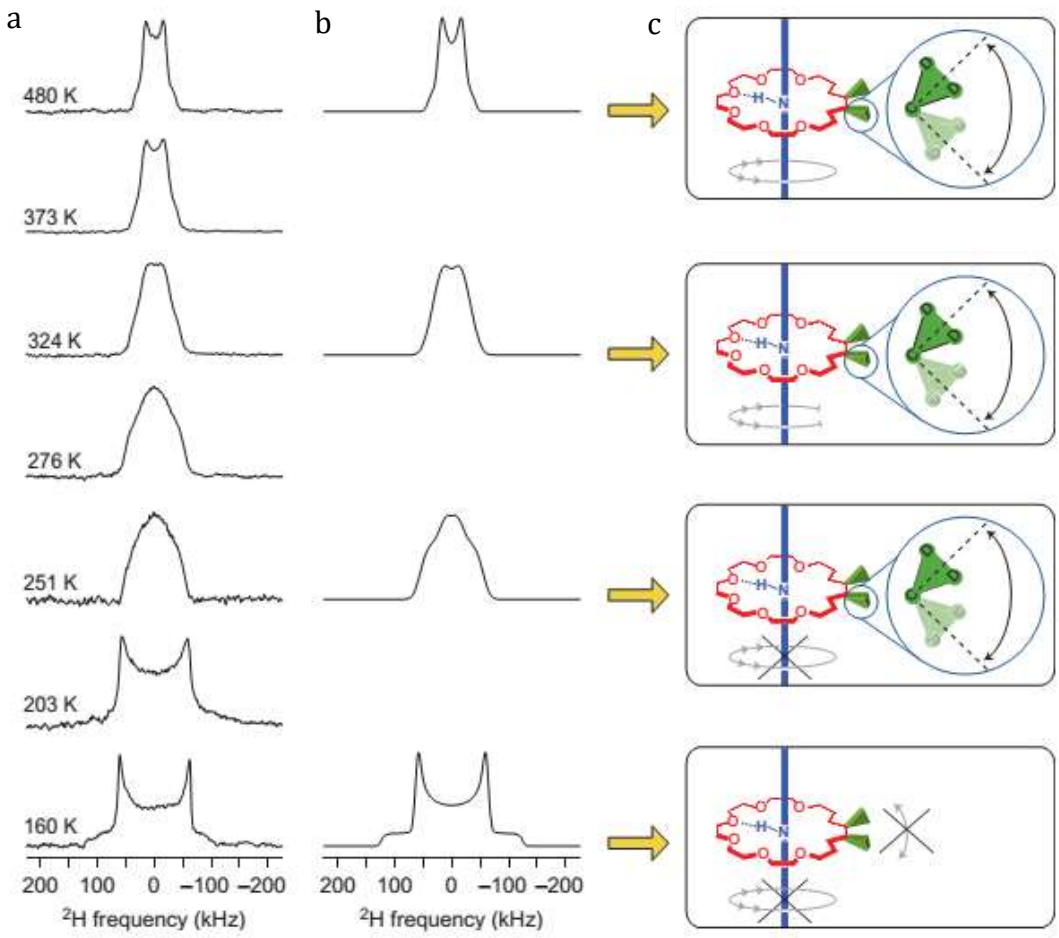

*Figure 1.13. (a) Experimental and (b) simulated ^{2}H SSNMR patterns were determined to identify the nature of the dynamic motions occurring inside activated **UWDM-1** at various temperatures. (c) schematic representations of the dynamic behaviour of the macrocycle inside the MOF. Reprinted with permission from ref 56.*

After successful ordering of a [2]rotaxane with a single recognition site and observation of rotational motion of the macrocyclic wheel in the solid state, Loeb and co-workers were focused to find out whether the translational motion of a macrocyclic component in a molecular shuttle could be transferred into the highly organized and dense material; to develop a MOF material with molecular shuttle linkers that can undergo translational motion in the highly organized and dense material. To this end, a tetra-carboxylic acid H-shaped [2]rotaxane linker with two identical benzimidazole recognition sites and a single [24]crown-8 ether, **24C8** was prepared (Scheme 1.9).[58]

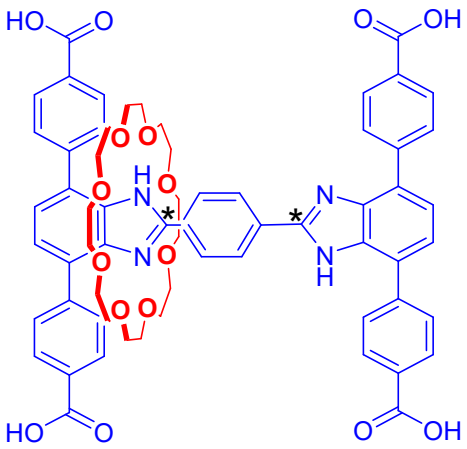

*Scheme 1.9. A neutral tetra-carboxylic acid H-shaped [2]rotaxane linker designed to exhibit shuttling motion of the **24C8** macrocycle inside the MOF.*[58]

The neutral [2]rotaxane linker was combined with $Zn(BF_4)_2.xH_2O$ in a 1:1:2 mixture of DMF/DMSO/EtOH with a drop of HBF_4 and heated at 85 °C for 48 h to yield a robust 3-D Zn-based MOF, in which each MIM linker is coordinated to four Zn_4O clusters. The as-synthesized material was described as **UWDM-4**-HBF_4 since single X-ray structure indicates the MIMs are in the mono-protonated state (Fig. 1.14a). The material consists of pseudo-interpenetrated cubic lattices in which the triphenyl struts form the sides of the cubes and the crossbars containing two benzimidazole recognition sites and a single [24]crown-8 ether (**24C8**) macrocycle connect the cubes (Fig. 1.14b). These repeating units assemble to make the whole framework with open channels (Fig. 1.14c). In **UWDM-4**-HBF_4, the wheels inside the MOF reside on the charged site due to much stronger non-covalent interactions. Thus, to observe shuttling of the macrocyclic wheel along the axle, the [2]rotaxane was neutralized using a proton sponge to produce **UWDM-4**. VT ^{13}C SSNMR spectra of an activated ^{13}C-enriched sample of **UWDM-4** were acquired to identify if the MIM could function as the molecular shuttle inside the MOF. The data analysis indicated that the macrocycle inside the MOF undergoes rapid shuttling between two recognition sites at high temperatures and slower shuttling when the sample is cooled.

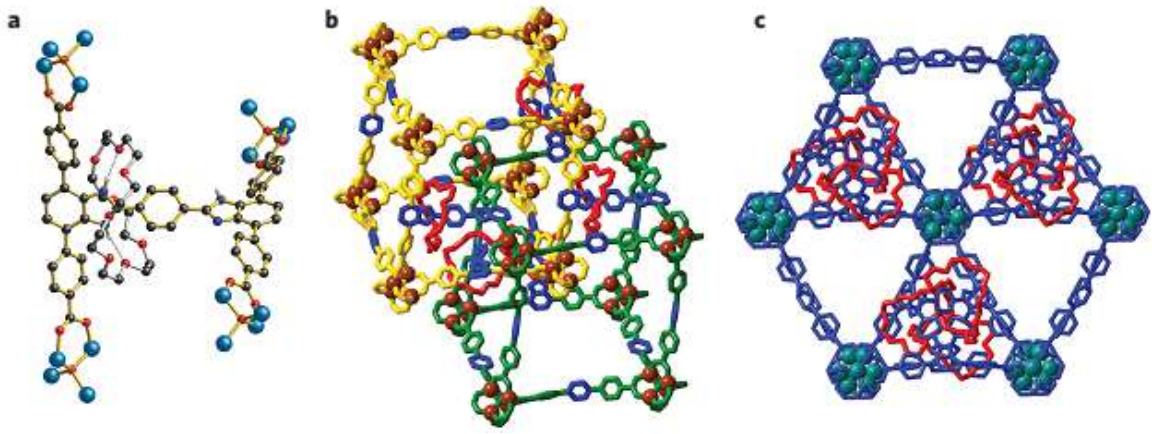

*Figure 1.14. The single X-ray structure of **UWDM-4**-HBF$_4$ indicating (a) the basic repeated unit showing the MIM is coordinated to four Zn$_4$O clusters (b) Two cubes of the lattice formed by the triphenyl struts (green and yellow) are linked by crossbars (axle in blue and wheel in red); only crossbars linking these two cubes are shown. (C) a view down the c-axis showing the open channels in which rings are separated from each other. Reprinted with permission from ref 58.*

Creation of such these solid-state materials that can exhibit rotational and translational motion are promising for the future development of molecular switches inside the condensed materials and eventually the ability of the materials to operate as molecular machines.

1.5 Scope of Dissertation

Although, it was proven that coupling of MIM ligands with the robust architecture of MOFs can produce materials that display robust dynamics, there is still need to develop dynamic materials that show switchable properties for eventual function as molecular machines. Design MIMs using new recognition motifs and the study of their dynamic properties both in solution and solid-state are important steps on the long path to the generation of solid-state nanoscale devices and molecular machines. The remaining chapters of this dissertation will describe how a *new* recognition motif was used to develop a molecular shuttle as well as rigid rotaxane linkers which could be incorporated into MOFs

to produce robust structures which show dynamic motion related to the wheel component in the solid state.

1.6 References

[1] b) J.-P. Sauvage, C. Dietrich-Buchecker, (eds) *Molecular Catenanes, Rotaxanes and Knots: A Journey Through the World of Molecular Topology*, Wiley-VCH, **1999**; b) G. A. Breault, C. A. Hunter, P. C. Mayers, *Tetrahedron*, **1999**, *55*, 5265; c) R. S. Forgan, J.-P. Sauvage, J. F. Stoddart, *Chem. Rev.,* **2011**, *111*, 5434; d) F. Aricó, J. D. Badjic, S. J. Cantrill, A. H. Flood, K–F. Leung, Y. Liu, J. F. Stoddart, *Top Curr Chem*., **2005**, *249*, 203.

[2] a) B. Hudson, J. Vinograd, *Nature*, **1967**, *216*, 647; b) D. A. Clayton, J. Vinograd, *Nature*, **1967**, *216*, 652.

[3] S. A. Wasserman, N. R. Cozzarelli, *Science* **1986**, *232*, 951.

[4] a) H. Wu, J. W. Lustbader, Y Liu, R. E. Canfield, W. A. Hendrickson, *Structure,* **1994**, 2, 545; b) N. L. Daly, D. J. Craik, *Curr. Opin. Chem. Biol.,* **2011**, *15*, 362; c) L.F. Liu, R.E. Depew, J.C. Wang, *J. Mol. Biol.* **1976**, *106*, 439; d) L. F. Liu, C. C. Liu, B. M. Alberts, *Cell*, **1980**, *19*, 697; E) J. R. Wagner, J. S. Brunzelle, K. T. Forest, R. D. Vierstra, *Nature*, **2005**, *438*, 325; f) D. Bölinger, J. I. Suzkowska, H. P. Hsu, L. A. Mirny, M. Kardar, J. N. Onuchic, P. Virnau, *PLoS Comput. Biol.,* **2010**, *6*, e1000731.

[5] a) V. Balzani, M. Gomez-Lopez, J. F. Stoddart, *Acc. Chem. Res.,* **1998**, *31*, 405; b) V. Balzani, A. Credi, F. M. Raymo, J. F. Stoddart, *Angew. Chem. Int. Ed*., **2000**, *39*, 3348; c) V. Balzani, A. Credi, B. Ferrer, S. Silvi, M. Venturi, *Top Curr. Chem.*, **2005**, *262*, 1; d) V. Balzani, *Pure Appl. Chem.,* **2008**, *80*, 1631; e) J. F. Stoddart, *Angew. Chem. Int. Ed.,* **2014**, *53*, 11102.

[6] a) F. M. Raymo, J. F. Stoddart, In: F. Diederich, P. J. Stang (eds) *Templated organic synthesis*, Wiley-VCH, Weinheim, **1999**; b) J. E. Beves, B. A. Blight, C. J. Campbell, D. A. Leigh, R. T.

McBurney, *Angew Chem. Int. Ed.,* **2011**, *50*, 9260; C) J. D. Crowley, S. M. Goldup, A.-L. Lee, D. A. Leigh, R. T. McBurney, *Chem. Soc. Rev.,* **2009**, *38*, 1530.

[7] a) D. B. Amabilino, J. F. Stoddart. *Chem. Rev.,* **1995**, *95*, 2725; b) T. J. Hubin, A. G. Kolchinski, A. L. Vance, D. H. Busch. *Adv. Supramol. Chem.,* **1999**, *6,* 237; c) S. J. Cantrill, A. R. Pease, J. F. Stoddart. *J. Chem. Soc., Dalton Trans.,* **2000**, 3715; d) K. E. Griffiths, J. F. Stoddart, *Pure Appl. Chem.,* **2008***, 80*, 485. e) V.N. Vukotic, S.J. Loeb, *Polyrotaxane Metal-Organic* Frameworks" *in: Metal-Organic Framework Materials*, John Wiley & Sons, Inc., New York, **2014**.

[8] a) J.-M. Lehn, *Supramolecular Chemistry: Concepts and perspectives*, VCH, Weinheim, **1995**; b) D. Philp, J. F. Stoddart. *Angew. Chem., Int. Ed. Engl.,* **1996**, *35*, 1154; c) J. W. Steed, J. L. Atwood, *Supramolecular Chemistry*, Wiley, New York, **2000**; d) S. J. Loeb, J. Tiburcio, S. J. Vella, J. A. Wisner, *Org. Biomol. Chem.*, **2006**, *4*, 667; e) Y. K. Agrawal, C. R. Sharma. *Rev. Anal. Chem.,* **2005**, *24*, 35.

[9] a) F. Aricó, J. D. Badjic, S. J. Cantrill, A. H. Flood, K. C.-F. Leung, Y. Liu, J. F. Stoddart, *Topics in Current Chemistry*, **2005**, *249*, 203; b) I. Yoon, M. Narita, T. Shimizu, M. Asakawa, *J. Am. Chem. Soc.,* **2004**, *126*, 16740; c) N. Kameta, K. Hiratani, Y. Nagawa, *Chem. Commun.,* **2004**, *51*, 466; d) M. Xue, Y. Yang, X. Chi, X. Yan, F. Huang, *Chem. Rev.,* **2015**, *115*, 7398.

[10] C. Reuter, W. Wienand, G. M. Hubner, C. Seel, F. Vögtle, *Chem. Eur. J.*, **1999**, *5*, 2692.

[11] J. Yin, S. Dasgupta, J. Wu, *Org. Lett.,* **2010**, *12*, 1712.

[12] a) M. R. Sambrook, P. D. Beer, J. A. Wisner, R. L. Paul, A. R. Cowley, F. Szemesa, M. B. G. Drew, *J. Am. Chem. Soc.*, **2005**, *127*, 2292; b) D. A. Leigh, M. A. F. Morales, E. M. Perez, J. K. Y. Wong, C. G. Saiz, A. M. Z. Slawin, A. J. Carmichael, D. M. Haddleton, A. M. Brouwer, W. J. Buma, G. W. H. Wurpel, S. Leon, F. Zerbetto, *Angew. Chem., Int. Ed.*, **2005**, *44*, 3062; c) S. J. Loeb, *Chem. Soc. Rev.,* **2007**, *36*, 226.

[13] a) E. A. Neal, S. M. Goldup, *Chem. Commun.,* **2014**, *50*, 5128; b) S. Erbas-Cakmak, D. A. Leigh, C. T. McTernan, A. L. Nussbaumer, *Chem. Rev.,* **2015**, *115*, 10081; c) E. R. Kay, D. A. Leigh, *Angew. Chem. Int. Ed.,* **2015**, *54*, 10080; d) A. Credi, S. Silvi, M. Venturi, (eds) *Molecular machines and motors, Top. Curr. Chem.*, **2014**, 1-342.

[14] E. R. Kay, D. A. Leigh, F. Zerbetto, Angew. *Chem., Int. Ed.,* **2007**, *46*, 72.

[15] a) R. Jahn, D. Fasshauer, *Nature,* **2012**, *490*, 201; b) M. Piccolino, *Nat. Rev. Mol. Cell Biol.* **2000**, *1*, 149; c) K. Kinbara, T. Aida, *Chem. Rev*., **2005**, *105*, 1377.

[16] a) M. Nakanishi-Matsui, M. Sekiya, R. K. Nakamoto, M. Futai, *Biochim. Biophys. Acta, Bioenerg.,* **2010**, *1797,* 1343; b) R. K. Nakamoto, J. A. B. Scanlon, M. K. Al-Shawi, *Arch. Biochem. Biophys.,* **2008**, *476*, 43. c) S. Hayashi, H. Ueno, A. R. Shaikh, M. Umemura, M. Kamiya, Y. Ito, M. Ikeguchi, Y. Komoriya, R. Iino, H. Noji, *J. Am. Chem. Soc.,* **2012**, *134*, 8447.

[17] G. J. E. Davidson, S. Sharma, S.J. Loeb, *Angew. Chem. Int. Ed.*, **2010**, *49*, 4938; b) L. Raehm, J. M. Kern, J.P. Sauvage, *Chem. A Eur. J.*, **1999**, *5*, 3310; c) N. D. Suhan, L. Allen, M. T. Gharib, E. Viljoen, S. J. Vella, S. J. Loeb, *Chem. Commun.*, **2011**, *47*, 5991; d) S. J. Loeb, J. Tiburcio, S. J. Vella, *Chem. Commun.*, **2006**, 1598.

[18] a) P. Linnartz, S. Bitter, C. A. Schalley, *Eur. J. Org. Chem.,* **2003**, 4819; b) M. Zhang, B. Zheng, F. Huang, *Chem. Commun*., **2011**, *47*, 10103; c) K.-D. Zhang, X. Zhao, G.-T. Wang, Y. Liu, Y. Zhang, H.-J. Lu, X.-K. Jiang, Z.-T. Li, *Tetrahedron,* **2012**, *68*, 4517; d) G. Yu, C. Han, Z. Zhang, J. Chen, X. Yan, B. Zheng, S. Liu, F. Huang, *J. Am. Chem. Soc.,* **2012**, *134*, 8711.

[19] a) S. Wenger, *J. Am. Chem. Soc.,* **2002**, *124*, 12786; b) S. I. Jun, J. W. Lee, S. Sakamoto, K. Yamaguchi, K. Kim, *Tetrahedron Lett*., **2000**, *41*, 471; c) V. Sindelar, S. Silvi, A. E. Kaifer, *Chem. Commun.,* **2006**, 2185; d) Sobransingh, D.; A. E. Kaifer, *Org. Lett.,* **2006**, *8*, 3247.

[20] a) M. Linke, J.-C. Chambron, V. Heitz, J.-P. Sauvage, V. Semetey*, Chem. Commun.,* **1998**, 2469; b) F. G. Gatti, S. Leon, J. K. Y. Wong, G. Bottari, A. Altieri, M. A. F. Morales, S. J. Teat, C. Frochot, D. A. Leigh, A. M. Brouwer, F. Zerbetto, *Proc. Natl. Acad. Sci. U.S.A.,* **2003**, *100*, 10.

[21] a) L. Jiang, J. Okano, A. Orita, J. Otera, *Angew. Chem., Int. Ed.,* **2004**, *43*, 2121; b) P. Ghosh, G. Federwisch, M. Kogej, C. A. Schalley, D. Haase, W. Saak, A.; Lutzen, R. M. Gschwind, *Org. Biomol. Chem.,* **2005**, *3*, 2691.

[22] P. R. Ashton, P. J. Campbell, P. T. Glink, D. Philp, N. Spencer, J. F. Stoddart, E. J. T. Chrystal, S. Menzer, D. J. Williams, P. A. Tasker, *Angew. Chem., Int. Ed. Engl.,* **1995**, *34*, 1865.

[23] a) D. B. Smithrud, E. M. Sanford, I. Chao, S. B. Ferguson, D. R. Carcanague, J. D. Evanseck, K. N. Houk, F. Diederich, *Pure Appl. Chem.,* **1990**, *62*, 2227; b) N. T. Southall, K. A. Dill, A. D. J. Haymet, *J. Phys. Chem. B*, **2002**, *106*, 521; c) C. Spickermann, T. Felder, C. A. Schalley, B. Kirchner, *Chem. -Eur. J.,* **2008**, *14*, 1216.

[24] P. R. Ashton, I. Baxter, M. C. T. Fyfe, F. M. Raymo, N. Spencer, J. F. Stoddart, A. J. P. White, D. J. Williams, *J. Am. Chem. Soc.,* **1998**, *120*, 2297; b) F. M. Raymo, K. N. Houk, J. F. Stoddart, *J. Am. Chem. Soc.,* **1998**, *120*, 9318.

[25] S. J. Vella, J. Tiburcio, J. W. Gauld, S. J. Loeb, *Org. Lett.,* **2006**, *8*, 3421.

[26] P. R. Ashton, V. Balzani, O. Kocian, L. Prodi, N. Spencer, J. F. Stoddart, *J. Am. Chem. Soc.,* **1998**, *120*, 11190.

[27] a) A. Martinez-Cuezva, A. Pastor, G. Cioncoloni, R.-A. Orenes, M. Alajarin, M. D. Symes, J. Berna, *Chem. Sci.,* **2015**, *6*, 3087; b) D. A. Leigh, P. J. Lusby, A. M. Z. Slawin, D. B. Walker, *Chem. Commun.,* **2012**, *48*, 5826; c) U. Letinois-Halbes, D. Hanss, J. M. Beierle, J.-P. Collin, J.-P. A. Sauvage, *Org. Lett.,* **2005**, *7*, 5753; d) Y. Nakatani, Y. Furusho, E. Yashima, *Angew. Chem., Int. Ed.,* **2010**, *49*, 5463.

[28] V. Bermudez, N. Capron, T. Gase, F. G. Gatti, F. Kajzar, D. A. Leigh, F. Zerbetto, S. Zhang, *Nature,* **2000**, *406*, 608.

[29] F. G. Gatti, S. Leon, J. K. Y. Wong, G. Bottari, A. Altieri, M. A. F. Morales, S. J. Teat, C. Frochot, D. A. Leigh, A. M. Brouwer, F. Zerbetto, *Proc. Natl. Acad. Sci. U.S.A.,* **2003**, *100*, 10.

[30] M. R. Panman, B. H. Bakker, D. d. Uyl, E. R. Kay, D. A. Leigh, W. J. Buma, A. M. Brouwer1, J. A. J. Geenevasen, S. Woutersen, *Nature Chem.*, **2013**, *5*, 913.

[31] a) A. Coskun, D. C. Friedman, H. Li, K. Patel, H. A. Khatib, J. F. Stoddart, *J. Am. Chem. Soc.*, **2009**, *131*, 2493; b) I. Yoon, et al., *Chem. A Eur. J.*, **2009**, *15*, 1115; c) L. Jiang, J. Okano, A. Orita, J. Otera, *Angew. Chem., Int. Ed.,* **2004**, *43*, 2121.

[32] a) R. A. Bissell, E. Cordova, A. E. Kaifer, J. F. Stoddart, *Nature,* **1994**, *369*, 133. b) M. J. Barrell, D. A. Leigh, P. J. Lusby, A. M. Z. Slawin, *Angew. Chem., Int. Ed.,* **2008**, *47*, 8036; c) A. Coskun, M. Banaszak, R. D. Astumian, J. F. Stoddart, B. A. Grzybowski, *Chem. Soc. Rev.,* **2012**, *41*, 19.

[33] P.-L. Anelli, N. Spencer, J. F. Stoddart, *J. Am. Chem. Soc.,* **1991**, *113*, 5131.

[34] D. Sobransingh, A. E. Kaifer, *Org. Lett.,* **2006**, *8*, 3247; b) X. Ma, Q. Wang, D. Qu, Y. Xu, F. Ji, H. Tian, *Adv. Funct. Mater.,* **2007**, *17*, 829.

[35] S. I. Jun, J. W. Lee, S. Sakamoto, K. Yamaguchi, K. Kim, *Tetrahedron Lett.,* **2000**, *41*, 471.

[36] a) J. O. Jeppesen, S. A. Vignon, J. F. Stoddart, *Chem. Eur. J.,* **2003**, *9*, 4611; b) V. Balzani, A. Credi, M. Venturi, *Chem. Soc. Rev*., **2009**, *38*, 1542; c) H. X. Deng, M. A. Olson, J. F. Stoddart, O. M. Yaghi, *Nature Chem*., **2010**, *2,* 439.

[37] a) M. Clemente-León, A. Credi, M. V. Martinez-Diaz, C. Mingotaud, J. F. Stoddart, *Adv. Mater*., **2006**, *18*, 1291; b) W. D. Zhou, J. L. Xu, H. Y. Zheng, X. D. Yin, Z. C. Zuo, H. B. Liu, Y. L. Li, *Adv. Funct. Mater.,* **2009**, *19*, 141.

[38] N. Noujeim, K. Zhu, V. N. Vukotic, S. J. Loeb, *Org. Lett.,* **2012**, *14*, 2484.

[39] a) K. Zhu, V. N. Vukotic, S. J. Loeb, *Angew. Chem. Int. Ed*., **2012**, *51*, 2168; b) K. Zhu, V. N. Vukotic, N. Noujeim, S. J. Loeb, *Chem. Sci.,* **2012**, *3*, 3265.

[40] V. Blanco, A. Carlone, K. D. Hänni, D. A. Leigh, B. Lewandowski, *Angew. Chem. Int. Ed.,* **2012**, *51*, 5166.

[41] B. Lewandowski, G. De Bo, J. W. Ward, M. Papmeyer, S. Kuschel, M. J. Aldegunde, P. M. E. Gramlich, D. Heckmann, S.M. Goldup, D.M. D'Souza, A.E. Fernandes, D.A. Leigh, *Science*, **2013**, *339*, 189.

[42] a) B. Long, K. Nikitin, D. Fitzmaurice, *J. Am. Chem. Soc.,* **2003**, 125, 15490; b) K. Nikitin, D. Fitzmaurice, *J. Am. Chem. Soc.,* **2005**, *127*, 8067; c) C. S. Vogelsberg, M. A. Garcia-Garibay, *Chem. Soc. Rev.,* **2012**, *41*, 1892;

[43] S. Angelos, Y.W. Yang, K. Patel, J.F. Stoddart, J.I. Zink, Angew. *Chem., Int. Ed.,* **2008,** *47*, 2222; b) Weiss, J. Coord. *Chem. Rev.,* **2010**, *254*, 2247; c) Y. Liu, A. H. Flood, P. A. Bonvallett, S. A. Vignon, B. H. Northrop, H. R. Tseng, J. O. Jeppesen, T. J. Huang, B. Brough, M. Baller, S. Magonov, S. D. Solares, W. A. Goddard, C. M. Ho, J. F. Stoddart, *J. Am. Chem. Soc.,* **2005**, *127*, 9745; d) M. Cavallini, F. Biscarini, S. Leon, F. Zerbetto, G. Bottari, D. A. Leigh, *Science*, **2003**, *299*, 531.

[44] K. K. Cotí, M. E. Belowich, M. Liong, M. W. Ambrogio, Y. A. Lau,H. A. Khatib,ac J. I. Zink, N. M. Khashab, J. F. Stoddart, *Nanoscale*, **2009**, *1*, 16.

[45] a) D. A. Leigh, M. A. Morales, E. M. Perez, J. K. Wong, C. G. Saiz, A. M. Slawin, A. J. Carmichael, D. M. Haddleton, A. M. Brouwer, W. J. Buma, G. W. Wurpel, S. Leon, F. Zerbetto, *Angew. Chem., Int. Ed.,* **2005**, *44*, 3062; b) Q. Li, G. Fuks, E. Moulin, M. Maaloum, M. Rawiso, I. Kulic, J. T. Foy, N. Giuseppone, *Nat. Nanotechnol.,* **2015**, *10*, 161; c) E. Katz, O. Lioubashevsky, I. Willner, *J. Am. Chem. Soc.,* **2004**, *126*, 15520.

[46] J. Berna, D. A. Leigh, M. Lubomska, S. M. Mendoza, E. M. Perez, P. Rudolf, G. Teobaldi, F. Zerbetto, Nat. Mater., **2005**, *4*, 704.

[47] a) H. Furukawa, N. Ko, Y. B. Go, N. Aratani, S. B. Choi, E. Choi, A. O. Yazaydin, R. Q. Snurr, M. O'Keeffe, J. Kim, O. M. Yaghi, *Science*, **2010**, *329*, 424; b) M. Eddaoudi, J. Kim, N. Rosi, D. Vodak, J. Wachter, M. O'Keeffe, O. M. Yaghi, *Science*, **2002**, *295*, 469; c) P. Nugent, Y. Belmabkhout, S. D. Burd, A. J. Cairns, R. Luebke, K. Forrest, T. Pham, S. Ma, B. Space, L. Wojtas,

M. Eddaoudi, M. J. Zaworotki, *Nature*, **2013**, *495*, 80; d) J. J. Perry, J. A. Perman, M. J. Zaworotko, *Chem. Soc. Rev.*, **2009**, *38*, 1400.

[48] a) R. J. Kuppler, D. J. Timmonsb, Q.-R. Fanga, J.-R. Lia, T. A. Makala, M. D. Younga, D. Yuana, D. Zhaoa, W. Zhuanga, H.-C. Zhoua, *Coordin. Chem. Rev.*, **2009**, *253*, 3042. b) J. R. Li, J. Sculley, H. C. Zhou, *Chem. Rev.*, **2012**, *112*, 869; c) L. E. Kreno, J. T. Hupp, R. P. Van Duyne, *Analytical Chemistry*, **2010**, *82*, 8042; d) R. Ricco, L. Malfatti, M. Takahashi, A. J. Hillad, P. Falcaro, *J. Mater. Chem. A,* **2013**, *1*, 13033 e) O. K. Farha, J. T. Hupp, *ACC. Chem. Res.*, **2010**, *43*, 1166; f) R. Ananthoji, J. F. Eubank, F. Nouar, H. Mouttaki, M. Eddaoudi, J. P. Harmon, *J. Mater. Chem.*, **2011**, *21*, 9587.

[49] O. M. Yaghi, G. Li, H. Li, *Nature*, **1995**, *378*, 703.

[50] a) S. J. Loeb, *Chem. Commun*., **2005**, 1511 b) V. N. Vukotic, S. J. Loeb, **2012**, *Chem. Soc. Rev*., *41*, 5896.

[51] a) W. D. Zhou, J. L. Xu, H. Y. Zheng, X. D. Yin, Z. C. Zuo, H. B. Liu, Y. L. Li, *Adv. Funct. Mater.,* **2009**, *19*, 14; b) Y. Kohsaka, K. Nakazono, Y. Koyama, S. Asai, T. Takata, *Angew. Int. Ed.,* **2011**, *50*, 4872; c) Frampton M. J., Anderson H. L., Angew. *Chem. Int. Ed.,* **2007**, *46*, 1028; d) M. Horie, T. Sassa, D. Hashizume, Y. Suzaki, K. Osakada, T. Wada, Angew. *Chem. Int. Ed.,* **2007**, *46*, 4983; e) U. Rauwald, J. d. Barrio, X. J. Loh, O. A. Scherman, *Chem. Commun.,* **2011**, *47*, 6000.

[52] S. J. Loeb, *Chem. Commun.,* **2005**, 1511;

[53] V. N. Vukotic, S. J. Loeb, *Chem. Soc. Rev.,* **2012,** *41*, 5896.

[54] H. Deng, M. A. Olson, J. F. Stoddart, O. M. Yaghi, *Nature Chem.,* **2010**, *2*, 439.

[55] a) K. Kim, *Chem. Soc. Rev.,* **2002**, *31*, 96; b) K. Zhu, S. J. Loeb, *Top. Curr. Chem.,* **2014**, *354*, 213.

[56] V. N. Vukotic, K. J. Harris, K. Zhu, R. W. Schurko S. J. Loeb, *Nature Chem.,* **2012**, *4*, 456.

[57] V. N. Vukotic, C. A. O'Keefe, K. Zhu, K. J. Harris, C. To, R. W. Schurko, S. J. Loeb, *J. Am. Chem. Soc.,* **2015**, *137*, 9643.

[58] K. Zhu, K. J. Harris, V. N. Vukotic, R. W. Schurko S. J. Loeb, *Nature Chem.,* **2015**, *7*, 514.

CHAPTER 2

2.1 [2]Pseudorotaxane Formation Between Rigid Y-shaped 2,4,5-Triphenylimidazolium Axles and [24]Crown-8 Ether Wheels

2.1.1 Introduction

The efficient host-guest interaction between electron-rich macrocyclic wheels and charged, electron-poor axles allows for the formation of [2]pseudorotaxanes and these interpenetrated species are essential precursors for the synthesis of permanently interlocked [2]rotaxanes via the threading-followed-by-stoppering protocol.[1] Therefore, the development of new templating motifs for [2]pseudorotaxane formation and the detailed study of their structure are of paramount importance for the development of new types of mechanically interlocked molecules (MIMs) and their eventual application in molecular systems as switches or machines.[2]

As part of our efforts to prepare rigid and compact MIMs for inclusion in metal-organic framework (MOF) materials,[3] we recently completed an in-depth study on the formation of [2]pseudorotaxanes utilizing T-shaped 2,4,7-triphenyl substituted benzimidazolium cations as the axles and various 24 membered crown ethers as the wheels.[4] It was shown that, although the interaction of dibenzo[24]crown-8 (**DB24C8**) with either the imidazolium[5] (Ka = 8 M^{-1}) or phenylbenzimidazolium[6] (K_a = 54 M^{-1}) cation is quite weak, the extra phenyl substituents on the T-shaped cations had a dramatic effect, raising the association constant by several orders of magnitude compared to those found for simple imidazolium or benzimidazolium derivatives (*e.g.*, 1.78 x 10^3 M^{-1} for the parent T-shaped axle with $R_1 = R_2 = H$).[4]

Although the 2,4,7-triphenylbenzimidazolium cations provide an excellent core for constructing rigid MIMs, such as [2]rotaxane molecule shuttles,[6] it was still of interest to

develop other [2]pseudorotaxane systems that could be used in combination with these new T-shaped axles. As part of this continuing efforts, we report herein the use of rigid, Y-shaped 2,4,5-triphenylimidazolium axles for the formation of [2]pseudorotaxanes with [24]crown-8 (**24C8**) and **DB24C8** and a comparison of these two systems; T- and Y-shaped. It should be noted that Tiburcio[7] Clarkson[8] and Gibson[9] have reported that when imidazolium groups are linked by alkyl chains the association constant can be effectively increased for interactions with crown ethers and cryptands but this type of flexible axle was not suitable for our purposes.

2.1.2 Results and Discussion

Synthesis of a series of Y-shaped axles ([**1a**]$^+$ - [**1e**]$^+$) was accomplished as outlined in Scheme 2.1. Either an electron-donating OMe group or an electron-withdrawing COOMe group was installed at the 2-position (R_1) or the 4- and 5-position (R_2) on the imidazole ring. The key step in the synthesis of these axles was the condensation between a 4-substituted aldehyde containing R_1 and a 4,4'-substituted benzil unit containing R_2 groups in the presence of ammonium acetate.[10] Axle [**2**]$^+$ was included to determine the effect of fusing the phenyl groups at the 4- and 5-positions.[11]

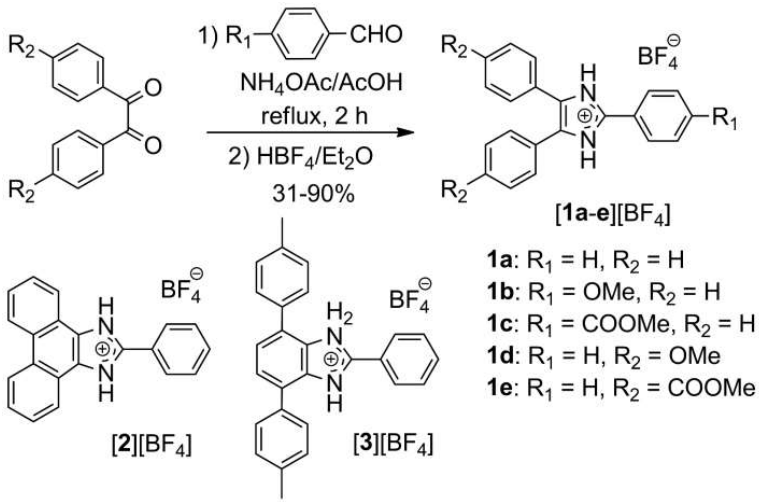

Scheme 2.1. Synthesis of 2,4,5-triphenylimidazolium axles.

The formation of [2]pseudorotaxanes from axles ([**1a**]$^+$-[**1e**]$^+$ and [**2**]$^+$ and macrocyclic wheels **24C8** and **DB24C8** were monitored by ^{1}H NMR spectroscopy in CD_3CN solution at 298 K. A 1:1 binding stoichiometry was determined for all combinations of axle and wheel as evidenced by integration of complexed and uncomplexed peaks in the ^{1}H NMR spectra (see experimental 2.2.4). Exchange between complexed and uncomplexed components was slow on the NMR timescale and association constant (K_a) values were determined using the single-point method from solutions containing equimolar amounts of axle and wheel at concentrations of 1.0 x 10^{-2} M.[12] The results of this study are summarized in Table 2.1.

Table 2.1. Association constants[a] for [2]pseudorotaxane formation showing the effect of axle substitution.

Y-Shaped Axle			Association Constant, K_a (M^{-1} x 10^{-2})[b]	
	R_1	R_2	**DB24C8**	**24C8**
[**1a**]$^+$	H	H	3.0	4.6
[**1b**]$^+$	OMe	H	2.8	3.8
[**1c**]$^+$	COOMe	H	5.6	8.0
[**1d**]$^+$	H	OMe	1.9	3.5
[**1e**]$^+$	H	COOMe	5.1	8.7
[**2**]$^+$	H	H	1.1	5.7

[a] Measured using ^{1}H NMR spectroscopy (CD_3CN, 1.0 x 10^{-2} M, 298 K). [b]Errors are estimated to be less than 10%. Ion pairing was assumed to be negligible in CD_3CN as measurements at different concentrations for [**1c⊂DB24C8**]$^+$ were within experimental error.[13]

As an illustration of the formation of [2]pseudorotaxanes under these experimental conditions, Fig. 2.1 shows ^{1}H NMR spectra for the Y-shaped axle [**1c**]$^+$ with an electron-withdrawing ester function at the 2-position, the macrocyclic wheel **DB24C8** and the [2]pseudorotaxane [**1c⊂DB24C8**]$^+$. Variations in chemical shift upon mixing axle and wheel clearly demonstrate the interpenetrated nature of the host-guest interaction. The most significant chemical shifts upon complexation are to higher frequency for the *NH* and *c* resonances on the axle, indicative of significant NH···O hydrogen-bonding and accompanying CH···O interactions between axle and wheel. Shifts to lower frequency for aromatic protons *d, e* and *f* on the axle and *g* and *h* on the wheel also occur due to π-stacking interactions between the somewhat electron poor phenyl rings attached to the imidazolium ring and the electron rich catechol rings of **DB24C8**. Similar shifts to higher frequency for *NH* and *c* resonances are observed for [2]pseudorotaxanes formed with **24C8** but changes to the aromatic protons *d, e* and *f* on the axle are minimal, consistent with the lack of π-stacking interactions in these species.

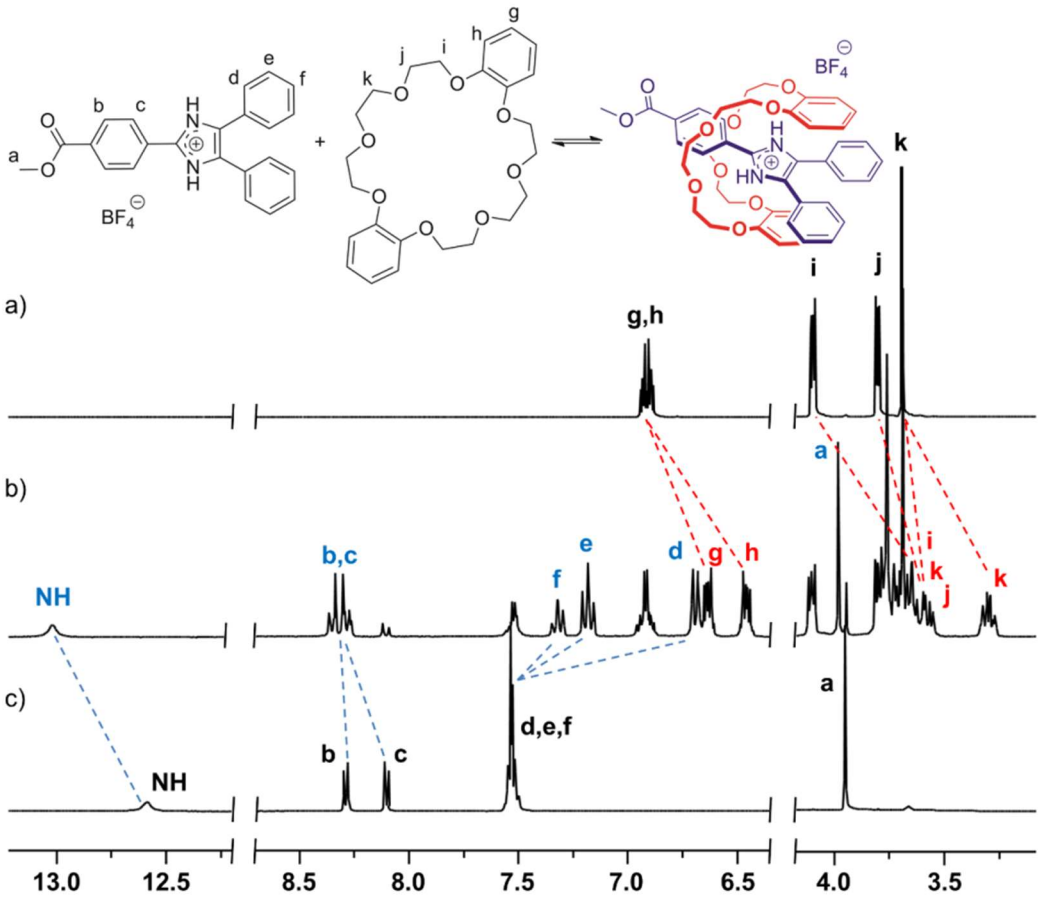

Figure 2.1. ^{1}H NMR spectra (500 MHz, CD_3CN) of: a) ***DB24C8****, b) equimolar amounts axle* ***[1c]***$^+$ *and wheel* ***DB24C8*** *at a concentration of 1.0 x 10^{-2} M demonstrating formation of [2]pseudorotaxane* ***[1c⊂DB24C8]***$^+$*, c) axle* ***[1c]***$^+$*.*

When either R_1 or R_2 is an electron-withdrawing ester group, the hydrogen-bonding, ion-dipole, and π-stacking interactions are all strengthened due to an increase in acidity of hydrogen bond donors and an increase in charge on the imidazolium rings. Conversely, the presence of an electron-donating OMe group lowers the association constant by weakening these same interactions. The effect is more pronounced for R_1 because substitution at the 2-position results in a more direct effect on the imidazolium moiety. Van't Hoff plots for **[1a⊂24C8]**$^+$ and **[1a⊂DB24C8]**$^+$ showed that the interaction between axle and wheel is primarily enthalpically driven[14] (see experimental section 2.2) similar to our T-shaped

system and consistent with the use of a rigid axle with limited degrees of motion. Hammett plots[15] for both crown ether wheels as a function of R_1 and R_2 were linear and support the straightforward effect of added EDG/EWG substituents on hydrogen-bonding as described, albeit for a limited set of data encompassing only H, OMe and COOMe groups (see section 2.2.7). Axle [**2**]$^+$, which is analogous to [**1a**]$^+$ but contains a fused ring system, shows a marked decrease in association constant with **DB24C8** when compared to [**1a**]$^+$. This is presumably the result of eliminating the supporting CH···O and π-stacking interactions that the freely rotating phenyl substituents present in axles [**1a**]$^+$ - [**1e**]$^+$, producing a K_a value closer to that observed for a simple unsubstituted benzimidazolium cation. This decrease does not occur for **24C8** because that interaction is driven almost exclusively by significant NH$^+$···O bonding.

The single-crystal X-ray structure* of [2]pseudorotaxane [**1c⊂DB24C8**][BF_4] (R_1 = COOMe, R_2 = H) is shown in Fig. 2.2; only one of the two identical molecules in the asymmetric unit is shown.[16,17] There are three hydrogen-bonding type interactions between axle and wheel; two significant charge-assisted NH···O hydrogen bonds (average; 2.87 Å, 177°) and two sets of much weaker, but directional, CH···O interactions (average 3.89 Å, 153°) to the COOMe-Ph ring (average; 4.18 Å, 150°). This hydrogen-bonding array is accompanied by significant ion-dipole interactions between the cationic charge on the imidazolium ring and the crown ether oxygen atoms. The NH···O and CH···O interactions to the COOMe-Ph ring are consistent with shifts observed for the *NH* and *c* protons in solution by ^{1}H NMR spectroscopy. Some degree of π -stacking can be inferred from the close approach of the aromatic rings from the phenyl groups at the 4- and 5-positions on the imidazolium unit with the electron-rich

* Synthetic experiment details for all new compounds, ^{1}H and ^{13}C NMR spectra, NOESY spectra, van't Hoff and Hammet plots are available in section 2.2 of this chapter. Crystallographic data for the X-ray structure reported in this chapter has been deposited with the Cambridge Crystallographic Data Centre as supplementary publication no. 990746.

catechol rings of **DB24C8** (*i.e.*, average; 3.53 Å between the phenyl *ipso* carbons and an O-bound aromatic carbon of **DB24C8**).[12]

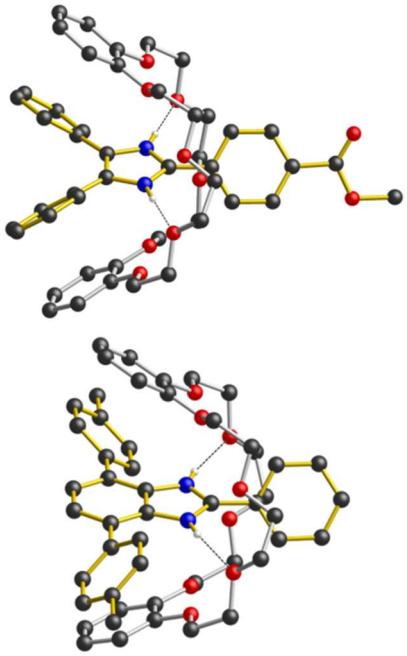

*Figure 2.2. Ball-and-stick representations of the cationic portions of the single-crystal X-ray structures of [2]pseudorotaxanes [**1c**⊂**DB24C8**)][BF_4] (top) and [**3**⊂**DB24C8**)][BF_4] (bottom). The N-bonded H-atoms involved in hydrogen-bonding are shown but all others are omitted for clarity.*

A direct comparison can be made between the results of [2]pseudorotaxane formation obtained in this study utilizing these new Y-shaped axles and our recent investigation[4] into analogous T-shaped axles, also with **24C8** and **DB24C8**. Fig. 2.3 shows a plot of association constant for [2]pseudorotaxane formation as a function of axle structure (T-shaped versus Y shaped) and crown ether type (**24C8** or **DB24C8**).

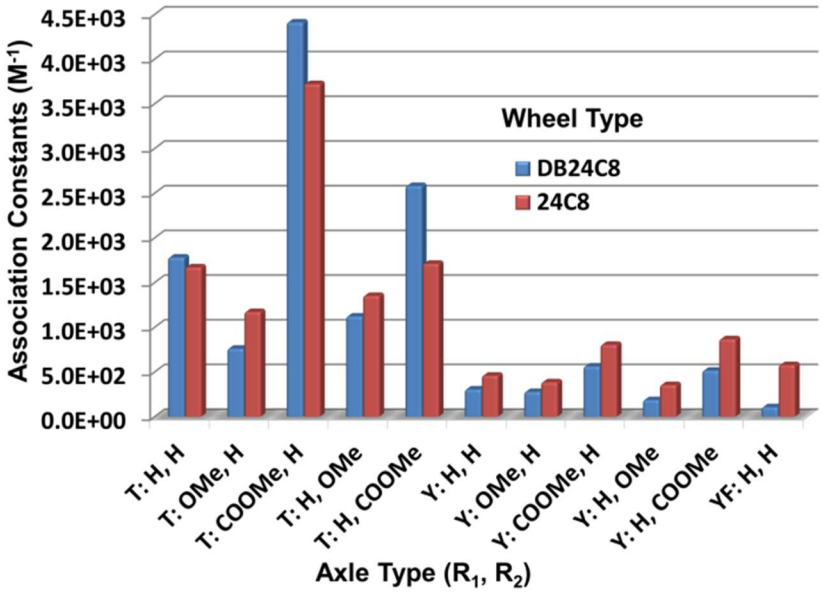

Figure 2.3. A plot of association constant for [2]pseudorotaxane formation as a function of axle shape (T versus Y, YF = Y-shaped with fused ring system) and crown ether wheel. All K_a values were determined by ^{1}H NMR spectroscopy (500 MHz) in CD_3CN solution at 298 K. Values for the T-shaped axles were taken from reference 4.

Although it is clear that the T-shaped axle produced [2]pseudorotaxanes that are more favorable, it is important to note that the association constants obtained herein for the Y shaped system are not weak as they are comparable to the ubiquitous secondary ammonium axles pioneered by Stoddart and used in a wide variety of MIM applications with crown ethers.[18] Fig. 2.4 summarizes the variation in templating ability for a range of imidazolium and benzimidazolium axles studied to date and qualitatively illustrates the relationship between structure and efficiency of [2]pseudorotaxane formation in these systems.

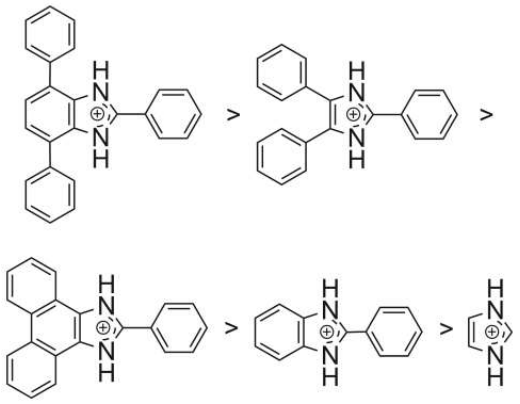

Figure 2.4. Qualitative ranking of imidazolium and benzimidazolium axles in order of their ability to form interpenetrated [2]pseudorotaxane structures with the 24-membered crown ether ***DB24C8****.*

2.1.3 Conclusions

Both the T- and Y-shaped systems have characteristics which are inherently unique: 1) a moderate (Y shaped) to strong (T-shape) association between axle and crown ether wheel due to the rigid shape of the axle cation, 2) a modular synthesis which allows for the incorporation of a wide variety of functionalized aromatics onto the molecular scaffold utilizing commercially available materials with well-established coupling methodologies and 3) the potential to easily incorporate this new template into MIMs by incorporating the appropriate functional group at R_1 for condensation, olefin metathesis or cross-coupling reactions. Indeed, the difference in association constants between the T and Y-shaped axles offers the possibility of utilizing both of these templating motifs in a single system where recognition sites with different binding strengths could potentially be utilized to produce switching phenomena. The ultimate goal for these new templating motifs with rigid cores is to develop versions that can act as efficient MIM linkers for MOF formation. This could be achieved by incorporation of metal binding groups at the R_1 position for either the T- or Y-shaped template; this work is in progress.

2.2 Experimental

2.2.1 General Comments

4,4′-Bis(methyloxycarbonyl)benzil was synthesized according to literature procedures.[19] All association constant (K_a) values were determined using the single point method.[20] All chemicals were obtained from Sigma-Aldrich and used without further purification. The solvents were dried using an Innovative Technologies Solvent Purification System. ^{1}H, ^{13}C and 2D NMR spectra were recorded on a Brüker Avance 500 instrument. High resolution mass spectra (HR-MS) were performed on a Micromass LCT electrospray ionization (ESI) time-of-flight (ToF) spectrometer. Melting points were recorded on a Stanford Research Systems, Opti Melt MPA100 instrument. FT-IR spectra (4000 – 400 cm^{-1}) were measured as thin films on a Bruker Alpha FT-IR instrument equipped with a Platinum single reflection diamond ATR module. The single crystal X-ray data were collected on a Bruker D8 Venture dual source diffractometer with a Photon 100 detector operated at 50 kV and 30 mA using $Cu_{K\alpha}$ radiation. Crystallographic data for the X-ray structure have been deposited with the Cambridge Crystallographic Data Center as supplementary publication no. 990746. Copies of the data can be obtained free of charge on application to CCDC at email: deposit@ccdc.cam.ac.uk.

2.2.2 Procedure for the Synthesis of 2,4,5-triphenylimidazolium salts [1a-1e][BF_4]

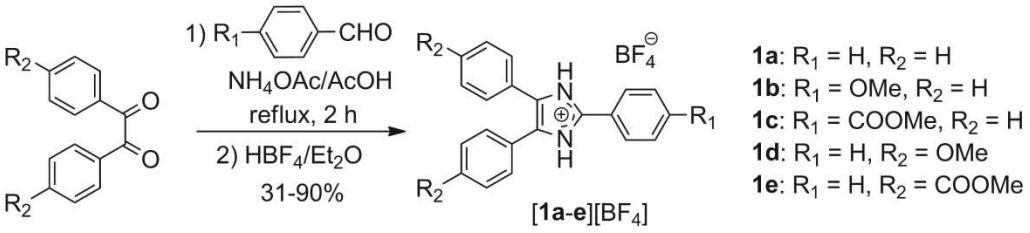

*Scheme 2.2. Procedure for the synthesis of 2,4,5-triphenylimidazolium salts [**1a-1e**][BF_4].*

The corresponding 4,4' substituted benzil (2.38 mmol, 1 eq.), *p*-substituted benzaldehyde (2.83 mmol, 1 eq.) and ammonium acetate (35.7 mmol, 15 eq.) were dissolved in acetic acid (9 mL). The reaction mixture was heated to 100 °C and stirred for 2 h. It was then cooled and neutralized with NH_4OAc and water (4 mL). The resulting solid was filtered, washed with water and dried under vacuum. The pure 2,4,5-triphenylimidazole was dissolved in a minimum amount of THF (7 mL) and tetrafluoroboric acid - diethyl ether complex (2.38 mmol, 1 eq.) was added. The mixture was stirred for 10 min and of diethyl ether (10 mL) was added. The resulting solid precipitated from solution and was collected by filtration, washed with ether and air dried.

[1a][BF_4]: (R_1 = R_2 = H, Yield 88 %): MP 172-174 °C (dec). ^{1}H NMR (CD_3NO_2, 500 MHz, 293 K): δ (ppm) = 12.51 (s, 2H), 8.05 (d, 2H, *J* = 7.0 Hz) 7.75-7.68 (m, 3H), 7.58 (d, 4H, *J* = 7.5 Hz), 7.52-7.47 (m, 6H);^{13}C NMR (CD_3CN, 125 MHz, 294 K): δ (ppm) = 140.5, 128.7, 125.9, 125.8, 125.7, 125.1, 124.3, 122.9, 122.7, 118.6; IR (neat) = 3209, 1647, 1598, 1491, 1467, 1445, 1324, 1280, 1201, 996, 776, 764, 695, 597, 517, 502 cm^{-1}; HR-MS (ESI-ToF) *m/z* found: 297.1404 $[M+H]^+$, $[C_{21}H_{17}N_2]^+$, calc: 297.1392.

[1b][BF_4]: (R_1 = OMe, R_1 = H, Yield 89 %): MP 260-264 °C (dec). ^{1}H NMR (CD_3NO_2, 500 MHz, 294 K): δ (ppm) = 12.32 (s, 2H), 8.01 (d, 2H, *J* = 9.0 Hz), 7.56 (d, 4H, *J* = 7.5 Hz), 7.51-7.46 (m, 6H), 7.20 (d, 2H, *J*=9.0 Hz), 3.91 (s, 3H); ^{13}C NMR (CD_3NO_2, 125 MHz, 295 K): δ (ppm) = 159.6, 140.6, 126.1, 125.2, 124.9, 124.8, 124.3, 122.5, 111.2, 109.9, 51.2; IR (neat): 3303, 1645, 1610, 1506, 1443, 1303, 1266, 1189, 1026, 989, 958, 834, 770, 735, 692, 511 cm^{-1}; HR-MS (ESI-ToF) *m/z* found: 327.1496 $[M+H]^+$, $[C_{22}H_{19}N_2O]^+$, calc: 327.1497.

[1c][BF_4]: (R_1 = COOMe, R_2 = H, Yield 95 %): MP 272-275 °C (dec). ^{1}H NMR (CD_3NO_2, 500 MHz, 295 K): δ (ppm) = 12.97 (s, 2H), 8.26 (d, 2H, *J* = 8.5 Hz), 8.16 (d, 2H, *J* = 8.5 Hz), 7.59(d, 4H, *J* = 8.0 Hz), 7.54-7.47 (m, 6H), 3.94 (s, 3H). ^{13}C NMR (CD_3NO_2, 125 MHz, 295 K): δ (ppm)

= 161.8, 139.2, 129.9, 126.4, 126.3, 126.1, 125.2, 124.4, 123.1, 122.2, 121.7, 48.0; IR (neat) = 3275, 1720, 1651, 1430, 1277, 1015, 862, 765, 722, 699, 520 cm^{-1}; HR-MS *m/z* found: 355.1453 $[M+H]^+$, $[C_{23}H_{19}N_2O_2]^+$, calc: 355.1447.

[1d][BF_4]: (R_1 = H, R_2 = OMe, Yield 85 %): MP 255-258 °C (dec). ^1H NMR (CD_3NO_2, 500 MHz, 294 K): δ (ppm) 12.19 (s, 2H), 8.01 (d, 2H, *J* = 7.0 Hz), 7.73-7.66 (m, 3H), 7.50 (d, 4H, *J* = 9.0 Hz), 7.02 (d, 4H, *J* = 9.0 Hz), 3.84 (s, 6H); ^{13}C NMR (CD_3NO_2, 125 MHz, 295 K): δ (ppm) = 157.0, 139.7, 128.9, 125.8 (2 peaks), 124.8, 122.8, 118.0, 114.6, 110.5, 50.8; IR (neat) = 3238, 1648, 1613, 1503, 1301, 1254, 1182, 1031, 836, 804, 777, 701, 689, 584, 533, 500, 417 cm^{-1}; HR-MS (ESI-ToF) *m/z* found: 357.1604 $[M+H]^+$, $[C_{23}H_{21}N_2O_2]^+$, calc: 357.1603.

[1e][BF_4]: (R_1 = H, R_2 = COOMe, Yield 31%): MP 285-289 °C (dec). ^1H NMR (CD_3NO_2, 500 MHz, 295 K): δ (ppm) = 12.86 (s, 2H), 8.09-8.06 (m, 6H), 7.77-7.69 (m, 7H), 3.91 (s, 6H); ^{13}C NMR (DMSO, 125 MHz, 294 K): δ (ppm) =165.9, 145.3, 132.3, 132.2, 130.4, 130.0, 129.7, 129.6, 129.2, 127.6, 123.8, 52.6; IR (neat) = 3197,2953, 1714, 1645, 1611, 1436, 1279, 1196, 1113, 1059, 987, 955, 863, 777, 721, 702, 684 cm^{-1}; HR-MS (ESI-ToF) *m/z* found: 413.1521 $[M+H]^+$, $[C_{25}H_{20}N_2O_4]^+$, calc: 413.1501.

2.2.3. 2-Phenyl-1H-phenanthro[9,10-d]imidazolium salt [2][BF_4]

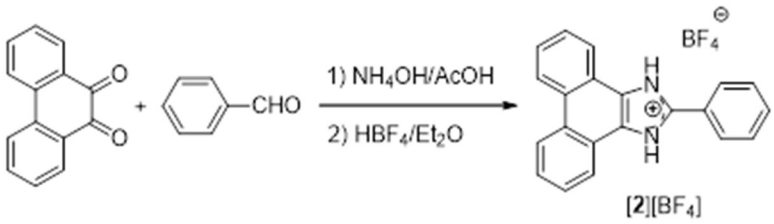

*Scheme 2.3. 2-Phenyl-1H-phenanthro[9,10-d]imidazolium salt [**2**][BF_4].*

The procedure for [**2**][BF_4] is the same as described above for [**1a**][BF_4] but uses 9,10-phenanthrenequinone (1.50 g, 7.20 mmol) as the starting material. It should be noted that

2-phenyl-1H-phenanthro[9,10-d]imidazole and its corresponding imidazolium salt are known compounds previously prepared by a different method.[21] Our spectroscopic characterization was consistent with the original published data for the charged [**2**]$^+$ species in solution. However, the tetrafluoroborate salt [**2**][BF_4] is a new compound. The crude product was recrystallized from nitromethane. Yield: 2.10 g, 76%, MP 253-256 °C. ^{1}H NMR (CD_3CN, 500 MHz, 293 K): δ (ppm) = 13.04 (s, 2H), 8.85 (d, 2H, *J* = 8.0 Hz), 8.40 (d, 2H, *J* = 7.5 Hz), 8.19 (d, 2H, *J* = 7.5 Hz), 7.85-7.78 (m, 7H). ^{13}C NMR (CD_3CN, 125 MHz, 294 K): δ (ppm) =147.6, 134.5,130.9, 129.7, 129.3, 129.0, 128.8, 126.9, 124.9, 123.0, 122.7, 120.5; IR (neat) = 3245, 1654, 1562, 1462, 995, 956, 754, 721, 697,614, 517, 484, 426 cm^{-1}. HR-MS (ESI-ToF) *m/z* found: 295.1239 [M+H]$^+$, [$C_{21}H_{16}N_2$]$^+$, calc = 295.1235.

2.2.4 ^{1}H NMR Studies of [2]Pseudorotaxanes

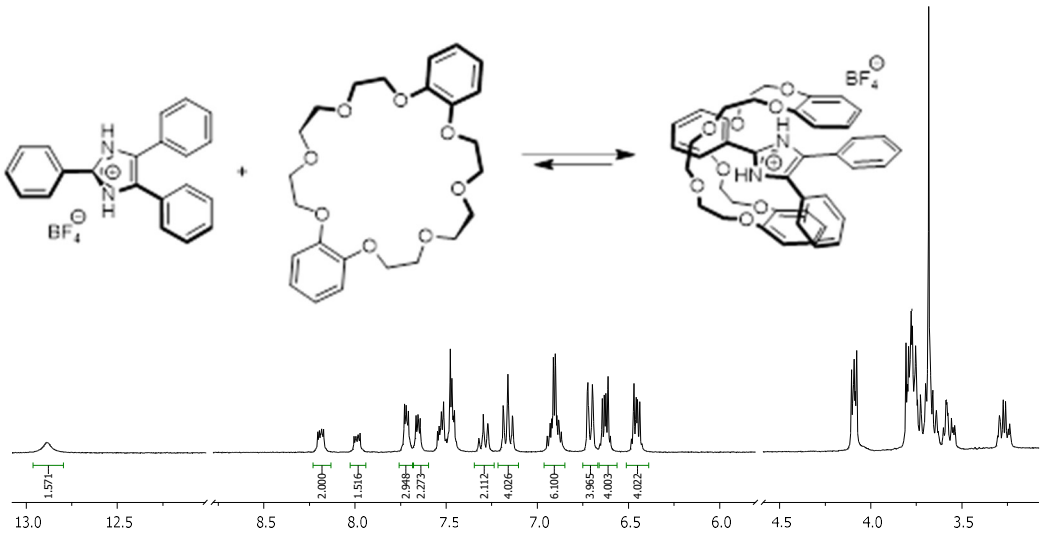

*Figure 2.5. ^{1}H NMR spectra in CD_3CN: 1.0 x 10^{-2} M solution of [**1a**][BF_4] with 1 eq. of **DB24C8** showing formation of [2]pseudorotaxane [**1a**⊂**DB24C8**][BF_4].*

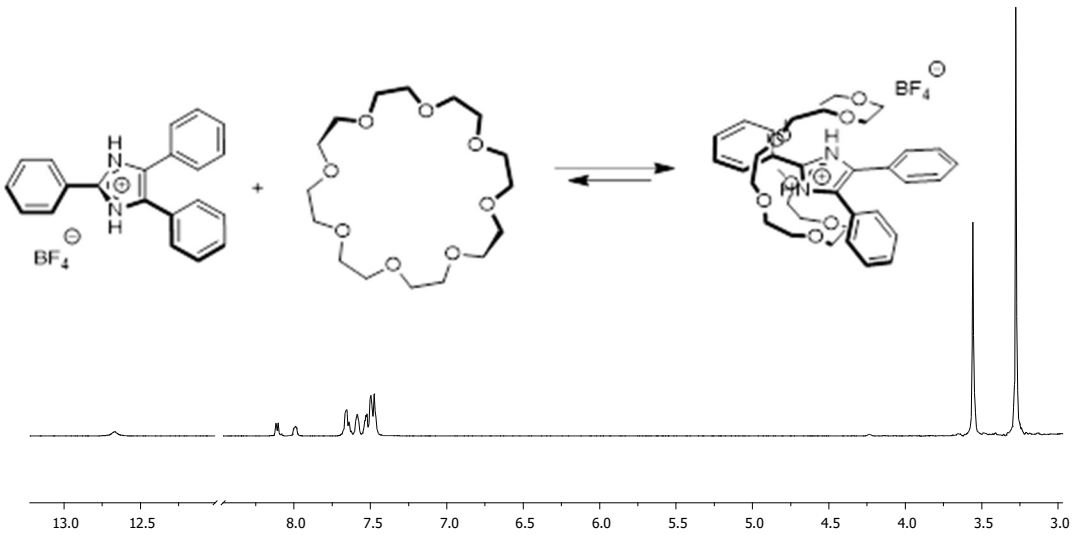

*Figure 2.6. ^{1}H NMR spectra in CD_3CN: 1.0 x 10^{-2} M solution of [**1a**][BF_4] with 1 eq. of **24C8** showing formation of [2]pseudorotaxane [**1a**⊂**24C8**][BF_4].*

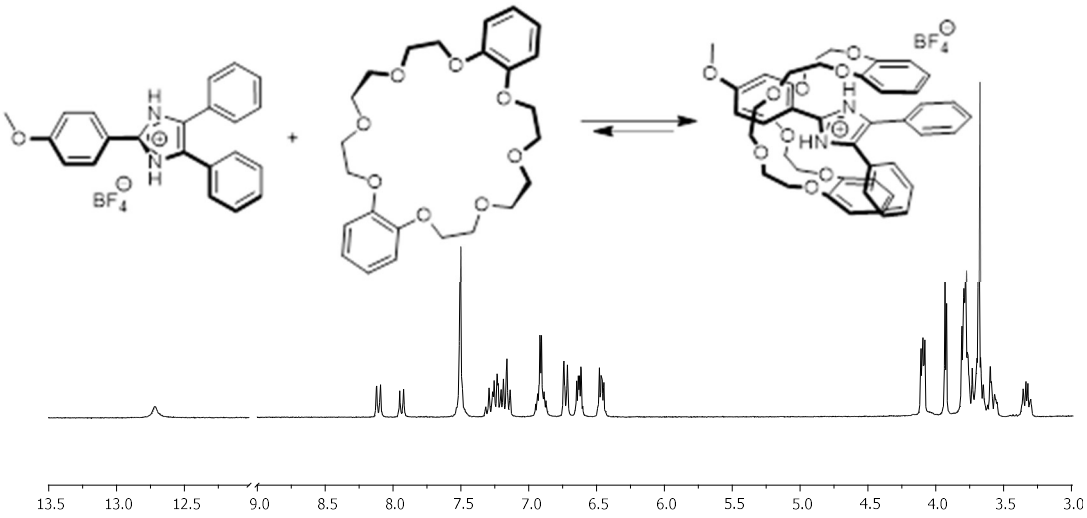

*Figure 2.7. ^{1}H NMR spectra in CD_3CN: 1.0 x 10^{-2} M solution of [**1b**][BF_4] with 1 eq. of **DB24C8** showing formation of [2]pseudorotaxane [**1b**⊂**DB24C8**][BF_4].*

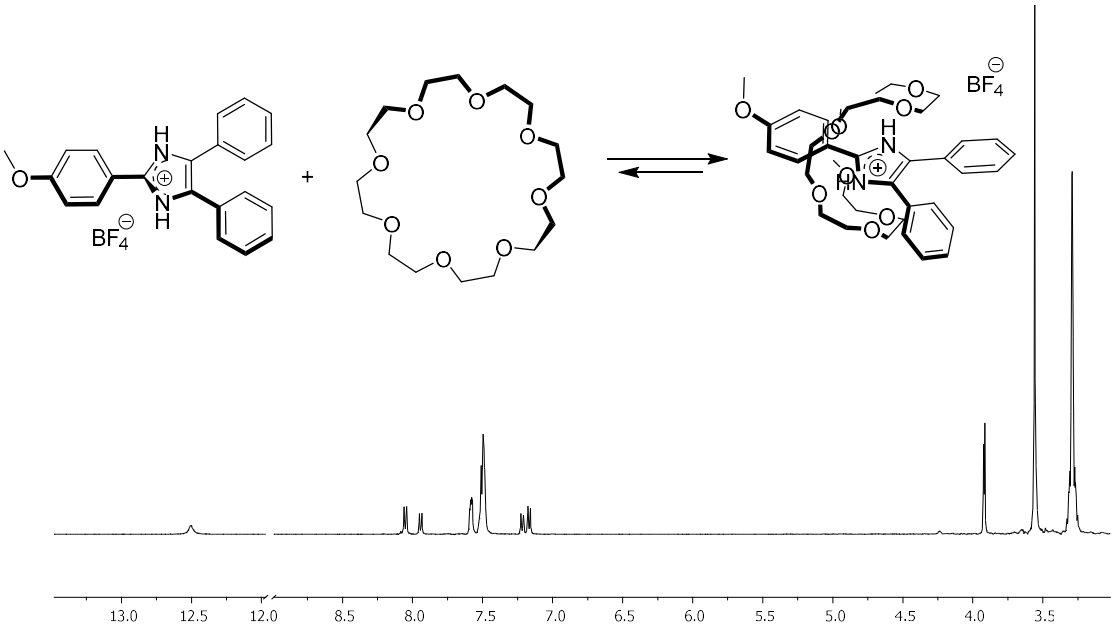

*Figure 2.8. ^{1}H NMR spectra in CD_3CN: 1.0 x 10^{-2} M solution of [**1b**][BF_4] with 1 eq. of **24C8** showing formation of [2]pseudorotaxane [**1b**⊂**24C8**][BF_4].*

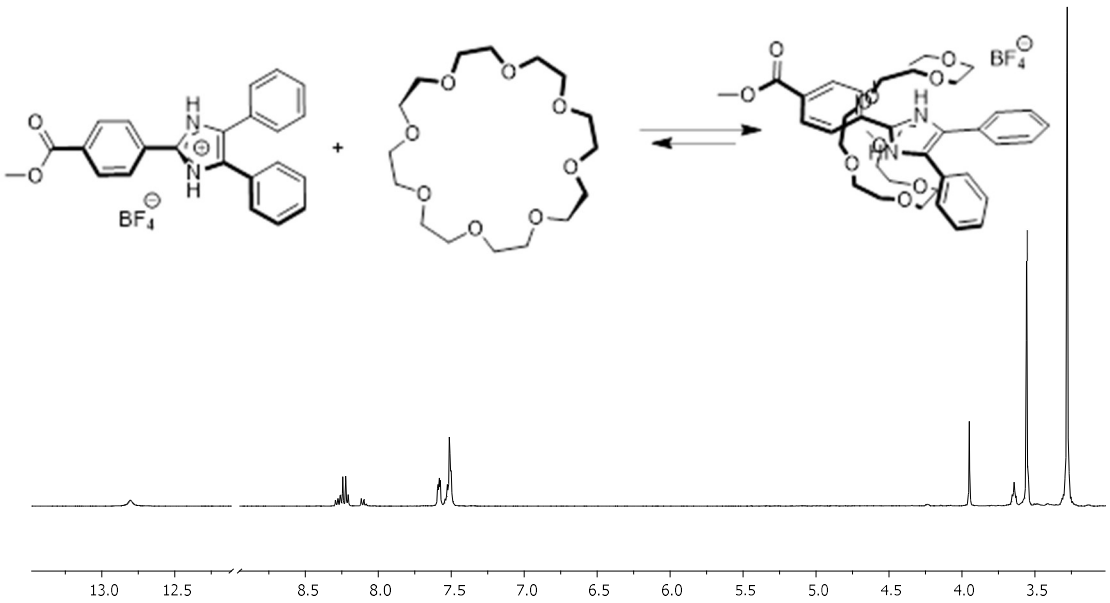

*Figure 2.9. ^{1}H NMR spectra in CD_3CN: 1.0 x 10^{-2} M solution of [**1c**][BF_4] with 1 eq. of **24C8** showing formation of [2]pseudorotaxane [**1c**⊂**24C8**][BF_4].*

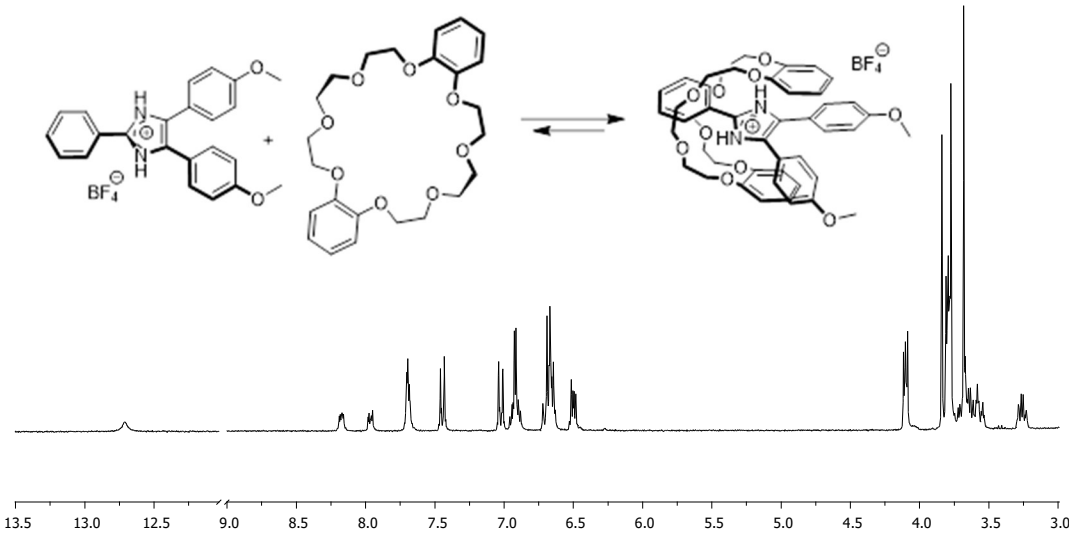

*Figure 2.10. ^{1}H NMR spectra in CD_3CN: 1.0 x 10^{-2} M solution of [**1d**][BF_4] with 1 eq. of **DB24C8** showing formation of [2]pseudorotaxane [**1d**⊂**DB24C8**][BF_4].*

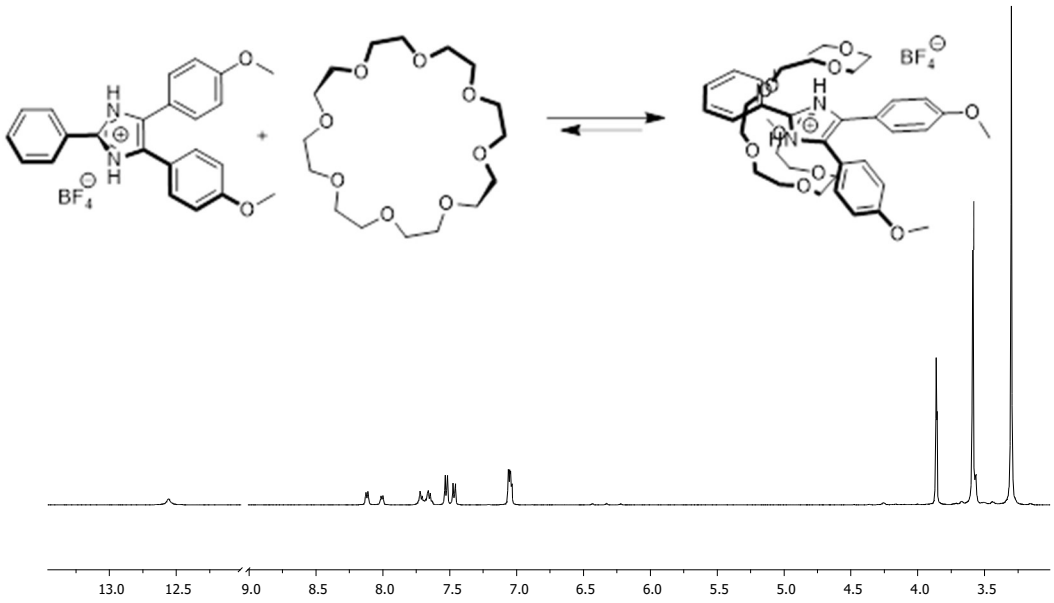

*Figure 2.11. ^{1}H NMR spectra in CD_3CN: 1.0 x 10^{-2} M solution of [**1d**][BF_4] with 1 eq. of **24C8** showing formation of [2]pseudorotaxane [**1d**⊂**24C8**][BF_4].*

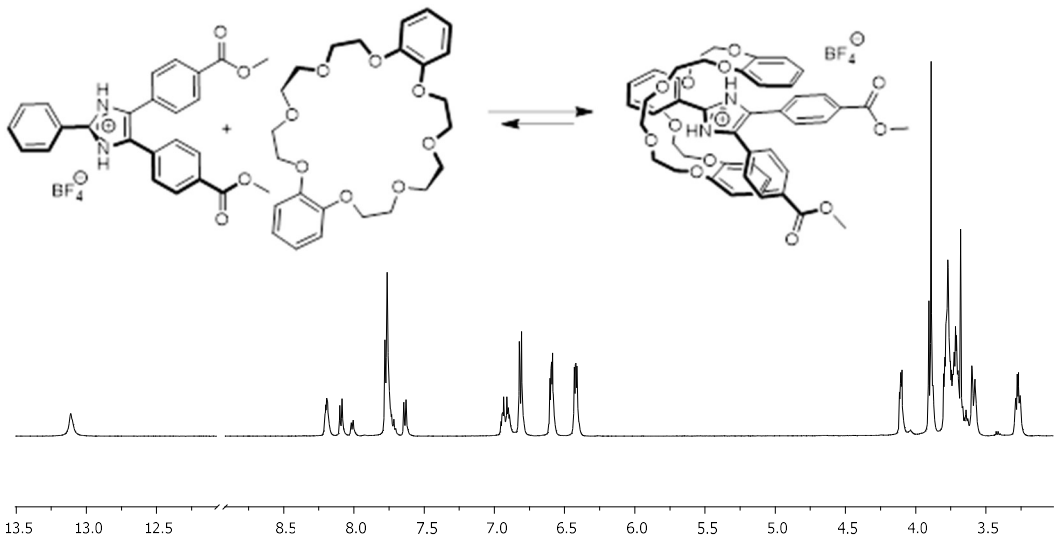

*Figure 2.12. ^{1}H NMR spectra in CD_3CN: 1.0 x 10^{-2} M solution of [**1e**][BF_4] with 1 eq. of **DB24C8** showing formation of [2]pseudorotaxane [**1e**⊂**DB24C8**][BF_4].*

s

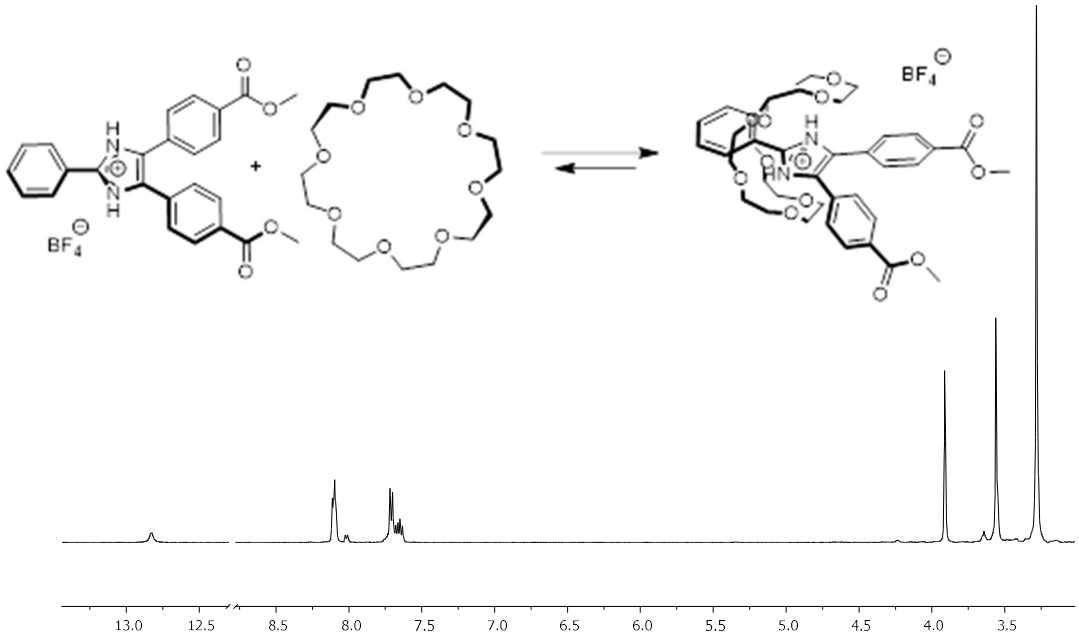

*Figure 2.13. ^{1}H NMR spectra in CD_3CN: 1.0 x 10^{-2} M solution of [**1e**][BF_4] with 1 eq. of **24C8** showing formation of [2]pseudorotaxane [**1e**⊂**24C8**][BF_4].*

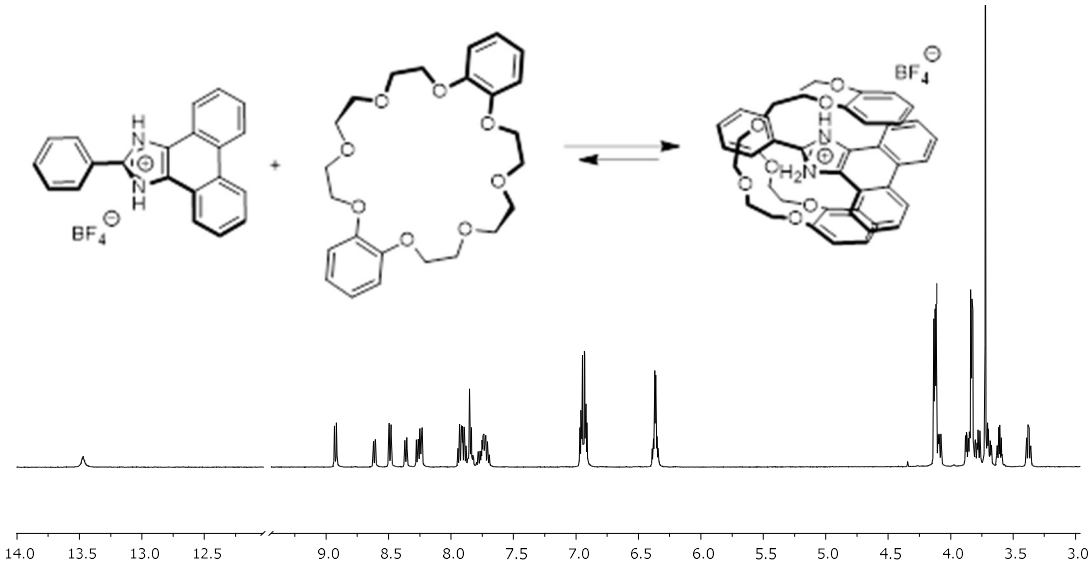

*Figure 2.14. ^{1}H NMR spectra in CD_3CN: 1.0 x 10^{-2} M solution of [**2**][BF_4] with 1 eq. of **DB24C8** showing formation of [2]pseudorotaxane [**2**⊂**DB24C8**][BF_4].*

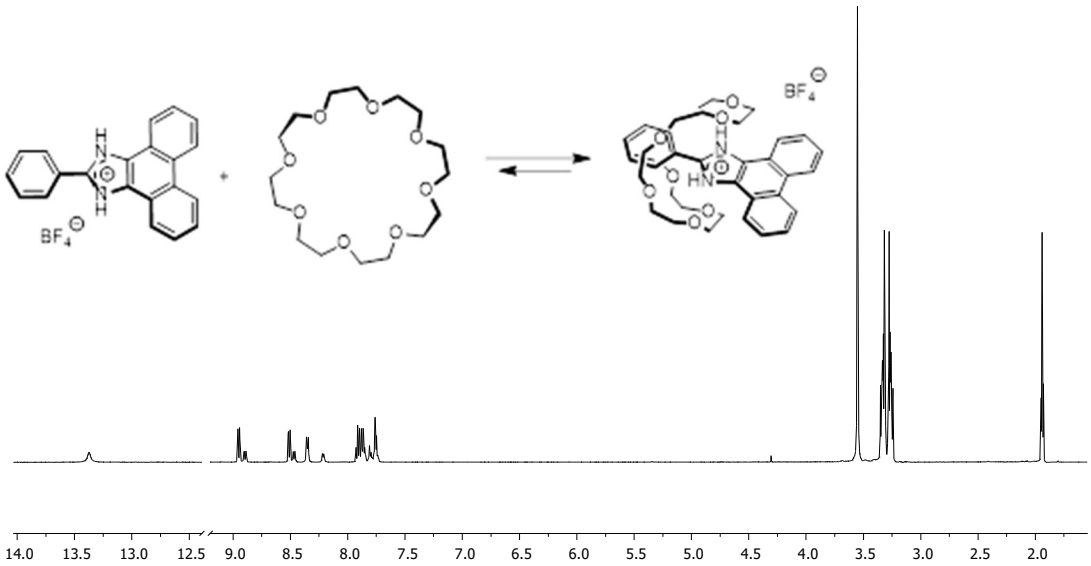

*Figure 2.15. ^{1}H NMR spectra in CD_3CN: 1.0 x 10^{-2} M solution of [**2**][BF_4] with 1 eq. of **24C8** showing formation of [2]pseudorotaxane [**2**⊂**24C8**][BF_4].*

2.2.5 2D-NMR Studies

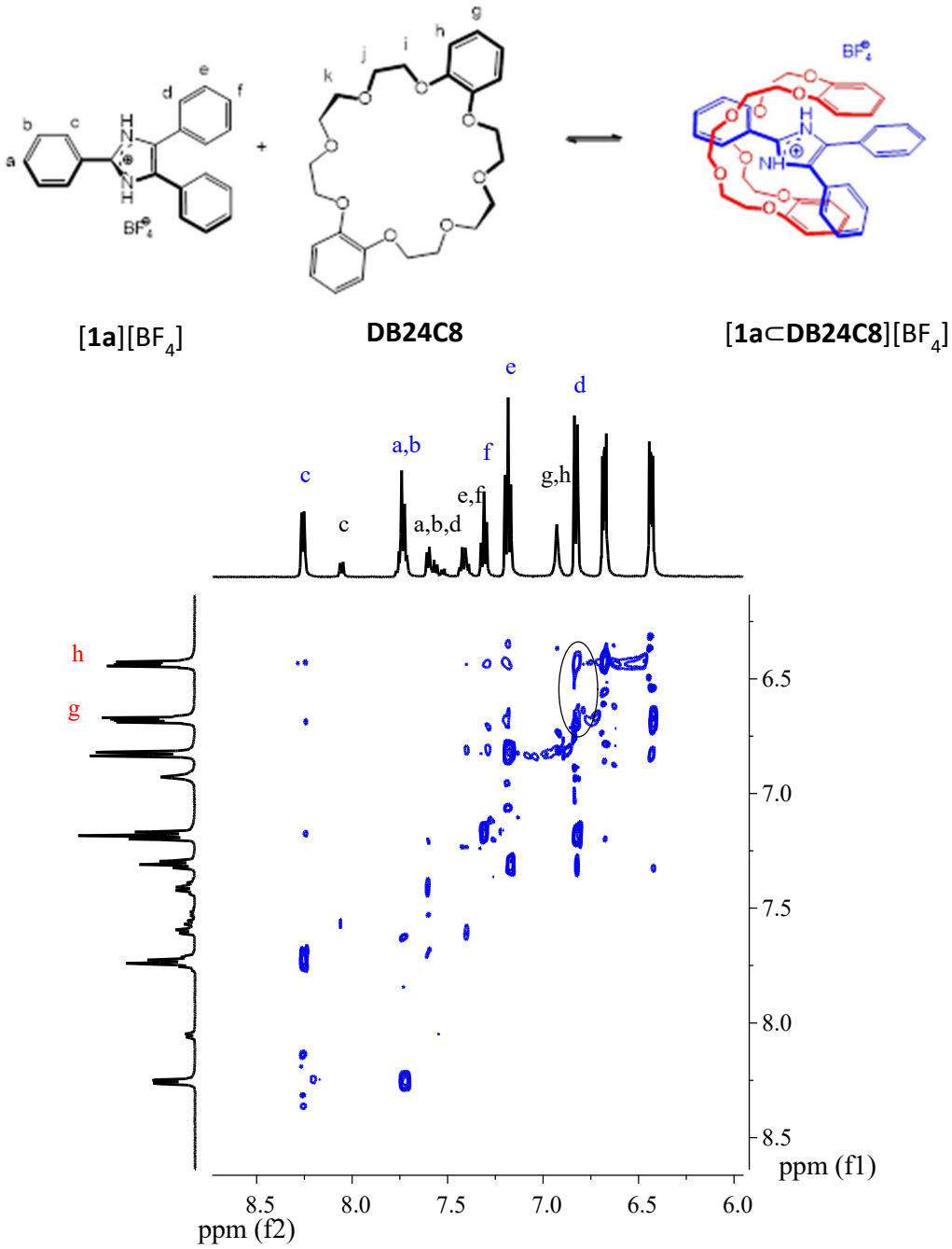

*Figure 2.16. Partial 2D-NOESY spectrum of [**1a⊂DB24C8**][BF_4] (500 MHz, CD_2Cl_2, 298 K). This verifies the interactions between axle and wheel are the same as observed in the X-ray crystal structure.*

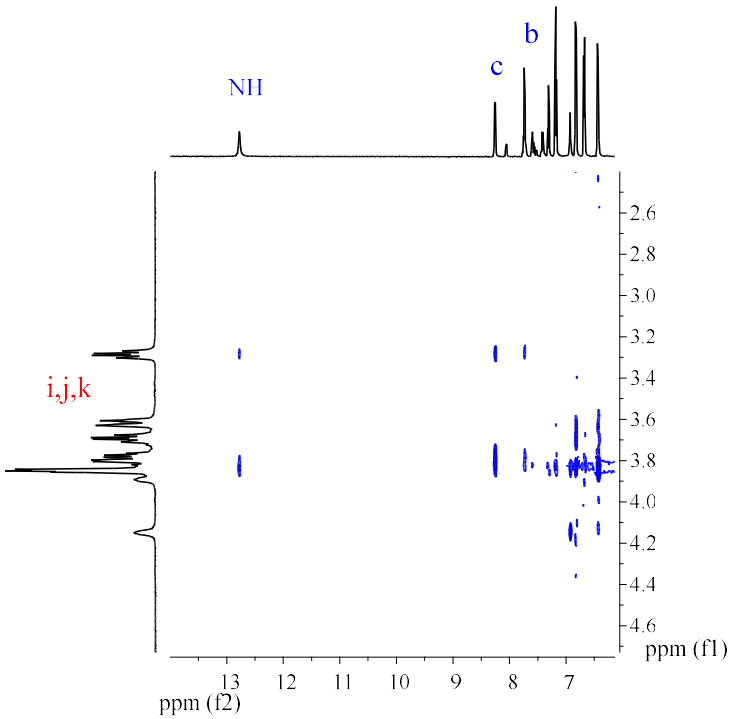

*Figure 2.17. Partial 2D-NOESY spectrum of [**1a⊂DB24C8**][BF_4] (500 MHz, CD_2Cl_2, 298 K). This verifies the interactions between axle and wheel are the same as observed in the X-ray crystal structure.*

2.2.6 Van't Hoff Plots

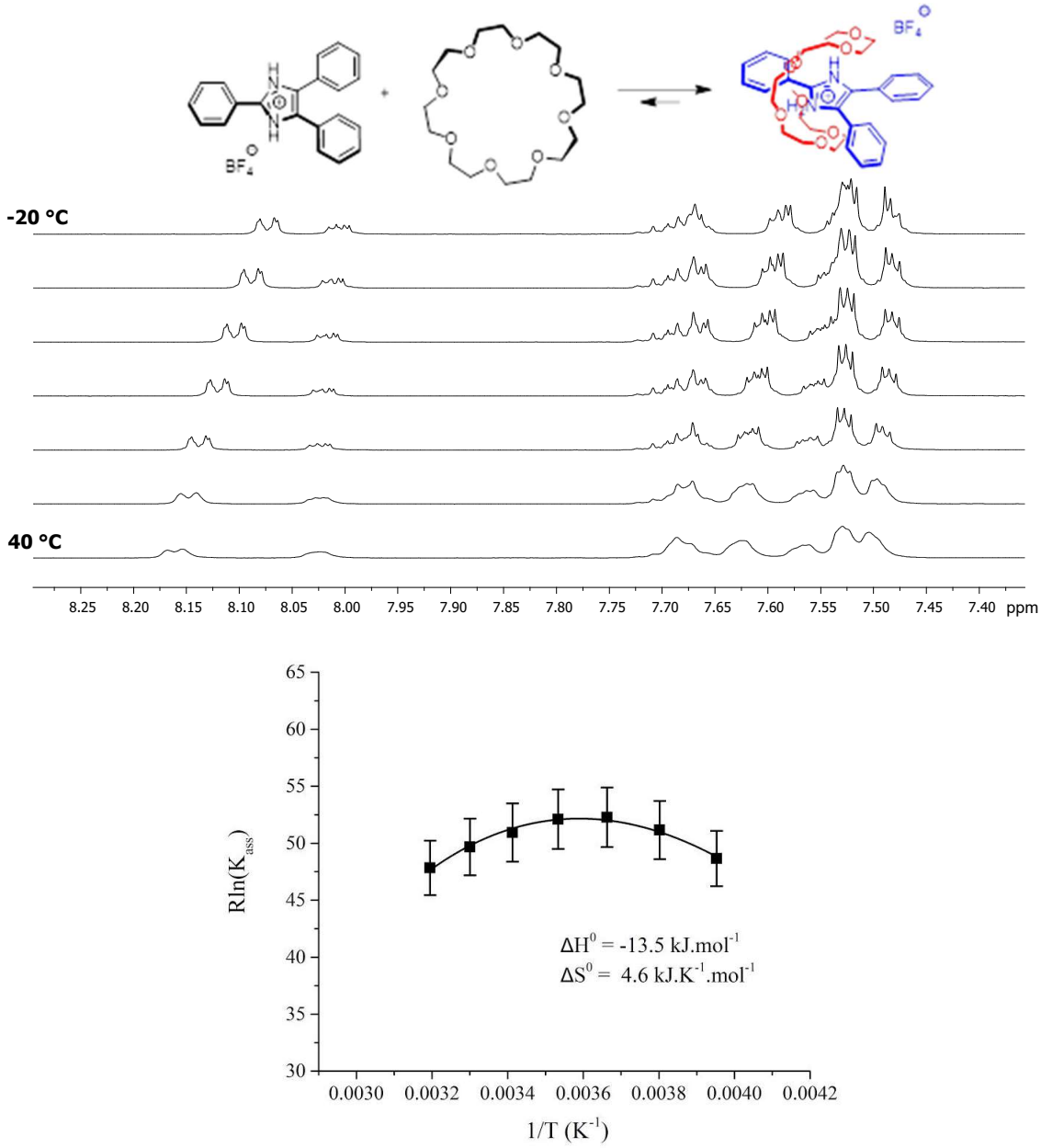

$RlnK_a = -(\Delta H_0/T) + \Delta Cp°lnT + (\Delta S_0 - \Delta Cp°)$

$\Delta H_0 = 193.9\ KJmol^{-1}$, $\Delta S_0 = 4.0\ kJK^{-1}mol^{-1}$, $\Delta Cp° = -696.2\ JK^{-1}mol^{-1}$

$\Delta H° = \Delta H_0 + T\ \Delta Cp°$

$\Delta S° = \Delta S_0 + \Delta Cp°lnT$

Figure 2.18. Variable temperature ^1H NMR spectra and van't Hoff plot for ***[1a⊂24C8]****.*

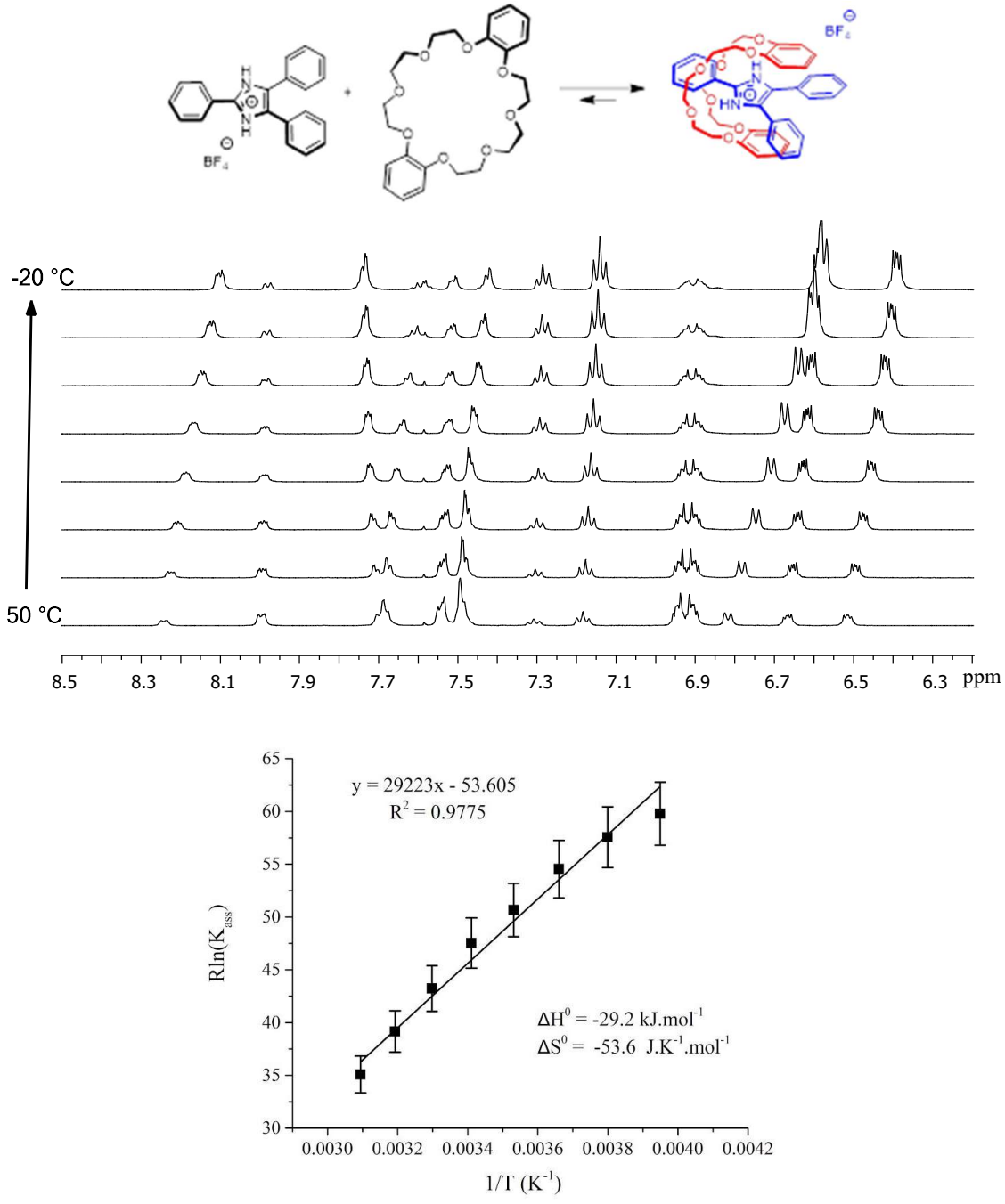

Figure 2.19. Variable temperature ^{1}H NMR spectra and van't Hoff plot for ***[1a⊂DB24C8]****.*

2.2.7 Hammett Plots

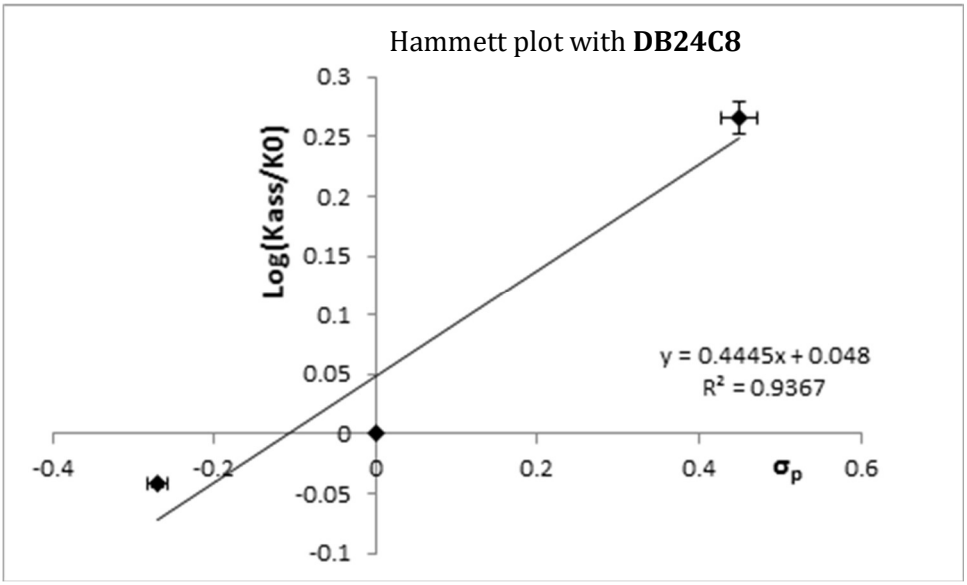

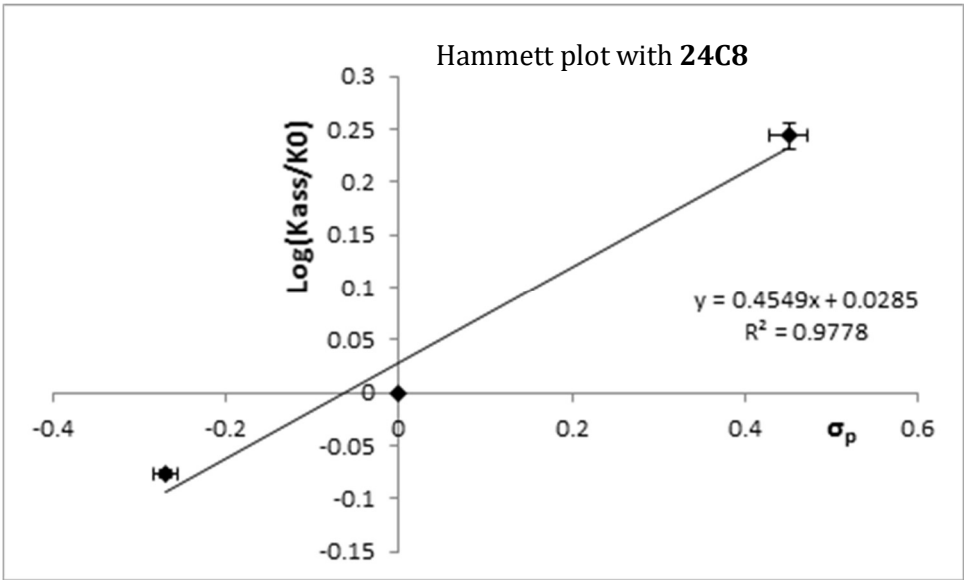

*Figure 2.20. Hammett plots for **DB24C8** and **24C8** (variation of R_1).*

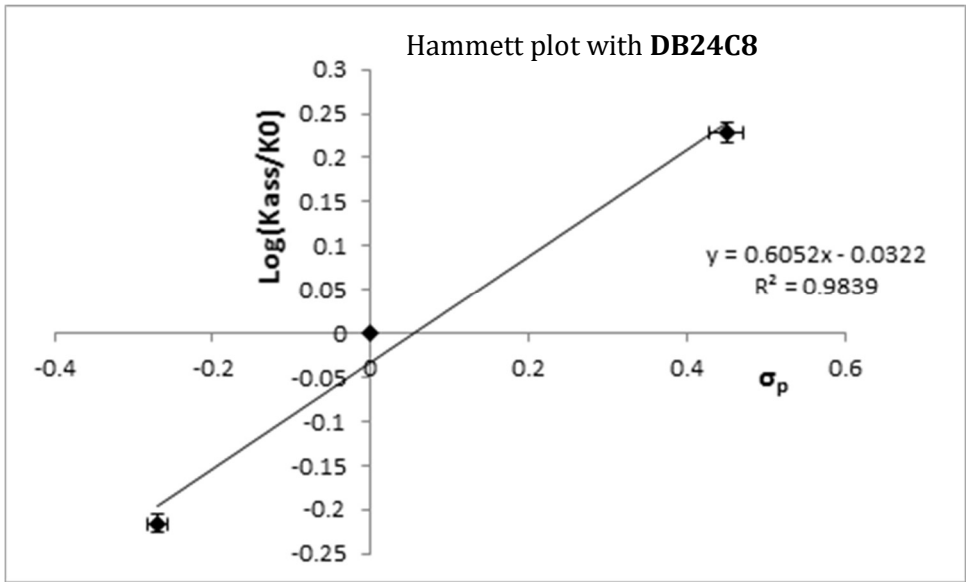

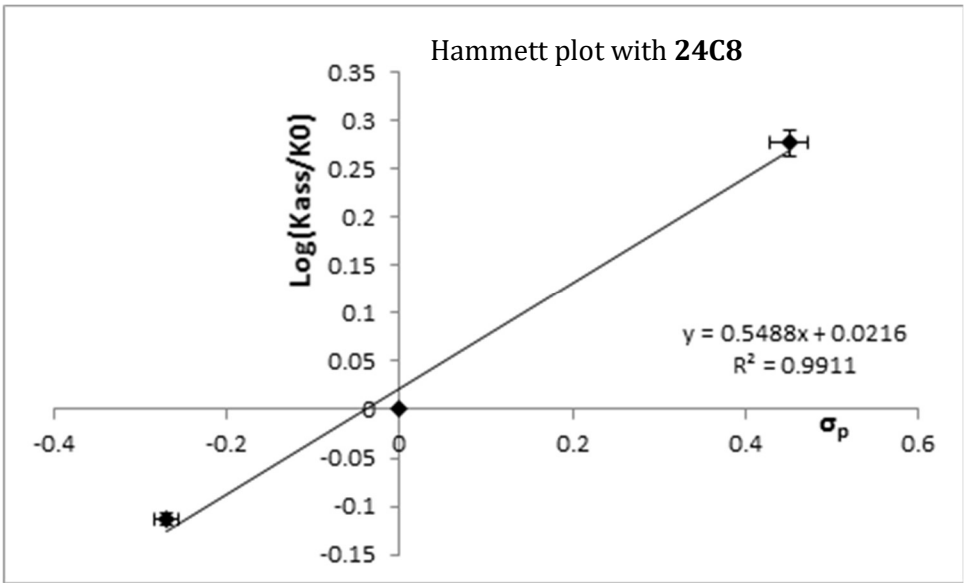

*Figure 2.21. Hammett plots for **DB24C8** and **24C8** (variation of R_2)*

2.3 References

[1] a) D. Thibeault, J.-F. Morin, *Molecules,* **2010**, *15*, 3709; b) F. Huang, H. W. Gibson, *Progr. Polym. Sci.,* **2005**, *30*, 982; c) C. Zhang, S. Li, J. Zhang, K. Zhu, N. Li, F. Huang, *Org. Lett.,* **2007**, *9*, 5553; d) M. Zhang, K. Zhu, F. Huang, *Chem. Commun.,* **2010**, *46*, 8131; e) Y. Makita, N. Kihara, T. Takata*, J. Org. Chem.,* **2008**, *73*, 9245. f) S. Suzuki, K. Nakazono, T. Takata, *Org. Lett.,* **2010**, *12*, 712; g) Y. Koyama, T. Matsumura, T. Yui, O. Ishitani, T. Takata, *Org. Lett.,* **2013**, ***15***, 4686; h) T. Yuki, Y. Koyama, T. Matsumura, T. Takata, *Org. Lett.,* **2013**, *15*, 4438; i) J.-L. Ko, S.-H. Ueng, C.-W. Chiu, C.-C. Lai, Y.-H. Liu, S.-M. Peng, S.-H. Chiu, Chem. Eur. J., **2010**, *16*, 6950; j) T.-C. Lin, C.-C. Lai, S.-H. Chiu, Org. Lett., 2009, *11*, 613; k) A. B. Braunschweig, W. R. Dichtel, O. S. Miljanic, M. A. Olson, J. M. Spruell, S. I. Khan, J. R. Heath, J. F. Stoddart, Chem. Asian J., **2007**, *2*, 634; l) A. B. Braunschweig, C. M. Ronconi, J.-Y. Han, F. Arico, S. J. Cantrill, J. F. Stoddart, S. I. Khan, A. J. P White, D. Williams, J. Eur. J. Org. Chem., **2006**, 1857; m) S. J. Rowan, S. J. Cantrill, J. F. Stoddart, Org. Lett., 1999, *1*, 129; n) S. J. Loeb, J. A. Wisner, Angew. Chem., Int. Ed., **1998**, *37*, 2838; o) K. Zhu, V. N. Vukotic, N. Noujeim, S. J. Loeb, Chem. Sci., **2012**, *3*, 3265.

[2] a) V. Balzani, A. Credi, M. Venturi*, Molecular Devices and Machines – Concepts and Perspectives for the Nanoworld*, Wiley InterScience, Wiley-VCH, Weinheim, **2008**; b) E. K. Kay, D. A. Leigh, F. Zerbetto, *Angew. Chem. Int. Ed.,* **2007**, *46*, 72; c) A. Coskun, M. Banaszak, R. D. Astumian, J. F. Stoddart, B. A. Grzybowski, *Chem. Soc. Rev.,* **2012**, *41*, 19; d) G. J. E. Davidson, S. Sharma, S. J. Loeb, *Angew. Chem., Int. Ed.,* **2010**, *49*, 4938; e) S. J. Loeb, J. Tiburcio, S. J. Vella, *Chem. Commun.,* **2006**, 1598; f) N. D. Suhan, L. Allen, M. T. Gharib, E. Viljoen, S. J. Vella, S. J. Loeb, *Chem. Commun.,* **2011**, *47*, 5991; g) S. Grunder, P. L. McGrier, A. C. Whalley, M. M. Boyle, C. Stern, J. F. Stoddart, *J. Am. Chem. Soc.,* **2013**, *135*, 17691; h) Y. Yamada, N. Mihara, Shibano, S. K. Sugimoto, K. Tanaka, J. Am. Chem. Soc., 2013, *135*, 11505; i) S. Dong, J. Yuan, F. Huang, *Chem. Sci.,* **2014**, *5*, 247.

[3] a) S. J. Loeb, *Rotaxanes as Ligands: From Molecules to Materials In Organic Nanostructures InterScience,* Wiley-VCH, Weinheim, **2008**, Ed. J. W. Steed, J. L. Atwood, pp 33; b) S. J. Loeb, *Chem. Soc. Rev.,* **2007**, *36*, 226; c) G. J. E. Davidson, S. J. Loeb, *Angew. Chem. Int. Ed.,* **2003**, *42*, 74; d) D. J. Hoffart, S. J. Loeb, *Angew. Chem., Int. Ed.,* **2005**, *44*, 901; e) D. J. Hoffart, S. J. Loeb, *Supramol. Chem.,* **2007**, *19*, 89; f) L. K. Knight, V. N. Vukotic, E. Viljoen, C. B. Caputo, S. J. Loeb, *Chem. Commun.,* **2009**, 5585; g) V. N. Vukotic, S. J. Loeb, *Chem. Eur. J.,* 2010, *16*, 13630; h) D. J. Mercer, V. N. Vukotic, S. J. Loeb, *Chem. Commun.,* **2011**, *47*, 896; i) V. N. Vukotic, K. J. Harris, K. Zhu, R. W. Schurko, S. J. Loeb, *Nat. Chem.,* **2012**, *4*, 456; j) N. C. Frank, D. J. Mercer, S. J. Loeb, *Chem. Eur. J.,* **2013**, *19*, 14076.

[4] N. Noujeim, K. Zhu, V. N. Vukotic, S. J. Loeb, *Org. Lett.,* **2012**, *14*, 2484.

[5] S. Kiviniemi, M. Nissinen, M. T. Jorma-Jalonen, K. Rissanen, M. Lämsä, J. Pursiainen, *New J. Chem.,* **2000**, *24*, 47.

[6] K. Zhu, V. N. Vukotic, S. J. Loeb, *Angew. Chem., Int. Ed.,* **2012**, *51*, 2168.

[7] a) D. Castillo, P. Astudillo, J. Mares, F. J. Gonzalez, A. Vela, J. Tiburcio, *Org. Biomol. Chem.,* **2007**, *5*, 2252; b) S. I. Moreno-Olivares, R. Cervantes, J. Tiburcio, *J. Org. Chem.,* **2013**, *78*, 10724.

[8] L. Li, G. J. Clarkson, *Org. Lett.,* **2007**, *9*, 497.

[9] M. Lee, Z. Niu, D. V. Schoonover, C. Slebodnick, H. W. Gibson, *Tetrahedron*, **2010**, *66*, 7077.

[10] a) W. Lin, L. Long, L. Yuan, Z. Cao, B. Chen, W. Tan, *Org. Lett.,* **2008**, *10*, 5577; b) A. Kikuchi, F. Iwahori, J. Abe, *J. Am. Chem. Soc.,* **2004**, *126*, 6526.

[11] N. Kishikawa, M. Wada, Y. Ohba, K. Nakashima, N. Kuroda, J. *Chromatogr. A,* **2004**, *1057*, 83.

[12] a) J. C., Jr. Adrian, C. S. Wilcox, *J. Am. Chem. Soc.,* **1991**, *113*, 678; b) S. J. Loeb, J. Tiburcio, J. A. Wisner, *Org. Biomol. Chem.,* **2006**, *4*, 667.

[13] a) J. W. Jones, H. W. Gibson, *J. Am. Chem. Soc.,* **2003**, *125*, 7001; b) H. W. Gibson, H. Wang, K. Bonrad, J. W. Jones, C. Slebodnick, L. N. Zackharov, A. L. Rheingold, B. Habenicht, P. Lobue, A. E. Ratliff, *Org. Biomol. Chem.,* **2005**, *3*, 2114; c) H. W. Gibson, H. Wang, C. Slebodnick, J. Merola, W. Scott Kassel, A. L. Rheingold*, J. Org. Chem.,* **2007**, *72*, 3381; d) H. W. Gibson, J. W. Jones, L. N. Zakharov, A. L. Rheingold, C. Slebodnick, *Chem. Eur. J.,* **2011**, *17*, 3192.

[14] a) J. R. Horn, D. Russell, E. A. Lewis, K. P. Murphy, *Biochemistry,* **2001**, *40*, 1774; b) J. R. Horn, J. F. Brandts, K. P. Murphy, *Biochemistry,* **2002**, *41*, 7501; c) D. B. Smithrud, T. B. Wyman, Diederich, F. *J. Am. Chem. Soc.,* **1991**, *113*, 5420; d) D. A. Stauffer, R. E. Barrans, Jr. D. A. Dougherty, *J. Org. Chem.,* **1990**, *55*, 2762.

[15] a) L. P. Hammett, *J. Am. Chem. Soc.,* **1937**, *59*, 96; b) C. Hansch, A. Leo, R. W. Taft, *Chem. Rev.*, **1991**, *91*, 165.

[16] The SHELXTL library in Bruker APEX2 software package was used for solution and refinement of the X-ray structure. See G. M. Sheldrick, *Acta Cryst.,* **2008**, *A64*, 112.

[17] Images of the X-ray structure were generated using CrystalMaker®: CrystalMaker Software Ltd, Oxford, England (www.crystalmaker.com).

[18] P. R. Ashton, E. J. T. Chrystal, P. T. Glink, S. Menzer, C. Schiavo, N. Spencer, J. F. Stoddart, P. A. Tasker, A. J. P. White, D. J. Williams, *Chem.–Eur. J.,* **1996**, *2*, 709.

[19] M. H. Petersen, S. A. Gevorgyan, F. C. Krebs, *Macromolecules*, **2008**, *41*, 8986.

[20] J. C., Adrian Jr., C. S. Wilcox, *J. Am. Chem. Soc.,* **1991**, *113*, 678.

[21] N. Kishikawa, M. Wada, Y. Ohba, K. Nakashima, N. Kuroda, J. *Chromatogr. A,* **2004**, *1057*, 83.

CHAPTER 3

3.1 Rigid, Bistable Molecular Shuttles Combining T-shaped Benzimidazolium and Y-shaped Imidazolium Recognition Sites

3.1.1 Introduction

Mechanically interlocked molecules (MIMs), such as rotaxanes and catenanes, have attracted great interest because of their potential to operate as molecular switches and machines in mechanical and electronic devices.[1] Among these MIMs, [2]rotaxane molecular shuttles, composed of a linear dumbbell-shaped axle with two distinct recognition sites and a single macrocyclic wheel, have been widely studied.[2] A bistable molecular shuttle can adopt two translational co-conformations with different molecular arrangements depending on the relative positioning of the two interlocked components. Switching of the co-conformations can then be induced by shuttling of the wheel between the two sites in response to an environmental stimulus such as a chemical, electrochemical or photochemical input.[3]

Almost all [2]rotaxane molecular shuttles characterized to date, have large and flexible structures and function efficiently in solution.[4] However, we are interested in incorporating these nanoscale switches into highly-organized, solid-state materials and have therefore sought out structures with rigid axles and linear tracks as building blocks. The first new MIM template identified for this purpose was that between T-shaped 2,4,7-triphenyl substituted benzimidazolium axles and 24-membered crown ether wheels.[5] This motif was used to prepare H-shaped, degenerate [2]rotaxane molecular shuttles exhibiting spontaneous shuttling between two equivalent recognition sites in solution; the rate could be controlled by either acid-base chemistry or lithium ion coordination.[6] Very recently, we also demonstrated that this compact and rigid, MIM can be incorporated into the solid-state

where it can undergo this same translation shuttling motion inside the highly organized lattice of a metal-organic framework (MOF) material.[7]

Although the T-shaped benzimidazolium cations turned out to be excellent candidates for developing rigid MIM molecular shuttles, there is still a need for new templating motifs to be used in conjunction with this T-shaped recognition site in order to produce unsymmetrical axles and eventually bistable molecular shuttles. To this end, we recently reported the formation of [2]pseudorotaxanes utilizing a similar, rigid Y-shaped 2,4,5-triphenylimidazolium axle and 24-membered crown ether wheels: [24]-crown-8 (**24C8**) and dibenzo-[24]-crown-8 ether (**DB24C8**).[8] Despite a weaker interaction between the crown ether wheel and the imidazolium axle for the Y-shaped system (relative to the T-shaped axle), the difference in association constants was seen as an opportunity to incorporate both of these templating motifs into a single entity and thus generate a bistable molecular shuttle that could eventually be utilized as a rigid linker in a MOF material.

Herein, novel [2]rotaxane molecular shuttles were synthesized through a threading-followed-by-stoppering[9] methodology under mild conditions and their shuttling characteristics systematically investigated. The combination of T-shaped benzimidazolium and Y-shaped imidazolium components results in a linear axle with two non-equivalent recognition sites possessing different binding strengths for a single 24-membered crown ether (**24C8** or **DB24C8**) wheel.

3.1.2 Results and Discussion

3.1.2.1 Synthesis of [2]rotaxane molecular shuttles

In a typical one-pot reaction, a Y-shaped [2]pseudorotaxane with a terminal aldehyde group on the axle was condensed with an equivalent of 1,2-diamino-3,6-diphenylbenzene followed by oxidation with atmospheric O_2 using a catalytic amount of $ZrCl_4$.[10] The crude products were treated with triethylamine to produce the neutral [2]rotaxanes [**2⊂DB24C8**]

and [**2**⊂**24C8**] in 63% and 59% yields respectively. Since the protonated forms of these rotaxanes can also undergo molecular shuttling, the neutral species were converted to their dicationic forms [**2**-H_2⊂**DB24C8**][BF_4]$_2$ and [**2**-H_2⊂**24C8**][BF_4]$_2$, by addition of two equivalents of HBF_4. See Scheme 3.1 for details.

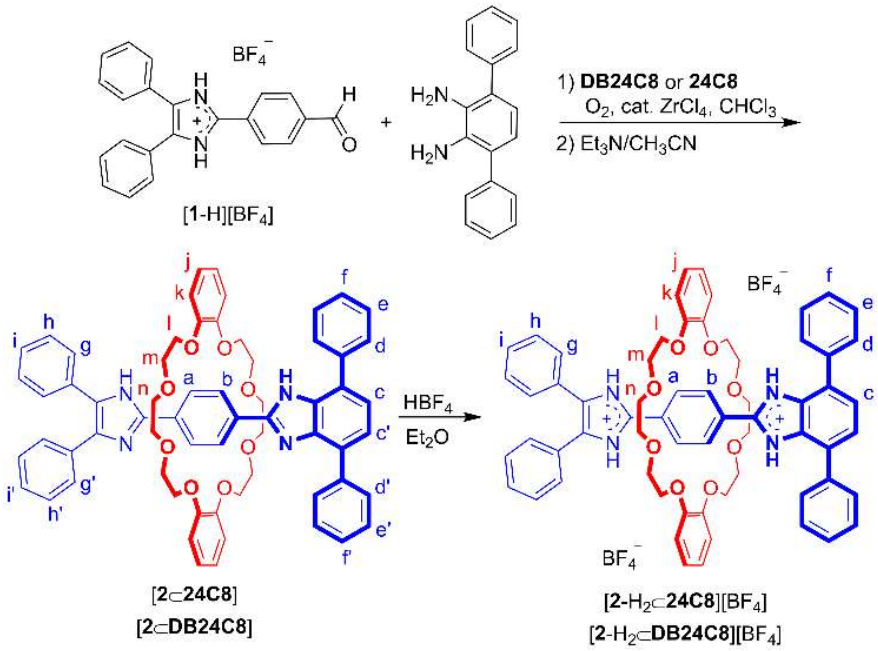

Scheme 3.1. Preparation of neutral and dicationic [2]rotaxane molecular shuttles ***[2⊂24C8]***, ***[2⊂DB24C8]***, ***[2***-H_2⊂***24C8]***$^{2+}$ *and* ***[2***-H_2⊂***DB24C8]***$^{2+}$ *from Y-shaped [2]pseudorotaxanes and T-shaped stoppering groups (****DB24C8*** *versions shown only). Labelling is for assignment of* ^{1}*H NMR resonances.*

3.1.2.2 Spectroscopic characterization of molecular shuttles

The ^{1}H NMR spectra of the neutral species are relatively simple since rapid translation of the macrocyclic ring along the axle at a rate faster than the NMR timescale results in only averaged signals for the complexed and uncomplexed species. This is not surprising, since, deprotonation of the imidazolium and benzimidazolium recognition sites eliminates significant ion-dipole and π-stacking interactions (for **DB24C8**) and reduces the degree of hydrogen bonding between axle and wheel. As shown in Fig. 3.1, only one set of peaks is observed for either neutral [2]rotaxane due to the average of hydrogen-bonded and free *NH*

and *CH* groups. Proton signals *NH*, *a* and *b* were assigned with the aid of 2D NOESY and HMBC spectroscopic measurements (see section 3.2.10).

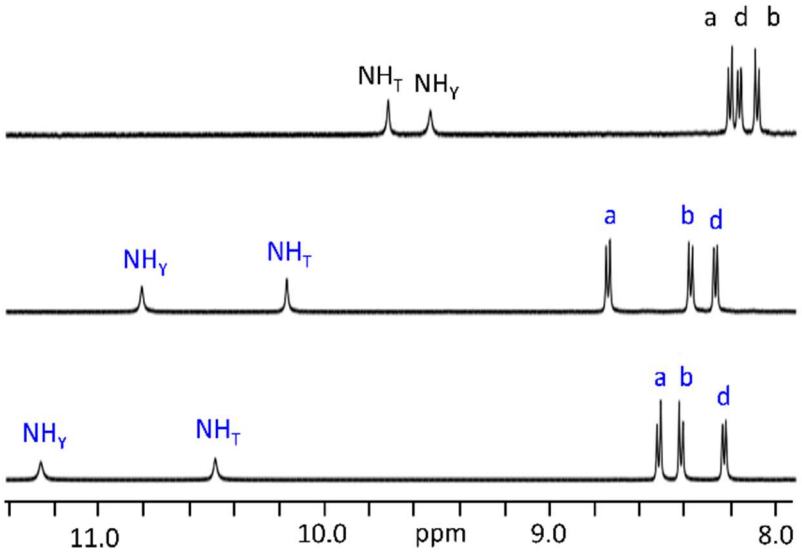

*Figure 3.1. Partial ^{1}H NMR spectra of neutral species (top to bottom), axle **2**, [**2**⊂**DB24C8**] and [**2**⊂**24C8**] (CD_2Cl_2, 298 K, 1.0 x 10^{-3} M). See Scheme 1 for labels; black = naked axle, blue = axle of rotaxane.*

A comparison of the chemical shifts of NH groups in the neutral axle [**2**], (δ = 9.72 and 9.58 ppm), with the neutral [2]rotaxanes, [**2**⊂**DB24C8**] (δ = 10.16 and 10.82 ppm) and [**2**⊂**24C8**] (δ = 10.40 and 11.20 ppm), clearly shows that there is hydrogen-bonding between the NH groups of the axles and crown ether oxygen atoms of the crown ethers. The Δδ values for the NH of the imidazole (+1.24 ppm for [**2**⊂**DB24C8**] and +1.64 ppm for [**2**⊂**24C8**]) are larger than for the benzimidazole NH (+0.44 ppm for [**2**⊂**DB24C8**] and +0.68 ppm for [**2**⊂**24C8**]). Thus, the NH of the imidazole ring experiences a stronger deshielding effect due to stronger hydrogen bonding with oxygen atoms on **DB24C8** and **24C8** and it can be inferred that in the neutral [2]rotaxanes the residual N-H···O interactions of electron-rich crown ethers with the neutral imidazole recognition site are preferred over those of the benzimidazole site. Since the interaction of a crown ether with a neutral recognition site is quite weak, it is likely

that this preference is simply driven by steric considerations – the Y-shaped site offers less steric hindrance and is thus preferred.

In contrast, the diprotonated [2]rotaxanes, [**2**-H_2⊂**DB24C8**]$^{2+}$ and [**2**-H_2⊂**24C8**]$^{2+}$, undergo slow exchange on the NMR timescale, wherein separate sets of peaks for both complexed and uncomplexed axle are observed. Fig. 3.2 shows the ^{1}H NMR spectra of the diprotonated species in CD_3CN at 298 K. In the case of [**2**-H_2⊂**DB24C8**]$^{2+}$, strong NH···O and CH···O hydrogen bonding interactions cause significant shifts to higher frequency for the *NH*, *a* and *b* resonances on the axle. Moreover, shifts to lower frequency for aromatic proton *c* on the axle and aromatic protons *j* and *k* on the wheel are indicative of efficient π-stacking interactions between the electron-poor benzimidazolium ring and electron-rich catechol rings of the crown ether. The ^{1}H NMR spectrum of [**2**-H_2⊂**24C8**]$^{2+}$ exhibits similar downfield shifts for *NH, a* and *b* resonances while the upfield shift for proton *c* is eliminated due to the lack of π-stacking interactions. Although the ^{1}H NMR spectra of dicationic systems shows resonances related to interactions of the wheel with both sites, larger Δδ for *b* (+0.40 ppm for [**2**⊂**DB24C8**]$^{2+}$ and +0.19 ppm for [**2**⊂**24C8**]$^{2+}$) versus *a* (+0.16 ppm for [**2**⊂**DB24C8**]$^{2+}$ and +0.11 ppm for [**2**⊂**24C8**]$^{2+}$) indicates that the wheel undergoes stronger interaction with the T-shaped benzimidazolium site than the Y-shaped imidazolium site. This preference corresponds to the larger association constants found for [2]pseudorotaxane formation between T-shaped benzimidazolium axles[5] and 24-membered crown ethers as compared to Y-shaped imidazolium axles.[8]

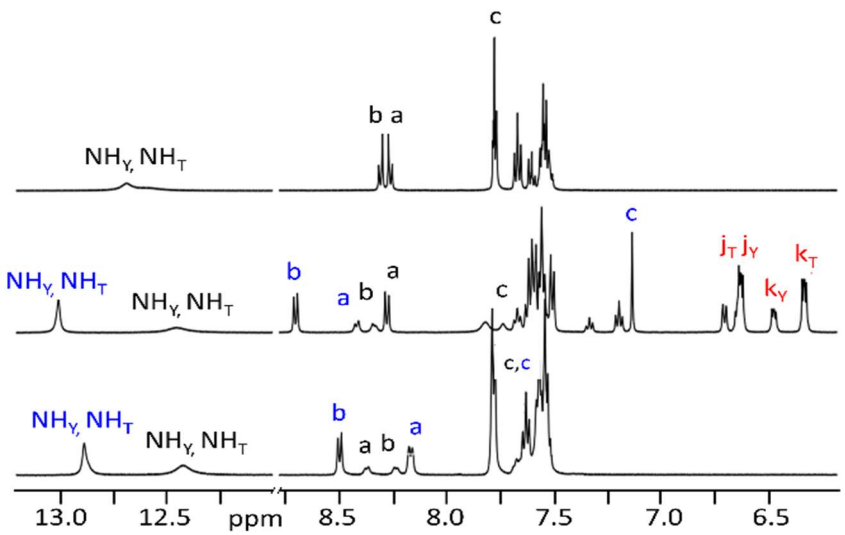

*Figure 3.2. ^{1}H NMR spectra of (top to bottom) axle **2**$^{2+}$, [**2**-H_2⊂**DB24C8**]$^{2+}$ and [**2**-H_2⊂**24C8**]$^{2+}$ (CD_3CN, 298 K, 1.0 x 10^{-3} M). See Scheme 1 for labels; black = uncomplexed axle, blue = complexed axle, red = wheel of rotaxane.*

3.1.2.3 Single-crystal X-ray diffraction studies

Single crystals suitable for X-ray diffraction were obtained for both of the protonated systems. Fig. 3.3 shows the results of these solid-state experiments for [**2**-H_2⊂**24C8**][BF_4]$_2$ and [**2**-H_2⊂**DB24C8**][BF_4]$_2$. The resulting structures display metric parameters which are in good agreement with the non-covalent interactions observed in solution. For [**2**-H_2⊂**DB24C8**]$^{2+}$, shown in Fig. 3 (top), the crown ether adopts a C-shaped conformation as it clamps around the benzimidazolium recognition site to allow for efficient π-stacking interaction (centroid-centroid, dihedral angles; 3.84 Å, 22°; 4.43 Å, 35°). This π-stacking array is accompanied by significant N$^+$···O ion-dipole interactions and directional hydrogen bonds; NH···O (2.86 Å, 163°; 2.89 Å, 166°) CH···O (3.60 Å, 158°; 3.66 Å, 152°) between the axle and wheel. The X-ray structure of [**2**-H_2⊂**24C8**]$^{2+}$ shown in Fig. 3 (bottom), is similar to [**2**-H_2⊂**DB24C8**]$^{2+}$ with similar NH…O charge-assisted hydrogen bonds (2.88 Å, 175°; 3.08 Å, 171°), and weaker CH···O interactions (3.41Å, 165°; 3.77Å, 156°).

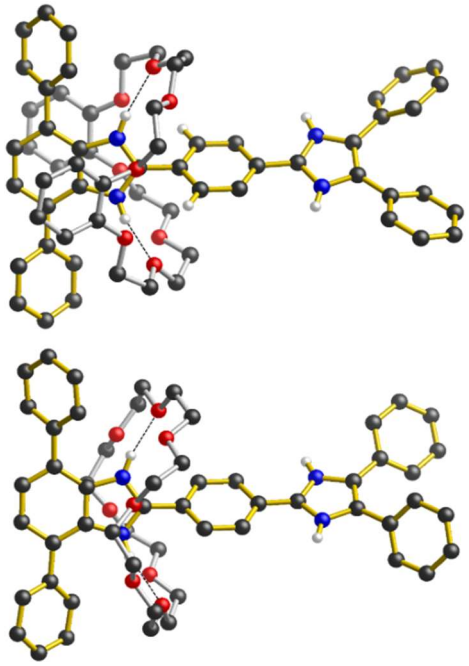

*Figure 3.3. Ball-and-stick representations[11] of the single-crystal X-ray structures of (top to bottom) [**2**-H_2⊂**DB24C8**]$^{2+}$ and [**2**-H_2⊂**24C8**]$^{2+}$. Color key: black = carbon, blue = nitrogen, red = oxygen; axle = gold bonds, wheel = silver bonds.*

3.1.2.4 Molecular Shuttling

In either the neutral or dicationic state, these new unsymmetrical [2]rotaxanes, contain two distinct recognition sites. This results in a competition between the two sites for the binding of the single macrocyclic wheel and leads to the *to and fro* motion described as molecular shuttling. As an example of this process, the two translational isomers (co-conformations) of the dicationic species [**2**-H_2⊂**24C8**]$^{2+}$ and their interconversion are shown in Fig. 3.4. The co-conformation with the **24C8** macrocycle interacting with the T-shaped recognition site is more favorable, *vide infra*.

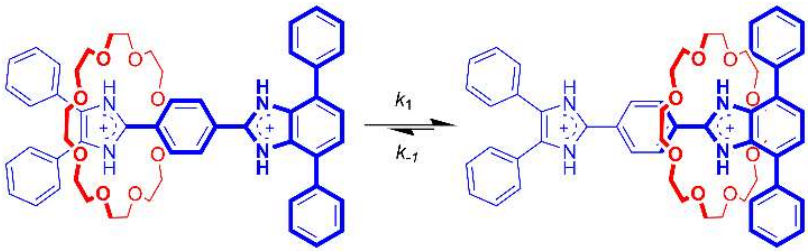

*Figure 3.4. Interconversion of the co-conformations of the [2]rotaxane molecular shuttle [**2**-H_2⊂**24C8**]$^{2+}$. The **24C8** macrocyclic wheel can occupy either of the two recognition sites; T-shaped benzimidazolium or Y-shaped imidazolium.*

The shuttling rates for the neutral species were difficult to determine as the exchange (shuttling) rate is fast on the NMR timescale and only a single set of resonances was observed for each co-conformation – *e.g.* two NH resonances representing an average of free and complexed sites for each of the T- and Y-shaped sites; see Fig. 3.1. Even at the lowest temperature accessible (183 K in CD_2Cl_2 for [**2**⊂**24C8**]), only broad signals for the free and complexed NH peaks could be observed; the limiting chemical shifts could not be determined. Thus, only a lower limit for the shuttling rates of *ca.* 1.0 x 10^6 s^{-1} at 298 K could be estimated from this data (see section 3.2.11). This is however, comparable to rates previously observed for H-shaped rotaxanes containing two similar T-shaped recognition sites.[8a] The distribution between the co-conformations (Y:T) for these neutral species was determined by using the NH chemical shifts observed for free axle **2** and a model, H-shaped rotaxane (see section 3.2.12). Thus, for the neutral [2]rotaxane molecular shuttles [**2**⊂**DB24C8**] and [**2**⊂**24C8**], the co-conformation with the macrocycle occupying the Y-shaped recognition site was preferred; Y:T, 77:23 and 69:31 respectively.

Since interconversion was observed to be slow on the NMR timescale exchange for the dicationic [2]rotaxanes, the shuttling rates could be determined directly by performing EXSY[12] experiments in CD_3CN at 298 K (see section 3.2.13). Both of the [2]rotaxanes exhibit a higher rate of wheel shuttling toward complexation with the T-shaped site (k_1 = 0.67 s^{-1} for [**2**-H_2⊂**DB24C8**]$^{2+}$ and k_1 = 5.66 s^{-1} for [**2**-H_2⊂**24C8**]$^{2+}$) than toward the Y-shaped site (k_{-1} =

0.26 s^{-1} for [**2**-H_2⊂**DB24C8**]$^{2+}$ and k_{-1} = 1.11 s^{-1} for [**2**-H_2⊂**24C8**]$^{2+}$). This can be understood by rationalizing that the stronger non-covalent interactions between the T-shaped site and the macrocyclic rings results in an increase in the barrier to motion of the wheels toward the Y-shaped site; *i.e.* stronger non-covalent interactions have to be broken to facilitate shuttling. The preferred location of the wheel was determined by integration of well resolved resonances (*a,b* for [**2**-H_2⊂**24C8**]$^{2+}$ and *j,k* for [**2**-H_2⊂**DB24C8**]$^{2+}$) from the respective ^{1}H NMR spectra. For the dicationic [2]rotaxane molecular shuttles [**2**-H_2⊂**DB24C8**]$^{2+}$ and [**2**-H_2⊂**24C8**]$^{2+}$, it was found that the co-conformation with the macrocycle occupying the T-shaped recognition site was preferred; Y:T, 32:68 and 24:76 respectively – the reverse of the trend observed for the neutral species.

Since solvent polarity is well known to have a profound effect on the π-stacking between aromatic rings,[13] N^+···O ion-dipole interactions and the degree of hydrogen bonding,[14] it was of interest to study the effect of solvent polarity on these new [2]rotaxane molecular shuttles. Accordingly, ^{1}H NMR spectra were recorded for [**2**-H_2⊂**DB24C8**]$^{2+}$ and [**2**-H_2⊂**24C8**]$^{2+}$ in a range of solvents from non-polar to highly polar (see section 3.2.14). The relative abundance of each co-conformer was then determined by integration of peaks related to proton *k* on the crown ether and *b* on the axle; the data summarized in Table 3.1, verifies that solvent polarity is an effective method to tune the ratio of these isomers in solution. The observed trend indicates that: 1) the interaction of the crown ether wheel with the T-shaped benzimidazolium site is more favorable in less polar solvents, 2) the non-covalent interactions between both of the recognition sites and the wheels are reduced by competition with the solvent, but the interactions with the benzimidazolium unit decrease to a larger degree than those with the imidazolium unit, 3) in the most polar solvent, DMSO, the electron-rich crown ether wheels actually prefers to reside at the imidazolium recognition

site. In this case, it is likely that DMSO actually out competes the crown ether for the T-shaped site resulting in the observed preference reversal.

*Table 3.1. Ratios of co-conformational isomers as a function of solvent polarity for the dicationic [2]rotaxane molecular shuttles [**2**-H_2⊂**DB24C8**]$^{2+}$ and [**2**-H_2⊂**24C8**]$^{2+}$.*

Solvent	ε[a]	Ratio of translational isomers Y:T[b]	
		[**2**-H_2⊂**24C8**]$^{2+}$	[**2**-H_2⊂**DB24C8**]$^{2+}$
C_6D_6	2.3	- [c]	5:95
$CDCl_3$	4.8	3:97	5:95
CD_2Cl_2	9.1	4:96	6:94
CD_3OD	32.6	14:86 [d]	20:80
CD_3NO_2	35.8	23:77	21:79
CD_3CN	37.5	24:76	32:68
$(CD_3)_2SO$	46.7	55:45	60:40

[a] Dielectric constants taken from reference.[15] [b] From integration of ^{1}H NMR data at 298 K. Errors estimated to be less than 5%. [c] Rotaxane was not soluble. [d] Peaks related to aliphatic protons on **24C8** were used to determine the ratio.

Finally, the reversal of the stability for the T- versus Y-shaped recognition sites towards binding a crown ether upon protonation/deprotonation can be used to design a pH sensitive, bistable molecular shuttle – an interlocked molecular switch driven by acid/base chemistry.[3c,3d] For example in CD_2Cl_2, the neutral [2]rotaxane, [**2**⊂**DB24C8**], prefers a co-conformation in which the **DB24C8** macrocycle occupies the Y-shaped, imidazole recognition site 77% of the time, but upon protonation the thermodynamic preference is reversed and the macrocycle prefers to occupy the T-shaped, benzimidazolium recognition site 94% of the time. This is summarized schematically in Fig. 3.5.

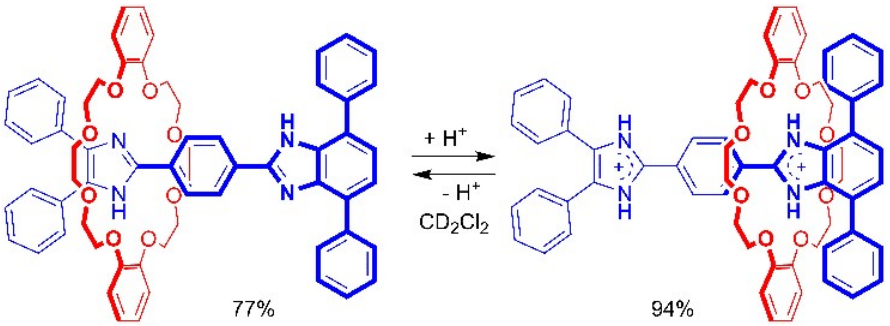

*Figure 3.5. Acid-base switching of a bistable, [2]rotaxane molecular shuttle between the neutral [**2**⊂**DB24C8**] and diationic [**2**-H_2⊂**DB24C8**]$^{2+}$ versions.*

3.1.3 Conclusions

Rigid and compact, bistable [2]rotaxanes can be constructed by combining T-shaped benzimidazolium and Y-shaped imidazolium recognition sites on a single axle with 24-membered crown ether wheels. The neutral forms, [**2**⊂**DB24C8**] and [**2**⊂**24C8**], undergo rapid shuttling of the macrocyclic wheel between the two recognition sites and it was determined that the interactions between the Y-shaped, imidazole unit and the macrocycles is most favorable. [**2**-H_2⊂**DB24C8**]$^{2+}$ and [**2**-H_2⊂**24C8**]$^{2+}$ can be prepared by protonation of the neutral species and both of these dications undergo much slower shuttling due to an increased barrier to the translational motion. For these charged systems, the preference for a particular co-conformation is dependent on the polarity of the solvent. In particular, for less polar solvents (*e.g.* CD_2Cl_2), interaction between the T-shaped benzimidazolium site and crown ether is favored almost exclusively. This correlation between co-conformer preference (Y versus T) and protonation state (neutral versus dicationic) allowed us to develop a new acid-base driven MIM switch.

3.2 Experimental

3.2.1 General Comments

4-(4,5-Diphenyl-1*H*-imidazol-2-yl)benzaldehyde, **1**, was synthesized according to the literature procedure.[17] All other chemicals were obtained from Sigma-Aldrich and used without further purification. Solvents were dried using an Innovative Technologies Solvent Purification System. Deuterated solvents were obtained from Cambridge Isotope Laboratories and used as received. ^{1}H, ^{13}C and 2D NMR spectra were recorded on a Brüker Avance 500 instrument with a working frequency of 500.1 MHz for ^{1}H and 125.7 MHz for ^{13}C; chemical shifts are quoted in ppm relative to tetramethylsilane using the residual solvent peak as a reference. ^{1}H-^{1}H NOESY and ^{1}H-^{13}C HMQC experiments were used to assign NMR resonances. Thin layer chromatography was performed using Teledyne Silica gel-60 F254 plates and viewed under UV light. Column chromatography was performed using Silicycle Ultra-Pure Silica Gel (230 – 400 mesh). High resolution mass spectra (HR-MS) were performed on a Micromass LCT electrospray ionization time-of-flight spectrometer. Melting points were recorded on a Stanford Research Systems, Opti Melt MPA100 instrument. Infrared spectra were recorded on a Bruker Alpha FT-IR spectrometer in the range of 4000–400 cm^{-1}.

3.2.2 Synthesis of [1-H][BF_4]

Tetrafluoroboric acid diethyl ether complex (185 µL, 1.36 mmol) was added to a solution of the 2,4,5-trisubstituted imidazole, **1** (400 mg, 1.23 mmol) in THF (10 mL). The mixture was stirred for 10 min and then 10 mL of ether was added and the solution stirred for 20 min resulting in a solid which was filtered, washed with more ether and dried under vacuum. Yield: 446 mg, 87%; MP 252-257 °C; ^{1}H NMR (CD_3CN, 500 MHz, 294 K): δ (ppm) = 12.53 (s, 2H), 10.13 (s, 1H), 8.19 (d, 4H, *J* = 1.5 Hz), 7.54-7.51 (m, 10H); ^{13}C NMR (CD_3CN, 125 MHz, 294 K): δ (ppm) = 192.8, 143.8, 139.6, 131.3, 131.2, 131.0, 130.1, 129.6, 128.9, 128.1,

127.4; IR (neat) = 3281, 1702, 1646, 1602, 1443, 1219, 1176, 1024, 832, 767, 732, 693, 518, 491 cm^{-1}; Anal. Calcd for $C_{22}H_{18}BF_4N_2O$: C, 63.95; H, 4.39; N, 6.78; Found: C, 62.95; H, 4.25; N, 6.52.

3.2.3 Synthesis of [2⊂DB24C8]

[**1**-H][BF_4] (200 mg, 0.48 mmol) and dibenzo-24-crown-8 ether (323 mg, 0.72 mmol) were solubilized in chloroform (20 mL). The resulting mixture was stirred for 15 min, then 1,2-diamino-3,6-di(4′-*t*-butylphenyl)benzene (187 mg, 0.72 mmol) and $ZrCl_4$ (11 mg, 0.048 mmol) were added. The reaction was allowed to stir at room temperature for 24 h and the solvent was removed in vacuum. The crude product was dissolved in CH_3CN (10 mL). The mixture was refluxed with 1 mL of triethylamine for 1 h and then cooled to room temperature. The off-white solid was filtered, washed with CH_3CN and air dried. Yield: 310 mg, 63%; MP 263-267 °C; ^{1}H NMR ($CDCl_3$, 500 MHz, 299 K): δ (ppm) = 10.67 (s, 1H), 10.09 (s, 1H), 8.64 (d, 2H, *J* = 8.5 Hz), 8.41 (d, 2H, *J* = 8.5 Hz), 8.35 (d, 2H, *J* = 7.0 Hz), 7.77 (d, 2H, *J* = 7.0 Hz), 7.59 (d, 2H, *J* = 7.5 Hz), 7.55 (d, 1H, *J* = 8.0 Hz), 7.40 (t, 2H, *J* = 7.5 Hz), 7.36 (t, 2H, *J* = 7.5 Hz), 7.31-7.28 (m, 5H), 7.20 (t, 2H, *J* = 7.5 Hz), 7.15 (t, 2H, *J* = 7.5 Hz), 7.09 (t, 2H, *J* = 7.5 Hz), 6.97-6.95 (m, 4H), 6.89-6.87 (m, 4H), 4.09-3.66 (m, 8H), 3.65 (t, 8H, *J* = 4.0 Hz), 2.86-2.82 (m, 4H), 2.80-2.77 (m, 4H); ^{13}C NMR (CD_2Cl_2, 125 MHz, 295 K): δ (ppm) = 152.5, 148.8, 146.4, 142.7, 138.9, 138.8, 137.8, 136.1, 133.6, 132.0, 131.9, 131.1, 129.7, 129.3, 128.8, 128.6, 128.5, 128.3, 128.2, 127.8, 127.6, 127.4, 126.7, 125.4, 123.3, 121.8, 121.2, 112.2, 69.7, 69.0, 68.7; IR (neat) = 3437, 3351, 2920, 1592, 1502, 1449, 1248, 1211, 1122, 1037, 923, 873, 764, 743, 693, 548 cm^{-1}; HR-MS (ESI-ToF) *m/z*: calcd for $[M+H]^+$, $[C_{64}H_{61}N_4O_8]^+$, 1013.4489; found 1013.4507.

3.2.4 Synthesis of [2⊂24C8]

The procedure is the same as stated above for **[2⊂DB24C8]** but using [**1**-H][BF_4] (200 mg, 0.48 mmol) and 24-crown-8 ether (254 mg, 0.72 mmol) in 10 mL of chloroform. As a result, an off-white solid was collected. Yield: 260 mg, 59%; MP 287-292 °C; ^{1}H NMR (CD_2Cl_2, 500 MHz, 296 K): δ (ppm) = 11.20 (s, 1H), 10.40 (s,1H), 8.47 (d, 2H, *J* = 8.5 Hz), 8.37 (d, 2H, *J* = 8.5 Hz), 8.18 (d, 2H, *J* = 8.5 Hz), 7.74 (d, 4H, *J* = 7.5 Hz), 7.60-7.52(m, 5H), 7.46 (t, 2H, *J* = 7.5 Hz), 7.43-7.36 (m, 3H), 7.34-7.30 (m, 4H), 7.24 (t, 2H, *J* = 7.5 Hz), 3.37-3.28 (m, 32H); ^{13}C NMR (CD_2Cl_2, 125 MHz, 297 K): δ (ppm) = 153.0, 146.2, 142.9,139.3,139.2, 138.3, 136.3, 133.7, 132.5, 132.4, 131.6, 129.9, 129.6, 128.9, 128.8, 128.7, 128.5, 128.4, 128.2, 128.0, 127.9, 127.8, 127.8, 127.5, 126.8, 125.5, 123.4, 122.2, 70.1; IR (neat) = 3247, 2871, 1481,1449, 1352, 1260, 1093, 1028, 936, 861,797, 757, 694 cm^{-1}; Anal. Calcd for $C_{56}H_{60}N_4O_8$: C, 73.34; H, 6.59; N, 6.11; Found: C,74.75;H, 6.86; N, 6.25.

3.2.5 Synthesis of [2-H_2⊂DB24C8][BF_4]$_2$

Tetrafluoroboric acid diethyl ether complex (57 μL, 0.42 mmol) was added to a solution of [**2⊂DB24C8**] (100 mg, 0.19 mmol) in CH_3CN (10 mL). After 10 min stirring at room temperature 20 mL ether was added. The white tetrafluoroborate salt precipitated, was filtered, washed with ether and air dried. Yield: 215 mg, 92%; MP 280 °C [decomp.]; ^{1}H NMR (CD_2Cl_2, 500 MHz, 294 K): δ (ppm) = 13.24 (s, 2H), 13.00 (s, 2H), 8.75 (d, 2H, *J* = 8.5 Hz), 8.59 (d, 2H, *J* = 8.5 Hz), 7.72-7.70 (m, 4H), 7.64-7.61 (m, 4H), 7.58-7.52 (m, 12 H), 7.05 (s, 2H), 6.62-6.60 (m, 4H), 6.28-6.26 (m, 4H), 3.85 (t, 4H, *J* = 10.5 Hz), 3.69-3.66 (m, 4H), 3.60-3.3.57 (m, 4H), 3.43-3.36 (m, 8H), 3.15-3.12 (m, 4H); ^{13}C NMR (CD_2Cl_2, 125 MHz, 293 K): δ (ppm) = 150.2,147.9, 143.8, 135.9, 133.2, 130.8, 130.6, 130.2, 129.9, 129.6, 129.2, 129.1, 129.0, 129.9, 127.8, 126.8, 126.6, 125.7, 125.7, 121.1, 112.9,70.5, 70.1, 68.5; IR (neat) = 3068, 2934, 2875, 1637, 1593, 1502, 1453, 1352, 1251, 1208, 1050, 947, 852, 748, 699, 593, 519 cm^{-1}; HR-MS (ESI-ToF) *m/z*: calcd for [M-2BF_4]$^+$, [$C_{64}H_{62}N_4O_8$]$^{2+}$, 507.2278; found 507.2186.

3.2.6 Synthesis of [2-H_2⊂24C8][BF_4]$_2$

The procedure is the same as stated above for [**2**-H_2⊂**DB24C8**][BF_4]$_2$ but using [**2**⊂**24C8**] (200 mg, 0.22 mmol) in 10 mL of CH_3CN. As a result, a white solid was collected. Yield: 226 mg, 95%; MP 190 °C [decomp]; ^{1}H NMR (CD_2Cl_2, 500 MHz, 297 K): δ (ppm) = 13.00 (s, 2H), 12.89 (s,2H), 8.50 (d, 2H, *J* = 8.5 Hz), 8.42 (d, 2H, *J* = 8.5 Hz), 7.78 (d, 4H, *J* = 7.0 Hz), 7.69 (s, 2H), 7.65-7.63 (m, 4H), 7.59 (t, 4H, *J* = 7.5 Hz), 7.54-7.46 (m, 8H), 3.19-3.15 (m, 16H), 2.99-2.95 (m, 16H); ^{13}C NMR (CD_2Cl_2, 125 MHz, 299 K): δ (ppm) = 150.9, 143.8, 136.5, 133.3, 130.7, 130.5, 129.9, 129.7, 129.6, 129.6, 129.1, 128.9, 128.6, 128.4, 127.8, 126.8, 126.6, 125.5, 71.0, 70.5; IR (neat) = 3112, 2886, 1637, 1488, 1350, 1259, 1088, 951, 847, 787, 773, 760, 697, 520 cm^{-1}; Anal. Calcd for $C_{56}H_{62}B_2F_8N_4O_8$: C, 61.55; H, 5.72; N, 5.13; Found: C, 59.76; H, 5.81; N, 5.38.

3.2.7 Synthesis of [2]

1,2-Diamino-3,6-di(4′-*t*-butylphenyl)benzene (120 mg, 0.46 mmol) and $ZrCl_4$ (7 mg, 0.031 mmol) were added to a solution of **1** (100 mg, 0.31 mmol) in CH_2Cl_2 (25 mL). After 24 hours stirring at room temperature, the solvent was removed in vacuum. The crude product was dissolved in CH_3CN (10 mL). The mixture was refluxed with 1 mL of triethylamine for 1 h and then cooled to room temperature. The pale yellow solid was filtered, washed with CH_3CN and air dried. Yield: 145 mg, 80%; MP 303-307 °C; ^{1}H NMR (DMSO-d_6, 500 MHz, 296 K): δ (ppm) = 12.86 (s, 1H), 12.73 (s, 1H), 8.42 (d, 2H, *J* = 8.5 Hz), 8.23 (d, 2H, *J* = 8.5 Hz), 8.19 (d, 2H, *J* = 8.5 Hz), 7.61-7.50 (m, 10H), 7.49-7.45 (m, 3H),7.43-7.40 (m, 2H), 7.32 (m, 3H, *J* = 7.5 Hz), 7.24 (t, 3H, *J* = 7.5 Hz); ^{13}C NMR (DMSO-d_6, 125 MHz, 296 K): δ (ppm) = 152.7, 145.4, 142.6, 138.7, 138.4, 138.0, 135.5, 134.1, 131.8, 131.4, 130.3, 130.0, 129.4, 129.4, 129.2, 129.2, 129.0, 128.8, 128.7, 128.4, 128.2, 128.0, 127.6, 127.1, 125.8, 125.6, 123.8, 121.8; IR (neat) = 3583, 1649, 1486, 1053765, 696, 518 cm^{-1}; HR-MS (ESI-ToF) *m/z*: calcd for $[M+H]^+$, $[C_{40}H_{29}N_4]^+$, 565.2392; found 565.2417.

3.2.8 Synthesis of [2-H_2][BF_4]$_2$

The procedure is the same as stated above for [**2**-H_2⊂**DB24C8**][BF_4]$_2$ but using **2** (70 mg, 0.12 mmol) and tetrafluoroboric acid diethyl ether complex (37 μL, 0.27 mmol) in 5 mL of CD_3CN. As a result, a yellow solid was collected. Yield: 71 mg, 77%; MP 215-219 °C; ^{1}H NMR (CD_3CN, 500 MHz, 295 K): δ (ppm) = 12.69 (br, 4H), 8.30 (d, 2H, *J* = 8.5 Hz), 8.26 (d, 2H, *J* = 8.5 Hz), 7.78-7.77 (m, 6H), 7.67 (t, 4H, *J* = 7.5 Hz), 7.60 (t, 2H, *J* = 7.5 Hz), 7.56-7.50 (m, 10H); ^{13}C NMR (CD_3CN, 125 MHz, 295 K): δ (ppm) = 150.8, 143.2, 136.2, 131.8, 131.3, 131.3, 131.3, 130.9, 130.1, 129.1, 128.9, 128.5, 127.7, 127.1, 126.2; IR (neat) = 3028, 2265, 1644, 1487, 1419, 1064, 1052, 1008, 849, 760, 696, 516 cm^{-1}; HR-MS (ESI-ToF) *m/z*: calcd for [M-$^2BF_4$]$^+$, [$C_{40}H_{29}N_4$]$^{2+}$, 283.1230; found *m/z* = 283.1183.

3.2.9 Schematics for the Synthetic Procedures

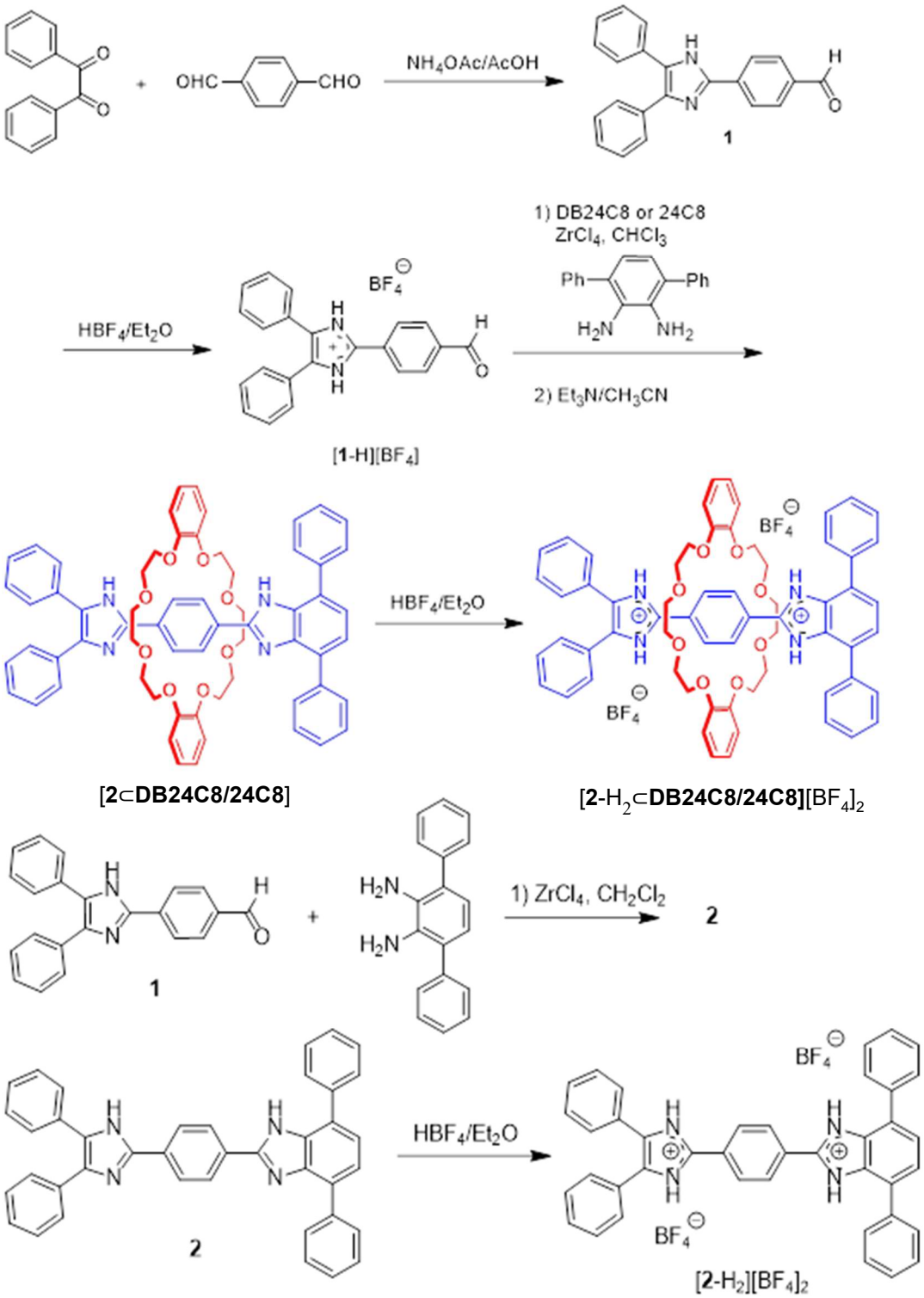

Figure 3.6. Summary of the synthetic procedures used in chapter 3.

3.2.10 2D-NMR Studies

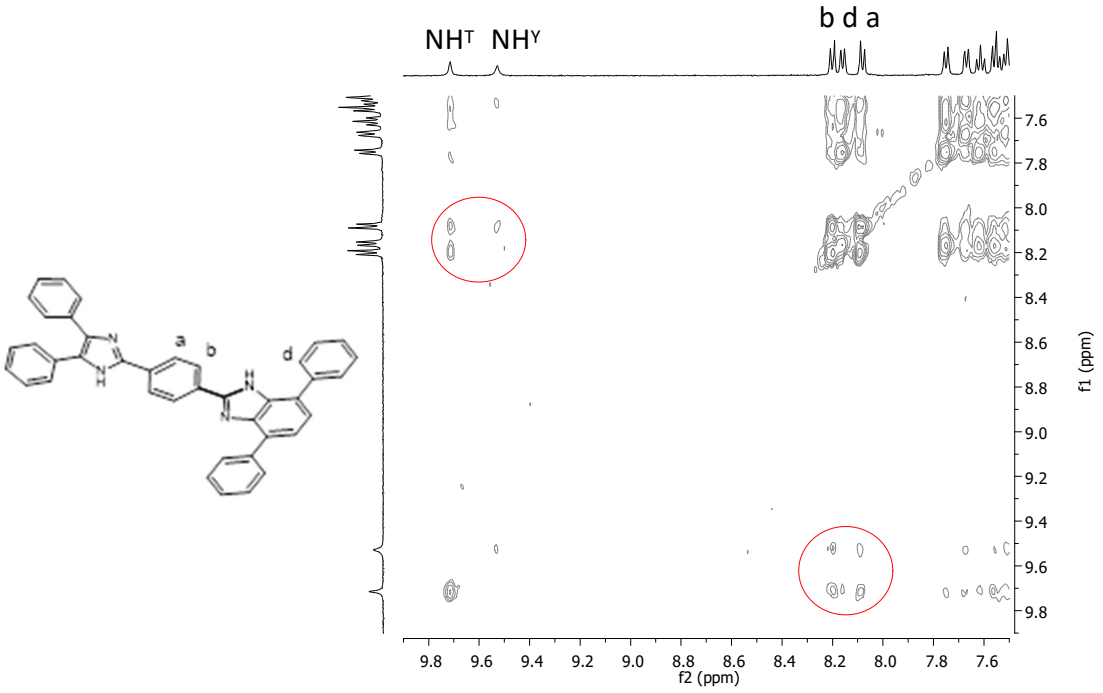

*Figure 3.7. Partial 2D-NOESY spectrum of [**2**] (500 MHz, CD_2Cl_2, 296 K, τ_m= 800 ms).*

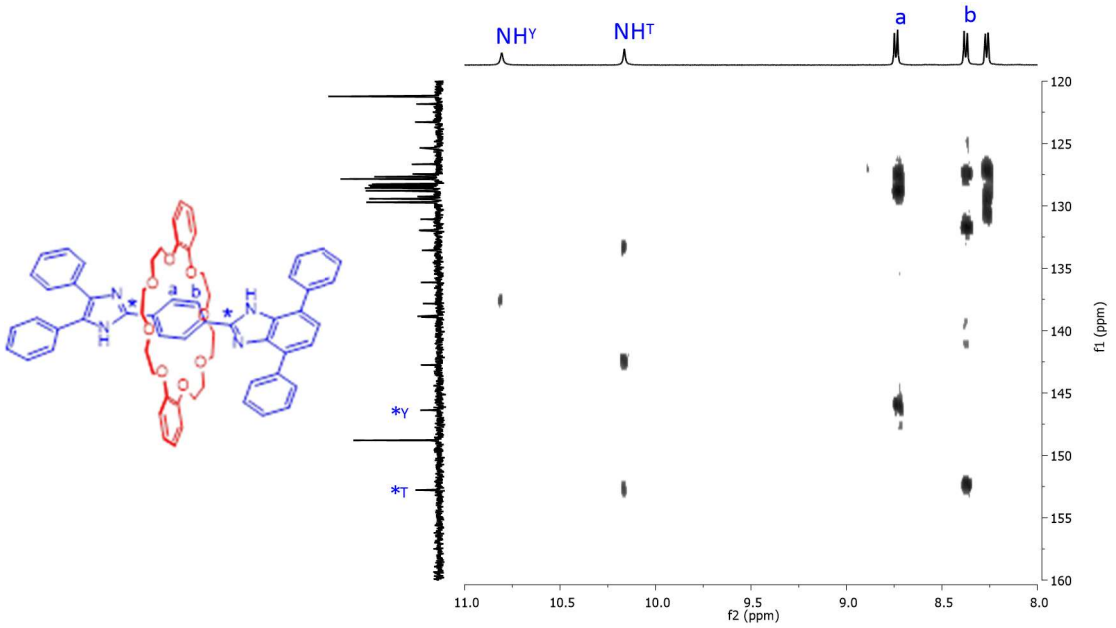

*Figure 3.8. Partial 2D-HMBC spectrum of [**2⊂DB24C8**] (500 MHz, CD_2Cl_2, 296 K).*

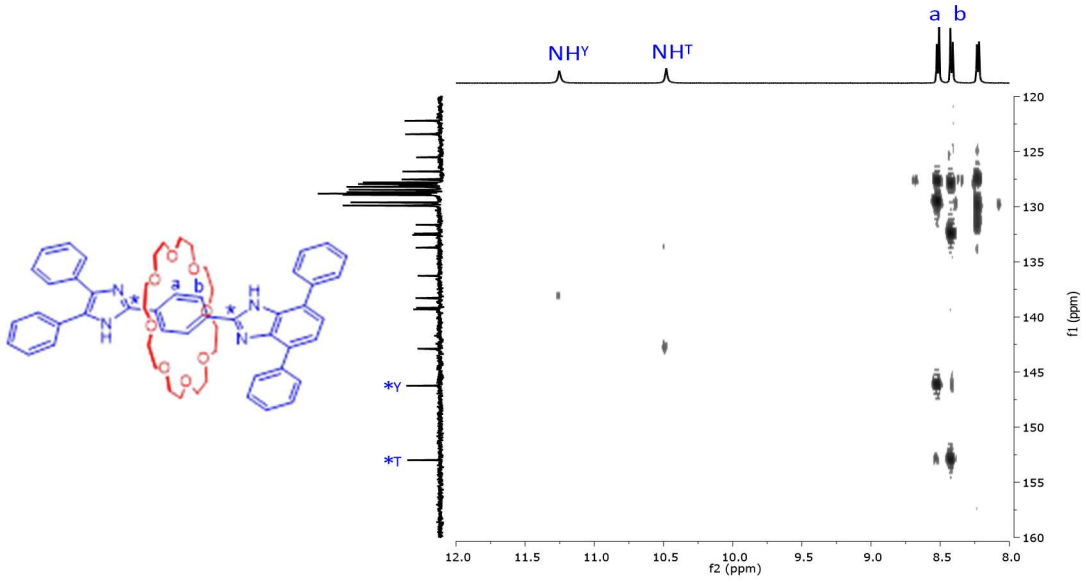

*Figure 3.9. Partial 2D-HMBC spectrum of [**2⊂24C8**] (500 MHz, CD_2Cl_2, 294 K).*

3.2.11 Co-conformation Distributions

*Table 3.2. Determination of the %Y and %T co-conformation distributions for neutral rotaxanes [**2**⊂**DB24C8**] and [**2**⊂**24C8**] using NH chemical shifts (δ, ppm) data.*

Compound	Average δ (NH)[a]	Limiting (*free*) δ (NH)	Limiting (*complexed*) δ (NH)	%T - %Y
H-shaped axle (see Figure 3.10)	-	9.75[b]	-	-
H-shaped **24C8** rotaxane (see Figure 3.10)	10.84	-	(11.93)[c]	-
H-shaped **DB24C8** rotaxane (see Figure 3.10)	10.70	-	(11.65)	-
T-Y axle, **2** (see Figure 3.1)	-	9.72 (T) 9.58 (Y)	-	-
Y-T rotaxane [**2**⊂**24C8**] (see Figure 3.1)	10.40 (T) 11.20 (Y)	-	-	**31 (T)** **69 (Y)**
Y-T rotaxane [**2**⊂**DB24C8**] (see Figure 3.1)	10.16 (T) 10.82 (Y)	-	-	**23 (T)** **77 (Y)**

[a] In CD_2Cl_2, at a concentration of 1.0 x 10^{-3} *M*. [b] Values taken from reference [17]. [c] Values in parentheses are those calculated from a combination of observed spectral values using model compounds; Fig-3.10. For example, for the first entry (11.93), the limiting chemical shift value for the free NH of the axle is 9.75 ppm and the averaged value for the 50:50 distribution for the symmetrical H-shaped [2]rotaxane is 10.84 ppm. Thus, it can calculated that the complexed value for the same rotaxane must be 11.93 ppm; *i.e.* +1.09 ppm downfield from the exchanged average signal, since the free value is -1.09 ppm upfield. These values can then be used as estimates of the free and complex chemical shift values for a macrocycle when it resides at the T-shaped recognition site in the new Y-T rotaxanes. These limiting values can then be compared to the position of the weighted average values for the new rotaxanes and the %T contribution determined; the %Y value is then simply determined by difference.

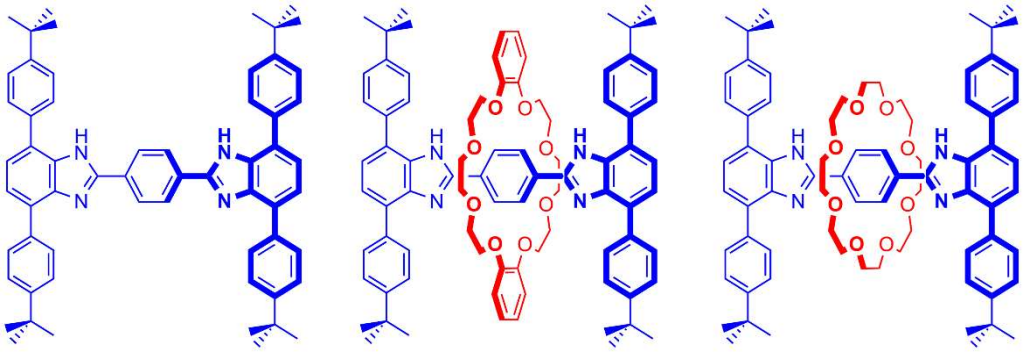

Figure 3.10. H-shaped axle and [2]rotaxane molecular shuttles used as models to estimate the limiting NH chemical shifts for the new Y-T molecular shuttles.

3.2.12 Variable Temperature ^{1}H NMR Study of [2⊂24C8]

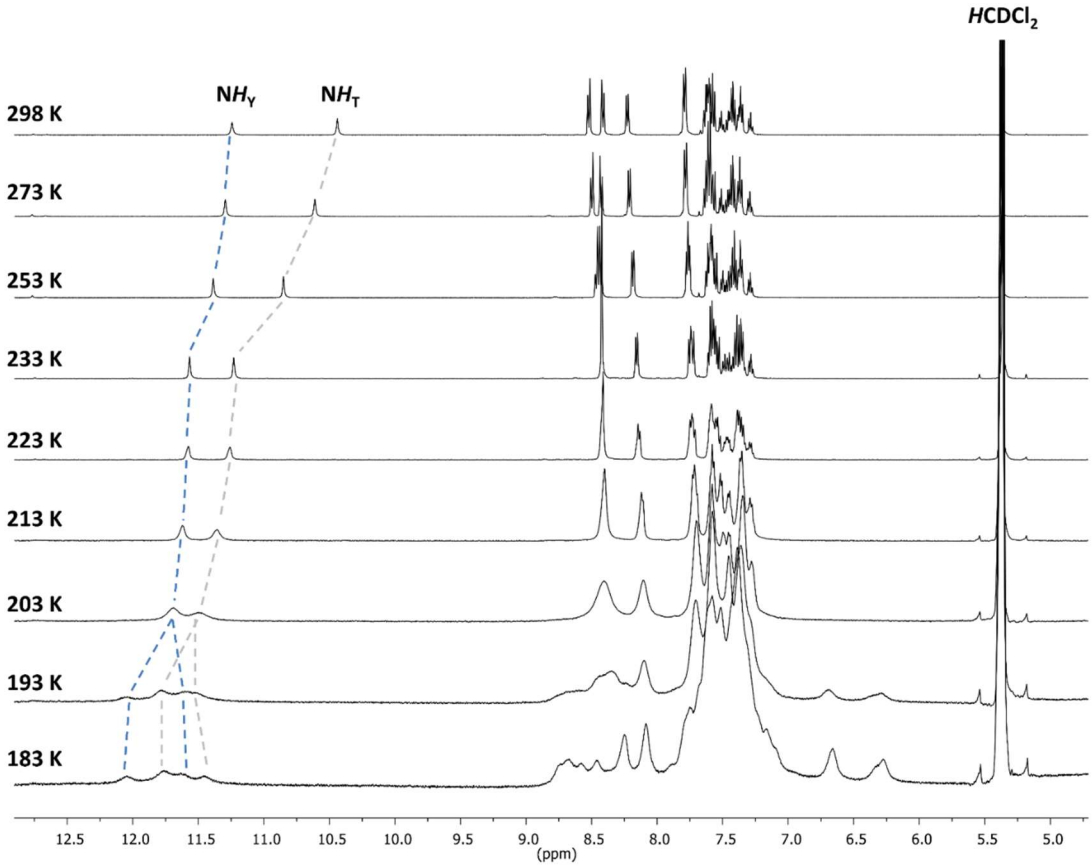

*Figure 3.11. Variable temperature ^{1}H NMR spectra for [**2⊂24C8**]*

3.2.13 2D-EXSY NMR Studies

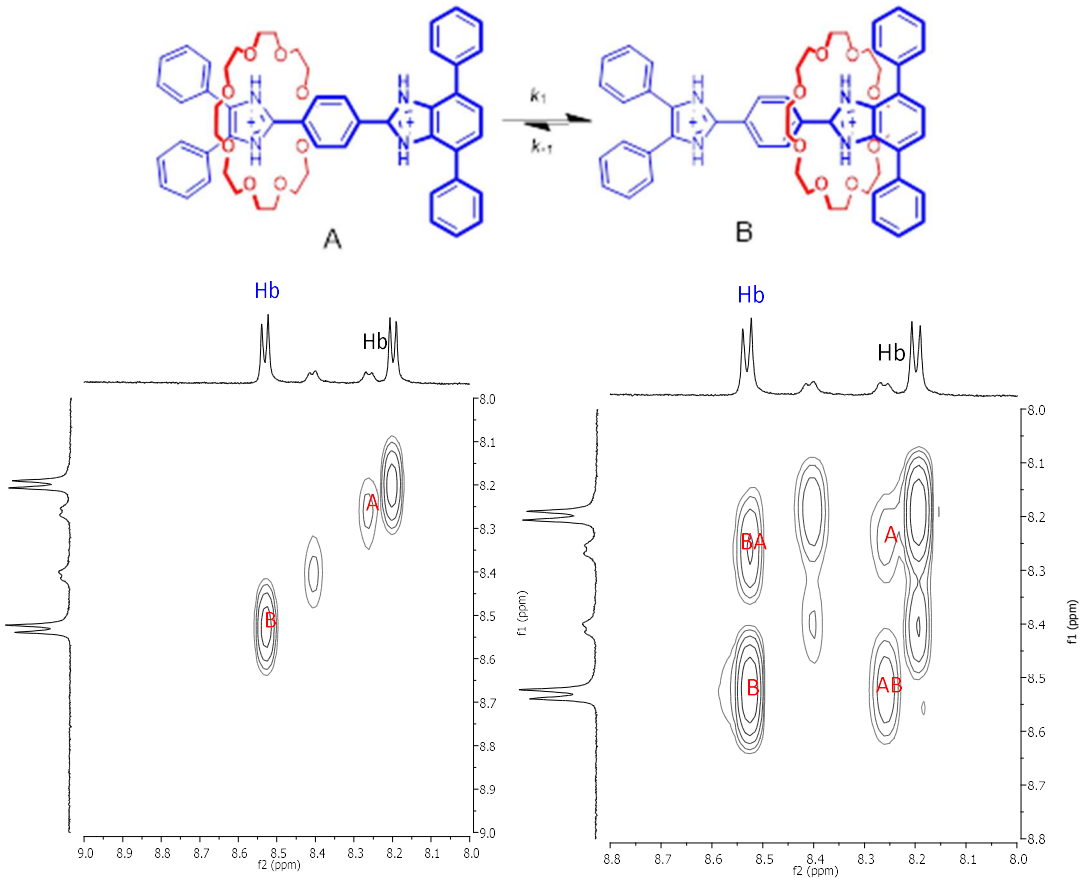

*Figure 3.12. Partial 2D-EXSY spectrum of [**2**-H_2⊂**24C8**]$^{2+}$ in CD_3CN (500 MHz) a) T = 292 K and τ_m = 5 ms; b) T = 296 K and τ_m = 500 ms.*

τ_m (ms)	I_{AA}	I_{BB}	I_{AB}
5	2319947.00	9929019.75	-
500	479584.25	5494293.00	1292090.00

K_1 = 5.664 s^{-1}, K_{-1} = 1.113 s^{-1}

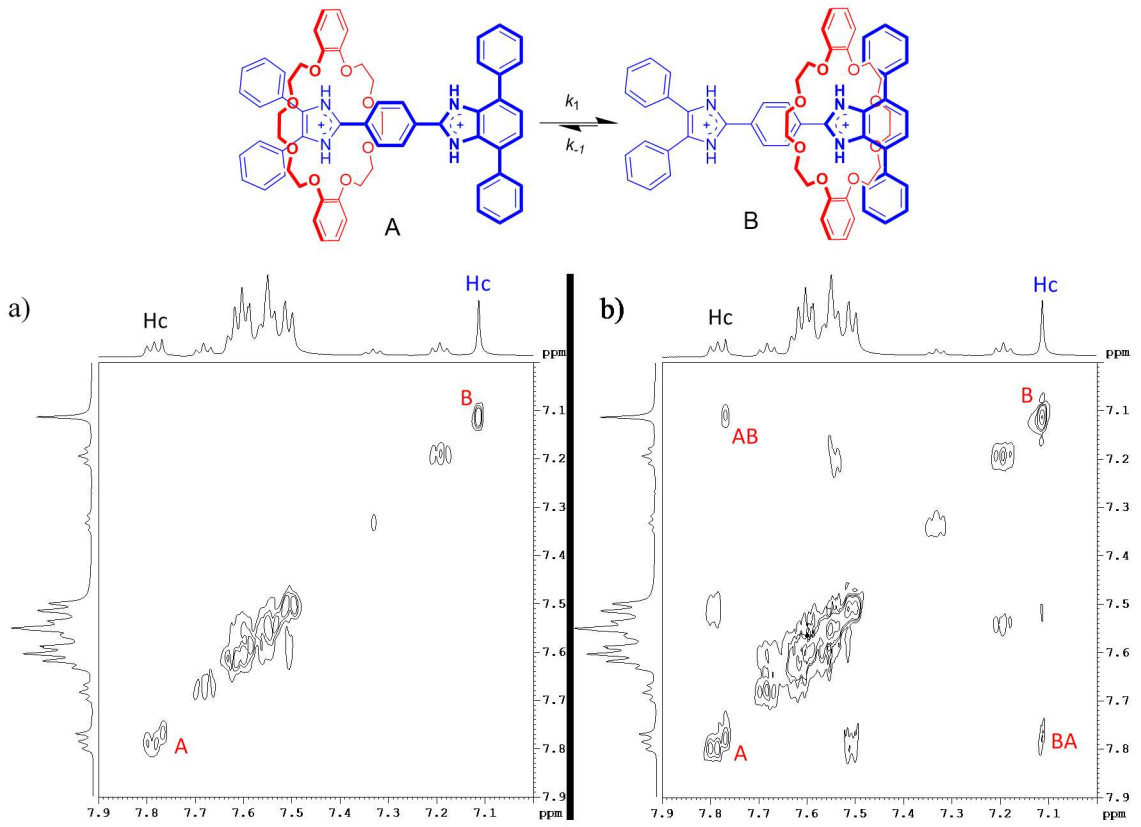

*Figure 3.13. Partial 2D-EXSY spectrum of [**2**-H_2⊂**DB24C8**]$^{2+}$ in CD_3CN (500 MHz) a) T = 295 K and τ_m = 5 ms; b) T = 295 K and τ_m = 500 ms.*

τ_m (ms)	I_{AA}	I_{BB}	I_{AB}	I_{BA}
5	2319947.00	9929019.75	-	-
500	70353566.00	358916919.00	35595481.00	30487959.00

K_1 = 0.666 s^{-1}, K_{-1} = 0.260 s^{-1}

3.2.14 ^{1}H NMR Studies in Various Solvents

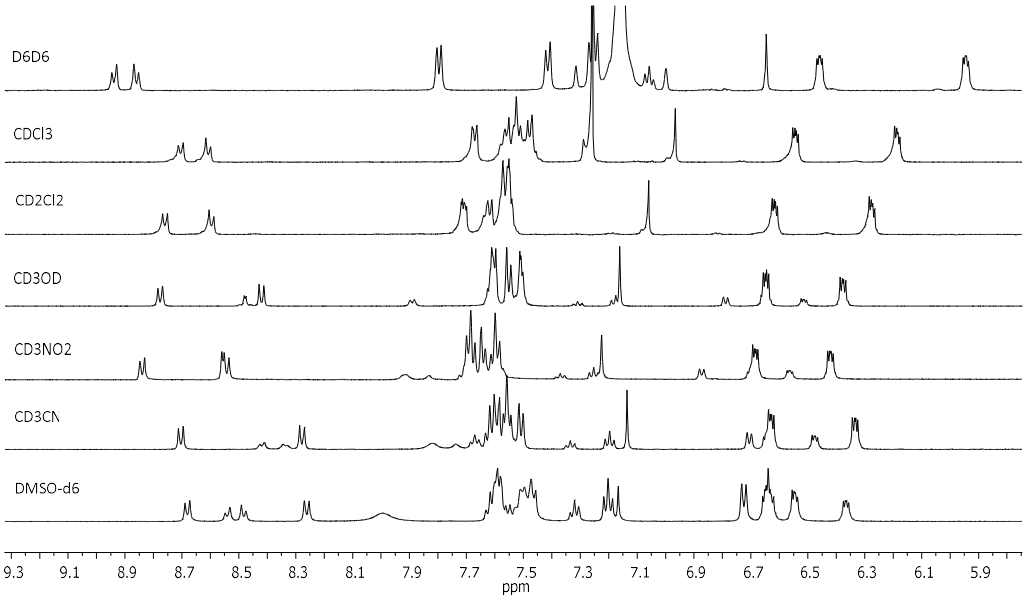

*Figure 3.14. Stacked ^{1}H NMR spectrum of [**2**-H_2⊂**DB24C8**]$^{2+}$ in various solvents*

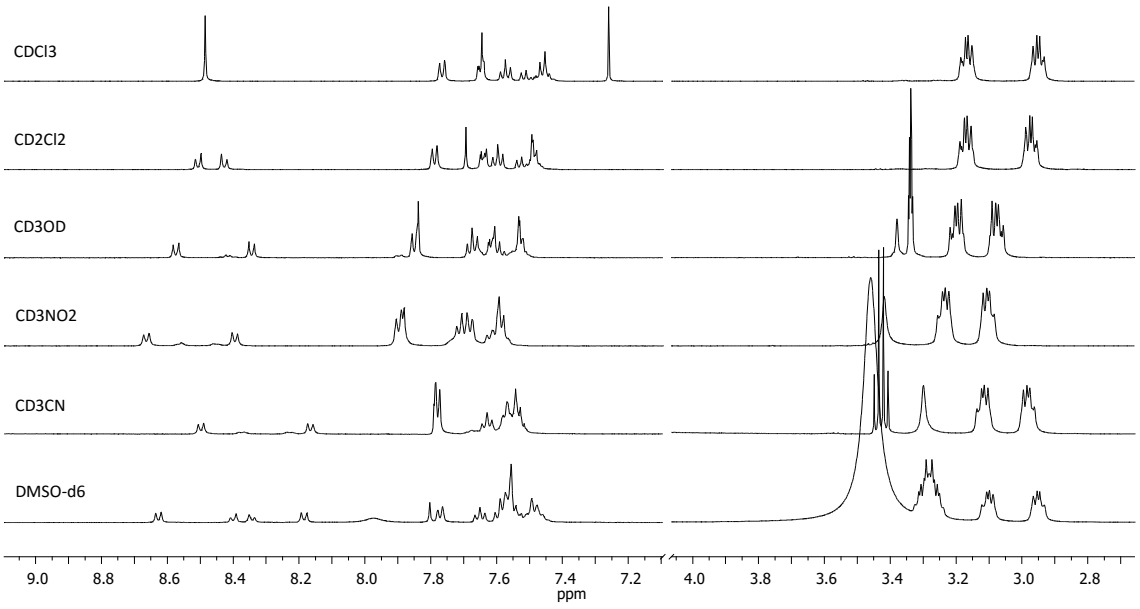

*Figure 3.15. Stacked ^{1}H NMR spectrum of [**2**-H_2⊂**24C8**]$^{2+}$ in various solvents*

3.2.15 Details of EXSY Experiments

All 2D-EXSY spectra were recorded on a Bruker Avance 500 MHz NMR spectrometer with τ_m = 500 and 5 ms. Shuttling rates were calculated by using the computer program EXSY CALC.[18] For the calculation, diagonal and cross-peak intensities for the exchanging NMR resonances are needed from two EXSY experiments at two different mixing times. In this work, one experiment was attained at 500 ms and the other at a very short mixing time of 5 ms.

The exchange matrix obtained by the program is shown below:

$$\begin{vmatrix} -R1 - k'1 & k'\text{-}1 \\ k'1 & -R2 - k'\text{-}1 \end{vmatrix}$$

In the matrix, k'_1 and k'_{-1} are exchange rates and R_1 and R_2 are the longitudinal relaxation rates.

3.2.16 Single-Crystal X-ray Diffraction Experiments

General: Crystals were frozen in paratone oil inside a cryoloop under a cold stream of N_2. Reflection data were collected on a Bruker APEX-II diffractometer using MoKα ([**2**-H_2⊂**DB24C8**][BF_4]$_2$) or CuKα ([**2**-H_2⊂**24C8**][BF_4]$_2$) radiation and a charge-coupled device (CCD) detector. For both data sets, decay was monitored using 50 standard data frames measured at the beginning and end of data collection. Diffraction data and unit-cell parameters were consistent with the assigned space groups. Lorentzian polarization corrections and empirical absorption corrections, based on redundant data at varying effective azimuthal angles, were applied to the data sets. The structures were solved by direct methods, completed by subsequent Fourier syntheses and refined using full-matrix least-squares methods against $|F^2|$ data. All non-hydrogen atoms were refined anisotropically and hydrogen atoms placed in idealized positions and refined using a riding model. Scattering factors and anomalous dispersion coefficients are contained in the SHELXTL program

library[19]. Details of the two structures can be obtained from the Cambridge Crystallographic Data Centre at www.ccdc.cam.ac.uk for CCDC accession numbers 1451524 and 1451525.

3.2.17 Single-Crystal X-ray Structure of [2-H_2⊂DB24C8][BF_4]$_2$

Crystals of [**2**-H_2⊂**DB24C8**][BF_4]$_2$ were of good quality. The unit cell contained two molecules of the dicationic [2]rotaxane ($C_{64}H_{62}N_4O_8$), four tetrafluoroborate anions (BF_4) and two molecules of CH_2Cl_2. The structure was solved in the triclinic space group P-1. All the non-hydrogen atoms were refined anisotropically and all the hydrogen atoms were placed in idealized positions and refined using a riding model. One of the tetrafluoroborate anions and the CH_2Cl_2 were disordered over two positions. These groups were restrained as rigid groups using SADI, DELU and SIMU commands and refined as two independent items using the PART command.

3.2.18 Single-Crystal X-ray Structure of [2-H_2⊂24C8][BF_4]$_2$

Crystals of [**2**-H_2⊂**24C8**][BF_4]$_2$ were of good quality. The unit cell contained four dicationic [2]rotaxanes ($C_{56}H_{66}N_4O_{10}$) and eight tetrafluoroborate anions (BF_4) as well as eight molecules of water. The structure was solved in the orthorhombic space group $Pna2_1$. All the non-hydrogen atoms were refined anisotropically and all the hydrogen atoms were placed in idealized positions and refined using a riding model. No restraints were required.

3.3 References

[1] a) J.-P. Sauvage, C. Dietrich-Buchecker, (eds) *Molecular Catenanes, Rotaxanes and Knots: A Journey Through the World of Molecular Topology*, Wiley-VCH, **1999**; b) C. P. Collier, G. Mattersteig, E. W. Wong, Y. Luo, K. Beverly, J. Sampaio, F. M. Raymo, J. F. Stoddart, J. R. Heath, *Science*, **2000**, *289*, 1172; c) E. K. Kay, D. A. Leigh, F. Zerbetto, *Angew. Chem. Int. Ed.* **2007**, *46*, 72; d) S. J. Loeb, *Chem. Soc. Rev.* **2007**, *36*, 226; e) V. Balzani, *Pure Appl. Chem.* **2008**, *80*, 1631;

f) M. J. Langton, P. D. Beer, *Acc. Chem. Res.***2014**, *47*, 1935; g) J. F. Stoddart, *Angew. Chem. Int. Ed.* **2014**, *53*, 11102; h) K. Zhu, S. J. Loeb, *Top. Curr. Chem.,* **2014**, *354*, 213; i) S. Erbas-Cakmak, D. A. Leigh, C. T. McTernan, A. L. Nussbaumer, *Chem. Rev*., **2015**, *115*, 10081.

[2] a) A. M. Brouwer, C. Frochot, F. G. Gatti, D. A. Leigh, L. Mottier, F. Paolucci, S. Roffia, G. W. H. Wurpel, *Science* **2001**, *291*, 2124; b) C. A. Stanier, S. J. Alderman, T. D. W. Claridge, H. L. Anderson, *Angew. Chem.* **2002**, *114*, 1847; *Angew. Chem. Int. Ed.* **2002**, *41*, 1769; c) X. Ma, H. Tian, *Chem. Soc. Rev.* **2010**, *39*, 70; d) A. C. Fahrenbach, C. J. Bruns, H. Li, A. Trabolsi, A. Coskun, J. F. Stoddart, *Acc. Chem. Res*. **2014**, 47, 482.

[3] a) R. A. Bissell, E. Cordova, A. E. Kaifer, J. F. Stoddart, *Nature* **1994**, *369*, 133; b) A. Altieri, G. Bottari, F. Dehez, D. A. Leigh, J. K. Y. Wong, F. Zerbetto, *Angew. Chem.* **2003**, *115*, 2398; c) S. J. Vella, J. Tiburcio, S. J. Loeb, *Chem. Commun*., **2007**, 4752; d) D. A. Leigh, A. R. Thomson, *Tetrahedron*, **2008**, *64*, 8411; e) A. Caballero, L. Swan, F. Zapata, P. D. Beer, *Angew. Chem. Int. Ed.,* **2014**, *53*, 11854; f) G. Ragazzon, M. Baroncini, S. Silvi, M. Venturi, A. Credi, *Nature Nanotech*., **2014**, *10*, 70; g) P. R. McGonigal, P. Deria, I. Hod, P. Z. Moghadam, A.-J. Avestro, N. E. Horwitz, I. C. Gibbs-Hall, A. K. Blackburn, D. Chen, Y. Y. Botros, W. R. Wasielewski, R. Q. Snurr, J. T. Hupp, O. K. Farha, J. F. Stoddart, *Proc. Natl. Acad. Sci. USA*, **2015**, *112*, 11161; h) S. Dong, J. Yuan, F. Huang, *Chem. Sci.,* **2014**, *5*, 247.

[4] a) J. O. Jeppesen, S. A. Vignon, J. F. Stoddart, *Chem. Eur. J.,* **2003**, *9*, 4611; b) V. Balzani, A. Credi, M. Venturi, *Chem. Soc. Rev*., **2009**, *38*, 1542; c) H. X. Deng, M. A. Olson, J. F. Stoddart, O. M. Yaghi, *Nature Chem*. **2010**, *2*, 439.

[5] N. Noujeim, K. Zhu, V. N. Vukotic, S. J. Loeb, *Org. Lett.,* **2012**, *14*, 2484.

[6] a) K. Zhu, V. N. Vukotic, S. J. Loeb, *Angew. Chem. Int. Ed*., **2012**, *51*, 2168; b) K. Zhu, V. N. Vukotic, N. Noujeim, S. J. Loeb, *Chem. Sci.,* **2012**, *3*, 3265.

[7] a) K. Zhu, C. O'Keefe, V. N. Vukotic, R. W. Schurko, S. J. Loeb, *Nature Chem*. **2015**, ***7***, 514; b) V. N. Vukotic, S. J. Loeb *Chem. Soc. Rev.* **2012**, *41*, 5896.

[8] N. Farahani, K. Zhu, N. Noujeim, S. J. Loeb, *Org. Biomol. Chem*., **2014**, 4824.

[9] a) P. R. Ashton, P. T. Glink, J. F. Stoddart, P. A. Tasker, A. J. P. White, D. J. Williams, *Chem. Eur. J.* **1996**, *2*, 729; b) S. J. Loeb, J. A. Wisner, *Chem. Commun*., **1998**, 2757. c) D. J. Mercer, J. Yacoub, K. Zhu, S. K. Loeb, S. J. Loeb, *Org. Biomol. Chem.* **2012**, *10*, 6094.

[10] a) P. N. Preston, *Chem. Rev*. **1974**, *74*, 279; b) R. Trivedi, S. K. De, R. A. Gibbs, *J. Mol. Catal. A*, **2006**, *245*, 8; c) Z. Zhang, L.Yin, Y. Wang, *Catal. Commun*. **2007**, *8*, 1126.

[11] Images for all X-ray crystal structures were generated using CrystalMaker® for Windows, CrystalMaker Software Ltd, Oxford, England (www.crystalmaker.com)

[12] J. C. Cobas, M. Martin-Pastor, EXSYCalc Ver 1.0; Mestrelab Research, Coruña, Spain, 2007.

[13] a) D. B. Smithrud, E. M. Sanford, I. Chao, S. B. Ferguson, D. R. Carcanague, J. D. Evanseck, K. N. Houk, F. Diederich, *Pure & Appl. Chem*., **1990**, *62*, 2227; b) M. S. Cubberley, B. L. Iverson, *J. Am. Chem. Soc.*, **2001**, *123*, 7560; c) S. J. Loeb, J. Tiburcio, S. J. Vella, *Chem. Commun.* **2006**, 1598; d) S. J. Vella, J. Tiburcio, S. J. Loeb, *Chem. Commun.* **2007**, 4752.

[14] a) G. R. Wiley, S. I. Miller, *J. Am. Chem. Soc.,* **1972**, 94, 3287; b) A. S. Lane, D. A. Leigh, A. Murphy, *J. Am. Chem. Soc.* **1997**, *119*, 11092; c) C. A. Hunter, Angew. Chem. Int. Ed. 2004, 43, 5310; d) S. J. Loeb, J. Tiburcio, S. J. Vella, *Chem. Commun.,* **2007**, 4752.

[15] Handbook of organic solvent properties, Ian M. Smallwood, consultant. London: Arnold; New York: Halsted Press, **1996**.

[16] W. Zheng, X. He, H. Chen, Y. Gao, H. Li, *Spectrochim. Acta Mol. Biomol. Spectrosc.,* **2014**, *124*, 97.

[17] K. Zhu, V. N. Vukotic, N. Noujeim, S. J. Loeb, *Chem. Sci.,* **2012**, *3*, 3265.

[18] J. C. Cobas, M. Martin-Pastor, EXSYCalc Ver 1.0; Mestrelab Research, Coruña, Spain, **2007**.

[19] G. M. Sheldrick, *Acta Cryst*. **2008**, *A64*, 112.

CHAPTER 4

4.1 Thermally Driven Dynamics of a Rotaxane Wheel about an Imidazolium Axle inside a Metal-Organic Framework

4.1.1 Introduction

Mechanically interlocked molecules (MIMs) are the core dynamic components of many molecular switches and machines.[1] The majority of these MIMs have large, flexible structures and function efficiently in solution[2] or in a few cases, soft matter.[3] There is however, interest in incorporating nanoscale devices based on MIMs into more organized materials such as crystalline solids.[4] To this end, we have sought out structures for MIMs with rigid axles and linear tracks in order to prepare compact linkers that could be incorporated into metal-organic framework (MOF) materials.[5] Initially, we identified the conformational changes and rotational dynamics of a variety of different sized macrocycles interlocked to a simple aniline-based axle driven by thermal input.[6] More recently, we have developed two new recognition motifs for 24-membered crown ether wheels based on compact, T-shaped 2,4,7-triphenylbenzimidazolium[7] and Y-shaped 2,4,5-triphenylimidazolium axles[8] and successfully combined these units to prepare rigid axles for [2]rotaxane molecular shuttles.[9] This allowed us to create MOF **UWDM-4** (**U**niversity of **W**indsor **D**ynamic **M**aterial) for which it was demonstrated that the large amplitude translational motion of a molecular shuttle could occur inside the organized lattice of a crystalline material[10].

Herein, we combine a Y-shaped 2,4,5-triphenylimidazolium recognition site with an *iso*phthalate coordinating group to create an axle with a single recognition site and incorporate this into a MOF (**UWDM-5**) using Zn^{II} ions. Using VT ^{2}H SSNMR, we have characterized the conformational and rotational motion of a **24C6** macrocycle as it undergoes

thermally driven dynamics around an imidazolium group on the axle. This represents only the second type of rotaxane-based MOF for which this type of motion in the solid-state has been characterized; following our recent work on the aniline/**24C6** based MOF materials **UWDM-1,**[6a] **UWDM-2** and **UWDM-3**.[6b]

4.1.2 Results and Discussion

4.1.2.1 Linker Synthesis and Characterization

A new unsymmetrical rotaxane linker for MOF construction was designed by combining an *iso*phthalic acid group – a well-known linker in MOF chemistry[11] – with our newly developed Y-shaped imidazolium-based template[8] for creating mechanically interlocked molecules. Preparation of the new tetracarboxylic linker **4**-H_4 is described in Scheme 4.1.

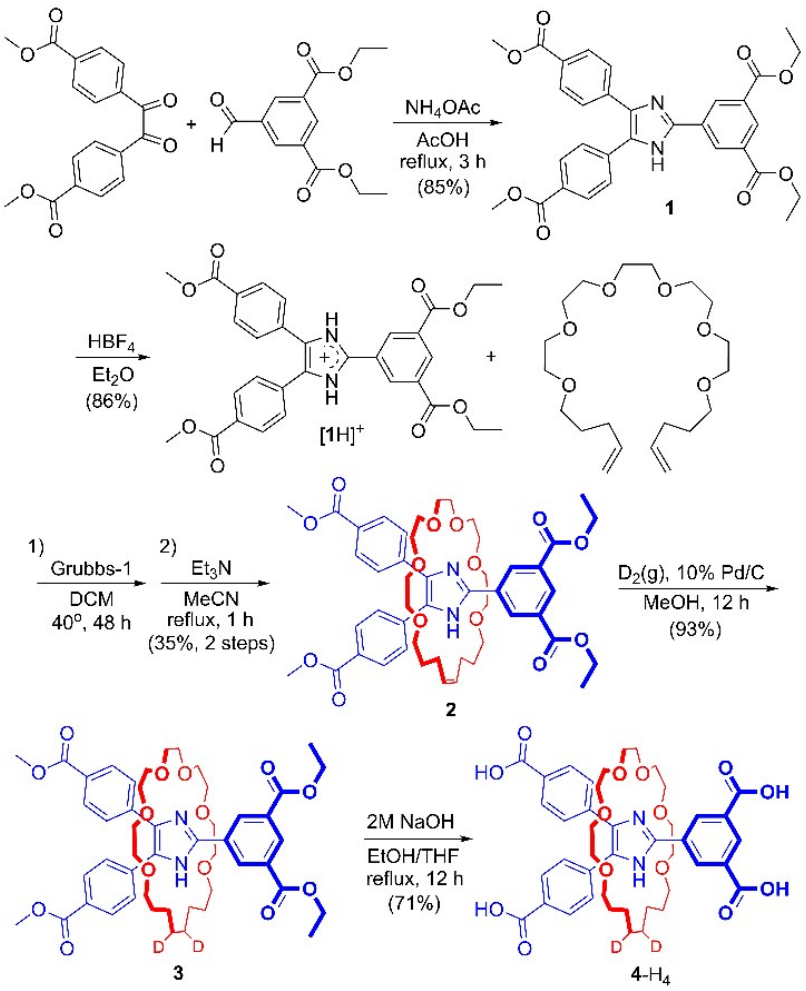

*Scheme 4.1. Preparation of interlocked linker **4**-H_4 with deuterium (D = ^{2}H) labels.*

Initially, 5-formyl-*iso*phthalic acid diethyl ester[12] and 4,4'-bis(methoxycarbonyl)benzil[13] were condensed with ammonium acetate to give the imidazole **1**. After protonation, [**1**-H]$^+$ was used as a template for the ring-closing metathesis (RCM), employing Grubbs' 1st generation catalyst, of a bis-olefin macrocycle precursor around the imidazolium group to form the interlocked compound **2** as a mixture of *E/Z* isomers (~70/30). Subsequent reduction of the double-bond using D_2(g) and Pd/C followed by hydrolysis yielded **4**-H_4 labelled with ^{2}H atoms for VT-SSNMR investigation (*vide infra*).

The linker **4**-H_4 was characterized in solution by ^{1}H and ^{13}C NMR spectroscopy as well as high-resolution electrospray-ionization mass spectrometry (HR-ESI MS) and in the solid

state by IR and single-crystal X-ray diffraction. Fig. 4.1 shows the solid-state structure of linker **4**-H_4. The neutral tetra-acid crystallizes as a zwitterionic imidazolium-carboxylate species; one of the carboxylic acid hydrogen atoms from the Y-shaped unit has been transferred to the imidazole nitrogen atom. The resulting imidazolium cation is stabilized by the presence of the interlocked, **24C6** ring and there are two relatively strong, charge-assisted hydrogen bonds between the imidazolium N-atoms and crown ether O-atoms; NH···O; 2.90 Å (170°) and 2.88 Å (168°).

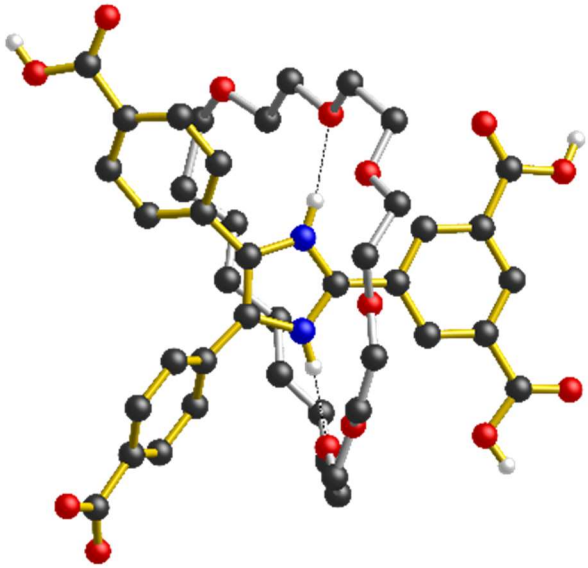

*Figure 4.1. X-ray structure of the interlocked linker **4**-H_4. The molecule crystallizes as a zwitterion; one of the four carboxylic acids H-atoms has been transferred to the imidazole ring. Only one of the two molecules in the asymmetric unit is shown. Only the hydrogen atoms of the imidazolium unit and the three protonated COOH groups are shown for clarity. Color key: red = O; blue = N; black = C; white = H; axle = gold bonds; silver = wheel*

4.1.2.2 MOF Synthesis and Characterization

The reaction of linker **4**-H_4 with $Zn(NO_3)_2{\cdot}(H_2O)_6$ in a solution of diethylformamide (DEF) containing a small amount of nitric acid (HNO_3) for 48 h at 85 °C, produced the MOF designated **UWDM-5** as X-ray quality crystalline material in 63% yield. The material was determined to have formula {[Zn_2(**4**-H)(NO_3)(DEF)](DEF)(H_2O)} by single-crystal X-ray diffraction. Fig. 4.2a and 4.2b show views of the coordinated [2]rotaxane linker [**4**-H]$^{3-}$ in

UWDM-5 emphasizing the relative positions of the axle and wheel, respectively. As was observed for the X-ray structure of the ligand, there are two hydrogen bonds between the imidazolium N-atoms and crown ether O-atoms: NH···O; 2.87 Å (175°) and 2.81 Å (164°); the relative rotational orientation of the crown ether with respect to the axle is also the same. Fig. 4.2c depicts the metal coordination node or secondary building unit (SBU) which involves two Zn^{II} ions, the four carboxylate groups of [**4**-H]$^{3-}$, a coordinated nitrate (NO_3^-) ion and a coordinated molecule of DEF.

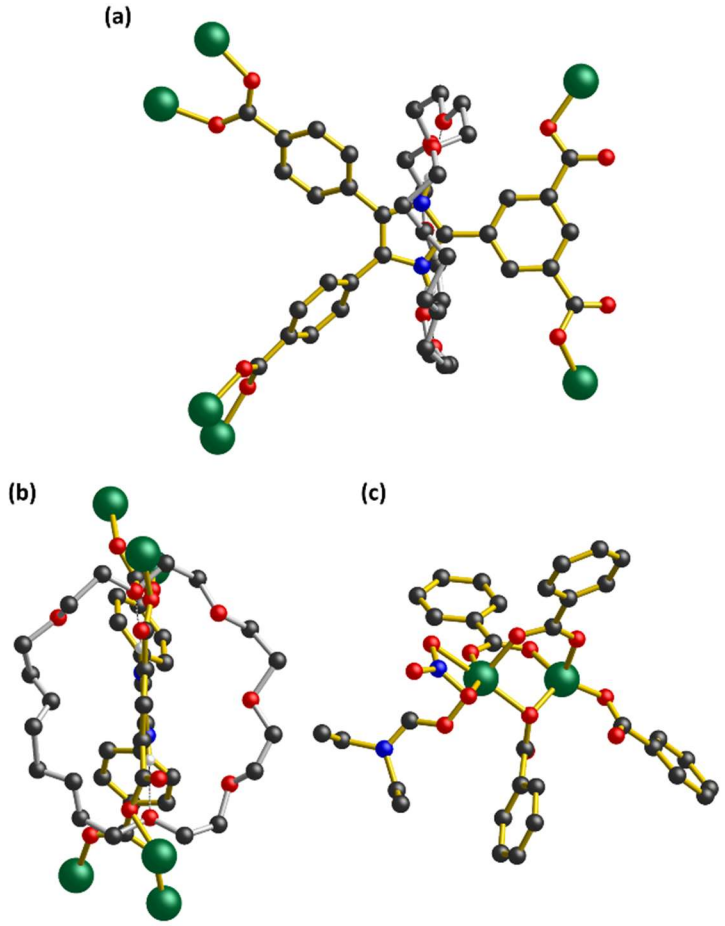

*Figure 4.2. X-ray structure of MOF **UWDM-5** showing the basic repeating units. a) Side-on view showing all of the linker bonds to Zn ions. b) An end-on view emphasizing the threading of the rigid axle through the macrocyclic wheel. c) The metal SBU showing the coordination environments of the two crystallographically independent Zn(II) ions to four carboxylates, one nitrate ion and one molecule of DEF. Only hydrogen atoms involved in intramolecular H-bonding are shown for clarity. Color key: green = Zn; red = O; blue = N; black = C; white = H; axle = gold bonds; silver = wheel bonds.*

One of the most interesting aspects of the MOF formulation is that the rotaxane imidazole core is protonated giving rise to an imidazolium recognition site encircled by a crown ether – "encapsulation" of the cation stabilizes the charge and drastically increases the pK_a of the imidazolium ion, making it very difficult to deprotonate.[9a,14] The charge on the cationic linker is balanced by the inclusion of a nitrate ion into the framework skeleton. This is consistent with both the observation that the free ligand **4**-H_4 adopts a zwitterionic form in the solid state and our previous characterization of MOFs with related benzimidazolium rotaxanes which remain protonated under basic, solvothermal conditions.[10]

Fig. 4.3a and 4.3b show views of the MOF lattice down the *c*-axis and *b*-axis respectively. Visually, it appears that the **24C6** wheels (red) are free from any steric interactions with the surrounding framework (blue) and that the Y-shaped diphenyl imidazolium unit provides enough spacing between adjacent recognition sites to avoid ring-ring interactions. This is important, since we have previously shown that macrocyclic rings that are within van der Waals distances of the MOF skeleton can undergo conformational changes but are impeded with respect to rotation.[6c]

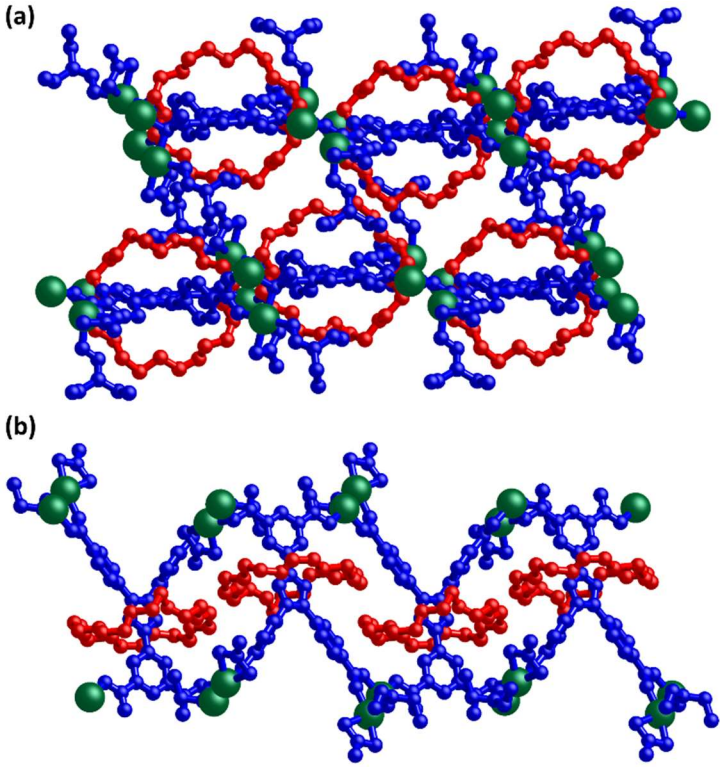

*Figure 4.3. X-ray structure of **UWDM-5** showing: a) a view down the c-axis showing that the macrocyclic wheels are clearly separated from each other in the plane of the macrocycle; b) a view down the b-axis showing that the macrocycles are clearly separated from each other between the layers. H-atoms are omitted for clarity. Color key: blue = MOF framework; red = macrocycles; teal = Zn ions.*

UWDM-5 is quite robust. Thermal gravimetric analysis (TGA) showed the loss of only a single DEF molecule per formula unit from the narrow channels upon heating to 150 °C; ~9% weight loss from 18% void space (as calculated by Mercury[15] using 1.2 Å probe). It should be noted that the channels occupied by solvent are completely separate from the cavities containing the **24C6** macrocycles. A VT powder X-ray diffraction (PXRD) experiment showed the material only undergoes very slight changes in structure over the temperature range of 25 – 150 °C (see section 4.2.10). The thermal stability of **UWDM-5** allowed us to study the thermally driven molecular dynamics of the interlocked **24C6** macrocycle inside the MOF material.

4.1.2.3 MOF Dynamics Characterized by ^{2}H SSNMR

VT ^{2}H SSNMR data for **UWDM-5** support the postulate that the macrocyclic **24C6** ring is in an unconstrained environment and therefore becomes increasingly mobile as temperature is increased (see section 4.2.12). The spectrum acquired at 192 K (Fig. 4.4a) was simulated as a single site (C_Q = 160(5) kHz, η_Q = 0.0(1)) and with motions occurring at rates that are too slow to affect the appearance of the ^{2}H powder pattern. Increasing the temperature to 226 K resulted in no significant change in the powder pattern. The spectrum acquired at 234 K indicates the onset of motion, and the spectrum at 276 K was simulated using the familiar two-site jump of the CD_2 groups through an angle of 75° (Fig. 4.4b). Increasing the temperature further induces the onset of partial rotation motion through 225° in 45° increments (Fig. 4.4c), in addition to the aforementioned two-site jump motion. The spectrum at 360 K was simulated with rates in the fast-motion limit (FML) for this combined motion (see section 4.2.13).

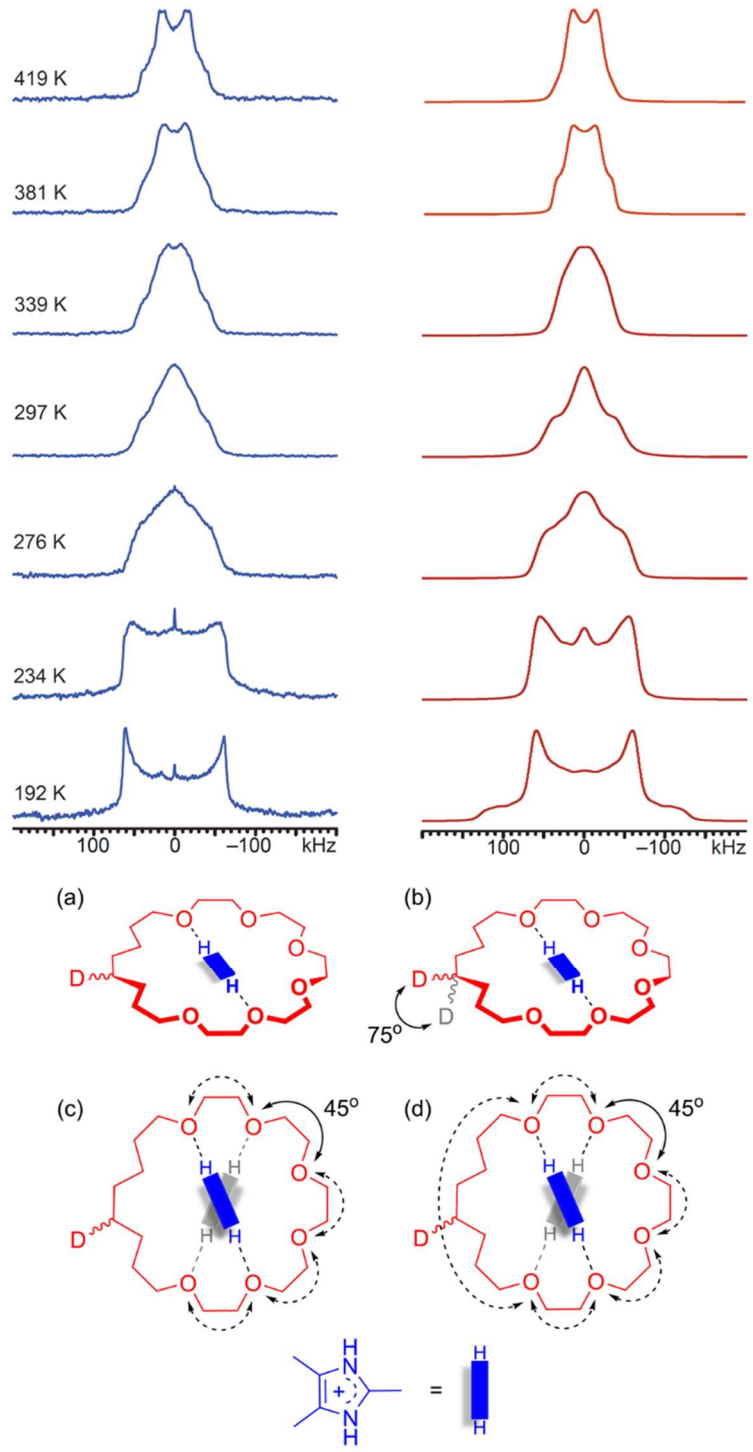

*Figure 4.4. Experimental (left) and simulated (right) ^{2}H SSNMR powder patterns as a function of temperature for **UWDM-5**. Illustrations (below) of the motions of the **24C6** macrocyclic ring relative to the framework axle: (a) the slow-motion limit (SML) where no motion is occurring on the NMR timescale, (b) the fast-motion limit (FML) for jumps between two sites separated by 75°, (c) partial rotation of the ring over 225° in 45° steps, (d) partial rotation of the ring over 225° in 45° steps combined with jumps over the alkyl portion of the ring resulting in full rotation.*

The spectra acquired at higher temperatures could not be simulated using the combined two-site jump and partial rotation model, nor could they be simulated with free rotation of the crown ether ring about an axis of $C_{n\geq3}$ symmetry. The simulation of the high-temperature spectra was achieved by considering an intermediate case between partial rotation and free rotation, combined with the two-site jump. Specifically, eight sites separated by 45° rotations were used, six corresponding to the hydrogen-bonding oxygen atom positions, and two corresponding to the alkyl portion of the ring (Fig. 4.4d). A rate matrix was constructed where jumps between the oxygen atom positions are occurring at rates in the FML (*i.e.*, v_{ex} >10^7 Hz) and jumps through the alkyl positions occur at a significantly slower rate in the intermediate-motion regime (IMR, *i.e.*, 50 to 1000 kHz). The spectra acquired from 381 to 419 K were simulated using this model, and excellent agreement with the experimental data was obtained.

The VT ^{2}H SSNMR spectra for **UWDM-5** are quite similar to those previously observed for **UWDM-1**, which features a Cu-paddlewheel MOF with the same macrocycle locked to a neutral aniline-based axle.[6a] It could be argued that the interaction between the macrocycle and the framework skeleton (axle) must be stronger for a charged imidazolium ion as compared to a neutral aniline – certainly this has been quantified to be true in solution.[16] Comparison of the SSNMR spectra for **UWDM-1 and UWDM-5** at low temperatures shows that, although the description of the motion is the same, the onset temperatures are slightly higher for **UWDM-5**. This may be the result of the stronger interactions between axle and wheel having a measurable effect on the barrier to motion at lower temperatures. However, this difference disappears at higher temperatures. Presumably the thermal energy required to induce conformational changes and eventually full rotation of the macrocycle inside a MOF is much greater that needed to overcome the non-covalent interactions between wheel and

axle; this suggests that energetic differences in initial axle/wheel template interactions are negligible as the amount of thermal energy available to the system is increased.

4.1.3 Conclusions

The unsymmetrical and extended structure of the new rotaxane linker [**4**-H]$^{3-}$ allows for formation of a MOF framework (**UWDM-5**) in which there is sufficient void space for a full range of dynamic motions by the interlocked **24C6** macrocyclic wheel. As the temperature is increased, the ring undergoes a series of conformational changes about the MOF framework axle. The larger size and higher charge of the imidazolium group relative to those of previously studied aniline axles (**UWDM-1**, **UWDM-2**, and **UWDM-3**), appear to only have a significant effect on the overall motion of the ring inside the MOF at lower temperatures, whereas these differences are insignificant at higher temperatures. Importantly, these results demonstrate that there may be a wide variety of MIMs that can be incorporated into MOFs exhibiting large scale dynamics and molecular switching in the solid state.

4.2 Experimental

4.2.1 General Comments

Diethyl-5-(hydroxylmethyl)*iso*phthalate, 5-bromopentene and pentaethylene-glycol were purchased from Aldrich and used as received. 5-Formyl*iso*phthalic acid diethyl ester was prepared according to literature procedure.[12] A modified method from that in the literature was used to synthesize 4,4'-bis(methoxycarbonyl)benzil.[13] Solvents were dried using an Innovative Technologies Solvent Purification System. Deuterated solvents were obtained from Cambridge Isotope Laboratories and used as received. Thin layer chromatography (TLC) was performed using Teledyne Silica gel 60 F_{254} plates and viewed under UV light. Column chromatography was performed using Silicycle Ultra-Pure Silica Gel (230 – 400 mesh). Flash column chromatography was performed using Teledyne Ultra-Pure

Silica/RP-C18 Silica Gel (230 – 400 mesh) on a Teledyne Isco Combiflash-R_f instrument. ^{1}H, ^{13}C, and all 2D solution NMR experiments were performed on a Bruker Avance III 500 instrument, with Larmor frequencies of 500.1 MHz for ^{1}H nuclei and 125.7 MHz for ^{13}C. Chemical shifts are quoted in ppm relative to tetramethylsilane (δ_{iso} = 0 ppm) using the residual solvent peak as a secondary reference standard. High resolution mass spectrometry (HR-MS) experiments were performed on a Waters Xevo G2-XS time-of-flight (ToF) instrument using lockspray for accurate mass determinations. ESI acquisitions were completed using a 1uL injection into a sample loop with a constant 5uL/min flow of 50:50 H_2O:CH_3CN (with 0.1% formic acid). All single crystal X-ray data were collected on a Brüker D8 diffractometer with a Photon 100 CCD detector operated at 50 kV and 30 mA with MoK_α radiation. Crystals were frozen in paratone oil inside a cryoloop and reflection data were integrated from frame data obtained from hemisphere scans. Powder XRD measurements were recorded on a Bruker D8 Discover diffractometer equipped with a GADDS 2D-detector and operated at 40 kV and 40 mA. CuK_α radiation was used and the initial beam diameter was 0.5 mm. Thermal gravimetric analyses were conducted on a Mettler Toledo TGA SDTA 851e instrument. Helium (99.99%) was used to purge the system with a flow rate of 30 mL/min. Samples were held at 25 ^{o}C for 30 min before heating up to 550 ^{o}C at 5 ^{o}C/min. Melting points were recorded on a Stanford Research Systems, Opti Melt MPA100 instrument. Infrared spectra were recorded on a Bruker Alpha FT-IR spectrometer in the range of 4000–400 cm^{-1}. ^{2}H solid-state NMR experiments were conducted using an Oxford 9.4 T ($\nu_0(^{1}H)$ = 400 MHz, $\nu_0(^{2}H$ = 61.4 MHz)) wide-bore magnet equipped with a Varian Infinity Plus console and a Chemagnetics 5 mm HX static probe. Samples were ground and tightly packed into 5 mm zirconia rotors. Temperatures were calibrated using the temperature-dependent ^{207}Pb isotropic chemical shift of $PbNO_3$, following a previously reported method.[17,18] Spectra were acquired using the quadrupolar-echo pulse sequence of the form 90°-τ_1-90°-τ_2-acquire, with

3.2 μs π/2 pulse lengths, 20 or 50 μs pulse spacings, and 0.5 s recycle delays. Chemical shifts were referenced to D_2O (δ_{iso} = 0 ppm). Simulations of the SML static ^2H powder patterns were generated using WSolids[19] and simulations of the powder patterns in the intermediate and fast motional regimes were performed using EXPRESS.[20] (See section 4.2.13).

4.2.2 Synthesis of 1

5-Formyl-*iso*-phthalic acid diethyl ester (1.5 g, 6.0 mmol), 4,4'-bis(methyloxycarbonyl)benzil (2.0 g, 6.0 mmol) and ammonium acetate (7.1 g, 0.09 mol) were dissolved in acetic acid (30 mL). The reaction mixture was heated to reflux for 2 h, cooled to room temperature and neutralized by NH_4OH. The yellow solid that precipitated was filtered, washed with H_2O and dried under vacuum. Yield: 2.8 g, 85%; MP 207-209 °C; ^1H NMR ($CDCl_3$, 500 MHz, 298 K): δ (ppm) = 10.36 (s, 1H), 8.83 (d, 2H, *J* = 1.5 Hz), 8.67 (s, 1H, *J* = 1.5 Hz), 8.00 (d, 4H, *J* = 8.5 Hz), 7.63 (br, 4H), 4.41 (q, 4H, *J* = 7.0 Hz), 3.93 (s, 6H), 1.41 (t, 6H, *J* = 7.0 Hz) .^{13}C NMR ($CDCl_3$, 125 MHz, 298 K): δ (ppm) = 167.0, 165.7, 145.5, 131.9, 130.8, 130.5, 130.5, 130.2, 129.5, 127.9, 61.9, 52.4, 14.5; IR (neat): 3279, 2986, 1717, 1699, 1607, 1434, 1273, 1233, 1101, 1016, 860, 777, 766, 718, 706, 693 cm^{-1}. HR-MS (ESI-ToF) *m/z*: calcd for $[M+H]^+$, $[C_{31}H_{29}N_2O_8]^+$, 557.1924; found 557.1924.

4.2.3 Synthesis of [1-H][BF_4]

Compound **1** (1.5 g, 2.7 mmol) was dissolved in THF (30 mL) and 1.1 eq of tetrafluoroboric acid diethyl ether complex (3.0 mmol, 402 μL) in ether added to the solution. After 10 min stirring at room temperature, diethyl ether (100 mL) was added. The resulting off-white precipitate was collected by filtration, washed 3 times with ether (10 mL) and dried under vacuum. Yield: 1.6 g, 90%; MP 159-164 °C. ^1H NMR (CD_3CN, 500 MHz, 295 K): δ (ppm) = 8.87 (d, 2H, *J* = 1.5 Hz), 8.77 (t, 1H, *J* = 1.5 Hz), 8.08 (d, 4H, *J* = 8.5 Hz), 7.64 (d, 4H, *J* = 8.0 Hz), 4.45 (q, 4H, *J* = .0 Hz), 3.90 (s, 6H), 1.42 (t, 6H, *J* = 7.0 Hz).^{13}C NMR (CD_3CN, 125 MHz, 295 K):

δ (ppm) = 166.9, 165.3, 144.4, 133.7, 133.6, 132.7, 132.3, 132.0, 131.2, 131.0, 129.7, 125.1, 62.9, 53.0, 14.4. IR (neat) = 2876, 1722, 1651, 1614, 1436, 1282, 1241, 1109, 1023, 957, 856, 774, 760, 708 cm^{-1}. HR-MS (ESI-ToF) *m/z*: calcd for $[M\text{-}BF_4]^+$, $[C_{31}H_{29}N_2O_8]^+$, 557.1924; found 557.1927.

4.2.4 Synthesis of 2

Compound [**1**-H][BF_4] (1.0 g, 1.6 mmol) and pentaethyleneglycol-dipent-4-enyl ether[21] (1.16 g, 3.1 mmol) were added to a Schlenk flask and dissolved in CH_2Cl_2 (25 mL). The flask was degassed and back-filled with N_2. Grubbs I catalyst (128 mg, 0.16 mmol) was added in one portion to the stirred solution and heated at 40 °C for 16 h after which another 25% catalyst was added over a period of 5 d. The progress of the reaction was monitored by ^{1}H NMR spectroscopy. After this time, the reaction was cooled to room temperature and the solvent was removed under reduced pressure. The residue obtained was washed with diethyl ether (50 mL), and then dissolved in methanol followed by addition of triethylamine (1 mL). The desired product (*E/Z* mixture ~70/30) was precipitated as an off-white solid and was filtered under vacuum. Yield: 482 mg, 34%; MP 162-164 °C; ^{1}H NMR (CD_3CN, 500 MHz, 295 K): (major product) δ (ppm) = 12.29 (s, 1H), 9.08 (d, 2H, *J* = 1.5 Hz), 8.58 (t, 1H, *J* = 1.5 Hz), 8.03 (d, 2H, *J* = 8.5 Hz). 7.95 (d, 2H, *J* = 8.5 Hz), 7.81 (d, 2H, *J* = 8.5 Hz), 7.69 (d, 2H, *J* = 8.5 Hz), 5.50 (t, 2H, *J* = 3.5 Hz), 4.43 (q, 4H, *J* = 7.0 Hz), 3.89 (s, 3H), 3.87 (s, 3H), 3.40-3.12 (m, 24H), 1.87-1.78 (m, 4H), 1.62-1.53 (m, 2H), 1.44-1.43 (m, 2H), 1.40 (t, 6H, *J* = 7.0 Hz).^{13}C NMR (CD_3CN, 125 MHz, 296 K): δ (ppm) = 167.6, 167.6, 167.4, 166.6, 166.6, 146.4, 146.1, 141.1, 138.8, 138.8, 137.2, 137.0, 133.4, 133.0, 132.6, 132.1, 132.0, 130.8, 130.5, 130.4, 130.3, 130.1, 130.1, 129.9, 129.9, 129.5, 129.3, 129.3, 129.2, 129.1, 72.1, 71.7, 71.2, 71.1, 71.0, 70.9, 70.7, 70.4, 70.4, 70.3, 69.2, 62.3, 62.2, 52.7, 52.6, 52.5, 30.7, 29.4, 29.2, 25.3, 14.7. IR (neat) = 3255, 2867, 1717, 1609, 1425, 1279, 1240, 1106, 1027, 969, 863, 774, 765, 706 cm^{-1}. HR-MS (ESI-ToF) *m/z*: calcd for $[M+H]^+$, $[C_{49}H_{63}N_2O_{14}]^+$, 903.4279; found 903.4262.

4.2.5 Synthesis of 3

Pd/C 10wt% (41 mg, 0.04 mmol) was added to a Schlenk flask and a balloon of D_2 gas was attached to the flask with an adapter that allowed the balloon to be closed off from the reaction flask. The flask was evacuated by vacuum and then back filled with N_2. Compound **2** (350 mg, 0.39 mmol) was dissolved in the mixture of MeOH/THF (10 mL: 3 mL) and transferred to the flask via syringe. A slight vacuum was applied to the reaction mixture until the solvent began to bubble, at which point the balloon was opened to the flask. The mixture stirred vigorously for 24 h under ambient conditions. The solid was filtered and the filtrate was concentrated under reduced pressure to yield a white solid. Yield: 326 mg, 93%; MP 174 °C. ^{1}H NMR (CD_3CN, 500 MHz, 292 K): δ (ppm) = 12.29 (s, 1H), 9.12 (d, 2H, *J* = 1.5 Hz), 8.57 (t, 1H, *J* = 1.5 Hz), 8.03 (d, 2H, *J* = 8.5 Hz), 7.93 (d, 2H, *J* = 8.0 Hz), 7.86 (d, 2H, *J* = 8.5 Hz), 7.70 (d, 2H, *J* = 8.5 Hz), 4.42 (q, 4H, *J* = 7.0 Hz), 3.89 (s, 3H), 3.87 (s, 3H), 3.47-3.14 (m, 24H), 1.39 (t, 6H, *J* = 7.0 Hz), 1.35-1.25 (m, 4H), 1.16-1.10 (m, 4H).^{13}C NMR (CD_3CN, 125 MHz, 294 K): δ (ppm) = 167.6, 167.3, 166.5, 146.2, 141.0, 139.0, 137.1, 133.4, 132.6, 132.1, 130.5, 130.0, 129.8, 129.5, 129.4, 129.2, 72.0, 70.9, 70.9, 70.7, 70.4, 69.9, 62.3, 52.7, 52.5, 30.0, 26.1, 14.7. IR (neat) = 2868, 1720, 1609, 1435, 1276, 1230, 1101, 997, 775, 764, 716, 632 cm^{-1}. HR-MS (ESI-ToF) *m/z*: calcd for $[M+H]^+$, $[C_{49}H_{63}D_2N_2O_{14}]^+$, 907.4561; found, 907.4536.

4.2.6 Synthesis of 4-H_4

Compound **3** (250 mg, 0.28 mmol) was dissolved in a mixture of EtOH/THF (20 mL: 6 mL) followed by addition of 1M NaOH (20 mL). The reaction mixture was heated at 80 °C for 24 h, concentrated in vacuum and carefully acidified with 1M HNO_3 to pH 4 to obtain a white precipitate. The resulting solid was filtered and washed with acidic water (pH = 4) and dried under vacuum. Yield: 202 mg, 89%; MP > 300 °C. ^{1}H NMR (CD_3OD, 500 MHz, 296 K): δ (ppm) = 9.05 (s, 2H), 8.92 (s, 1H), 8.16 (d, 4H, *J* = 8.5), 8.75 (d, 4H, *J* = 8.5), 3.89-3.85 (m, 2H), 3.71-3.62 (m, 7H), 3.41-3.12 (m, 15H), 1.29-1.11 (m, 8H), 1.07-1.03 (m, 4H). ^{13}C NMR (DMSO,

125 MHz, 295 K): δ (ppm) = 176.7, 176.3, 154.5, 148.9, 146.8, 145.0, 141.2, 141.0, 140.9, 139.4, 138.9, 138.8, 138.3, 138.1, 137.8, 137.4, 80.3, 79.1, 79.0, 79.0, 78.7, 78.0. IR (neat) = 2867, 1713, 1246, 1079, 952, 777, 702, 441 cm^{-1}. HR-MS (ESI-ToF) *m/z*: calcd for $[M+H]^+$, $[C_{43}H_{51}D_2N_2O_{14}]^+$, 823.3622; found 823.3622.

4.2.7 Preparation of MOF, UWDM-5, {[Zn_2(H-4)(DEF)(NO_3)]·(DEF)(H_2O)}

4-H_4 (78 mg, 0.095 mmol) and $Zn(NO_3)_2{\cdot}6H_2O$ (57 mg, 0.19 mmol) were dissolved in DEF (10 mL), to which 3 drops of HNO_3 were added. The solution was transferred through a 13 mm syringe filter (0.2 μm PTFE membrane) to five 20 mL scintillation vials and heated at 85 °C in a programmable heating oven for two days. 67 mg of a colorless crystalline product was collected and washed with DEF several times to yield pure **UWDM-5**. The DEF was then replaced with DCM (3 × 30 mL) over a five-day period. Finally, the solid was filtered and dried under high vacuum for 6 h (47 mg, 63%).

4.2.8 Schematic Representation of Steps Involved in the Preparation of Precursor 1

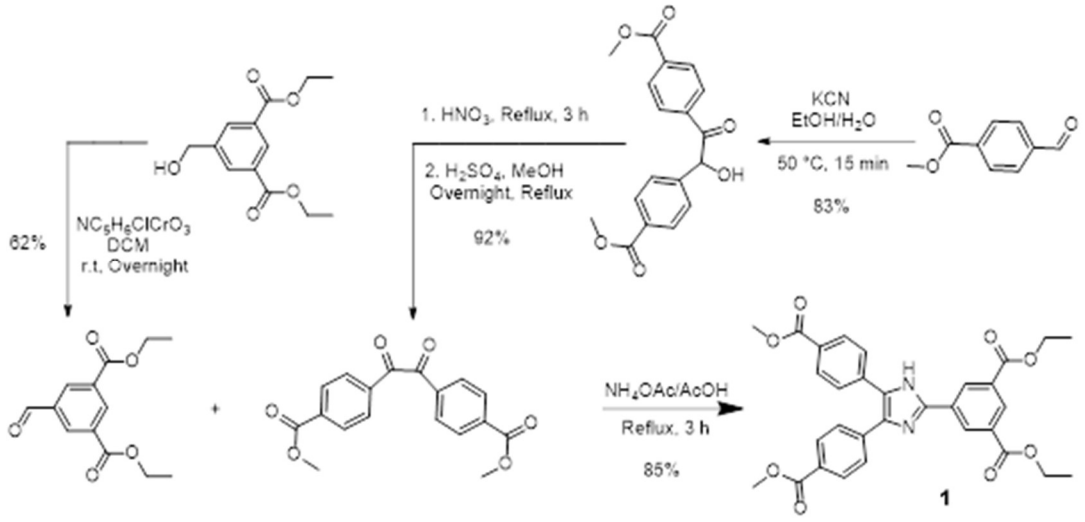

*Scheme 4.2. Initial synthetic steps involved in the preparation of precursor **1**.*

4.2.9 Optical Microscopy of UWDM-5

*Figure 4.5. Optical microscopy image of X-ray quality crystals of **UWDM-5**.*

4.2.10 Variable Temperature Powder X-ray Diffraction Studies

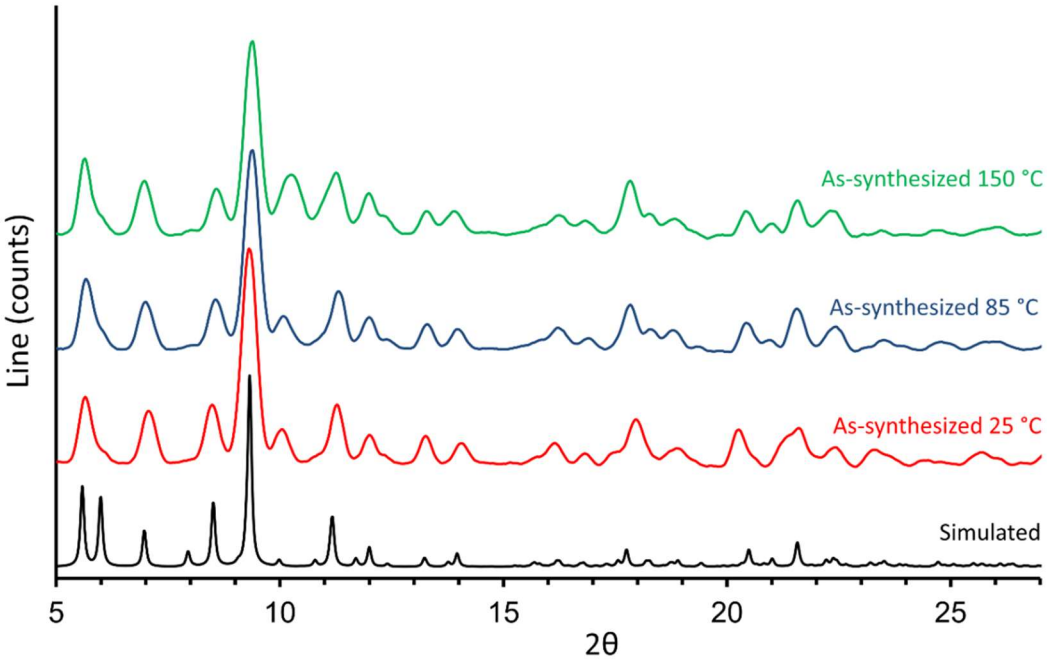

*Figure 4.6. Variable temperature powder-XRD results for **UWDM-5**.*

4.2.11 Thermogravimetric Analysis

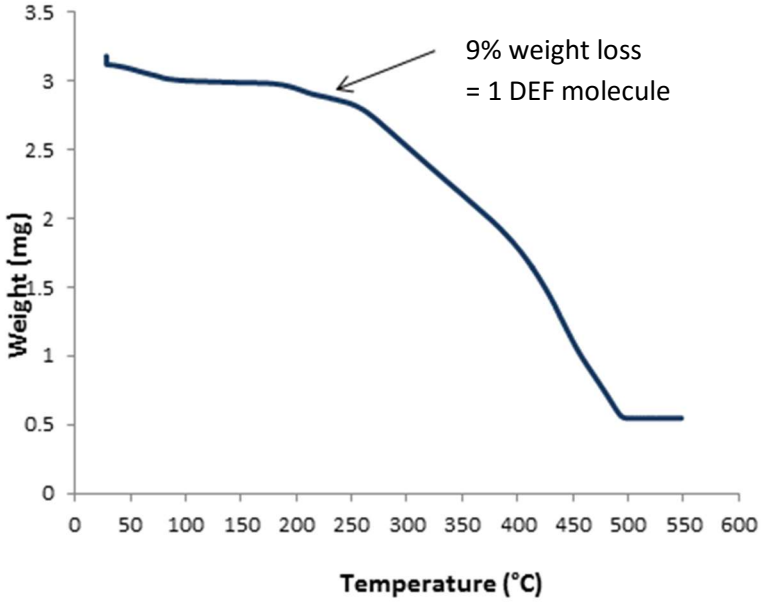

*Figure 4.7. Thermogravimetric analysis (TGA) curve for as-synthesized **UWDM-5**. (3.3 mg of dried **UWDM-5** was heated on a Mettler Toledo thermogravimetric analyzer from room temperature to 550 °C at a rate of 5 °C min^{-1} under N_2 flow).*

4.2.12 Single Crystal X-ray Diffraction Studies

General: Single crystal X-ray data sets were collected on a Brüker D8 Venture diffractometer, equipped with a PHOTON 100 detector, Kappa goniometer, and collected using a Mo sealed tube source (MOFs) or a Cu high brilliance IμS microfocus source (ligands). Crystals were frozen in paratone oil inside a cryoloop using the cold N_2 stream. Reflection data were integrated using Bruker APEX II software. Decay was monitored using 50 standard data frames measured at the beginning and end of data collection. Diffraction data and unit-cell parameters were consistent with assigned space groups. Lorentzian polarization corrections and empirical absorption corrections, based on redundant data at varying effective azimuthal angles, were applied to the data sets. The structures were solved by direct methods, completed by subsequent Fourier syntheses and refined using full-matrix least-squares methods against $|F^2|$ data. When practical, non-hydrogen atoms were refined

anisotropically and hydrogen atoms placed in idealized positions and refined using a riding model. Scattering factors and anomalous dispersion coefficients are contained in the SHELXTL program library[22] and figures drawn with CrystalMaker[23] software. Details can be obtained from the Cambridge Crystallographic Data Centre at www.ccdc.cam.ac.uk for CCDC accession numbers 1473089 and 1473090.

4.2.12.1 Single Crystal X-ray Structure of Linker 4-H_4

Crystals of compound **4**-H_4 were of good quality. The unit cell contained four molecules of the neutral [2]rotaxane ($C_{43}H_{52}N_2O_{14}$) in the form of a zwitterion along with molecules of methanol (CH_3OH). The structure was solved in the triclinic space group P-1 (#2) with Z = 4. The asymmetric unit consists of two molecules of **4**-H_4 and two and a half molecules of methanol. A portion of the crown ether macrocycle (O9-C26-C27-O10-C28-C29-O11-C30-C31-O11) was disordered with a partially occupied methanol molecule. All non-hydrogen atoms were refined anisotropically by full matrix least squares calculations based on F^2. Two bonds of the macrocycle (O114-C136; C136-C137) were restrained to have bond distances of 1.43 and 1.54 Å respectively using the DFIX command. Atoms C26A and C43 of the macrocycle were restrained to have isotropic thermal parameters using the command ISOR. All hydrogen atoms were placed in geometric positions using a riding model. A summary of the crystal data, solution and refinement parameters are presented in Table 4.1.

*Table 4.1. Crystal data, solution and refinement parameters for Linker **4**-H_4.*

CCDC number	1473089	**V (Å^3)**	4416.2 (7)
Formula	$(C_{43}H_{52}N_2O_{14})(CH_3OH)_{1.25}$	**Z**	4
Formula weight	860.92	**ρ, g cm^{-3}**	1.295
Crystal system	Triclinic	**μ, mm^{-1}**	0.098
Space group	P-1 (#2)	**Reflections used**	14525
T (K)	173(2)	**variables**	1193
a (Å)	12.3786(11)	**restraints**	14
b (Å)	18.9667(17)	**R1 [$I > 2\sigma(I)$][a]**	0.0946
c (Å)	19.5578(18)	**R1 (all data)**	0.1602
α (°)	99.4946(13)	**R2w [$I > 2\sigma(I)$][b]**	0.2323
β (°)	91.6514(13)	**R2w (all data)**	0.2806
γ (°)	102.2399(13)	**GOF on F^2**	1.032

[a] $R1 = \Sigma ||F_o| - |F_c|| / \Sigma |F_o|$; [b] $R2w = [\Sigma[w(F_o^2 - F_c^2)^2] / \Sigma[w(F_o^2)^2]]^{1/2}$, [b]where $w = q[\sigma^2(F_o^2) + (aP)^2 + bP]^{-1}$.

4.2.12.2 Single Crystal X-ray Structure of Linker UWDM-5

Crystals of compound **UWDM-5** were of good quality. The unit cell contained four equivalent repeating unit with formula ($Zn_2C_{63}H_{90}N_7O_{16}$). The structure was solved in the monoclinic space group $P2_1/n$ (#14) with Z = 4. The asymmetric unit consists of two Zn(II) ions, one linker [**4**-H]$^{3-}$ containing four carboxylate groups, an imidazolium core and an encircling **24C6** macrocycle, one coordinated nitrate ion and one coordinated molecule of diethylformamide (DEF). In addition it was calculated that one molecule of DEF and one molecule of water per formula unit were present in the channel; these were taken into account using the program SQUEEZE prior to final refinement. All non-hydrogen atoms were

refined isotropically followed by anisotropic refinement by full matrix least squares calculations based on F^2. All hydrogen atoms were placed in geometric positions using a riding model. The nitrate ion was restrained to have a trigonal planar geometry using the command FLAT. The command SIMU was used to restrain the thermal parameters of the nitrate ion to be approximately equivalent. The C38-C39-C40 and C37-C38-C39 bond angles were restrained to have 1-3 distances of 2.45 Å using the command DANG. A summary of the crystal data, solution and refinement parameters are presented in Table 4.2.

*Table 4.2 Crystal data, solution and refinement parameters for **UWDM-5**.*

CCDC number	1473090	**V (Å^3)**	6011.7 (5)
Formula	$C_{63}H_{90}N_7O_{16}Zn_2$	**Z**	4
Formula weight	1332.15	**ρ, g cm^{-3}**	1.472
Crystal system	Monoclinic	**μ, mm^{-1}**	0.875
Space group	$P2_1/n$ (#14)	**Reflections used**	10414
T (K)	173(2)	**variables**	649
a (Å)	19.1594(9)	**restraints**	39
b (Å)	12.3790(6)	**R1 [$I > 2\sigma(I)$][a]**	0.1030
c (Å)	25.4170(12)	**R1 (all data)**	0.1430
α (°)	90	**R2w [$I > 2\sigma(I)$][b]**	0.2687
β (°)	94.241(2)	**R2w (all data)**	0.3138
γ (°)	90	**GOF on F^2**	1.084

[a] $R1 = \Sigma ||F_o| - |F_c|| / \Sigma |F_o|$; [b] $R2w = [\Sigma[w(F_o^2 - F_c^2)^2] / \Sigma[w(F_o^2)^2]]^{1/2}$, [b]where $w = q[\sigma^2(F_o^2) + (aP)^2 + bP]^{-1}$.

4.2.13 Solid-State NMR Experiments

^{2}H Solid-state NMR experiments were conducted using an Oxford 9.4 T ($\nu_0(^{1}H)$ = 400 MHz,$\nu_0(^{2}H$ = 61.4 MHz)) wide-bore magnet equipped with a Varian Infinity Plus console and a Chemagnetics 5 mm HX static probe. Samples were ground and tightly packed into 5 mm zirconia rotors. Temperatures were calibrated using the temperature-dependent ^{207}Pb isotropic chemical shift of $PbNO_3$, following a previously reported method.[24,25] Spectra were acquired using the quadrupolar-echo pulse sequence of the form 90°-τ_1-90°-τ_2-acquire, with 3.2 μs π/2 pulse lengths, 20 or 50 μs pulse spacings, and 0.5 s recycle delays. Chemical shifts were referenced to D_2O (δ_{iso} = 0 ppm). Simulations of the slow-motion limit static ^{2}H powder patterns were generated using WSolids[26] and simulations of the powder patterns in the intermediate and fast motional regimes (*vide infra*) were done with EXPRESS.[27]

4.2.13.1 ^{2}H SSNMR Studies of UWDM-5

Deuterium (^{2}H) solid-state NMR (SSNMR) is ideally suited to the study of dynamic processes occurring over a wide range of temperatures in the solid state.[27] We have demonstrated its application to the study of several metal-organic frameworks (MOFs) with dynamic interlocked components (*i.e.*, crown ether molecules threaded around an axle).[28-31] In general, it has been shown that three types of motion occur for the crown ether rings within MOFs: two-site jumps, partial rotations, and full rotations. The two-site jump motion consists of each of the deuterons in the CD_2 group moving between two distinct positions separated by a rotation angle, β. The jumping motion occurs about an axis perpendicular to the CD_2 plane (*i.e.*, about the C-C bond). For partial rotation, the crown ether ring rotates about the axle, jumping between sites such that the hydrogen-bond donor on the axle can interact with each of the oxygen atoms on the ring; however, rotation through the alkyl portion of the ring does not occur. Full rotation corresponds to complete, free rotation of the ring, with jumps through the alkyl portion as well.

The variable temperature (VT) ^{2}H SSNMR spectra acquired for **UWDM-5**, along with simulated lineshapes, are shown in Fig. 4.8. The rates for the three types of the motion used in the simulations are shown in Table 4.3. The spectrum acquired at 192 K was simulated with the absence of motion, or equivalently, rates in the slow motion limit (SML, i.e., $\nu_{ex} < 10^3$ Hz), which are too slow to produce any noticeable changes in the powder pattern. Increasing the temperature up to 226 K does not produce any appreciable changes in the powder pattern; however, at 234 K, drastic changes in the powder pattern are observed, which could be simulated as a two-site jump motion with an angle of 75° and a rate in the intermediate motion regime (IMR). The fast motion limit (FML, *i.e.*, $\nu_{ex} > 10^7$ Hz) for the two-site jump motion is reached at 276 K. The spectra acquired above 276 K could not be simulated by considering only the two-site jump motion, and instead were simulated with the onset of the partial rotation motion, combined with the two-site jump. The FML of this combined motion is reached at 339 K. The spectra acquired at higher temperatures could not be simulated using the combined partial rotation and two-site jump, nor with full rotation combined with the two-site jump, as full rotation about a $C_{n\geq3}$ axis would yield in an axially symmetric pattern. Instead, an intermediate dynamical model between partial and full rotation was used, where jumps through the alkyl portion of the ring are possible, but occurring at a slower rate than the jumps between the oxygen positions on the ring. Simulations using this intermediate between partial and full rotation yield agreement with experimental spectra. Full descriptions and pictures of these motions are pictured in Fig. 4.4 in this chapter, and described in more detail in previous publications by our research groups.

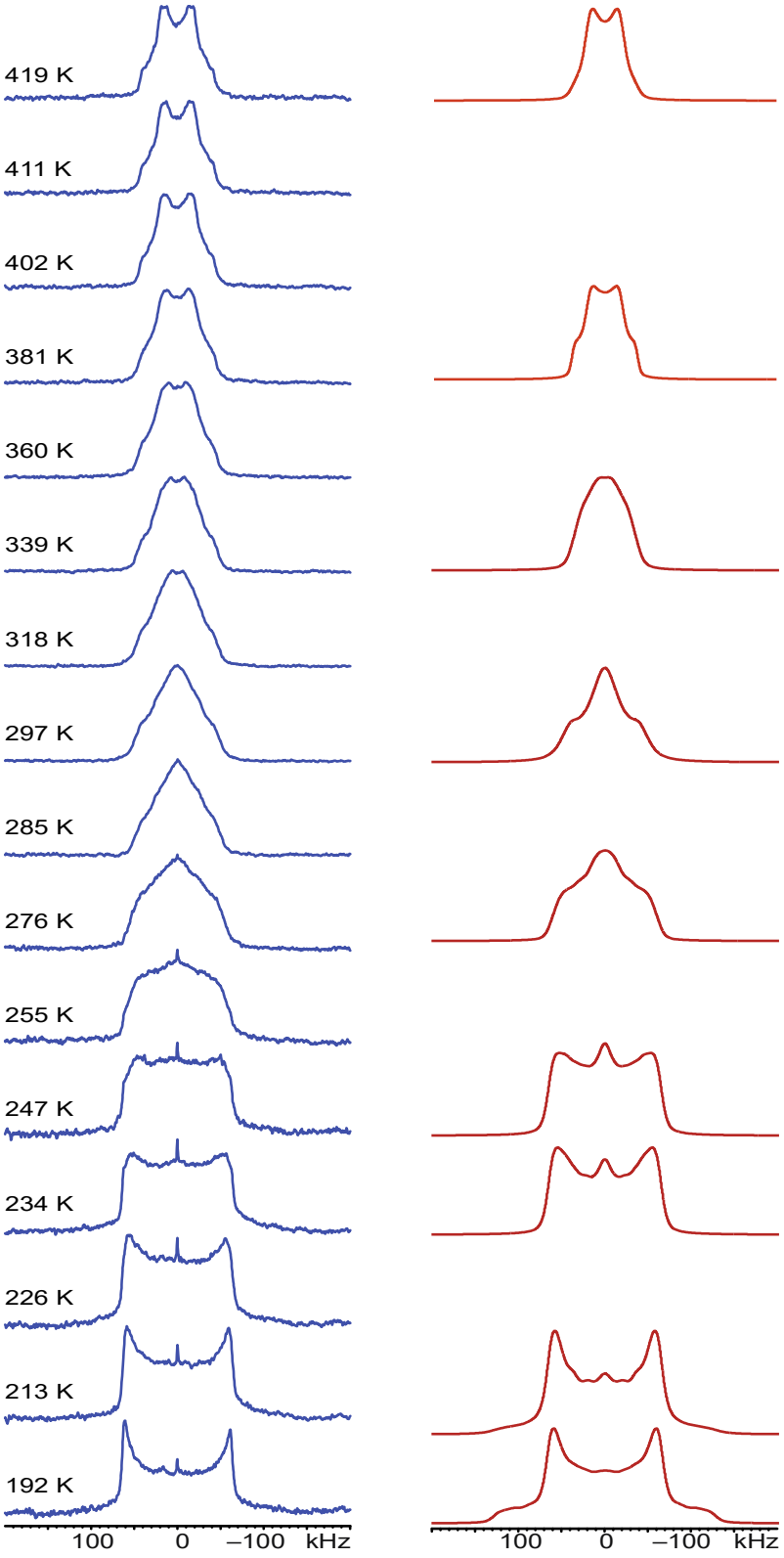

Figure 4.8. Experimental (blue) and simulated (red) VT ^{2}H SSNMR spectra of ***UWDM-5****.*

*Table 4.3. Rates of motion used in the simulation of experimental data for **UWDM-5**.*

Temperature (K)	Two-site Jump Rate (Hz)	Partial Rotation Rate (Hz)	Full Rotation Rate (Hz)
192	0	0	0
234	10^5	0	0
276	10^7	10^3	0
297	$>10^7$	10^5	0
339	$>10^7$	$>10^7$	10^4
381	$>10^7$	$>10^7$	$5x10^5$
419	$>10^7$	$>10^7$	10^6

4.3 References

[1] a) J.-P. Sauvage, C. Dietrich-Buchecker, (eds) *Molecular Catenanes, Rotaxanes and Knots: A Journey Through the World of Molecular Topology*, Wiley-VCH, **1999**; b) C. P. Collier, G. Mattersteig, E. W. Wong, Y. Luo, K. Beverly, J. Sampaio, F. M. Raymo, J. F. Stoddart, J. R. Heath, *Science*, **2000**, *289*, 1172; c) E. K. Kay, D. A. Leigh, F. Zerbetto, *Angew. Chem. Int. Ed.* **2007**, *46*, 72; d) V. Balzani, *Pure Appl. Chem.,* **2008**, *80*, 1631; e) M. J. Langton, P. D. Beer, *Acc. Chem. Res.,* **2014***, 47*, 1935; f) J. F. Stoddart, *Angew. Chem. Int. Ed.,* **2014**, *53*, 11102; g) K. Zhu, S. J. Loeb, *Top. Curr. Chem.,* **2014**, *354*, 213; h) S. Erbas-Cakmak, D. A. Leigh, C. T. McTernan, A. L. Nussbaumer, *Chem. Rev*., **2015**, *115*, 10081.

[2] a) V. Balzani, A. Credi, M. Venturi, *Chem. Soc. Rev*., **2009**, *38*, 1542; b) J.-P. Collin, F. Durola, J. Frey, V. Heitz, F. Reviriego, J.-P. Sauvage, Y. Trolez, K. Rissanen, *J. Am. Chem. Soc.,* **2010**, *132*, 6840; c) M. J. Langton, S. W. Robinson, I. Marques, V. Felix, P. D. Beer, *Nat. Chem*., **2014**, *6*, 1039.

[3] a) G. Du, E. Moulin, N. Jouault, E. Buhler, N. Giuseppone, *Angew. Chem. Int. Ed*., **2012**, *51*, 12504; b) M. Xue, Y. Yang, X. Chi, X. Yan, F. Huang, *Chem. Rev*., **2015**, *115*, 7398; c) C. J. Bruns, J. F. Stoddart, *Acc. Chem. Res*., **2014**, *47*, 2186; d) Fasano, V. Baroncini, M. Moffa, M. Iandolo, D.

Camposeo, A. Credi, A. Pisignano, D., *J. Am. Chem. Soc.,* **2014**, *136*, 14245; e) N. D. Suhan, S. J. Loeb, S. H. Eichhorn, *J. Am. Chem. Soc.,* **2013**, *135*, 400;

[4] a) I. Aprahamian, T. Yasuda, T. Ikeda, S. Saha, W. R. Dichtel, K. Isoda, T. Kato, J. F. Stoddart, *Angew. Chem. Int. Ed.,* **2007**, *46*, 4675; b) H. X. Deng, M. A. Olson, J. F. Stoddart, O. M. Yaghi, *Nat. Chem*., **2010**, *2*, 439; c) C. J. Bruns, D. Fujita, M. Hoshino, S. Sato, J. F. Stoddart, M. Fujita, *J. Am. Chem. Soc.,* **2014**, *136*, 12027; d) D. A. Tramontozzi, N. D. Suhan, S. H. Eichhorn and S. J. Loeb, *Chem. Eur. J.,* **2010**, *16*, 4466.

[5] a) G. J. E. Davidson, S. J. Loeb. *Angew. Chem. Int. Ed. Engl*., **2003**, *42*, 74; b) S. J. Loeb, *Chem. Soc. Rev*., **2007**, *36*, 226; d) V. N. Vukotic, S. J. Loeb. *Chem. Soc. Rev*., **2012**, *41*, 5896; c) V. N. Vukotic and S. J. Loeb, in *Encyclopedia of Inorganic and Bioinorganic Chemistry*, ed. L. R. MacGillivray, C. M. Lukehart. Wiley & Sons, Ltd: Chichester, UK, **2014**. DOI: 10.1002/9781119951438.eibc2193; d) D. J. Mercer, J. Yacoub, K. Zhu, S. K. Loeb, S. J. Loeb, *Org. Biomol. Chem.,* **2012**, *10*, 6094; e) V. N. Vukotic and S. J. Loeb, *Chem. Eur. J.,* **2010**, *16*, 13630; f) L. K. Knight, V. N. Vukotic, E. Viljoen, C. B. Caputo and S. J. Loeb, *Chem. Commun.,* **2009**, 5585; g) D. J. Hoffart and S. J. Loeb, *Angew. Chem. Int. Ed.,* **2005**, *44*, 901; h) D. J. Mercer, V. N. Vukotic and S. J. Loeb, *Chem. Commun.,* **2011**, *47*, 896. S. J. Loeb, *Chem. Commun.,* **2005**, *41*, 1511.

[6] a) V. N. Vukotic, K. J. Harris, K. Zhu, R. W. Schurko, S. J. Loeb, *Nat. Chem*., **2012**, *4*, 456; b) K. Zhu, V. N. Vukotic, C. A. O'Keefe, R. W. Schurko, and S. J. Loeb, *J. Am. Chem.,* **2014**, *136*, 7403; c) V. N. Vukotic, C. A. O'Keefe, K. Zhu, K. J. Harris, C. To, R. W. Schurko, and S. J. Loeb, *J. Am. Chem. Soc.,* **2015**, *137*, 9643.

[7] N. Noujeim, K. Zhu, V. N. Vukotic, S. J. Loeb, *Org. Lett*., **2012**, *14*, 2484.

[8] N. Farahani, K. Zhu, N. Noujeim, S. J. Loeb, *Org. Biomol. Chem.,* **2014**, 4824.

[9] a) K. Zhu, V. N. Vukotic, S. J. Loeb, *Angew. Chem. Int. Ed.,* **2012**, *51*, 2168; b) K. Zhu, V. N. Vukotic, N. Noujeim, S. J. Loeb, *Chem. Sci*., **2012**, 3, 3265; c) N. Farahani, K. Zhu, S. J. Loeb, *ChemPhysChem.,* **2016**, DOI: 10.1002/cphc.201600128.

[10] K. Zhu, C. O'Keefe, V. N. Vukotic, R. W. Schurko, S. J. Loeb, *Nat. Chem.,* **2015**, *7*, 514.

[11] X. Lin, I. Telepeni, A. J. Blake, A. Dailly, C. M. Brown, J. M. Simmons, M. Zoppi, G. S. Walker, M. Thomas, T. J. Mays, P. Hubberstey, N. R. Champness, M. Schroder, *J. Am. Chem. Soc.,* **2009**, 131, 2159.

[12] Y. Kobuke, J. T. Dy, K. Ogawa, A. Satake, A. Ishizumi, *Chem. Eur. J.,* **2007**, *13*, 3491.

[13] M. H. Petersen, S. A. Gevorgyan, F. C. Krebs, *Macromolecules,* **2008**, *41*, 8986.

[14] K. Nakazono, T. Takata, *Chem. Eur. J.,* **2010**, *16*, 13783.

[15] Mercury version 3.8, Cambridge Crystallographic Data Centre (CCDC). C. F. Macrae, I. J. Bruno, J. A. Chisholm, P. R. Edgington, P. McCabe, E. Pidcock, L. Rodriguez-Monge, R. Taylor, J. van de Streek, P. A. Wood, *J. Appl. Cryst.,* **2008**, *41*, 466.

[16] The Y-shaped imidazolium unit shows strong interactions with crown ethers through hydrogen bonding and ion-dipole interactions (see ref. 8), while only one weak residual hydrogen bonding exists between neutral aniline axles and crown ethers.

[17] A. Bielecki, D. P. Burum, *J. Magn. Reson.,* **1995**, *220*, 215.

[18] K. Eichele, R. E. Wasylishen, WSolids: Solid-State NMR Spectrum Simulation Package **2001**.

[19] R. L. Vold, G. L. Hoatson, *J. Magn. Reson.,* **2009**, *198*, 57.

[20] N. Chandrakumar, *Spin-1 NMR*; Springer, **1996**.

[21] A. F. M. Kilbinger, S. J. Cantrill, A. W. Waltman, M. W. Day, R. H. Grubbs, *Angew. Chem. Int. Ed.,* **2003**, *42*, 3281.

[22] SHELX G. M. Sheldrick, Acta Cryst., 2008, A64, 112.

[23] Images generated using CrystalMaker®; *CrystalMaker Software* Ltd, Oxford, England (www.crystalmaker.com).

[24] A. Bielecki, D. P. Burum, *J. Magn. Reson.,* **1995**, *220*, 215.

[25] K. Eichele, R. E. Wasylishen, WSolids: Solid-State NMR Spectrum Simulation Package **2001**.

[26] R. L. Vold, G. L. Hoatson, *J. Magn. Reson.,* **2009**, *198*, 57.

[27] N. Chandrakumar, *Spin-1 NMR*; Springer, 1996.

[28] V. N. Vukotic, K. J. Harris, K. Zhu, R. W. Schurko, S. J. Loeb, *Nat. Chem.,* **2012**, *4*, 456.

[29] K. Zhu, V. N. Vukotic, C. A. O'Keefe, R. W. Schurko, S. J. Loeb, *J. Am. Chem. Soc.,* **2014**, *136*, 7403.

[30] K. Zhu, C. A. O'Keefe, V. N. Vukotic, R. W. Schurko, S. J. Loeb, *Nat. Chem.*, **2015**, *7*, 514.

[31] V. N. Vukotic, C. A. O'Keefe, K. Zhu, K. J. Harris, C. To, R. W. Schurko, S. J. Loeb, *J. Am. Chem. Soc.,* **2015**, 137, 9643.

CHAPTER 5

5.1 Dynamics of a Rotaxane Wheel about a Bis(imidazole) Axle Inside a Zr-Based Metal Organic Framework

5.1.1 Introduction

Mechanically interlocked molecules (MIMs) have two advantages as molecular machines. First a wide variety of supramolecular assemblies with different structures and functions can be developed using combination of various organic molecules. Second, even though the relative motion of the MIM components is independent to some extent, the interlocked skeleton confines or control its direction.[1] Although almost all MIM-based molecular machines and devices operate efficiently in solution environment,[2] they are not compatible with typical solid-state technology wherein controlled cooperative molecular motion of individual MIMs is necessary.[3] This challenge can be addressed by transferring nanoscale MIMs into condensed and highly-organized materials.[4] Using nanoscale molecular machines in the solid state or other condensed material could affect the properties and function of the material at the macroscopic level.[5] To this end, we developed a series of Cu-based MOFs, **UWDM-1** (University of Windsor Dynamic Material) using [2]rotaxanes which contain a rigid aniline-based axle and a variety of different-sized macrocycles and identified dynamic properties of the wheel inside the pores of the MOFs.[6] More recently, T-shaped 2,4,7-triphenylbenziimidazolium templating motif[7] was used to develop a rigid degenerate molecular shuttle.[8] Then, this [2]rotaxane molecular shuttle was used to create a prototype Zn-based MOF, **UWDM-4** for which it was demonstrated translational motion of its macrocyclic ring in the solid state.[9] Later, a new recognition site using a rigid, Y-shaped 2,4,5- triphenylimidazolium axle was designed[10] and it was demonstrated that the Y-shaped recognition site is an excellent core to develop rigid MIMs such as bistable [2]rotaxane

molecular shuttles.[11] To identify the dynamic properties of the Y-shaped templating motif in the solid state, this Y-shaped axle was combined with an isophthalate coordinating group to create a MIM linker with an imidazole recognition site and incorporated into a Zn-based MOF, **UWDM-5**. Using variable-temperature (VT) ^{2}H solid-state NMR spectroscopy (SSNMR), it was observed that the interlocked macrocyclic component can undergo conformational changes and rotational motion by a thermal input.[12] Although, it was demonstrated that the Y-shaped MIM ligand can undergo dynamic motion inside the solid state, it was still of interest to develop other MIM ligands using Y-shaped axle that could be used in combination with metal ions to create MOF materials which show dynamic properties.

Based on the previous studies on the structures and properties of MIM-based MOFs, dynamic motion can only be observed in MOF materials with robust and stable frameworks which show high degree of porosity. However, only a few of known MOFs exhibit sufficient stability required for the intended applications.[13] To address this challenge, we targeted MOFs created from Zr-based nodes and carboxylate-terminated linkers. Zr-based MOFs are known to possess high chemical, mechanical and thermal stability due to strong ionic bonding between Zr(IV) sites and negatively charged carboxylate ions.[14] To this end, we report herein the preparation of a MOF designated **UWDM-6** containing a [2]rotaxane MIM linker with a bis(imidazole) core and demonstrate that the interlocked macrocyclic component can undergo dynamic motion inside the solid state.

5.1.2 Results and Discussion

5.1.2.1 Linker Synthesis and Characterization

It has been established by Farha,[15] Yaghi[16] and others[17] that symmetrical tetracarboxylic ligands (*e.g.* tetracarboxyphenylporphyrin (H_4-TCPP-H_2) and 1,3,6,8-tetrakis(*p*-benzoicacid)pyrene (H_4TBAPy)) can be linked to Zr clusters to form 3-periodic Zr-based MOFs. Varying the complexity of these ligands has been a popular strategy for the

construction of Zr-based MOF materials with high porosity and stability.[18] With this in mind, a new symmetrical tetracarboxylic [2]rotaxane linker was designed by combining two Y-shaped imidazolium-based templates. Scheme 5.1 describes the synthesis of the new tetracarboxylic acid linker, **6**. Initially, two nitrogen atoms of bis(imidazole) **1** were protected using trimethylsilylethoxymethyl chloride (SEMCl) followed by a bromination reaction to yield the tetrabromo substituted bis(imidazole). The bromide groups of the protected bis(imidazole) were then replaced by 4-ethoxycarbonylphenyl groups via a Suzuki-coupling reaction to yield **2**. After removal of the SEM protecting groups and protonation, [**4**-H_2]$^{+2}$ was used as a template for ring closing metathesis (RCM), employing Grubb I catalyst. The RCM reaction allowed clipping of a bis-olefin macrocycle precursor around the bis(imidazolium) recognition site to give [2]rotaxane **4** as a mixture of *E/Z* isomers (*ca.* 60:40). Finally, hydrogenation of the residual double bond using D_2(g) and Pd/C followed by treatment with base to hydrolyze the four ester groups gave the neutral MIM linker **6.**

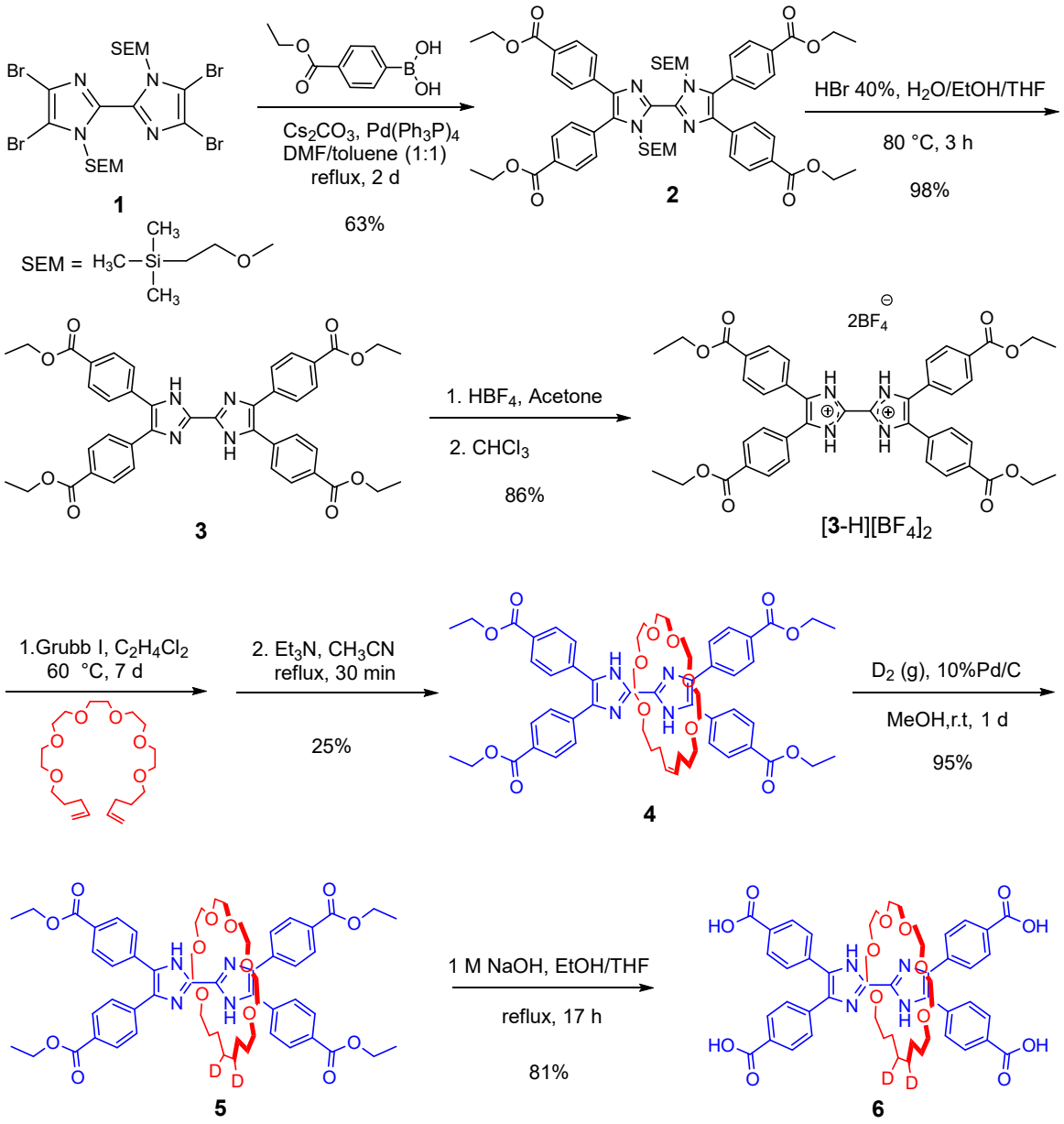

*Scheme 5.1. Synthesis of interlocked linker **6** with deuterium (D=²H) labels.*

The linker **6** was characterized in solution by ^{1}H and ^{13}C NMR spectroscopy as well as high-resolution electrospray-ionization mass spectrometry (HR-ESI MS). Fig. 5.1 shows the ^{1}H NMR spectrum of compound **6** in CD_3OD.

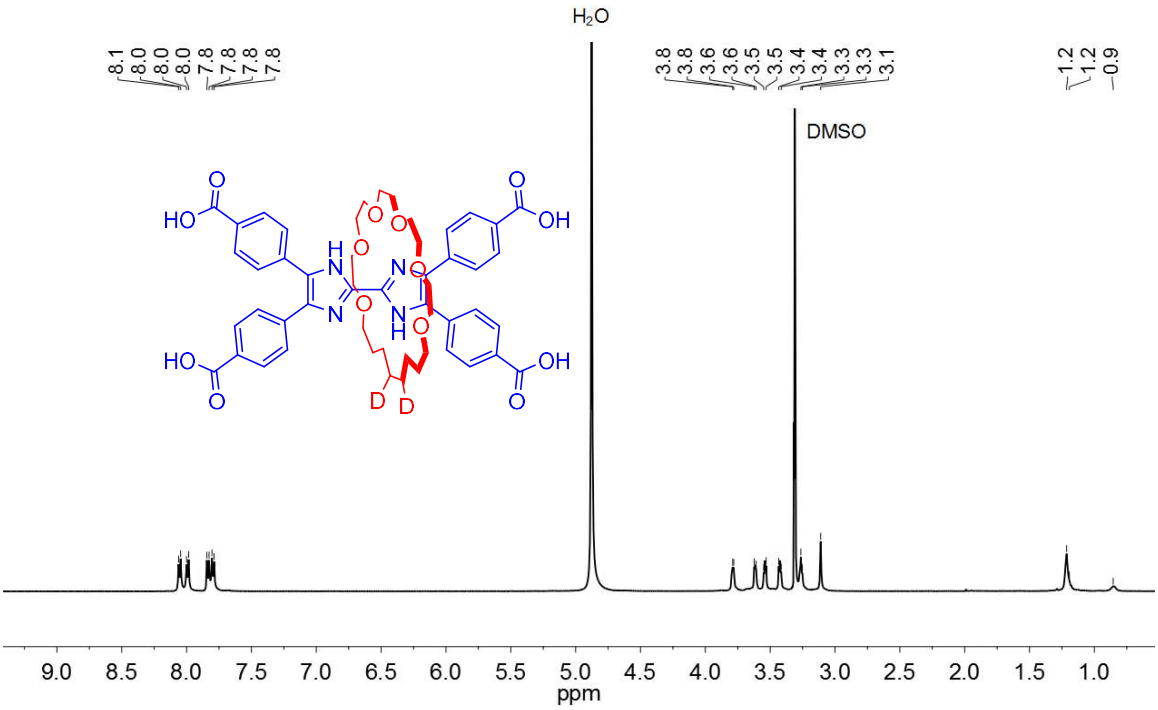

*Figure 5.1. ^{1}H NMR spectrum of interlocked linker **6** in CD_3OD at 298 K.*

Further, the structure of **5** was confirmed by single-crystal X-ray diffraction which revealed the axle and wheel are clearly interlocked with two hydrogen bonding interactions between bis(imidazole) N-H groups on the axle and two oxygen atoms of **24C6** ring; N-H···O; 2.11 Å (165°) and 1.15 Å (154°).

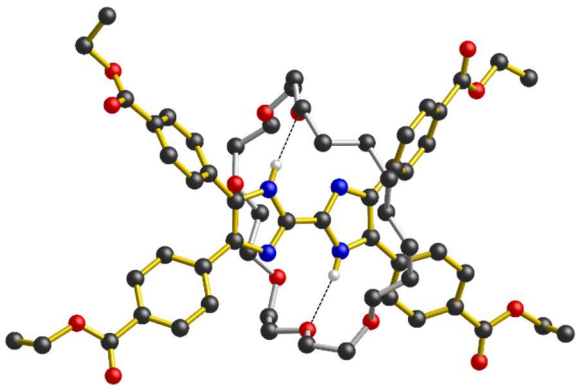

*Figure 5.2. X-ray structure of the interlocked linker **5** showing two N-H…O hydrogen bonding interactions between the axle and wheel components. Only hydrogen atoms of bis(imidazole) unit are shown for clarity. Color Key: black= carbon, red = oxygen, blue = nitrogen, gold bond = axle, silver bond = wheel.*

5.1.2.2 MOF Synthesis and Characterization

The solvothermal reaction of MIM linker **6**, $ZrCl_4.8H_2O$ and benzoic acid in N,N'-diethylformamide (DEF) at 120 °C for 20 h yielded the MOF designated **UWDM-6** as a X-ray-quality crystalline material. **UDMW-6** crystallizes in the tetragonal space group P4 with unit cell parameters a =b = 19.687(4) Å and c = 15.980(3) Å. The single X-ray analysis determined the SBU (secondary binding unit) with formula of $[Zr_6(\mathbf{6})_2(\mu_3\text{-}OH)_8(H_2O)_8]$. **UWDM-6** adopts a rare **scu-a** topology in which a $Zr_6(\mu_3\text{-}O)_8(H_2O)_8^{8+}$ node is linked by eight carboxylates from the rectangular linker **6**. To the best of our knowledge, the scu-a network was missing in Zr-MOFs as connectivity of 8-connected Zr_6 cluster to 4-connected D_{4h} and D_{2h} linkers may not be the thermodynamically favored outcome.[19] Thus, **UWDM-6** can be considered the prototype for the construction of Zr-MOFs with scu topology.

Fig. 5.3a shows a ball-and-stick representation of a single unit of the neutral MIM linker **6** coordinated to four Zr(IV) clusters. Figs. 5.3b,c illustrate a view down the c-axis of the crystal, in ball-and-stick and space-filling models, respectively. Fig. 5.3d shows a view down the a- and b- axes in a ball-and-stick model. It appears that the large channels of the MOF provide enough void space for the **24C6** rings (red in space-filling models) to be free from any steric interactions with the neighboring macrocycles and surrounding framework (blue).

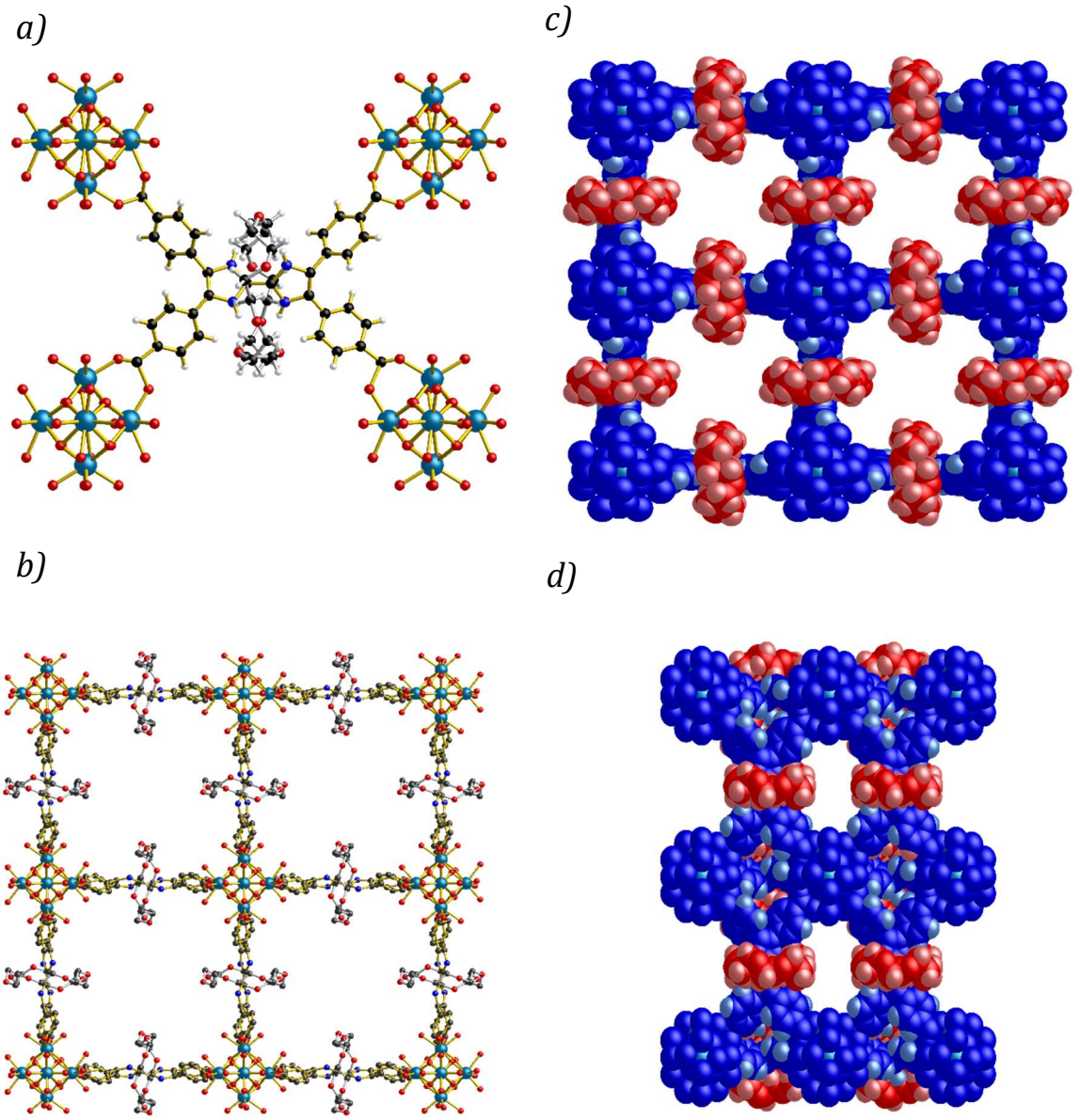

*Figure 5.3. X-ray structure of **UWDM-6** determined by single crystal X-ray diffraction. (a) a ball-stick representation of the basic repeating unit of MIM linker **6** linked to four $Zr_6(O)_8(H_2O)_8^{8+}$ clusters. (b) a ball-stick representation of a view down c-axis showing the channels (c) As in b, but a space-filling model; (d) a space-filling representation of a view down a- and b- axis.*

The powder X-ray diffraction (PXRD) pattern of as-synthesized **UWDM-6** is in excellent agreement with the simulated PXRD pattern indicating the bulk phase purity of the material (Fig 5.4). Thermogravimetric analysis (TGA) of a non-activated sample of **UWDM-6**

showed weight loss attributed to removal of free solvent molecules from the pores (*i.e.* H_2O and DEF followed by decomposition of the macrocycle at 250 °C[6, 20] and eventual decomposition of the MOF framework at approx. 400 °C.

Interestingly, when the material was desolvated using solvent exchange from DEF to CH_2Cl_2 and drying under vacuum,[21] significant changes appeared in the PXRD pattern of **UWDM-6**. However, the original PXRD pattern of **UDWM-6** was restored when the dried sample was resolvated with DEF which is indicative of a reversible phase change of the material due to removal of DEF from the pores (Fig. 5.4). Moreover, VT-PXRD data also revealed that this material goes through similar a phase change over a temperature range of 100-200 °C (see experimental Fig. 5.9). Thus, this material can undergo a reversible structural transformation without any structural collapse. Unfortunately, broadness of the PXRD pattern did not allow for indexing the new phase and determination of cell parameters.[22] Conversion between the phases can be attributed to reversible conformational changes in the MIM linkers which bring the Zr (IV) nodes closer together and reduces the pore volume.[23] This type of structural transformation is a known feature for some of similar Zr-based MOFs which are described as soft porous crystals (SPCs).[24] For example, some MOFs display this reversible 'breathing' behavior in response to external stimuli, which structural transformation leads to significant pore volume changes in a reversible manner.[24,25]

Although, **UWDM-6** goes through a phase change in response to removal of solvent molecules from the pores, thermal stability of the material allowed us to study the thermally-driven molecular motion of the interlocked **24C6** wheels inside the MOF. Therefore, the material was activated to provide enough void space for macrocycles to undergo uninhibited motion by replacing the coordinated benzoate ions with hydroxide ions and removing the free molecules inside the channels (see section 5.2.9)

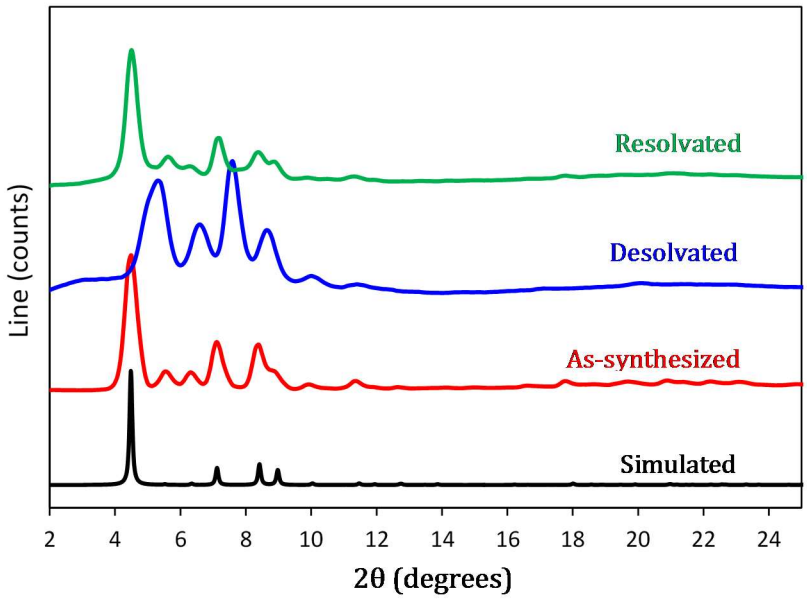

*Figure 5.4. Powder X-ray diffraction spectra of **UWDM-6.** Black: simulated spectrum from the single crystal structure. Red: as-synthesized, Blue: desolvated sample prepared using exchange of solvent from DEF to CH_2Cl_2 and then drying under vacuum at r.t. for 1 h and Green: desolvated sample resoaked in DEF for 24 h.*

5.1.2.3 Dynamics in the Solid State

^{2}H SSNMR spectra of activated **UWDM-6** were obtained over a wide temperature range (185-411 K) to characterize the dynamics[26] of the **24C6** rings in the solid state. To this end, MIM synthesized by RCM was labelled with deuterium atoms by reduction of double bond via addition of D_2 gas. Experimental and simulated VT ^{2}HNMR spectra of activated **UWDM-6** are shown in Fig. 5.5 (see section 5.2.16) The static spectrum obtained at 181 K simulated as a single site and indicates that there are no motions that affect the ^{2}H quadrupole interactions on the NMR time scale (Fig. 5.5a). Increasing the temperature to 298 K produces a change in the powder pattern which was simulated using two site jumps of the CD_2 group with the rate in the fast motion limit (FML) through an angle of 75° (Fig. 5.5b). Starting at 411 K, the CD_2 reorientation is accompanied with partial rotation of **24C8** through 225° in 45°

steps at a rate of 5 ×10^5 Hz (Fig. 5.5c). Although, the single X-ray structure of **UWDM-6** showed that the ring is in an unconstrained environment, no full rotation of the macrocylce around the axle was observed. Even though the subtle phase change that is observed does not effect the gross structure of the lattice, it may involve subtle changes that affect the mobility of the macrocycle.

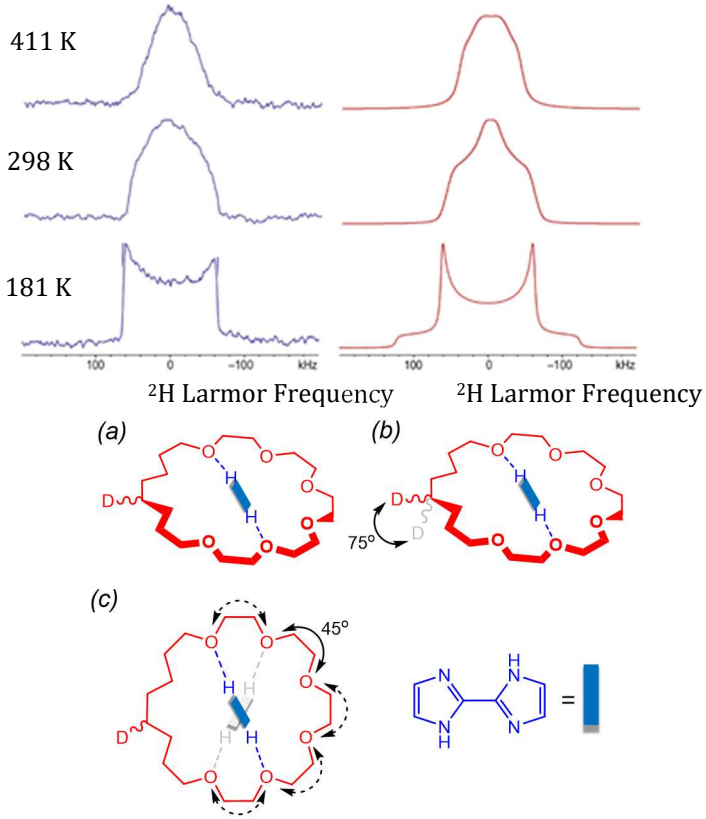

*Figure 5.5. Experimental (left) and simulated (right) ^{2}H SSNMR powder pattern as a function of temperature for **UWDM-6**. Illustration (below) of motions of the **24C6** macrocyclic ring relative to the framework axle: (a) the slow motion limit (SML) where no motion is occurring on the NMR time scale (b) the fast motion limit (FML) for jumps between two sites 75° apart, and (c) partial rotation of the ring over 225° in 45° steps.*

The VT ^{2}H SSNMR patterns for **UWDM-6** is clearly different from those previously observed for **UWDM-5**, which contains a Zn-based MOF with the same macrocyclic wheel encircling an imidazolium axle.[12] It appears that the non-covalent interactions between the wheel and bis(imidazole) recognition site is stronger as compared to imidazolium which

prevents the complete rotation of the macrocycle around the framework skeleton. Apparently, the thermal energy needed for full rotation of the ring is much greater in **UWDM-6**. Moreover, comparison of the SSNMR data for **UWDM-5** and **UWDM-6** shows that both two site jumps and partial rotation occur at higher temperatures for **UWDM-6**. This can be understood by rationalizing that the stronger interactions between the axle and wheel which results in a noticeable effect on the barrier to motion.

5.1.2.4 Protonation of UWDM-6

The overall charge on the MIM linker is an extremely important property that affects the interaction of the macrocyclic wheel with the recognition site[8,11] and may give rise to different dynamic properties for the MOF.[9] Since Zr-based MOFs are known to possess high chemical stability,[14] this feature provided the opportunity to post-synthetically, protonate the bis(imidazole) unit of the MIMs inside the MOF to study the dynamic properties of the protonated version of **UWDM-6**. We therefore developed a non-destructive method to protonate the MIM linker inside the MOF material. Accordingly, activated **UWDM-6** was treated with triflic acid (CF_3SO_3H) in ethanol at 60 °C to yield a protonated MOF, designated **UWDM-6**.$(HOTf)_2$ (see section 5.2.11). The degree of protonation was quantified by monitoring the amount of $CF_3SO_3^-$ (OTf^-) anion present in the material, using ^1H and ^{19}F NMR after decomposing the sample in a 10% D_2SO_4/DMSO-d_6 mixture. The ^{19}F signals of the OTf^- were integrated against the ^1H NMR signals of the MIM ligand utilizing an internal standard 1,2-dibromo,4,5-diflourobenzene (see experimental Fig. 5.12). Protonation was also indicated by solid-state ^{19}F NMR spectroscopy in which an OTf^- signal appeared after treatment of **UWDM-6** with acid. Gratifyingly, PXRD experiment for **UWDM-6**.$(HOTf)_2$ showed no significant changes as compared to the pattern of activated **UWDM-6** which inferred that no change in the basic internal structure of **UWDM-6** occurred after treatment with acid (see experimental Fig. 5.14).

We also found that the protonated MOF can be easily converted back to its neutral state by soaking the sample in DEF at 90 °C without any significant effect on the structural integrity of the rigid MOF skeleton.

To determine if the macrocycle could undergo rotational motion about the bis(imidazolium) unit inside the solid-state lattice of the MOF, a d_2-labelled sample of **UWDM-6**.$(HOTf)_2$ was subjected to VT ^{2}H SSNMR. VT ^{2}HNMR spectra of **UWDM-6**.$(HOTf)_2$ are shown together with spectral simulations in Fig. 5.6.

The spectrum obtained at 185 K could not be simulated as a single site, but simulated using two site jumps of the CD_2 group through an angle of 78° at a rate of 5×10^6 Hz which indicates the motions could not be frozen even at low temperature (Fig. 5.5a). Increasing the temperature increased the rate of two site jumps such that at 253 K, the ring undergoes CD_2 reorientations with the rate in the fast motion limit (FML). At 343 K, two site jumps occurs through an angle of 70° which is accompanied with partial rotation of **24C8** through 225° in 45° steps at a rate of 1×10^5 Hz (Fig. 5.5b). At 388 K and above, the spectra clearly indicate that the macrocycle is undergoing partial rotations with the rate in the fast motion limit (FML), in combination with the conformational changes. Comparison of the VT ^{2}H SSNMR spectra for **UWDM-6**.$(HOTf)_2$ and **UWDM-6** at low temperatures demonstrate that, although the description of the motion is the same, the onset temperatures are much lower for **UWDM-6**.$(HOTf)_2$.

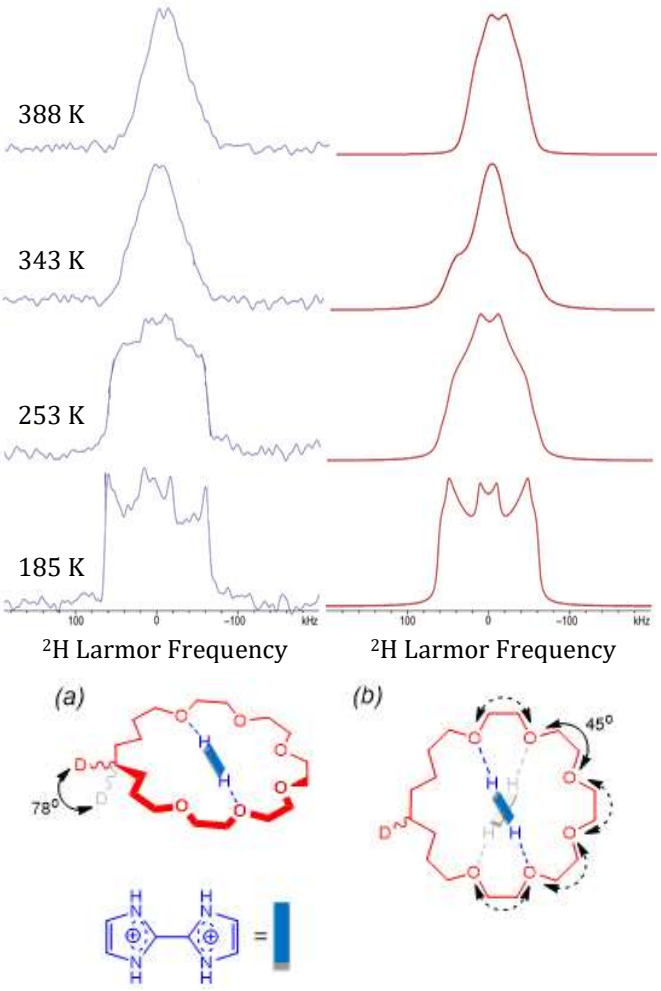

*Figure 5.6. Experimental (left) and simulated (right) ^{2}H SSNMR powder pattern as a function of temperature for **UWDM-6**.(HOTf)$_2$. Illustration (below) of motions of the **24C6** macrocyclic ring relative to the framework axle: (a) two site jumps separated by 78° (b) partial rotation of the ring over 225° in 45° steps.*

5.1.2.5 Lithium Binding of UWDM-6

Although the demonstration of acid-base control of rotational motion in the solid state was gratifying, the access to a MOF containing bis(imidazole) units with N,N chelating sites, motivated us to explore other methods that might affect the dynamic motion inside the material. It is known that imidazole moieties exhibit high binding affinity toward a wide variety of metal ions.[27] MIMs with nitrogen donor atoms can also provide a chelating site and form stable complexes with metal atoms.[28] Thus, the structure of MIM linker **6**

consisting of a bis(imidazole) unit with two donor nitrogen atoms in close proximity to several oxygen atoms from the **24C6** macrocycle, might offer an effective chelating site to the metals.

At the first step toward understanding if the metal ions can be coordinated to the MIM with bis(imidazole) core, the Li^+ ion was tested for coordination in solution.[29] To this end, a sample of [2]rotaxane **5** was subjected to a ^1H NMR titration study in the mixture of $CDCl_3/CD_3CN$ (see experimental Fig. 5.16). Titration of [2]rotaxane **5** with lithium ions produced significant changes in chemical shifts which are consistent with strong binding of Li^+ to bis(imidazole) nitrogen atoms and the neighbouring macrocycle oxygen atoms ($K = 10^4$) (see section 5.2.13).

To identify whether or not the MIM is capable of Li-binding in the solid state MOF, a d_2-labelled sample of activated **UWDM-6** was treated with a lithium triflate (LiOTf) solution in a mixture of CH_3Cl/CH_3CN to give a Li-doped MOF, designated **UWDM-6**.LiOTf (see section 5.2.14). The presence of Li^+ ions inside the MOF was indicated by ^7Li NMR spectroscopy of a digested sample of **UWDM-6**.LiOTf (see experimental Fig. 5.18). Solid-state ^7Li NMR spectroscopy also showed two ^7Li signals, which were tentavily assigned as Li^+ ions coordinated to the cluster and Li^+ ions bound to the chelating site of the linker (see experimental Fig. 5.19). To characterize the mobility of the macrocycle inside the Li-doped MOF, **UWDM-6**.LiOTf was probed by VT ^2H SSNMR experiments (see Figure 5.23). The VT ^2H SSNMR data for **UWDM-6**.Li are quite similar to those observed for **UWDM-6.** It could be argued that the interaction of Li^+ with the chelating site of MIM does not significantly effect the rotational motion of the **24C6**. This might be thought of being analogous to the effect observed for protonation of **UWDM-6** or the lack of a significant increase in the barrier to rotation observed for **UWDM-5** when compared to **UWDM-1**. Alternatively, this result could

simply mean that the degree to which the Li+ ions are complexed is reduced as the temperature is increased.

5.1.3 Conclusion

The symmetrical tetracarboxylic structure of the new rotaxane linker **6** allows for formation of a highly porous and stable Zr-based MOF (**UWDM-6**) as a X-ray-quality crystalline material. **UWDM-6** is a prototype Zr-based MOFs with **scu** topology in which a $Zr_6(\mu_3\text{-}O)_8(H_2O)_8^{8+}$ node is linked by eight carboxylates from the rectangular linker **6**. Sufficient void space for a full range of dynamic motions along with thermal stability of **UWDM-6** allows study of the dynamic properties of the interlocked component in MOF using VT ^2H SSNMR. Moreover, high thermal and chemical stability of **UWDM-6** provide the opportunity to use post-synthetic approaches on the material using acid and Li^+ ion to study the effect of protonation and Li^+ doping on the internal dynamics of **UWDM-6**. VT ^2H SSNMR specra show that Li^+ doping does not significantly change the energy barrier to rotation, especially at higher temperatures. Whereas, SSNMR spectra of protonated **UWDM-6** are slightly different from **UWDM-6**. The onset temperatures are lower for protonated **UWDM-6,** however the description of the motion is the same. Although, it appears that the thermal energy required to induce conformational changes and partial rotation of the wheel is lower inside the protonated MOF, more studies are required to understand the SSNMR and motion behaviour of the macrocyclic wheel inside the MOF.

5.2 Experimental

5.2.1 General Comments

Starting materials were purchased from Aldrich and Alfa Aesar and 1,1-bis(trimethylsilylethoxymethyl)-4,4',5,5'-tetrabromo-2,2'-biimidazole (**1**) was obtained according to literature procedure.[30] Solvents were dried using an Innovative Technologies

Solvent Purification System. Deuterated solvents were obtained from Cambridge Isotope Laboratories and used as received. Thin-layer chromatography (TLC) was performed using Teledyne Silica gel 60 F_{254} plates which were viewed under UV light. Column chromatography was performed using Silicycle Ultra-Pure Silica Gel (230–400 mesh). Flash column chromatography was performed using Teledyne Ultra-Pure Silica/RP-C18 Silica Gel (230–400 mesh) on a Teledyne Isco Combiflash-R_f instrument. ^{1}H, ^{13}C, ^{19}F and all ^{2}D solution NMR experiments were performed on a Bruker Avance III 500 instrument, with Larmor frequencies of 500.1 MHz for ^{1}H nuclei, 125.7 MHz for ^{13}C and 470.5 MHz for ^{19}F. Chemical shifts are quoted in ppm relative to tetramethylsilane (d_{iso}=0 ppm) using the residual solvent peak as a secondary reference standard. ^{7}Li experiment was performed using aqueous LiCl as external standard on a Bruker US 300 instrument. High-resolution mass spectrometry (HRMS) experiments were performed on a Waters Xevo G2-XS time-of-flight (ToF) instrument using lockspray for accurate mass determinations. ESI acquisitions were completed using a 1 μL injection into a sample loop with a constant 5 μL min^{-1} flow of 50:50 H_2O/CH_3CN (with 0.1% formic acid). All single-crystal X-ray data were collected on a Bruker D8 diffractometer with a Photon 100 CCD detector operating at 50 kV and 30 mA with CuK_α radiation. Crystals were frozen in paratone oil inside a cryoloop and reflection data were integrated from frame data obtained from hemisphere scans. Powder XRD measurements were recorded on a Bruker D8 Discover diffractometer equipped with a GADDS 2D-detector and operated at 40 kV and 40 mA. CuK_α radiation was used and the initial beam diameter was 0.5 mm. Thermal gravimetric analyses were conducted on a Mettler Toledo TGA SDTA 851e instrument. Helium (99.99%) was used to purge the system with a flow rate of 30 mL min^{-1}. Samples were held at 25 °C for 10 min before heating up to 550 °C at 2 °C min^{-1}. Melting points were recorded on a Stanford Research Systems, Opti Melt MPA100 instrument. Infrared spectra were recorded on a Bruker Alpha FT-IR spectrometer in the range of 4000–400 cm.

5.2.2 Synthesis of 2

1 (2.2 g, 3.1 mmol), 4-ethoxycarbonylphenylboronic acid (4.8 g, 24.7 mmol), cesium carbonate (Cs_2CO_3) (5.1 g, 15.6 mmol) and a mixture of DMF/toluene (40 mL: 40 mL) were added to a round-bottom flask. The reaction mixture was degassed under N_2 followed by addition of 10% $Pd(Ph_3P)_4$ catalyst (361 mg, 0.3 mmol). The mixture was then heated to reflux for 2 d, cooled and filtered to remove unreacted Cs_2CO_3. The solvent was evaporated under reduced pressure. The crude product was extracted 3 times with $CHCl_3/H_2O$ (60:60 mL), dried with $MgSO_4$ and concentrated under vacuum.CH_3CN was then added to the residue and the precipitate was filtered and dried under vacuum to yield **2** as an off-white solid. Yield: 1.82 g, 63%; MP 186-188 °C; ^{1}H NMR ($CDCl_3$, 500 MHz, 296 K): δ (ppm) = 8.17 (d, 4H, *J* = 8.5 Hz), 7.91 (d, 4H, *J* = 8.5 Hz), 7.61(d, 4H, *J* = 8.5 Hz), 7.54 (d, 4H, *J* = 8.5 Hz), 5.91 (s, 4H), 4.44 (q, 4H, *J* = 7.0 Hz), 4.34 (q, 4H, *J* = 7.0 Hz), 3.53 (t, 4H, *J* = 8.5 Hz), 1.44 (t, 6H, *J* = 7.0 Hz) , 1.37 (t, 6H, *J* = 7.0 Hz), 0.838 (t, 4H, *J* = 8.5 Hz); ^{13}C NMR ($CDCl_3$, 125 MHz, 292 K): δ (ppm) = 166.6, 166.2, 138.5, 138.3, 137.6, 134.5, 131.6, 131.3, 131.2, 130.3, 129.7, 128.8, 126.8, 73.4, 66.3, 61.5, 61.0, 18.1, 14.5, 14.5; IR (neat) = 2990, 2954, 1721, 1699, 1608, 1408, 1271, 1081, 1017, 953, 838, 779, 709 cm^{-1}; HR-MS (ESI-ToF) *m/z*: calcd for $[M+H]^+$, $[C_{54}H_{67}N_4O_{10}Si_2]^+$, 987.4390; found 987.4361.

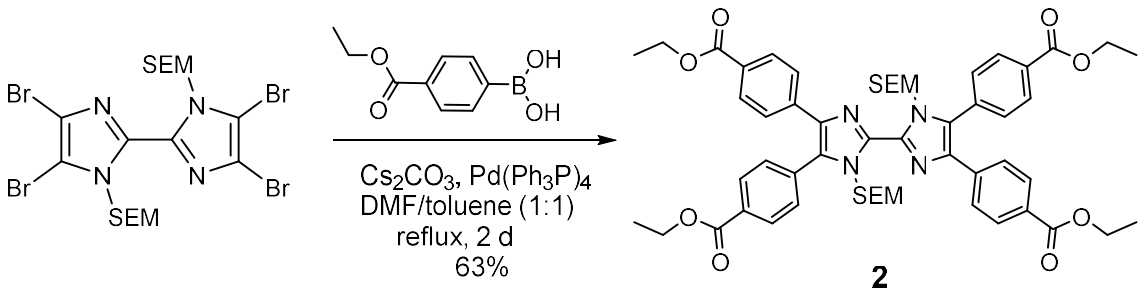

*Scheme 5.2. Synthesis of **2***

5.2.3 Synthesis of 3

2 (1.8 g, 1.9 mmol) was dissolved in a mixture of H_2O, EtOH and THF (100: 500: 400 mL) followed by addition of 40% aqueous HBr (100 mL). The mixture was heated at 80 °C for 3 h, the EtOH and THF were removed under vacuum and the resulting slurry was neutralized with K_2CO_3 to pH=7. The yellow precipitate weas filtered, washed with water and air dried. Yield: 1.4 g, 98%; MP 267-271 °C; ^{1}H NMR ($CDCl_3$, 500 MHz, 296K): δ (ppm) = 7.93 (d, 8H, *J* = 8.0 Hz), 7.38 (d, 8H, *J* = 6.5 Hz), 4.35 (q, 8H, *J* = 7.0 Hz), 1.37 (t, 12H, *J* = 7.0 Hz); ^{13}C NMR ($CDCl_3$, 125 MHz, 297 K): δ (ppm) = 165.8, 132.6, 132.5, 131.8, 131.7, 130.6, 128.3, 61.6, 14.4; IR (neat) = 3508, 2922, 1713, 1609, 1367, 1272, 1104, 1018, 852, 799, 770, 700, 580 cm^{-1}; HR-MS (ESI-ToF) *m/z*: calcd for $[M+H]^+$, $[C_{42}H_{39}N_4O_8]^+$, 727.2762 ; found 727.2769.

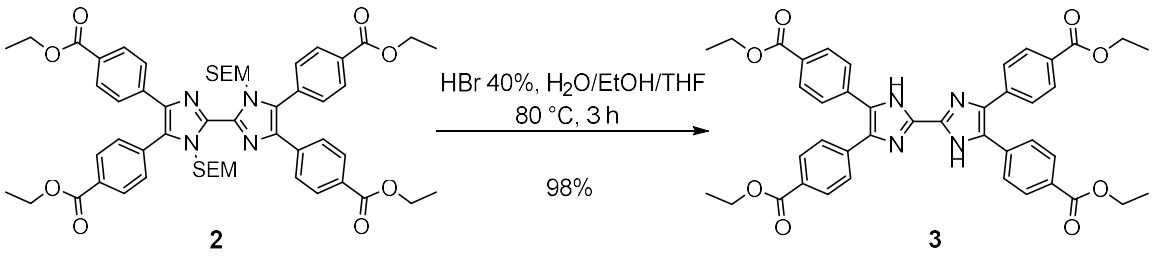

*Scheme 5.3. Synthesis of **3**.*

5.2.4 Synthesis of $[3\text{-}H][BF_4]_2$

Tetrafluoroboric acid diethyl ether complex (0.4 mL, 3.0 mmol) was added to a solution of **3** (1.0 g, 1.4 mmol) in acetone (30 mL). After 10 min stirring at room temperature, the solvent was removed under reduced pressure.The white product was then dissolved in chloroform (30 mL), filtered and air dried. Yield: 782 mg, 86%; MP 225-227 °C; ^{1}H NMR ($CDCl_3$, 500 MHz, 294K): δ (ppm) = 8.19 (d, 8H, *J* = 8.5 Hz), 7.84 (d, 8H, *J* = 8.5 Hz), 4.42 (q, 8H, *J* = 7.0 Hz), 1.42 (t, 12H, *J* = 7.0 Hz); ^{13}C NMR (CD_3CN, 125 MHz, 295 K): δ (ppm) = 166.5, 133.7, 133.4, 133.3, 132.3, 130.9, 129.3, 62.2, 14.4; IR (neat) = 3549, 2980, 1711, 1607, 1411, 1278,

1218, 1018, 861, 771, 699, 522 cm^{-1}; HR-MS (ESI-ToF) *m/z*: calcd for $[M\text{-}2BF_4]^+$, $[C_{42}H_{39}N_4O_8]^+$, 727.2762; found 727.2768.

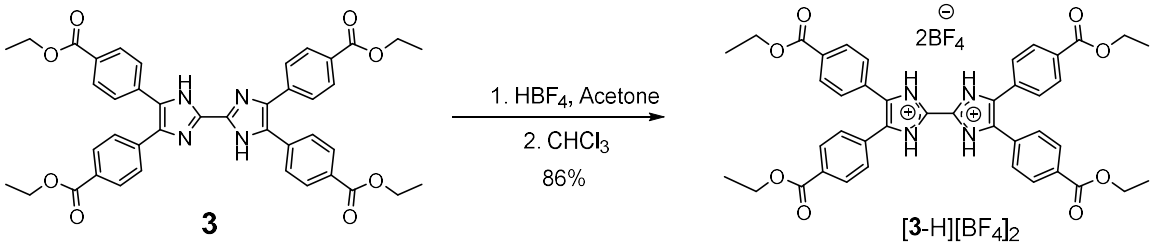

*Scheme 5.4. Synthesis of [**3**-H][BF_4]$_2$.*

5.2.5 Synthesis of 4

Compound [**3**-H][BF_4]$_2$ (780 mg, 0.9 mmol) and pentaethyleneglycol-dipent-4-enyl ether[2] (971 mg, 2.6 mmol) were added to a Schlenck flask and dissolved in 1,2-dichloroethane (200 mL). The flask was degassed and back-filled with N_2. Grubbs I catalyst (71 mg, 0.09 mmol) was added in one portion to the stirred solution and heated at 60 °C for 16 h after which another 45% catalyst was added over a period of 7 days. Progress of the reaction was monitored by ^{1}H NMR spectroscopy. After this time, the reaction was cooled to room temperature and the solvent was removed under reduced pressure. The residue was washed with diethyl ether (100 mL), dissolved in chloroform (20 mL) and neutralized with triethylamine (2 mL). The crude product was purified using flash column chromatography with a mixture of chloroform/aceton/triethylamine (10:0.5:0.1) as the eluent. The brown-yellow solid was collected, dissolved in CH_3CN (30 mL) followed by addition of riethylamine (1 mL). The desired product (E/Z mixture ~ 60/40) was precipitated as a yellow solid, filtered and air dried. Yield: 232 mg, 25%; MP 283-287 °C; ^{1}H NMR ($CDCl_3$, 500 MHz, 293K): (major product) δ (ppm) = 12.36 (s, 2H), 8.04 (d, 4H, *J* = 8.5 Hz), 8.00 (d, 4H, *J* = 8.5 Hz), 7.81 (d, 4H, *J* = 8.5 Hz), 7.77 (d, 4H, *J* = 8.5 Hz), 4.94 (t, 2H, *J* = 3.5 Hz), 4.39 (qui, 8H, *J* = 7.0 Hz), 3.74-3.73 (m, 4H), 3.67-3.66 (m, 4H), 3.52-3.48 (m, 4H), 3.36 (t, 4H, *J* = 5.0 Hz), 3.28 (t, 4H, *J*

= 6.5 Hz), 3.04 (s, 4H), 1.85-1.80 (m, 4H), 1.42 (q, 12H, *J* = 7.0 Hz), 1.31-1.21 (m, 4H); ^{13}C NMR (CD_2Cl_2, 125 MHz, 294 K): δ (ppm) = 166.6, 166.6, 140.6, 140.5, 140.3, 140.2, 137.9, 137.8, 136.3, 136.2, 130.3, 129.9, 129.9, 129.8, 129.8, 129.0, 129.0, 128.9, 128.9, 128.9, 127.9, 127.7, 71.8, 71.4, 71.1, 70.8, 70.6, 70.5, 70.4, 70.3, 70.3, 69.7, 69.7, 61.4, 61.2, 31.0, 30.4, 29.5, 28.5, 24.8, 14.6; IR (neat) = 3212, 2868, 1708, 1606, 1445, 1367, 1269, 1173, 1096, 1018, 972, 863, 776, 708 cm^{-1}; HR-MS (ESI-ToF) *m/z*: calcd for $[M+H]^+$, $[C_{60}H_{72}N_4O_{14}]^+$, 1073.5123; found 1073.5103.

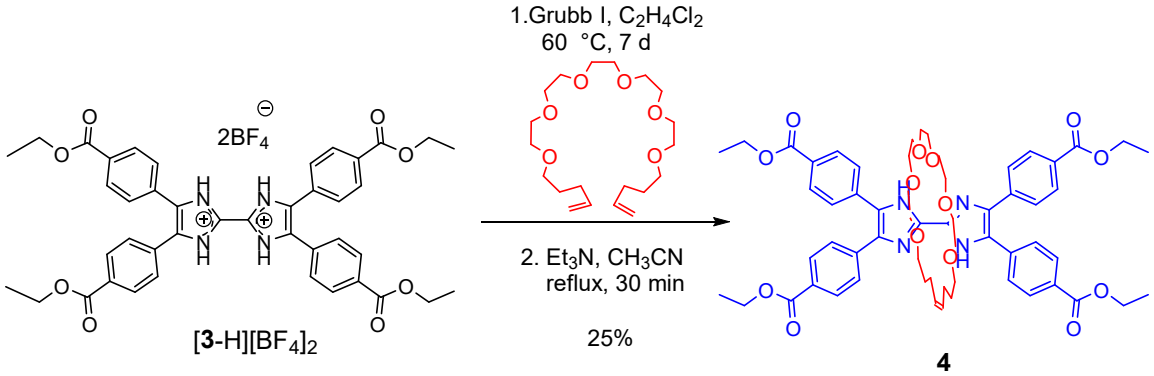

Scheme 5.5. Synthesis of ***4.***

5.2.6 Synthesis of 5

Pd/C 10wt% (23 mg, 0.02 mmol) was added to a Schlenck flask and a balloon of D_2 gas was attached to the flask with an adapter that allowed the balloon to be closed off from the reaction flask. The flask was evacuated by vacuum and then back filled with N_2. Compound **5** (230 mg, 0.2 mmol) was solubilized in THF (10 mL) and transferred to the flask via a syringe. A slight vacuum was applied to the reaction mixture until the solvent begins to bubble and then the balloon was opened to the flask. The mixture stirred for 24 h under ambient conditions. The solid was filtered and the filtrate was concentrated under reduced pressure to yield a yellow solid. Yield: 219 mg, 95%; MP > 300 °C; ^{1}H NMR ($CDCl_3$, 500 MHz, 297K): δ (ppm) = 12.35 (s, 2H), 8.04 (d, 4H, *J* = 8.5 Hz), 8.00 (d, 4H, *J* = 8.5 Hz), 7.82 (d, 4H, *J*

= 8.5 Hz), 7.77 (d, 4H, *J* = 8.5 Hz), 4.40 (qui, 8H, *J* = 7.0 Hz), 3.75-3.74 (m, 4H), 3.60-3.58 (m, 4H), 3.50 (t, 4H, *J* = 5.0 Hz), 3.37 (t, 4H, *J* = 5.0 Hz), 3.22 (t, 5H, *J* = 6.0 Hz), 3.07 (s, 4H), 1.56-1.52 (m, 4H), 1.42 (q, 12H, *J* = 7.5 Hz), 1.19-1.09 (m, 6H); ^{13}C NMR ($CDCl_3$, 125 MHz, 299 K): δ (ppm) = 166.8, 166.6, 140.3, 139.9, 137.7, 136.0, 129.8, 129.7, 129.4, 128.7, 128.6, 127.6, 71.3, 71.0, 70.4, 70.2, 70.1, 70.0, 69.2, 61.2, 61.0, 29.8, 29.6, 25.6, 25.5, 14.5; IR (neat) = 3208, 2768, 1709, 1607, 1269, 11.72, 1097, 1018, 940, 863, 776, 679 cm^{-1}; HR-MS (ESI-ToF) *m/z*: calcd for $[M+H]^+$, $[C_{60}H_{73}D_2N_4O_{14}]^+$, 1077.5400; found 1077.5366.

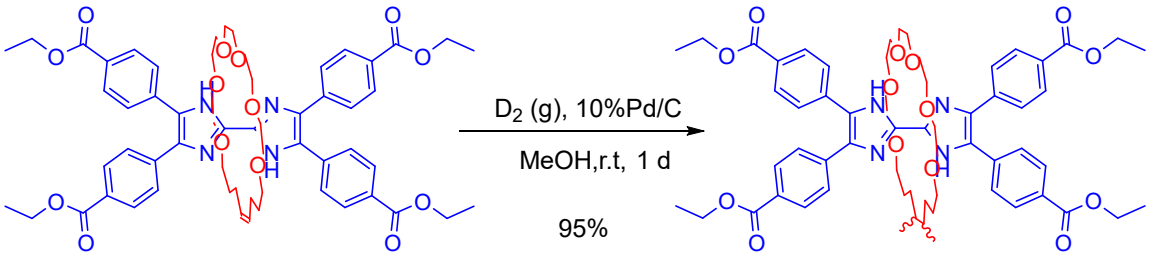

*Scheme 5.6. Synthesis of **5**.*

5.2.7 Synthesis of 6

Compound **6** (215 mg, 0.2 mmol) was dissolved in a mixture of EtOH/THF (7 mL: 7 mL) followed by addition of 1M NaOH (7 mL). the reaction mixture was heated at 80 °C for 17 h, concentrated in vacuum and carefully acidified with 1M HCl to pH= 5 to obtain a yellow precipitate. The resulting solid was filtered and washed with pH= 5 water and dried under vacuum. Yield: 156 mg, 81%; MP > 300 °C; ^{1}H NMR (CD_3OD, 500 MHz, 296K): δ (ppm) = 8.06 (d, 4H, *J* = 8.0 Hz), 8.99 (d, 4H, *J* = 8.0 Hz), 7.84 (d, 4H, *J* = 8.0 Hz), 7.80 (d, 4H, *J* = 8.0 Hz), 3.79 (m, 4H), 3.62 (m, 4H), 3.54 (t, 4H, *J* = 5.0 Hz), 3.42 (t, 4H, *J* = 5.0 Hz), 3.26 (t, 5H, *J* = 5.5 Hz), 3.11 (s, 4H); ^{13}C NMR (CD_3OD, 125 MHz, 298 K): δ (ppm) = 169.9, 169.6, 141.5, 141.0, 138.8, 137.1, 130.9, 129.8, 128.7, 72.3, 72.0, 71.5, 71.3, 71.2, 71.1, 70.3, 30.8, 30.7, 26.7, 26.6; IR (neat) = 2961, 2869, 1685, 1608, 1418, 1259, 1418, 1259, 1175, 1088, 1017, 862, 796, 704,

677, 547 cm^{-1}; HR-MS (ESI-ToF) *m/z*: calcd for $[M+H]^+$, $[C_{52}H_{57}D_2N_4O_{14}]^+$, 965.4148; found 965.4125.

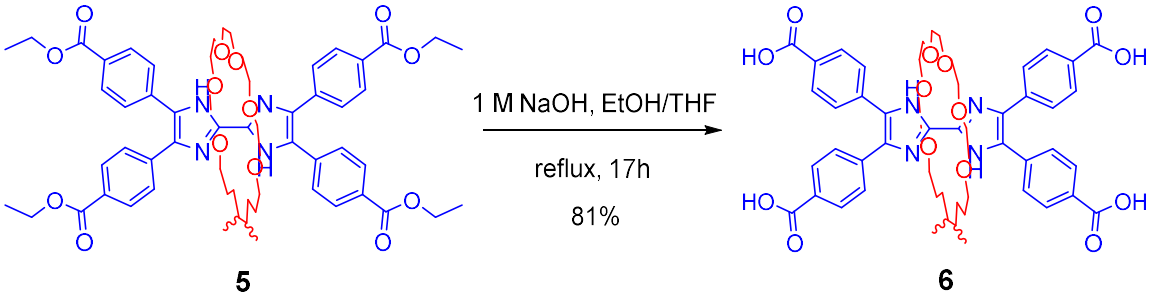

*Scheme 5.7. Synthesis of **6**.*

5.2.8 Synthesis of UWDM-6

$ZrCl_4.8H_2O$ (85 mg, 0.4 mmol) and benzoic acid (3500 mg, 28 mmol) were dissolved in DEF (15 mL). The mixture was heated at 80 °C for 1 h. After cooling to room temperature, ligand **6** (70 mg, 0.08 mmol) was added to the clear solution and the solution sonicated for 5 min. The yellow solution was transferred through a 25 mm syringe filter (0.2 μm PTFE membrane) to five 15 mL vials and heated at 120 °C in a programmable heating oven for 20 h. ThAe yellow crystalline product was collected.

5.2.9 Activation Procedure for UWDM-6

As-synthesized **UWDM-6** was soaked in 10 mL of DEF. The mixture was heated in an oven at 90 °C for 12 h. The solvent was replaced with fresh DEF and the mixture was returned to the oven. This procedure was repeated another four times over a 3-day period. The DEF was then replaced with DCM (6 × 30 mL) over a 3-day period. The solid was filtered, air dried and activated at 150 °C under vacuum for 2 h. Yield: 70 mg, 70%.

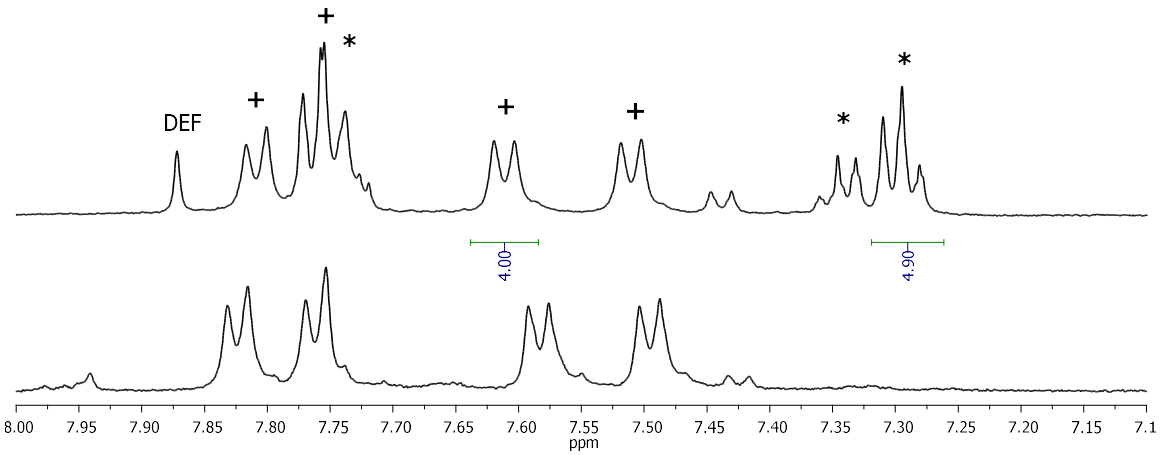

*Figure 5.7. ^{1}H NMR spectrum (500 MHz) of (a) as-synthesized and (b) activated **UWDM-6** peaks of ligand **6** and benzoic acid are denoted with (+) and (*), respectively. Samples were decomposed in K_3PO_4/D_2O/DMSO-d_6*

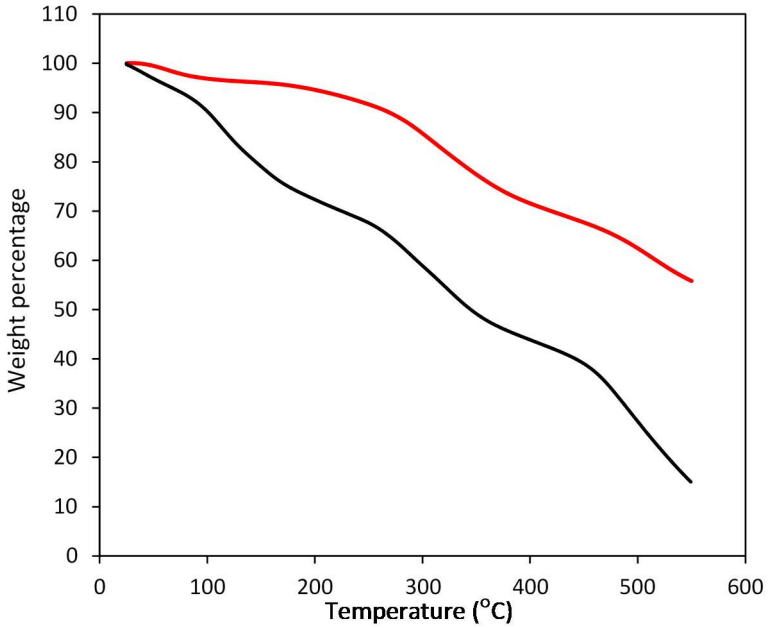

*Figure 5.8. Thermogravimetric analysis of as-synthesized (black) and Activated (red) **UWDM-6***

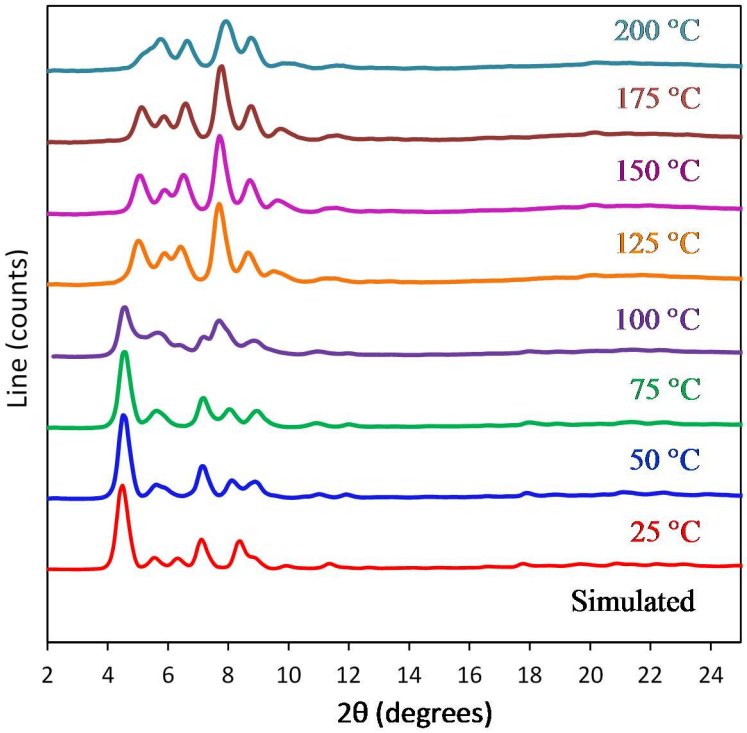

*Figure 5.9. Variable temperature powder X-ray diffraction spectra of **UWDM-6**.*

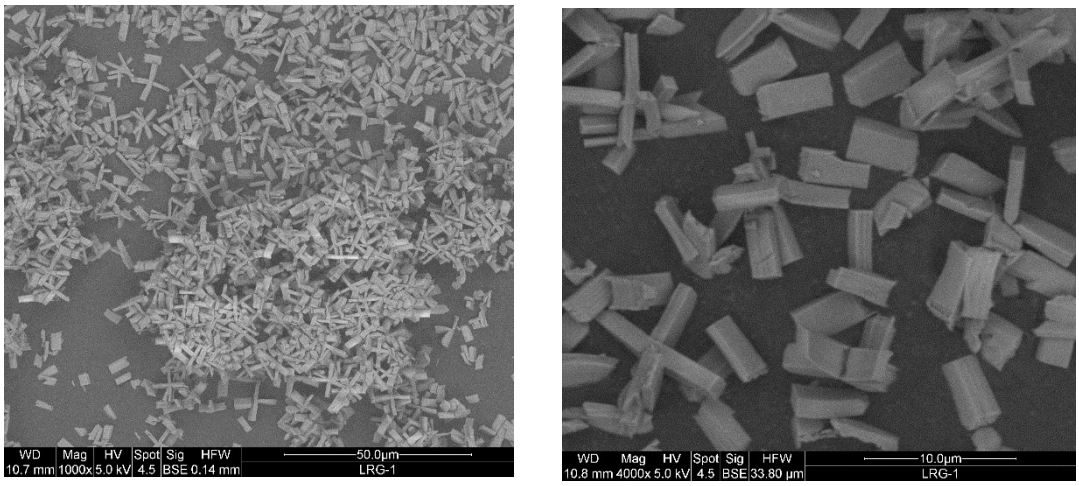

*Figure 5.10. SEM images of the crystalline product of **UWDM-6** at different magnifications.*

5.2.10 Chemical Stability of UWDM-6

As-synthesized **UWDM-6** (10 mg) was washed twice with DEF (3 mL) and soaked in 1 M aqueous HCl (5 mL) at room temperature for 17 h. Then, the solution was decanted and

the crystals were washed 3 times with DEF (3 mL) and finally, soaked in DEF (2 mL) at 45 °C for 24 h.

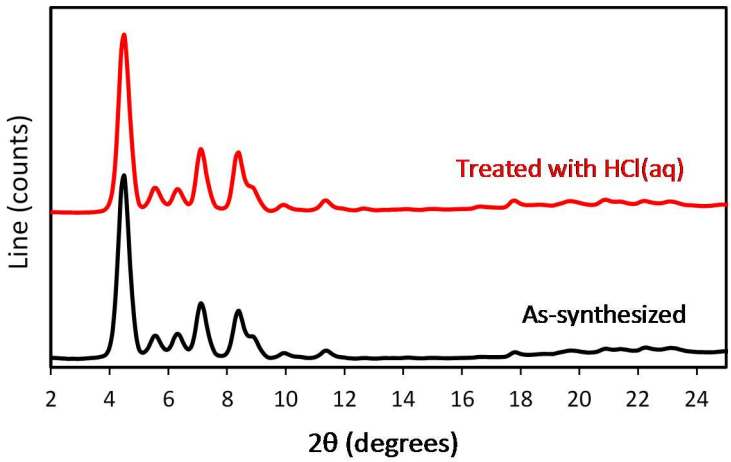

*Figure 5.11. Powder X-ray diffraction spectrum of **UWDM-6** after treatment with 1M HCl(aq) (top) in comparison to as-synthesized pattern (below).*

5.2.11 Protonation of UWDM-6

50 mg of activated **UWDM-6** was soaked in 2 M solution of triflic acid (CF_3SO_3H) in ethanol (15 mL) for 12 h at 60 °C. The solvent was replaced with the fresh triflic acid solution for another 12 h. The solid was filtered, quickly rinsed with the ethanol (2 mL) and DCM (15 mL) and activated under vacuum at 150 °C for 2 h.

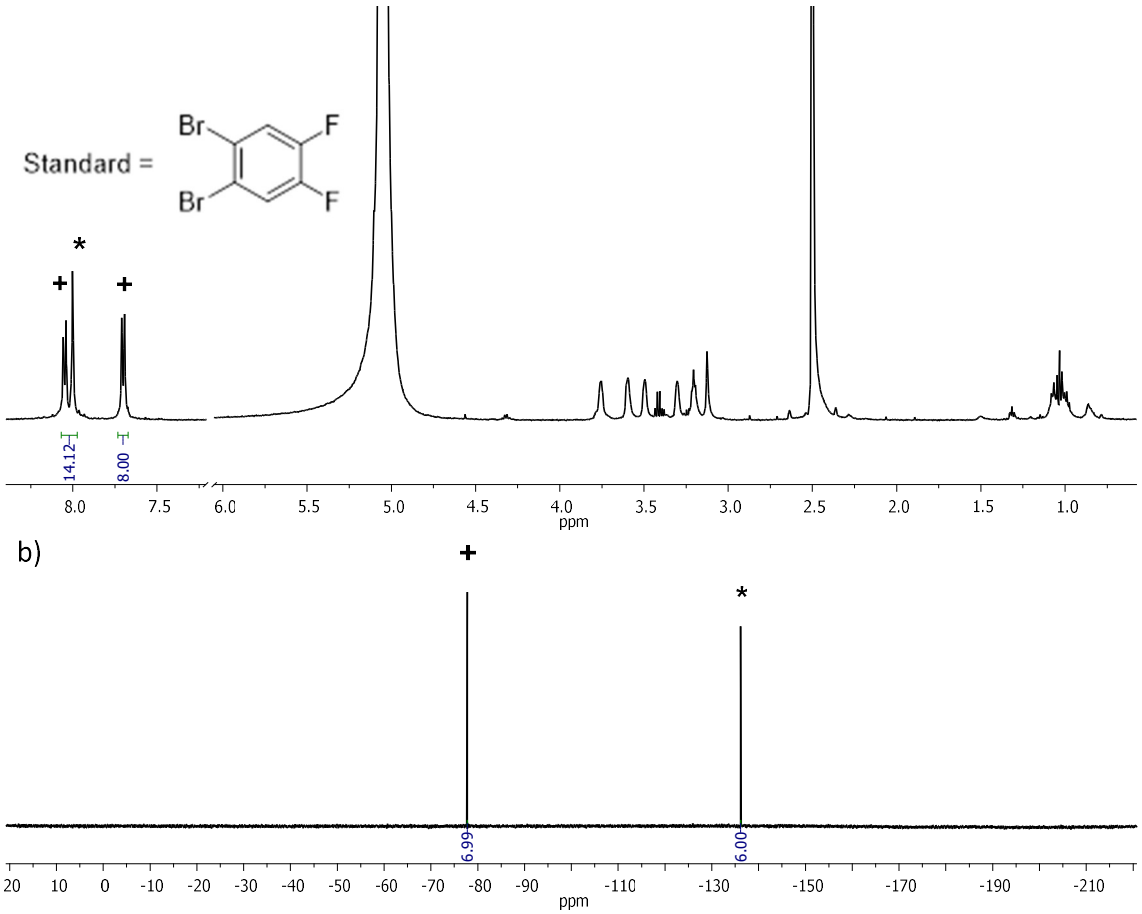

*Figure 5.12. (a) ^{1}H NMR and (b) ^{19}F NMR spectrum (500 MHz) of **UWDM-6**, after treatment with triflic acid (CF_3SO_3H); peaks for ligand **6** are denoted with (**+**) and peak for 1,2-dibromo, 4,5-diflourobenzene as the internal standard is denoted with (*****). Sample was decomposed in 10% D_2SO_4/DMSO-d_6.*

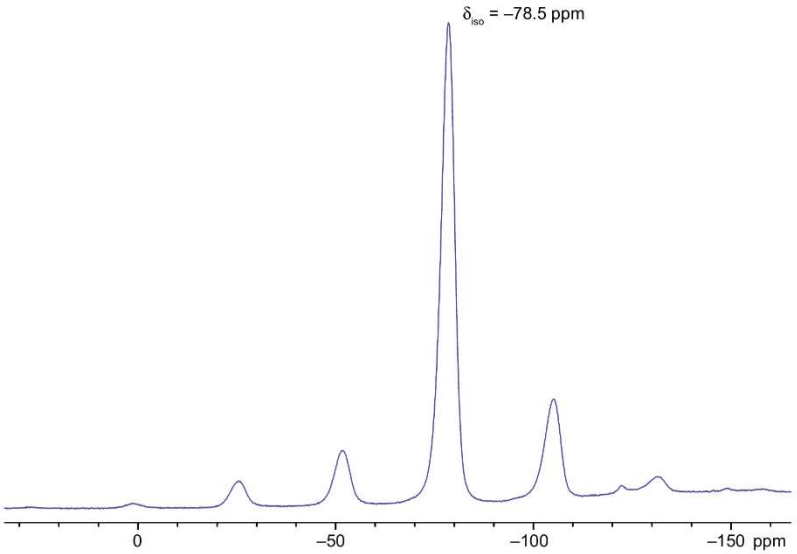

*Figure 5.13. Solid-state ^{19}F NMR spectrum of **UWDM-6**, after treatment with triflic acid (CF_3SO_3H).*

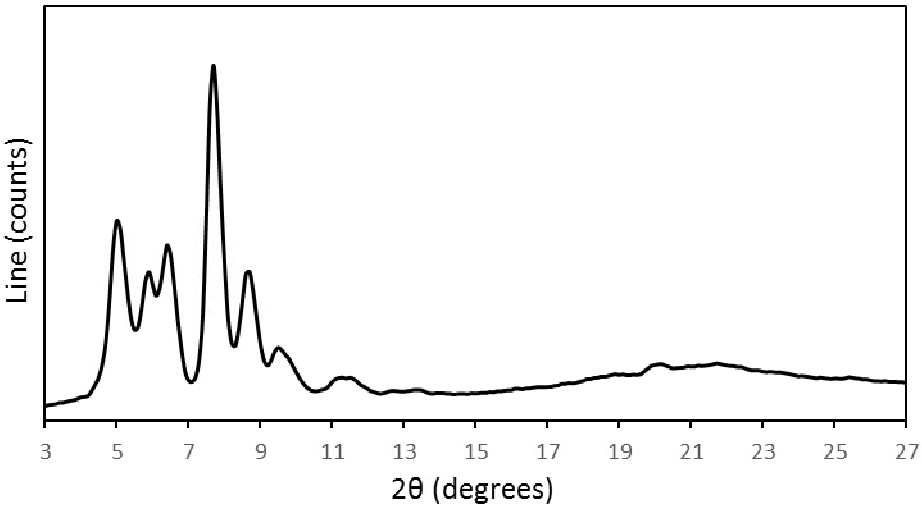

*Figure 5.14. Powder X-ray diffraction spectrum of **UWDM-6** after treatment with triflic acid (CF_3SO_3H).*

5.2.12 Deprotonation of protonated UWDM-6

A 10 mg sample of protonated **UWDM-6** was soaked in DEF (10 mL) and heated at 90 °C. The solvent was replaced every 24 h over a 3-day period. A ^{19}F NMR spectrum was recorded each day to monitor the deprotonation process.

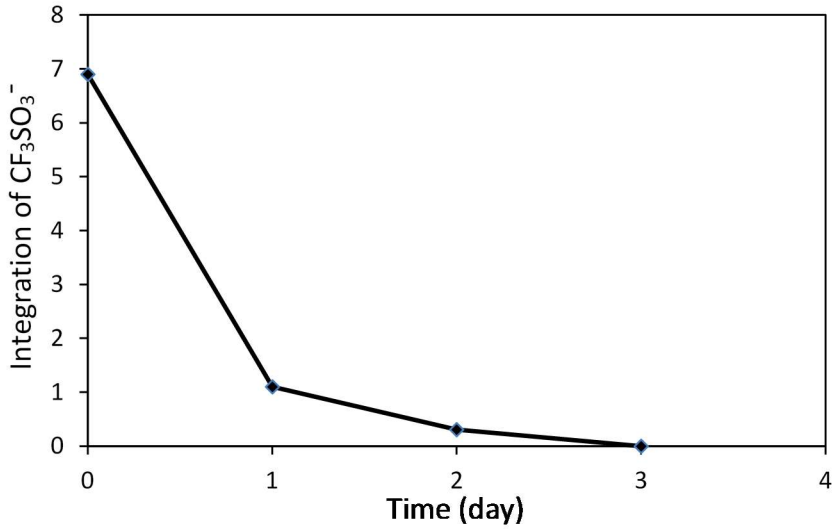

Figure 5.15. Plot of integration of $CF_3SO_3^-$ peak versus time obtained using ^1H NMR and ^{19}F NMR (500 MHz). Peak of 1,2-dibromo, 4,5-diflourobenzene was used as the internal standard.

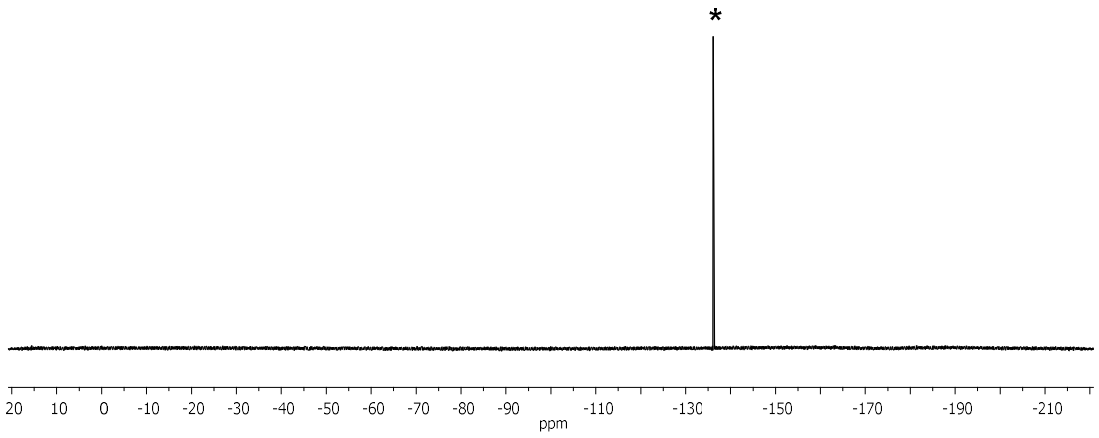

*Figure 5.16. ^{19}F NMR spectrum (500 MHz) of protonated **UWDM-6** after soaking in DEF at 90 °C for 3 days; peak for 1,2-dibromo, 4,5-diflourobenzene as the internal standard is denoted with (*). The peak of triflic acid was disappeared after 3 days. Sample was decomposed in 10% D_2SO_4/DMSO-d_6.*

5.2.13 Lithium Binding Constant Determination

A 2 mM solution of **5** in the mixture of $CDCl_3/CD_3CN$ (1.1 mg in 0.5 mL) was prepared in a 5-mm NMR tube. A 10 mM and 50 mM solution of lithium trifluoromethanesulfonate (LiOTf) in a mixture of $CDCl_3/CD_3CN$ (3.1 mg in 2 mL and 7.8 mg in 1 mL, respectively) were

prepared. An initial NMR spectrum of the solution of **5** was taken, and the initial chemical shift of the NH on the axle and CH protons on the axle and wheel were determined. The 10 mM solution of LiOTf was then added, initially in 10 μL portions, and ^{1}H NMR spectrum was recorded after each addition. After 1.6 equiv. addition of the guest, the aliquot size was increased to 20 μL. After a total of 300 μL had been added, the 50 mM solution of LiOTf was added in 10 and 20 μL portions. A total of 380 μL were added until no further change in the chemical shifts was observed. Association constants between ligand L and metal ions were calculated using the software HypNMR.[31] A 1:1 stoichiometry equilibrium model $L + M^{+} \rightarrow [LM]^{+}$ was used to fit the experimental titration data through a non-linear least-squares algorithm and obtain the log Ka values.

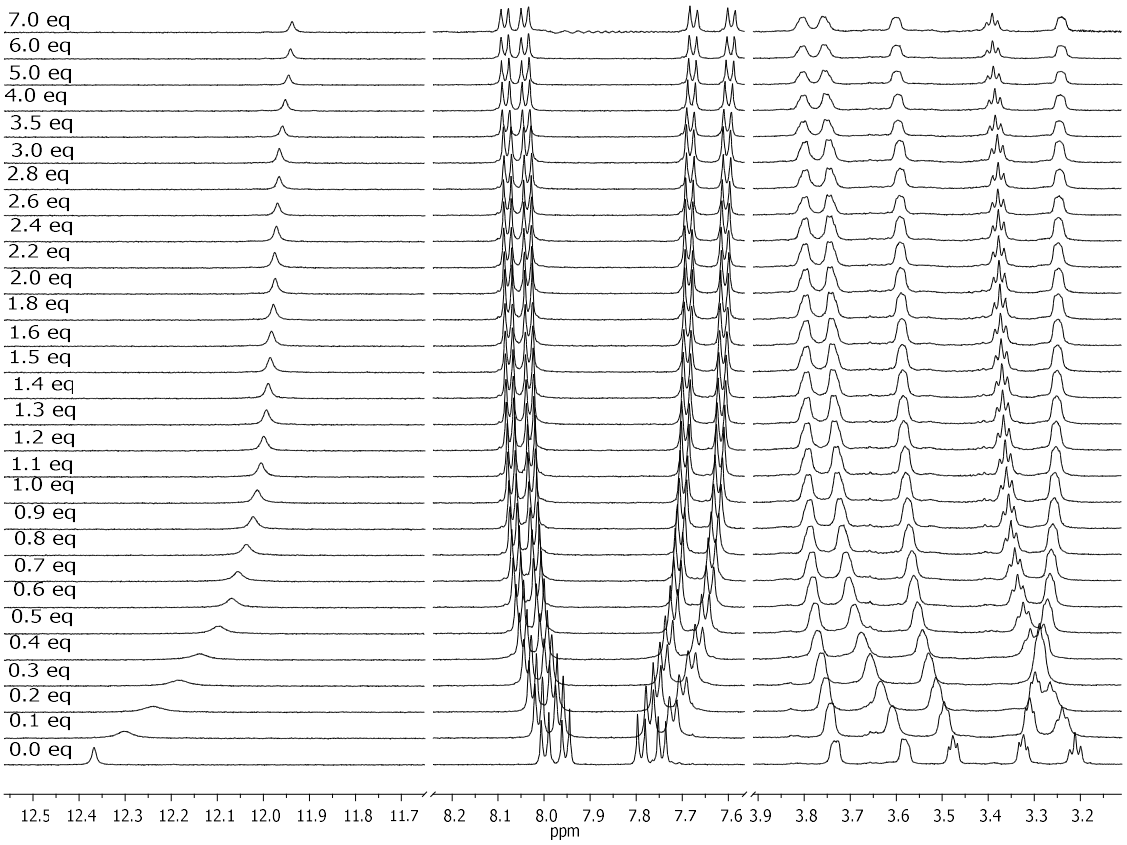

*Figure 5.17. Stacked ^{1}H NMR (500 MHz) resulting from titration of compound **5** against LiOTf solution.*

5.2.14 Lithium Binding for UWDM-6

50 mg of activated **UWDM-6** was soaked in the saturated solution of LiOTf in a mixture of $CHCl_3/CH_3CN$ (8:8 mL) for 12 h at room temperature. The solvent was replaced with fresh LiOTf solution for another 12 h. The solid was filtered, quickly rinsed with the mixture of $CHCl_3/CH_3CN$ (3:3 mL) and air dried. The MOF was activated under vacuum at 150 °C for 2 h.

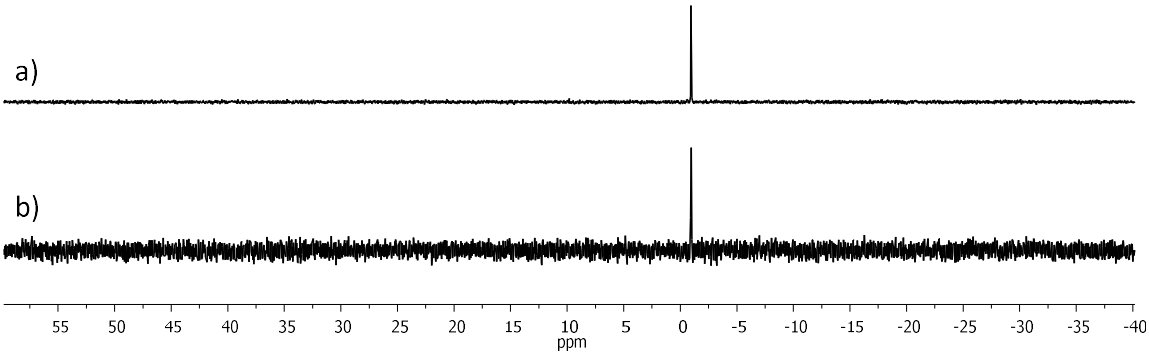

Figure 5.18. ^{7}Li NMR spectrum (300 MHz) of (a) LiOTf in 10% D_2SO_4/DMSO-d_6 (b) ***UWDM-6****, after soaking in saturated LiOTf solution for 24 h. Sample was decomposed in 10% D_2SO_4/DMSO-d_6.*

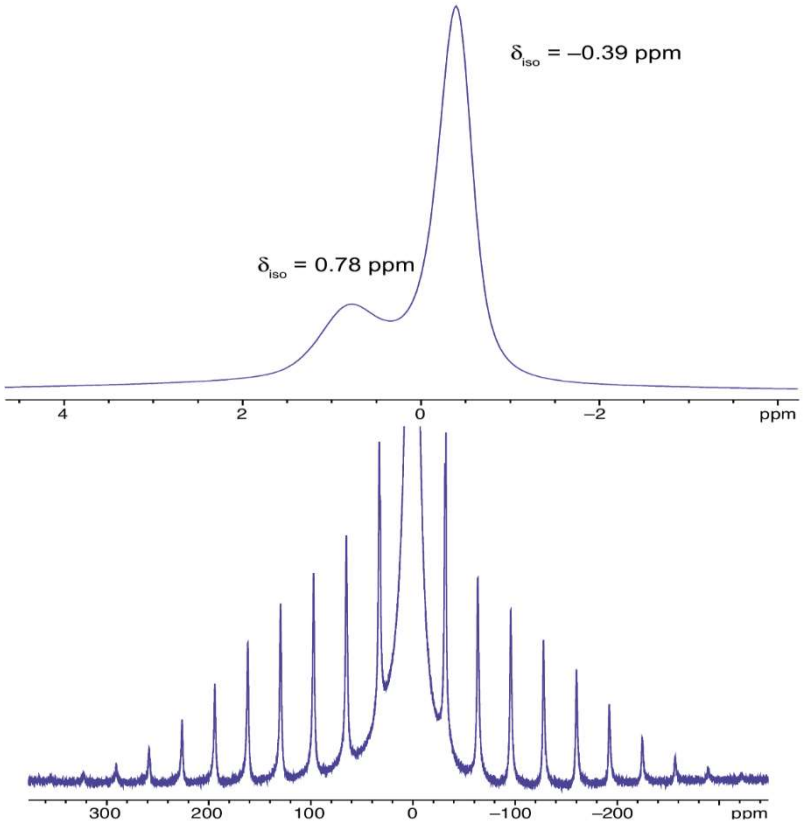

Figure 5.19. Solid-state ^{7}Li NMR spectrum of ***UWDM-6****, after soaking in saturated LiOTf solution for 24 h.*

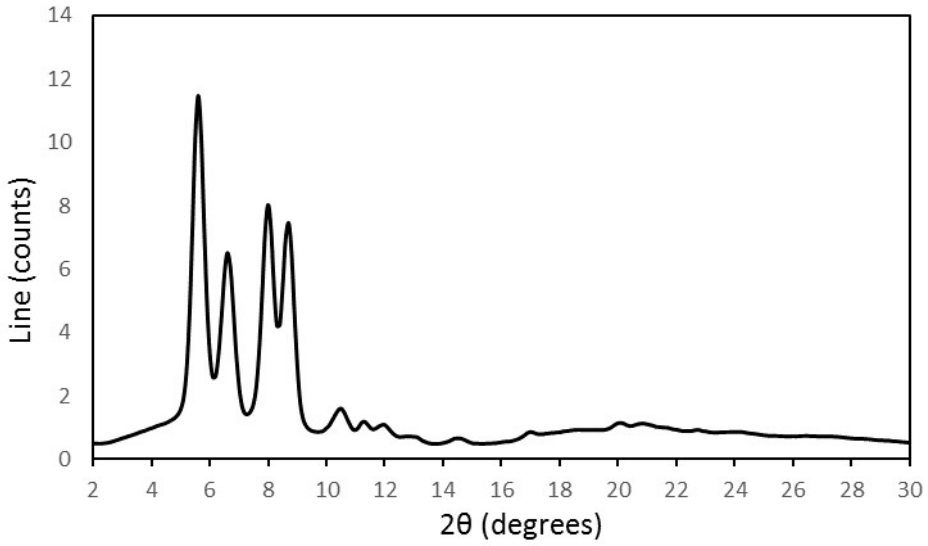

*Figure 5.20. Powder X-ray diffraction spectrum of **UWDM-6** after soaking in saturated LiOTf solution for 24 h and drying under vacuum at 150 °C for 2 h.*

5.2.15 Single Crystal X-ray Diffraction Studies

5.2.15.1 General

Single crystal X-ray data sets were collected on a Brüker D8 Venture diffractometer, equipped with a PHOTON 100 detector, Kappa goniometer, and collected using a Cu high brilliance IμS microfocus source. Crystals were frozen in paratone oil inside a cryoloop under a cold stream of N_2. Reflection data were integrated using Bruker APEX II software. Decay was monitored using 50 standard data frames measured at the beginning and end of data collection. Diffraction data and unit-cell parameters were consistent with assigned space groups. Lorentzian polarization corrections and empirical absorption corrections, based on redundant data at varying effective azimuthal angles, were applied to the data sets. The structures were solved by direct methods, completed by subsequent Fourier syntheses and refined using full-matrix least-squares methods against $|F^2|$ data. When practical, non-hydrogen atoms were refined anisotropically and hydrogen atoms placed in idealized positions and refined using a riding model. Scattering factors and anomalous dispersion

coefficients are contained in the SHELXTL program library[32] and figures drawn with CrystalMaker[33] and Diamond[34] software.

5.2.15.2 Single Crystal X-ray Structure of MIM 5

Crystals of MIM **5** were of good quality. The unit cell contained four molecules of the neutral [2]rotaxane ($C_{42}H_{40}N_4O_8$). The structure was solved in the orthorhombic space group $Pna2_1$ (#33) with Z = 4. All the non-hydrogen atoms were refined anisotropically and all the hydrogen atoms were placed in idealized positions and refined using a riding model. A summary of the crystal data, solution and refinement parameters are presented in Table 5.1.

*Table 5.1. Crystal data, solution and refinement parameters for MIM **5**.*

CCDC number	-	**V (Å^3)**	57188(4)
Formula	($C_{42}H_{40}N_4O_8$)	**Z**	4
Formula weight	1075.23	**ρ, g cm^{-3}**	1.249
Crystal system	Orthorhombic	**μ, mm^{-1}**	0.727
Space group	$Pna2_1$ (#33)	**Reflections used**	9851
T (K)	173	**variables**	924
a (Å)	20.4191(8)	**restraints**	338
b (Å)	24.7102(11)	**R1 [$I > 2\sigma(I)$][a]**	0.0825
c (Å)	11.3342(5)	**R1 (all data)**	0.1021
α (°)	90	**R2w [$I > 2\sigma(I)$][b]**	0.1801
β (°)	90	**R2w (all data)**	0.1938
γ (°)	90	**GOF on F^2**	1.138

[a] $R1 = \Sigma ||F_o| - |F_c|| / \Sigma |F_o|$; [b] $R2w = [\Sigma[w(F_o^2 - F_c^2)^2] / \Sigma[w(F_o^2)^2]]^{1/2}$, [b]where $w = q[\sigma^2(F_o^2) + (aP)^2 + bP]^{-1}$.

5.2.15.3 Single Crystal X-ray Structure of Compound UWDM-6

Crystals of **UWDM-6** were of good quality and size but only weakly diffracting as is common for many porous MOF materials. The structure was solved in the tetragonal space group P4 (#75) with Z = 4 for a formula of $[Zr_6(MIM)_2(O)_6(OH)_6][DEF]$. The non-hydrogen atoms of the framework were easily located and well behaved, although DFIX and DANG restraints were required to position the four methyl groups of the axle at chemically meaningful bond distance and angles. The non-hydrogen atoms of the macrocycle were much more difficult to locate. Several cycles of least squares refinement and the use of DFIX (O-C, C-C) and DANG (O-C-C, C-O-C and C-C-C) restraints were necessary to create a chemically sensible model. Assignment of the O-atoms in the ring was made by comparing displacement parameters and H-bonding distances to the framework. SIMU and DELU were used to restrain the displacement parameters of the macrocycle and even out the electron density associated with disordered portions of the molecule.

*Table 5.2. Crystal data, solution and refinement parameters for **UWDM-6**.*

CCDC number	-	**V (Å³)**	6193.4 (3)
Formula	$C_{68}H_{44}N_4O_{32}Zr_6$	**Z**	4
Formula weight	1896.20	**ρ, g cm^{-3}**	2.034
Crystal system	Tetragonal	**μ, mm^{-1}**	5.041
Space group	P4 (#75)	**Reflections used**	6455
T (K)	170(2)	**variables**	139
a (Å)	19.6869(4)	**restraints**	67
b (Å)	19.6869(4)	**R1 [$I > 2\sigma(I)$][a]**	0.0951
c (Å)	15.9799(3)	**R1 (all data)**	0.1355
α (°)	90	**R2w [$I > 2\sigma(I)$][b]**	0.2356

β (°)	90	**R2*w* (all data)**	0.2613
γ (°)	90	**GOF on F^2**	1.007

[a] $R1 = \Sigma ||F_o| - |F_c|| / \Sigma |F_o|$; [b] $R2w = [\Sigma[w(F_o^2 - F_c^2)^2] / \Sigma[w(F_o^2)^2]]^{1/2}$, [b]where $w = q[\sigma^2(F_o^2) + (aP)^2 + bP]^{-1}$.

5.2.16 Deuterium Solid-State NMR Experimental Details

SSNMR experiments were conducted using a Bruker Avance III HD console and an Oxford 9.4 T ($\nu_0(^1H)$ = 400 MHz, $\nu_0(^{19}F)$ = 376.1 MHz, $\nu_0(^7Li)$ = 155.4 MHz, $\nu_0(^2H)$ = 64.1 MHz) widebore magnet. ^{19}F SSNMR experiments were conducted on a Chemagnetics 4 mm HXY MAS probe (ν_{rot} = 10 kHz) using the Hahn echo pulse sequence (90°-τ_1-180°-τ_2-acquire) with a 2.75 μs π/2 pulse length, a 100 μs pulse spacing and a 1 s recycle delay. ^{19}F chemical shifts were referenced to isotropic shift of fluorobenzene ($\delta_{iso}(^{19}F)$ = –113.15 ppm). ^7Li SSNMR experiments also used the Chemagnetics 4 mm HXY MAS probe (ν_{rot} = 5 kHz), and a Bloch decay pulse sequence with a π/2 pulse length of 3.85 μs and a recycle delay of 2.5 s. ^7Li chemical shifts were referenced to a 1.0 M solution of LiCl in D_2O ($\delta_{iso}(^7Li)$ = 0 ppm). Variable-temperature (VT) ^2H SSNMR experiments were conducted on a Chemagnetics 5 mm HX static probe using the quadrupolar-echo pulse sequence (90°-τ_1-90°-τ_2-acquire) with π/2 pulse lengths of 3.125 μs, pulse spacings of either 30 or 50 μs and a 1 s recycle delay. ^2H isotropic shifts were referenced to D_2O ($\delta_{iso}(^2H)$ = 0 ppm). Temperatures were calibrated based on a previously reported method using the temperature-dependent ^{207}Pb isotropic shift of $Pb(NO_3)_2$.[35,36] Quadrupolar parameters were extracted from the slow-motion limit ^2H spectra using WSolids[37] and powder patterns in the intermediate and fast motion regimes were simulated using EXPRESS.[38]

Compound	Temperature (K)	Two-site jump rate (Hz)	Partial Rotation Rate (Hz)
Neutral	185	0	0
	298	$>10^7$	0
	411	$>10^7$	5×10^5
Protonated	185	5×10^5	0
	253	$>10^7$	0
	343	$>10^7$	1×10^5
	388	$>10^7$	$>10^7$

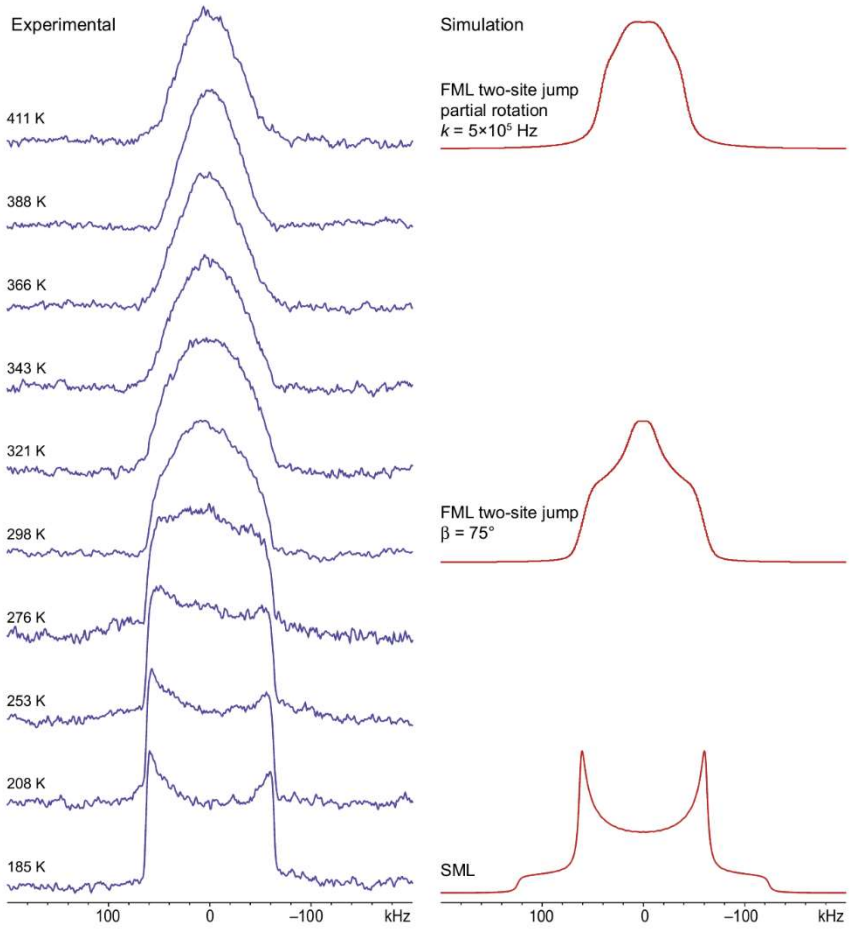

Figure 5.21. Experimental (blue) and simulated (red) VT ^{2}H SSNMR spectra of ***UWDM-6****.*

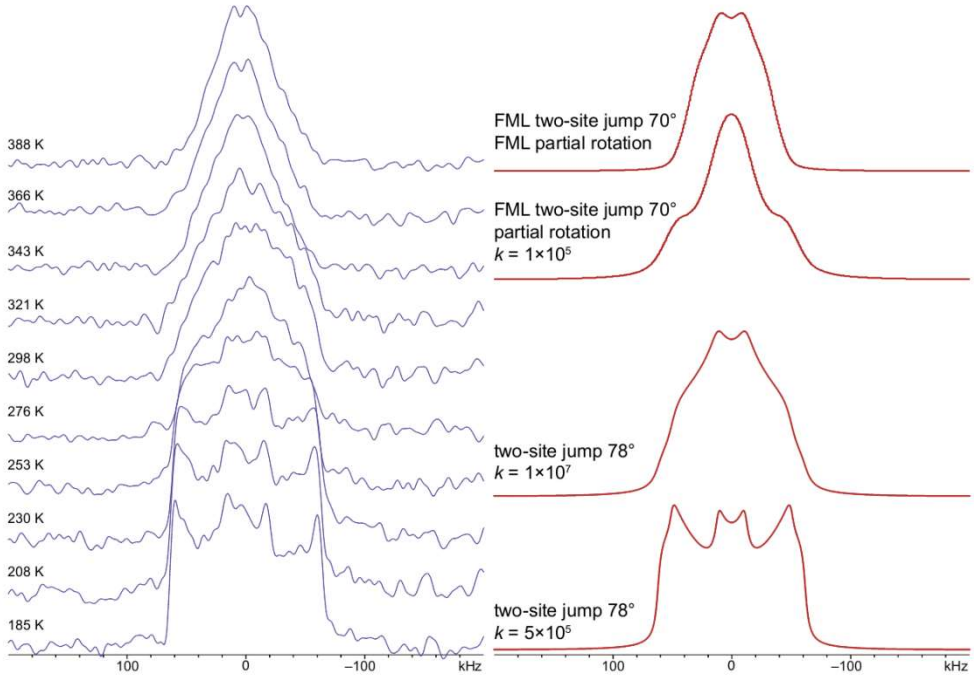

*Figure 5.22. Experimental (blue) and simulated (red) VT ^{2}H SSNMR spectra of **UWDM-6**.(HOTf)$_2$.*

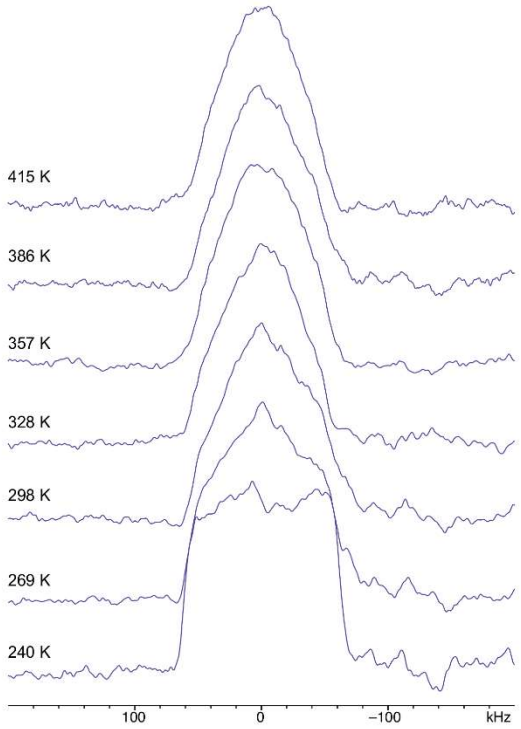

*Figure 5.23. Experimental VT ^{2}H SSNMR spectra of **UWDM-6**. LiOTf.*

5.3. References

[1] a) S. Saha, J. F. Stoddart, *Chem. Soc. Rev.*, **2007**, *36*, 77. b) E. R. Kay, D. A. Leigh, F. Zerbetto, *Angew. Chem.,* **2007**, *119*, 72; c) *Angew. Chem. Int. Ed.,* **2007**, *46*, 72.

[2] a) J. O. Jeppesen, S. A. Vignon, J. F. Stoddart, *Chem. Eur. J.,* **2003**, *9,* 4611; b) V. Balzani, A. Credi, M. Venturi, *Chem. Soc. Rev*., **2009**, *38*, 1542; c) H. X. Deng, M. A. Olson, J. F. Stoddart, O. M. Yaghi, *Nature Chem*., **2010**, *2,* 439.

[3] S. Erbas-Cakmak, D. A. Leigh, C. T. McTernan, A. L. Nussbaumer *Chem. Rev.,* **2015**, *115*, 10081.

[4] a) S. J. Loeb, *Chem. Commun*., **2005**, 1511 b) V. N. Vukotic, S. J. Loeb, **2012**, *Chem. Soc. Rev*., *41*, 5896.

[5] a) W. D. Zhou, J. L. Xu, H. Y. Zheng, X. D. Yin, Z. C. Zuo, H. B. Liu, Y. L. Li, *Adv. Funct. Mater.,* **2009**, *19*, 14; b) Y. Kohsaka, K. Nakazono, Y. Koyama, S. Asai, T. Takata, Angew. Int. Ed., **2011**, *50*, 4872; c) Frampton MJ, Anderson HL, Angew. *Chem. Int. Ed.,* **2007**, *46*, 1028; d) M. Horie, T. Sassa, D. Hashizume, Y. Suzaki, K. Osakada, T. Wada, Angew. *Chem. Int. Ed.,* **2007**, 46, 4983; e) U. Rauwald, J. del Barrio, X. J. Loh, O. A. Scherman, *Chem. Commun.,* **2011**, *47*, 6000.

[6] V. N. Vukotic, K. J. Harris, K. Zhu, R. W. Schurko S. J. Loeb, *Nature Chem.,* **2012**,*4*, 456.

[7] N. Noujeim, K. Zhu, V. N. Vukotic, S. J. Loeb, *Org. Lett.,* **2012**, *14*, 2484.

[8] a) K. Zhu, V. N. Vukotic, S. J. Loeb, *Angew. Chem. Int. Ed*., **2012**, *51*, 2168; b) K. Zhu, V. N. Vukotic, N. Noujeim, S. J. Loeb, *Chem. Sci.,* **2012**, *3*, 3265.

[9] K. Zhu, K. J. Harris, V. N. Vukotic, R. W. Schurko S. J. Loeb, *Nature Chem.,* **2015**, *7*, 514.

[10] N. Farahani, K. Zhu, N. Noujeim, S. J. Loeb, *Org. Biomol. Chem.,* **2014**, 4824.

[11] N. Farahani, K. Zhu, S. J. Loeb, *ChemPhysChem.,* **2016**, *17*, 1.

[12] N. Farahani, K. Zhu, C. A. O'Keefe, R. W. Schurko, S. J. Loeb, *ChemPlusChem.,* **2016**, DOI: 10.1002/cplu.201600176.

[13] a) J. H. Cavka, S. Jakobsen, U. Olsbye, N. Guillou, C. Lamberti, S. Bordiga, K. P. Lillerud, *J. Am. Chem. Soc.,* **2008**, *130*, 13850; b) K. S. Park, Z. Ni, A. P. Côté, J. Y. Choi, R. Huang, F. J. Uribe-Romo, H. K. Chae, M. O'keeffe, O. M. Yaghi, *Proc. Natl. Acad. Sci. U. S. A.,* **2006**, *103*, 10186; c) G. Férey, C. Mellot-Draznieks, C. Serre, F. Millange, J. Dutour, S. Surblé, I. Margiolaki, *Science*, **2005**, *309*, 2040; d) V. Colombo, S. Galli, H. J. Choi, G. D. Han, A. Maspero, G. Palmisano, N. Masciocchi, J. R. Long, *Chem. Sci.,* **2011**, *2*, 1311; e) F. Carson, E. Martínez-Castro, R. Marcos, G. González Miera, K. Jansson, X. Zou, B. Martín-Matute, *Chem. Commun.,* **2015**, *51*, 10864.

[14] a) J. E. Mondloch, W. Bury, D. Fairen-Jimenez, S. Kwon, E. J. DeMarco, M. H. Weston, A. A. Sarjeant, S. T. Nguyen, P. C. Stair, R. Q. Snurr, O. K. Farha, J. T. Hupp, *J. Am. Chem. Soc.,* **2013**, *135*, 10294; b) M. Carboni, C. W. Abney, S. Liu, W. Lin, *Chem. Sci.,* **2013**, *4*, 2396 c) V. Guillerm, F. Ragon, M. Dan-Hardi, T. Devic, M. Vishnuvarthan, B. Campo, A. Vimont, G. Clet, Q. Yang, G. Maurin, G. Férey, A. Vittadini, S. Gross, C. Serre, *Angew. Chem.,* **2012**, *124*, 9401; *Angew. Chem. Int. Ed.,* **2012**, *51*, 9267; d) J. H. Cavka, S. Jakobsen, U. Olsbye, N. Guillou, C. Lamberti, S. Bordiga, K. P. Lillerud, *J. Am. Chem. Soc.,* **2008**, *130*, 13850; e) D. Feng, W-C. Chung, Z. Wei, Z.-Y. Gu, H.-L. Jiang, D. J. Darensbourg, H.- C. Zhou, *J. Am. Chem. Soc.,* **2013**, *135*, 17105; f) H. Wu, T. Yildirim, W. Zhou, *J. Phys. Chem. Lett.,* **2013**, *4*, 925; g) J. B. Decoste, G. W. Peterson, H. Jasuja, T. G. Glover, Y.-G. Huang, K. S. Walton, *J. Mater. Chem. A,* **2013**, *1*, 5642.

[15] a) P. Deria, J. E. Mondloch, E. Tylianakis, P. Ghosh, W. Bury, R. Q. Snurr, J. T. Hupp, O. K. Farha, *J. Am. Chem. Soc.,* **2013**, *135,* 16801; b) J. E. Mondloch, M. J. Katz, N. Planas, D. Semrouni, Laura Gagliardi, J. T. Hupp O. K. Farha, *Chem. Commun.,* **2014**, *50*, 8944.

[16] W. Morris, B. Volosskiy, S. Demir, F. Gandara, P. L. McGrier, H. Furukawa, D. Cascio, J. F. Stoddart, O. M. Yaghi, *Inorg. Chem.,* **2012**, *51*, 6443.

[17] D. Feng, Z-Y. Gu, J.-R. Li, H.-L. Jiang, Z. Wei, H.-C. Zhou, Angew. *Chem. Int. Ed.,* **2012**, *51*, 10307.

[18] a) O. V. Gutov, W. Bury, D. A. Gomez-Gualdron, V. Krungleviciute, D. Fairen-Jimenez, J. E. Mondloch, A. A. Sarjeant, S. S. Al-Juaid, R. Q. Snurr, J. T. Hupp, T. Yildirim, O. K. Farha, *Chem. Eur. J.,* **2014**, *20*, 12389; b) T.-F. Liu, D. Feng, Y.-P. Chen, L. Zou, M. Bosch, S. Yuan, Z. Wei, S. Fordham, K. Wang, H.-C. Zhou, *J. Am. Chem. Soc.,* **2015**, *137*, 413.

[19] B. Wang, X.-L. Lv, D. Feng, L.-H. Xie, J. Zhang, M. Li, Y. Xie, J.-R. Li, H.-C. Zhou, *J. Am. Chem. Soc.,* **2016**, *138*, 6204.

[20] D. J. Hoffart, S. J. Loeb, *Angew. Chem. Int. Ed.,* **2005**, *44*, 901.

[21] V. N. Vukotic, S. J. Loeb, *Chem. Eur .J.,* **2010**, *16*, 13630.

[22] a) W. I. F. David, K. Shankland, N. Shankland, *Chem. Commun.,* **1998**, 931; b) A. Boultif, D. J. Louer, *Appl. Crystallogr.,* **1991**, *24*, 987; c) W. I. F. David, K. Shankland, J. van de Streek, E. Pidcock, W. D. S. Motherwell, J. C. J. Cole, *Appl. Crystallogr.,* **2006**, *39*, 910.

[23] K. Zhu, V. N. Vukotic, C. A. O'Keefe, R. W. Schurko, S. J. Loeb, *J. Am. Chem. Soc.,* **2014**, *136*, 7403;

[24] a) S. Horike, S. Shimomura, S. Kitagawa, *Nature Chem.,* **2009**, *1*, 695; (b) G. Férey, C. Serre, *Chem. Soc. Rev.,* **2009**, *38*, 1380; b) A. Schneemann, V. Bon, I. Schwedler, I. Senkovska, S. Kaskel, R. A. Fischer, *Chem. Soc. Rev.,* **2014**, *43*, 6062.

[25] P. Deria, D. A Gomez-Gualdron, W. Bury, H. T. Schaef, T. C. Wang, P. K. Thallapally, A. A. Sarjeant, Randall Q. Snurr, Joseph T. Hupp, Omar K. Farha, *J. Am. Chem. Soc.*, **2015**, *137*, 13183.

[26] a) M. A. Garcia-Garibay, *Proc. Natl. Acad. Sci. U. S. A.,* **2005**, *102*, 10771; b) W. Morris, R. E. Taylor, C. Dybowski, O. M. Yaghi, M. A. Garcia-Garibay, *J. Mol. Struct.,* **2011**, *1004*, 94; c) M. Hughs, M. Jimenez, S. Khan, M. A. Garcia-Garibay, *J. Org. Chem.,* **2013**, *78*, 5293.

[27] R. J. Sundberg, R. B. Martin, *Chem. Rev.,* **1974**, *74*, 471; b) R. Bhalla, M. Helliwell, C. David Garner, *Inorg. Chem.,* **1997**, *36,* 2944; c) S. B. Park, H. Alper, *Org. Lett.,* **2003**, *5*, 3209.

[28] a) S. Sharma, G. J. E. Davidson, S. J. Loeb, *Chem. Commun.,* **2008**, 582; b) G. Periyasamy, J.-P. Collin, J.-P. Sauvage, R. D. Levine, F. Remacle Chem. Eur. J., **2009**, *15*, 1310; c) F. Durola, J.

Lux, J.-P. Sauvage, *Chem. Eur. J.,* **2009**, *15*, 4124; d) J.-P. Collin, F. Durola, J. Lux, J.-P. Sauvage, *Angew. Chem.,* **2009**, *121*, 8684; *Angew. Chem. Int. Ed.,* **2009**, *48*, 8532; e) G. J. E. Davidson, S. Sharma, S. J. Loeb, *Angew. Chem.,* **2010**, *122*, 5058; *Angew. Chem. Int. Ed.,* **2010**, 49, 4938.

[29] For examples of lithium and metal-ion switchable MIMs see: a) S. A. Vignon, T. Jarrosson, T. Iijima, H. Tseng, J. K. M. Sanders, J. F. Stoddart, *J. Am. Chem. Soc.*, **2004**, *126*, 9884; c) T. Iijima, S. A. Vignon, H. Tseng, T. Jarrosson, J. K. M. Sanders, F. Marchioni, M. Venturi, E. Apostoli, V. Balzani, J. F. Stoddart, *Chem. Eur. J.,* **2004**, *10*, 6375; d) G. Kaiser, T. Jarrosson, S. Otto, Y.-F. Ng, A. D. Bond, J. K. M. Sanders, *Angew. Chem.,* **2004**, *116*, 1993; *Angew. Chem. Int. Ed.,* **2004**, *43*, 1959.

[30] C. h. Kirchner and B. Krebs, *Inorg. Chem*., **1987**, *26*, 3569; b) D. Sanchez-García, S. Borrós, S. Nonell, J. I. Borrell, C. Colominas, J. Teixidó, *J. Heterocyclic Chem.*, **2002**, *39*, 733.

[31] a) C. Frassineti, S. Ghelli, P. Gans, A. Sabatini, M.S. Moruzzi, A. Vacca, *Anal. Biochem.,* **1995**, *231*, 374; b) C. Frassineti, L. Alderighi, P. Gans, A. Sabatini, A.Vacca, S. Ghelli, *Anal. Bioanal. Chem.,* **2003**, *376*, 1041.

[32] SHELX G. M. Sheldrick, *Acta Cryst*. **2008**, *A64*, 112.

[33] Images generated using CrystalMaker®; *CrystalMaker Software* Ltd, Oxford, England (www.crystalmaker.com).

[34] DIAMOND 3.2i, CRYSTAL IMPACT, Postfach 1251, D-53002, Bonn, Germany **2009**.

[35] L. C. M. Van Gorkom, J. M. Hook, M. B. Logan, J. V Hanna, R. E. Wasylishen, *Magn. Reson. Chem.,* **1995**, *33*, 791.

[36] A. Bielecki, D. P. Burum, *J. Magn. Reson.* **1995**, *220*, 215.

[37] K. Eichele, R. E. Wasylishen, WSolids: *Solid-State NMR Spectrum Simulation Package* **2001**.

[38] R. L. Vold, G. L. Hoatson, *J. Magn. Reson.* **2009**, *198*, 57.

CHAPTER 6

6.1 Post-Synthetic Modification of a Zr-based MOF Containing a [2]Rotaxane Linker

6.1.1 Introduction

Metal-organic frameworks (MOFs), a class of porous materials, are materials comprising metal nodes coordinated to organic linkers by strong bonds.[1] Due to their robust structure and permanent porosity[2], MOFs have attracted great interest for a wide range of applications such as gas adsorption and storage,[3] chemical separations,[4] molecular sensing,[5] conductivity,[6] heterogeneous catalysis[7] and drug delivery[8]. One of their most attractive features is that chemical modification of the organic linkers can lead to changes in the topology of MOFs or modification of the internal surfaces to optimize their performance while keeping the same MOF skeleton. For example, elongation of the linker is a common approach to increase the surface area and porosity.[9] However, elongation or introduction of chemical functionality for desired applications is often challenging due to solubility and/or stability problems of the linker[10] and the formation of undesirable structures or side products.[10] These synthetic challenges can be addressed by post-synthetic modification (PSM) to include desired functional group within a MOF structure.[11] Some examples of this PSM strategy include organic functionalization at the metal node,[12] covalent modification of the organic linker,[13] and solvent-assisted linker exchange (SALE).[14] Studies have also demonstrated that lattice interpenetration can be prevented by utilizing small functional groups followed by post-synthetic removal of the functionalities to retain the MOFs' potential porosity.[15] Recently, Loeb *et al* developed a novel cubic MOF by mechanically interlocking a 24-membered polyether-based macrocycle around an organic linker which increases the solubility of the linker and prevents lattice interpenetration.[16] They, then used a PSM approach to remove the macrocyclic rings and produce a MOF with high porosity that was

not possible with the naked linker. However, it should be noted that yields for the post-synthetic removal of the ring varied between 40-90% and degradation of the crystals occurred as the reaction time was increased to >24 h and at temperatures >80 °C. For this PSM strategy be effective without damaging the MOF skeleton, MOFs with high chemical and thermal stability are required. Among the many MOFs, Zr-based MOFs that have been subjected to various PSMs[14,17] and they show high thermal (up to 500 °C), chemical (pH 1–10)[18] and mechanical stability.[18,19]

In chapter 5, we reported the design of a new Zr-based MOF (**UWDM-6**) with mesoporous channels which showed high thermal and chemical stability. **UWDM-6** consists of $Zr_6(OH)_8(O)_8^{+8}$ clusters linked by tetracarboxylate [2]rotaxane linkers containing bis(imidazole) axles and **24C6** wheels. Herein, we report the synthesis of a Zr-based MOF (**UWCM-1**) by a similar bis(imidazole) [2]rotaxane linker containing unreduced **24C6** wheels and post-synthetic removal of the macrocyclic wheel within the **UWCM-1** framework using a ring opening metathesis reaction with Hoveyda-Grubbs catalyst to increase the void space in the MOF.

6.1.2. Results and Discussion

6.1.2.1 Linker Synthesis and Characterization

Scheme 6.1 outlines the synthesis of all linkers used in this work. Linker [**1**-H_4⊂**24C6'**] was synthesized by a ring closing metathesis reaction using Grubbs I catalyst which allowed clipping of a **24C6** macrocyclic precursor around the dicationic axle [**1**-H_2][BF_4]$_2$ (see chapter 5), followed by subsequent deprotonation and hydrolysis *via* refluxing in a mixture of 1M NaOH/EtOH/THF. The "naked" linker **1**-H_4 (without the macrocycle) was also synthesized by hydrolyzing **1**in the same mixture.

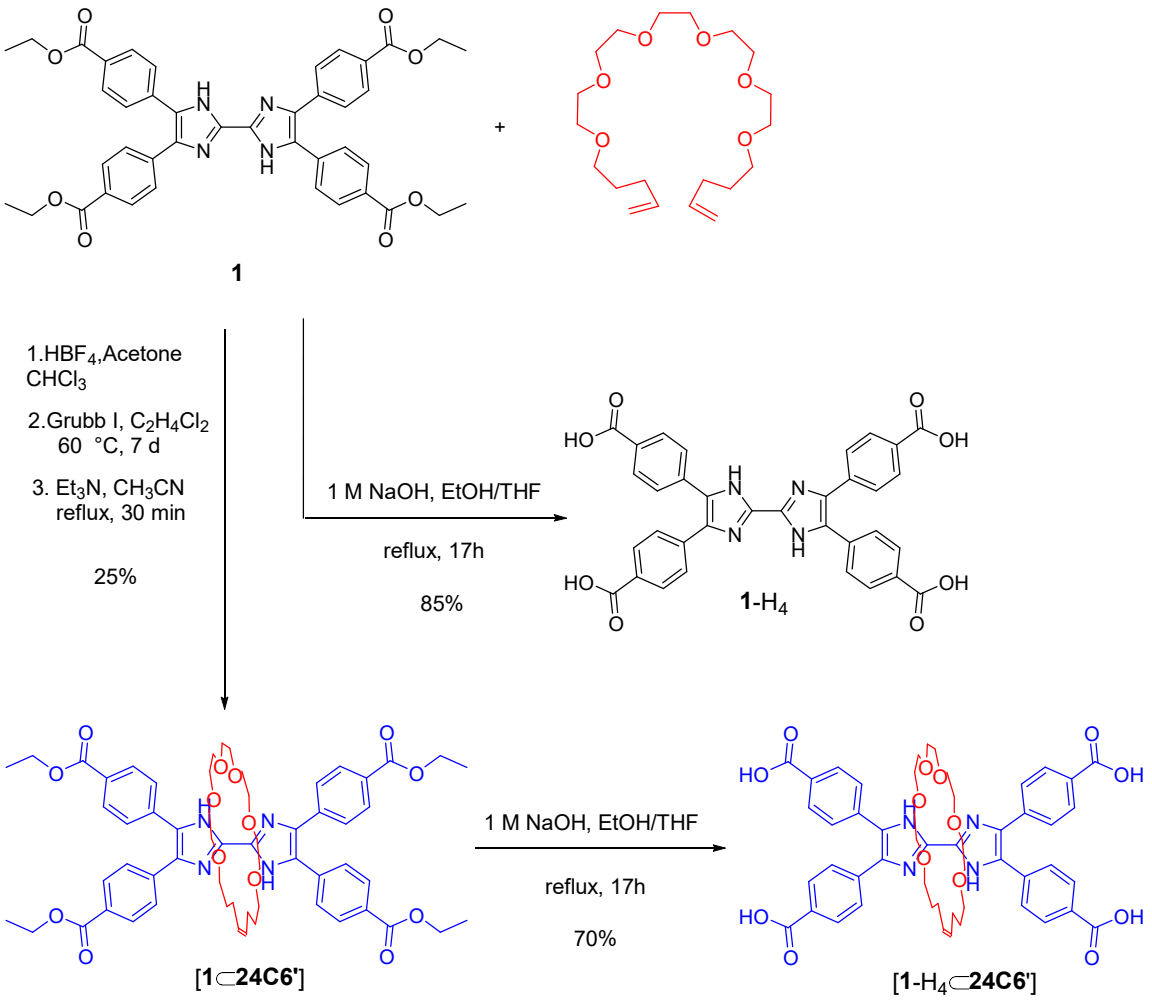

*Scheme 6.1. Synthesis of [2]rotaxane linker [**1**-H_4⊂**24C6'**] and naked linker **1**-H_4.*

6.1.2.2 MOF Synthesis and Characterization

The solvothermal reaction of MIM linker [**1**-H_4⊂**24C6'**], $ZrCl_4.8H_2O$ and benzoic acid in N,N'-diethylformamide (DEF) at 120 °C for 20 h , resulted in formation of a pale yellow crystalline material designated University of Windsor Crystalline Material-1 (**UWCM-1**). Powder X-ray diffraction (PXRD) showed that the PXRD pattern of **UWCM-1** is identical to the predicted pattern from the single crystal structure of **UWDM-6** which was synthesized under similar reaction condition to **UWCM-1** (see Figure 6.3). This reveals that **UWCM-1** adopts the same structure as **UWDM-6** with the $Zr_6(\mu_3\text{-}O)_8(OH)_8$ SBUs (secondary binding

units) connected by [**1-H_4⊂24C6'**] linkers. Due to desolvation, **UWCM-1** can also go through the phase change which was previously observed for **UWDM-6** (see chapter 5).

The identity of as-synthesized **UWCM-1** was also established by recording the ^{1}H NMR spectrum of the digested MOF which indicated the presence of tetracarboxylate MIM linker and benzoic acid with the ratio of 1:4 in the MOF. The benzoic acid signal corresponds to benzoic acid molecules which are coordinated to Zr clusters and could not be removed with regular washing at room temperature.[17a] ^{1}H NMR studies revealed that the benzoic acid could, however, be removed from the Zr nodes and replaced with −OH groups[17a] by soaking the material in DEF at 90 °C (see section 6.2 for details).

Attempts to utilize **1**-H_4 as a linker with Zr(IV) were also successful and yielded MOF product designated **UWCM-2**. In this case, the solvothermal reaction of linker **1**-H_4 with $ZrCl_4$ in presence of benzoic acid and DMF (dimethylformamide) at 120 °C for 24 h produced **UWCM-2** as a microcrystalline powder which was not suitable for single crystal analysis. The crystallinity of the powder was verified by PXRD measurement. PXRD demonstrated that **UWCM-2** adopts a different structure from **UWCM-1**, even though they appear to have similar cluster-cluster distances as inferred by the presence of very similar low angle diffraction peaks in 2theta. After being activated under vacuum at 150 °C, the PXRD pattern of **UWCM-2** was unaltered, which indicates the framework remains intact and does not undergo any significant phase change during the activation process (Figure 6.1). Decomposition of activated **UWCM-2** in K_3PO_4/D_2O/DMSO-d_6 gave a very similar ^{1}H NMR spectrum to the observed for the corresponding organic linker, further representing the robustness of the linker in the MOF (see experimental Figure 6.7). Moreover, thermogravimetric analysis (TGA) of an as-synthesized sample of **UWCM-2** showed that the material is stable up to 410 °C (see experimental Figure 6.8).

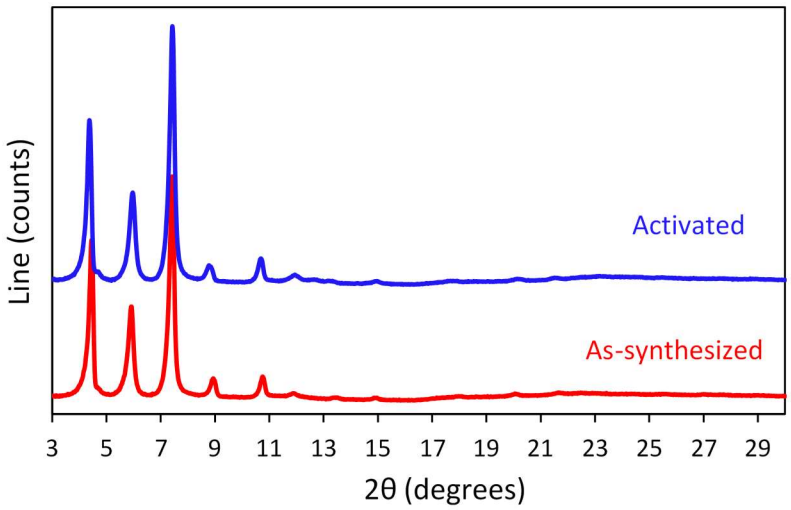

Figure 6.1. Powder X-ray diffraction spectra of as-synthesized (red) and activated (blue) ***UWCM-2****.*

In an effort to determine the potential benefits of removing the macrocyclic wheels from the structure of **UWCM-1**, PLATON[20] was used to calculate the void spaces. The calculations show that **UWCM-1** before and after removal of the wheels contains 65% and 77% void spaces, respectively.

6.1.2.3 Post-Synthetic Modification of UWCM-1

Post-synthetic removal of the macrocyclic wheel can be performed through cleavage of the olefin bond on the wheel resulting from the ring closing metathesis reaction. In the previous study, Loeb *et al* demonstrated that Hoveyda-Grubbs II catalyst could be utilized for the ring opening metathesis reaction with 24-membered macrocyclic rings linked around a benzo-bis-imidazole axle within the free volume of the MOF due to its high chemical stability and relatively small size which allows or diffusion within the pores of the framework.[16] Therefore, to perform the PSM on **UWCM-1**, 5% Hoveyda-Grubbs II catalyst was added to a sample of as-synthesized **UWCM-1** in dichloroethane (DCE) in a thick-walled glass and the reaction mixture heated to 80 °C for 20 h. The resultant material was then activated for further studies. It is worth noting that the ring opening reaction on the activated material was

not successful. This can be attributed to the deactivation of slowly-initiating Hoveyda-Grubbs catalyst by acidic Zr_6-oxo clusters due to the replacement of the benzoic acid groups with OH groups. After the ring removal reaction, the activated powder was digested in a K_3PO_4/D_2O/DMSO-d_6 and analyzed by ^{1}H NMR spectroscopy. Figure 6.2 represents the stacked plot of the digested **UWCM-1** before and after post-synthetic modification. Before the reaction, resonances corresponding to the [2]rotaxane linker [**1**-H_4⊂**24C6'**] were observed in the ^{1}H NMR spectrum. It was apparent that almost 100% of the macrocycle has been removed from the framework after the reaction as the signals in the ^{1}H NMR spectrum belong only to the naked linker.

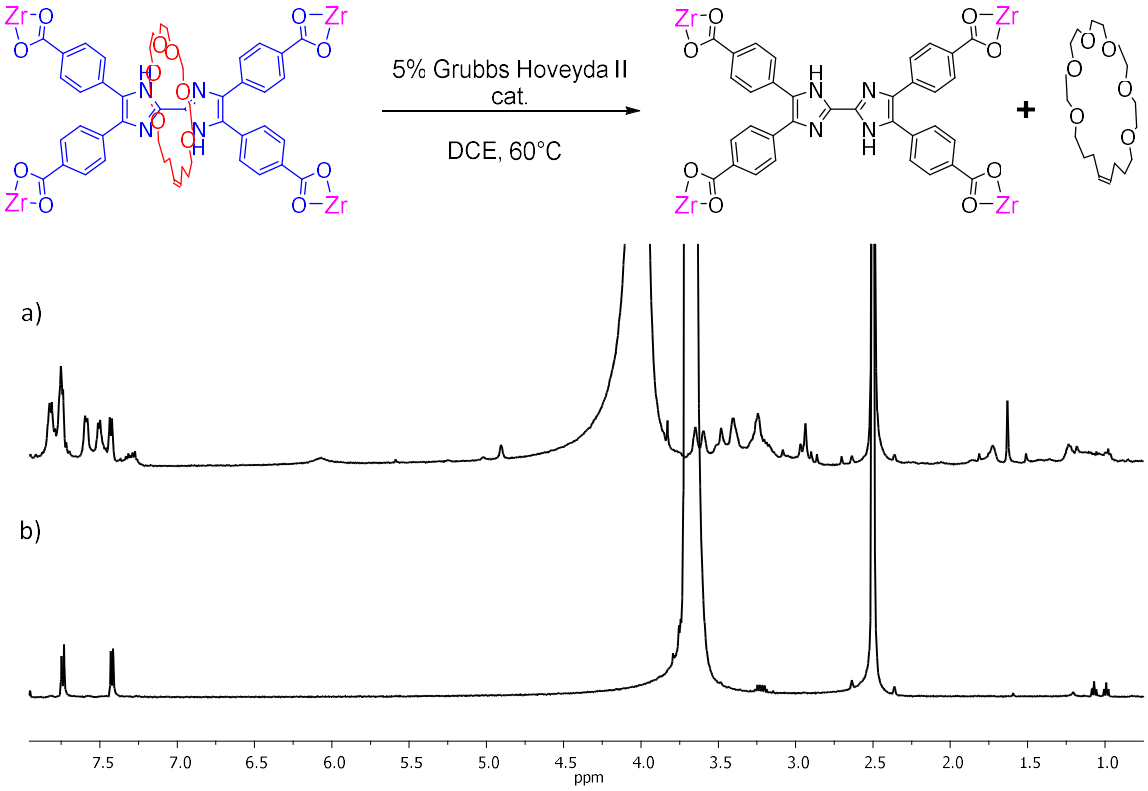

*Figure 6.2. Schematic representation of post-synthetic ring removal (top) and partial ^{1}H NMR spectra (500MHz) (below) of (a) activated **UWCM-1** and (b) activated **UWCM-1** after ring removal. Samples were decomposed in K_3PO_4/D_2O/DMSO-d_6.*

Powder X-ray diffraction (PXRD) measurements confirmed that the material retains its crystallinity, and interestingly it adopts a different topology which is identical to **UWCM-2**

(Figure 6.3). In MOF chemistry, topological transformation is a known phenomenon which can occur through conformational changes in the organic linker without breaking any of the coordination bonds during the transformation.[21] Thus, ring removal of **UWCM-1** causes conformational changes of the tetracarboxylate axle which leads to structural transformation of the MOF while the 8-connected Zr clusters still remain intact. After activation, PXRD showed that the post-synthetic material is stable and does not go through the phase change that previously observed for **UWCM-1**.

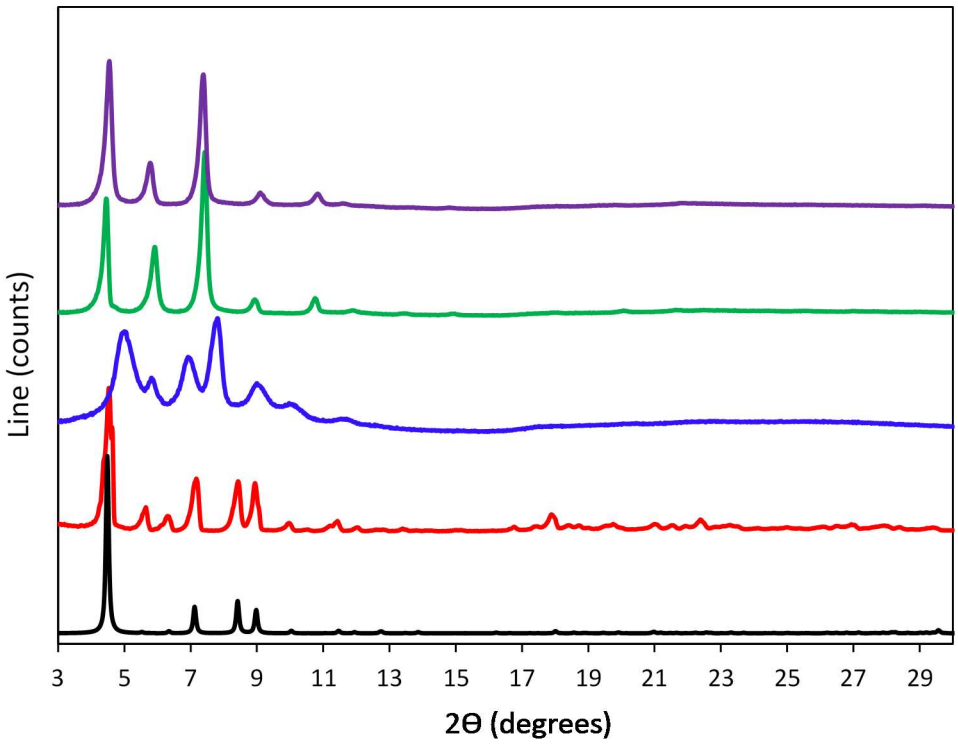

*Figure 6.3. Powder X-ray diffraction spectra of simulated from single crystal of **UWDM-6** (black), as-synthesized (red) and desolvated (blue) **UWCM-1**, as-synthesized **UWCM-2** (green) and **UWCM-1** after post-synthetic ring removal (purple).*

In order to assess the porosity of **UWCM-1** before and after post-synthetic ring removal as well as **UWCM-2**, N_2 adsorption isotherms at 77 K were measured for these materials. On the basis of the single crystal structure previously observed for **UWDM-6** and our knowledge of Zr-MOFs, surface area analysis of the materials by the BET method gave

surface areas that were much lower than our expectations. As the gas adsorption properties of MOFs are much sensitive to the method used to activate the material,[22] further studies are required to optimize the activation method of the materials and are essential to prove porosity.

6.1.3 Conclusion

Interlocking a 24-membered polyether-based macrocycle around a tetracarboxylic linker allowed for the formation of a 8-connected Zr-based MOF (**UWCM-1**) similar to **UWDM-6** which shows some degree of flexibility; whereas reaction of $ZrCl_4$ and the naked linker led to a rigid material (**UWCM-2**) but its structure could not be determined due to lack of X-ray quality single crystals of suitable size. Moreover, interlocking the macrocycle around the axle together with high chemical and thermal stability of Zr nodes allowed for the post-synthetic modification of **UWCM-1** with Hoveyda-Grubbs II catalyst, which removed the macrocycle. From PXRD measurements, we found that the PSM material adopts a rigid structure analogous to **UWCM-2,** as a result of a topological transformation which occurs through conformational changes in the linker. On the basis of this evidence, **UWCM-1** and **UWCM-2** were confirmed to possess similar 8-connected Zr nodes with the formula of $[Zr_6(\mathbf{6})_2(\mu_3\text{-}O)_8(OH)_8]$ but adopt different topologies.

6.2. Experimental

6.2.1 General Comments

Hoveyda Grubb II catalyst was purchased from Aldrich and compound **1**-H_4 and [**1⊂24C6'**] were obtained according to the procedure that stated in chapter 5. Solvents were dried using an Innovative Technologies Solvent Purification System. Deuterated solvents were obtained from Cambridge Isotope Laboratories and used as received. ^1H, ^{13}C, NMR experiments were performed on a Bruker Avance III 500 instrument, with Larmor

frequencies of 500.1 MHz for ^{1}H nuclei, 125.7 MHz for ^{13}C. Chemical shifts are quoted in ppm relative to tetramethylsilane (δ_{iso}=0 ppm) using the residual solvent peak as a secondary reference standard. High-resolution mass spectrometry (HRMS) experiments were performed on a Waters Xevo G2-XS time-of-flight (ToF) instrument using lockspray for accurate mass determinations. ESI acquisitions were completed using a 1 μL injection into a sample loop with a constant 5 μL min^{-1} flow of 50:50 H_2O/CH_3CN (with 0.1% formic acid). Powder XRD measurements were run on a PROTO AXRD powder diffractometer equipped with a Cu X-ray source, and a Mythen 1K silicon strip detector, operated at 30KV and 20mA. Scans were performed utilizing CuKα radiation, a 0.3mm divergence slit, and a step size of 0.02 degrees 2theata. Thermal gravimetric analyses were conducted on a Mettler Toledo TGA SDTA 851e instrument. Helium (99.99%) was used to purge the system with a flow rate of 30 mL min^{-1}. Samples were held at 25 °C for 10 min before heating up to 550 °C at 2 °C min^{-1}. Melting points were recorded on a Stanford Research Systems, Opti Melt MPA100 instrument. Infrared spectra were recorded on a Bruker Alpha FT-IR spectrometer in the range of 4000–400 cm.

6.2.2 Synthesis of [1-H_4⊂24C6']

Compound [**1⊂24C6'**] (200 mg, 0.2 mmol) was dissolved in a mixture of EtOH/THF (10 mL: 5 mL) followed by addition of 1M NaOH (10 mL). The reaction mixture was heated at 80 °C for 17 h, concentrated in vacuum and carefully acidified with 1M HCl to pH= 5 to obtain a yellow precipitate. The resulting solid was filtered and washed with pH = 5 water and dried under vacuum. Yield: 125 mg, 70%; MP > 300 °C; ^{1}H NMR (DMSO-d_6, 500 MHz, 298K): (major product) δ (ppm) = 12.39 (s, 2H), 7.99 (d, 4H, *J* = 8.5 Hz), 7.94 (d, 4H, *J* = 8.5 Hz), 7.77 (d, 4H, *J* = 8.5 Hz), 7.73 (d, 4H, *J* = 8.5 Hz), 4.91 (t, 2H, *J* = 3.5 Hz), 3.73-3.72 (m, 4H), 3.67-3.66 (m, 4H), 3.47-3.26 (m, 12H), 2.95 (s, 4H), 1.78-1.71 (m, 4H), 1.25-1.21 (m, 4H); ^{13}C NMR (DMSO-d_6, 125 MHz, 298 K): δ (ppm) = 167.4, 167.3, 139.6, 139.5, 139.5, 136.9, 136.7,

135.3, 135.2, 130.0, 130.0, 129.8, 129.8, 129.6, 129.0, 129.0, 128.5, 128.4, 127.2, 127.1, 70.8, 70.5, 70.2, 70.1, 69.9, 69.7, 69.6, 69.6, 69.5, 69.4, 68.8, 68.8, 29.6, 28.9, 27.8, 24.0; IR (neat) = 2871, 1682, 1608, 1418, 1314, 1279, 1177, 1124, 1095, 1017, 973, 942, 863, 800, 778, 727, 707, 683, 584, 546 cm^{-1}; HR-MS (ESI-ToF) *m/z*: calcd for $[M+H]^+$, $[C_{52}H_{57}N_4O_{14}]^+$,961.3866; found 961.3852.

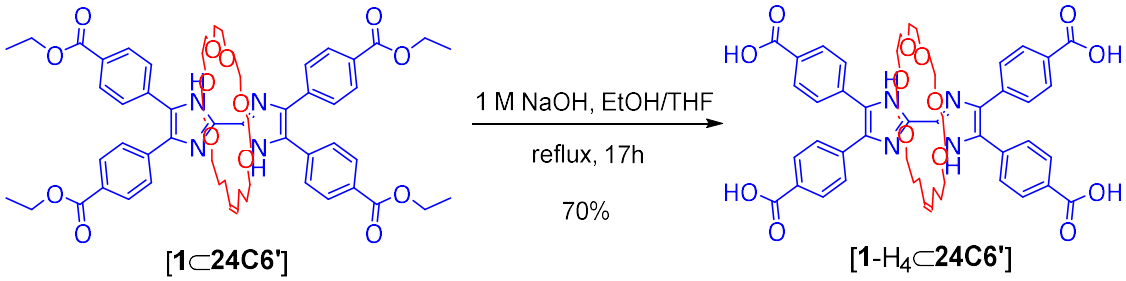

*Scheme 6.2. Synthesis of [**1**-H_4⊂**24C6'**]*

6.2.3 Synthesis of 1-H4

Compound **1** (200 mg, 0.3 mmol) was dissolved in a mixture of EtOH/THF (10 mL: 2 mL) followed by addition of 1M NaOH (10 mL). the reaction mixture was heated at 80 °C for 17 h, concentrated in vacuum and carefully acidified with 1M HCl to pH= 6 to obtain a yellow precipitate. The resulting solid was filtered and washed with water and dried under vacuum. Yield: 143 mg, 85%; MP 283-286 °C; ^{1}H NMR (1 drop cont. trifilic acid, DMSO-d_6, 500 MHz, 294K): δ (ppm) = 8.01 (d, 8H, *J* = 8.5 Hz), 7.68 (d, 8H, *J* = 8.5 Hz); ^{13}C NMR (1 drop cont. trifilic acid, DMSO-d_6, 125 MHz, 294 K): δ (ppm) = 167.0, 136.7, 134.8, 132.7, 130.4, 129.9, 128.3; IR (neat) = 2871, 1674, 1606, 1538, 1386, 1314, 1259, 1177, 1098, 1015, 972, 858, 789, 775, 699, 581, 511, 456 cm^{-1}; HR-MS (ESI-ToF) *m/z*: calcd for $[M+H]^+$, $[C_{34}H_{23}N_4O_8]^+$, 615.1510; found 615.1520.

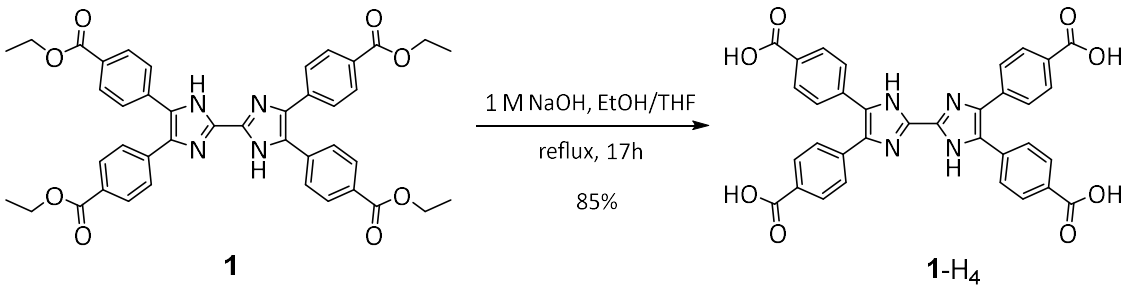

*Scheme 6.3. Synthesis of **1**-H_4*

6.2.4 Synthesis of UWCM-1

$ZrCl_4.8H_2O$ (129 mg, 0.6 mmol) and benzoic acid (5250 mg, 42 mmol) were dissolved in DEF (22 mL). The mixture was heated at 80 °C for 1 h. After cooling down to room temperature, ligand [**1**-H_4⊂**24C6'**] (105 mg, 0.12 mmol) was added to the clear solution and the solution sonicated for 5 minutes. The yellow solution was transferred through a 25 mm syringe filter (0.2 μm PTFE membrane) to six 15 mL vials and heated at 120 °C in a programmable heating oven for 20 h. a yellow crystalline product was collected.

6.2.5 Activation Procedure for UWCM-1

Half of as-synthesized **UWCM-1** Was soaked in 10 mL of DEF. the mixture was heated in an oven at 90 °C for 12 h. The solvent was replaced with fresh DEF and the mixture was returned to the oven. This procedure was repeated another four times over a 3-day period. After removing residual benzoic acids and impurities, DEF was then replaced with absolute methanol (2 × 20 mL) for 24 h. The methanol containing crystals were placed inside the supercritical dryer and the methanol was exchanged with CO_2 (L) over a period of 2 h. during this time, the chamber was vented for 5 min each 30 min and then filled with CO_2 again. Then, the chamber was sealed and the temperature and pressure were raised to 40 °C and 1300 psi, above the critical point of CO_2. After holding the chamber above the critical point for 1 h, the chamber was slowly vented over 18 h period. The dried crystals were transferred to a sealed container and kept in a desiccator. Yield: 53 mg, 70%.

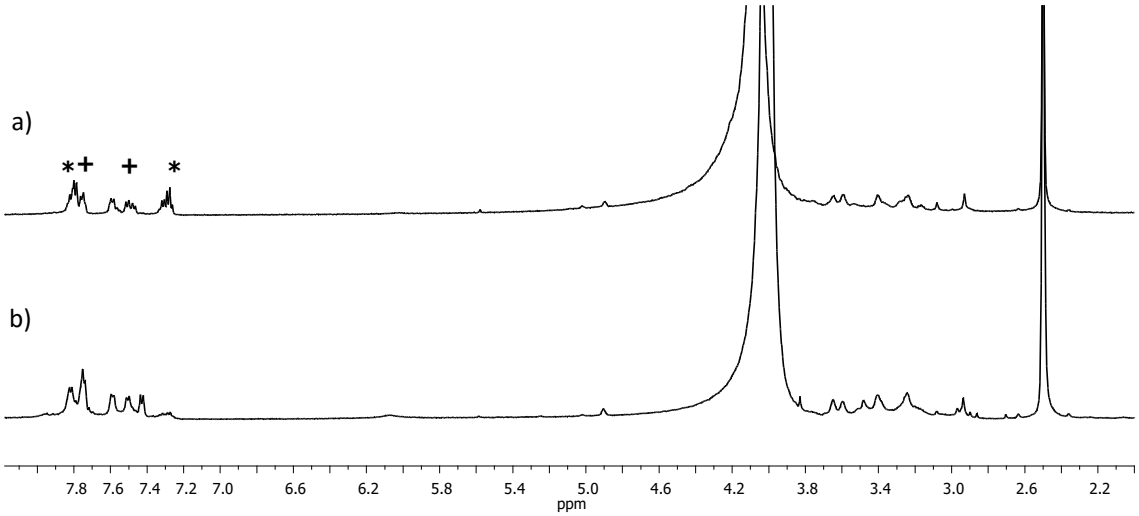

*Figure 6.4. Partial ^{1}H NMR spectra (500MHz) of (a) as-synthesized **UWCM-1** and (b) activated **UWCM-1;** peaks for ligand [**1**-H_4⊂**24C6'**] and benzoic acid are denoted with (**+**) and (*), respectively. Samples were decomposed in K_3PO_4/D_2O/DMSO-d_6.*

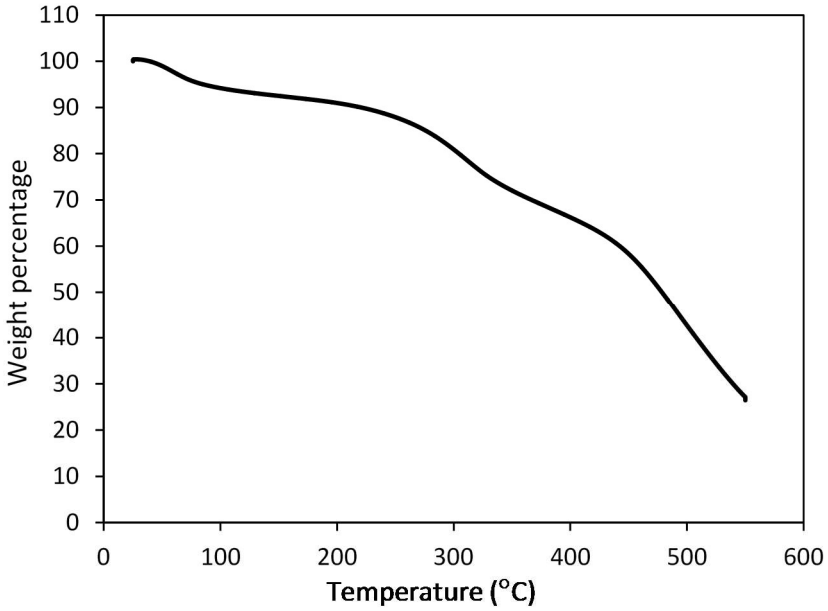

*Figure 6.5. Thermogravimetric analysis of activated **UWCM-1**.*

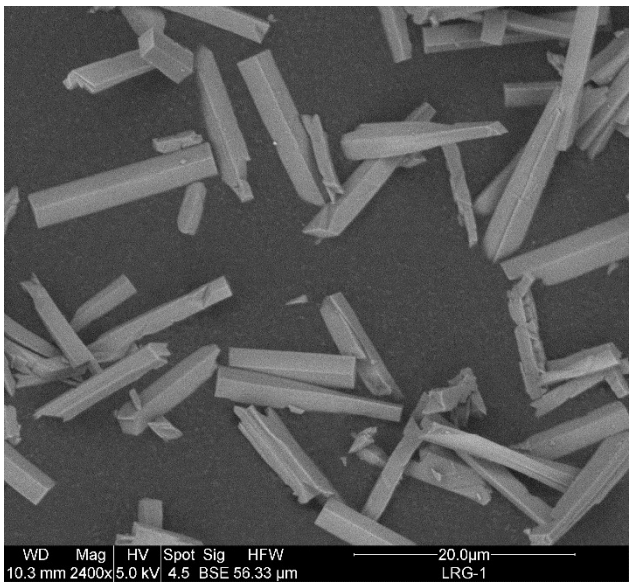

*Figure 6.6. SEM image of the microcrystalline product of **UWCM-1.***

6.2.6 Synthesis of UWCM-2

$ZrCl_4.8H_2O$ (46 mg, 0.2 mmol) and benzoic acid (1050 mg, 8.6 mmol) were dissolved in DMF (12 mL). The mixture was heated at 80 °C for 1 h. After cooling down to room temperature, ligand **1-H$_4$** (40 mg, 0.07 mmol) was added to the clear solution and the solution sonicated for 10 minutes. The yellow solution was transferred through a 25 mm syringe filter (0.2 µm PTFE membrane) to four 15 mL vials and heated at 120 °C in a programmable heating oven for one day to yield a yellow crystalline powder.

6.2.7 Activation Procedure for UWCM-2

As-synthesized **UWCM-2** was soaked in 10 mL of DMF and 0.1 mL of 2 M HCl was added. The mixture was heated in an oven at 90 °C for 24 h. The solvent was replaced with fresh DMF followed by addition of another 0.1 mL 2 M HCl and the mixture was returned to the oven for 24 h. after cooling at room temperature, the solution was removed and the solid was washed twice with DMF to remove HCl impurities. DMF was then replaced with absolute methanol (2 × 20 mL) for 24 h. the DEF was replaced with absolute Methanol (2 × 20 mL)

over a 1-day period and the material evacuated with supercritical CO_2 according to the procedure was used for **UWCM-1.**Yield: 60 mg, 90%.

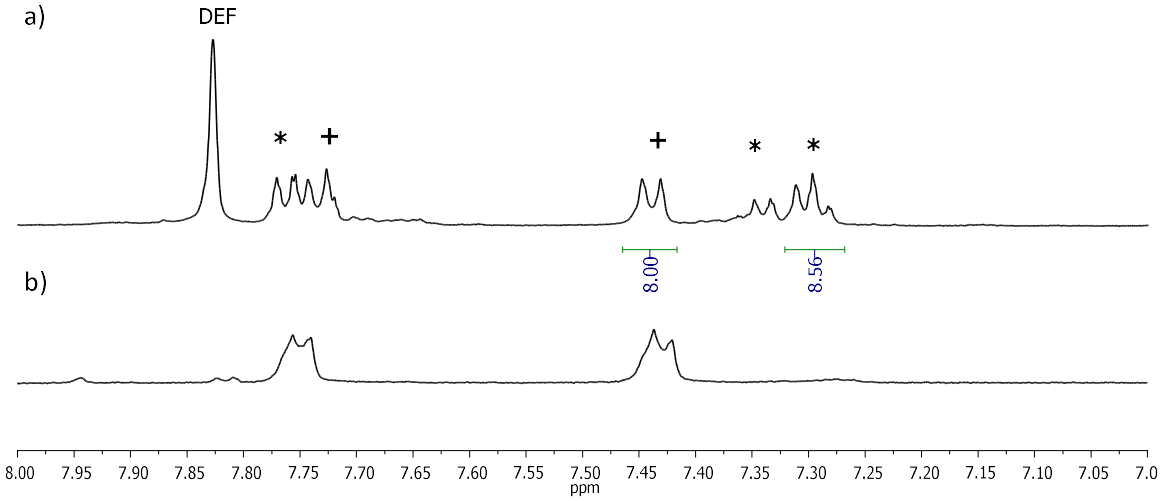

*Figure 6.7. Partial ^{1}H NMR spectra (500MHz) of (a) as-synthesized and (b) activated **UWCM-2**; peaks for ligand **1-H$_4$** and benzoic acid are denoted with (+) and (*), respectively. Samples were decomposed in K_3PO_4/D_2O/DMSO-d_6.*

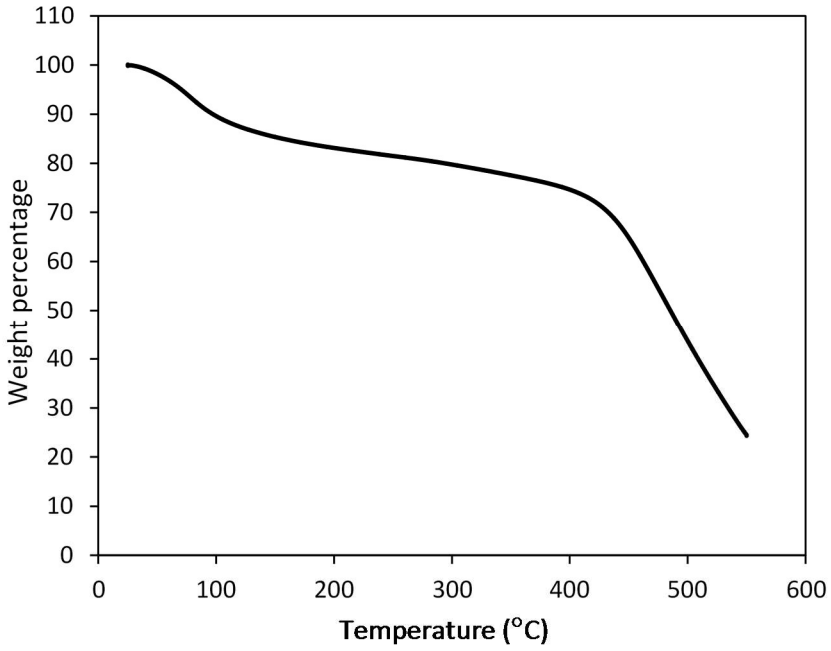

*Figure 6.8. Thermogravimetric analysis of activated **UWCM-2**.*

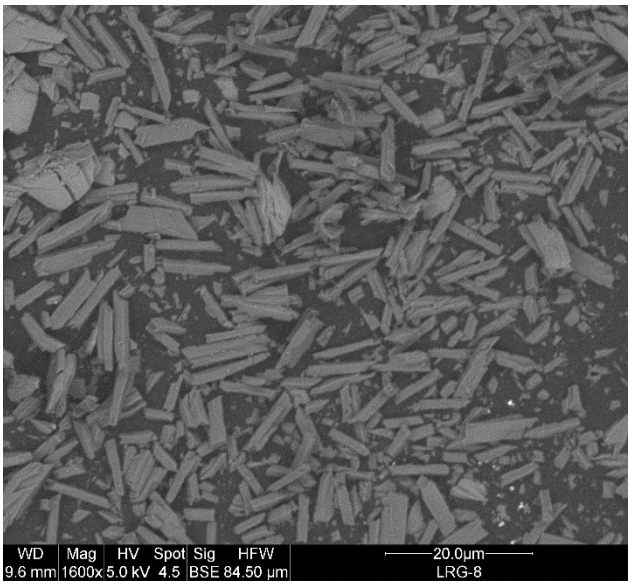

*Figure 6.9. SEM image of the microcrystalline product of **UWCM-2.***

6.2.8 Post-synthetic Modification of UWCM-1

The other half of as-synthesized **UWCM-1** was washed with fresh DEF (2 x 10 mL) and left to stand in DEF at room temperature. After 17 h, the solid was filtered and washed with Ethanol and followed by DCM to remove residual DEF. the material was then soaked in 3 mmL dry dichloroethane (DCE) in a thick-walled glass tube followed by addition of 5% Grubbs Hoveyda II Catalyst (1.5 mg). Nitrogen gas was bubbled through the reaction mixture for 10 min. Then, the glass tube was sealed with a Teflon screw cap and placed in an oil bath at 60 °C for 20 h. the material was then filtered, washed with DCM (3 x 5 mL).

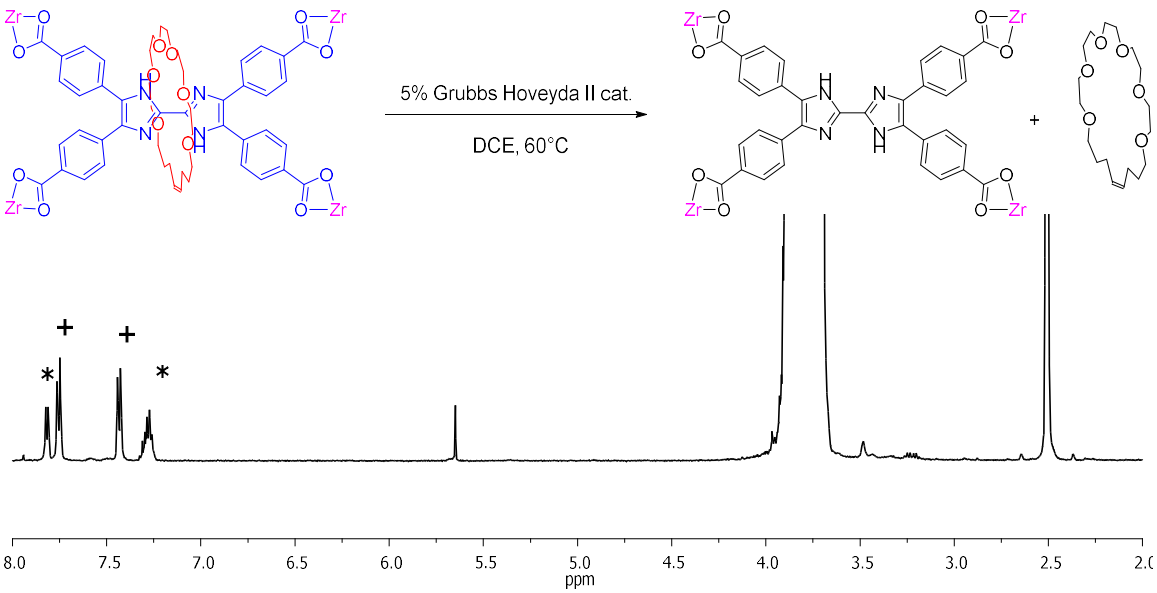

*Figure 6.10. ^{1}H NMR spectrum (500MHz) of **UWCM-1** after 24 h of exposure to Grubb hoveyda II catalyst in DCE at 60 °C; peaks for the ligand and benzoic acid are denoted with (+) and (*), respectively. Sample was decomposed in K_3PO_4/D_2O/DMSO-d_6.*

6.2.9 Activation Procedure for Post-synthetic UWCM-1

The procedure was the same as stated above for **UWCM-2.**

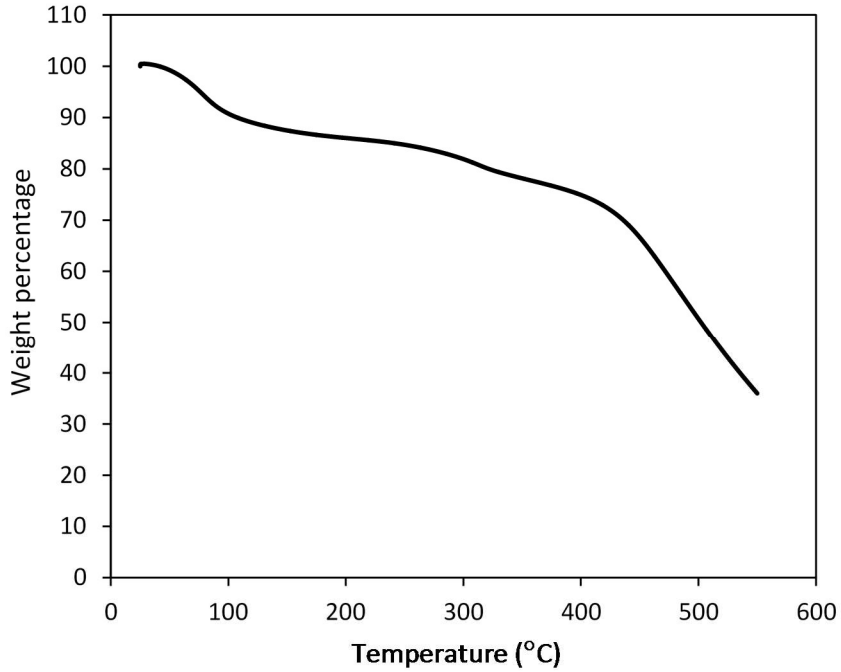

*Figure 6.11. Thermogravimetric analysis of activated **UWCM-1** after ring removal.*

6.3 References

[1] a) O. M. Yaghi, M. O'Keefe, N. W. Ockwig, H. K.Chae, M. Eddaoudi, J. Kim, *Nature*, **2003**, *423*, 705; b) G. Férey, Chem. Soc. Rev., 2008, 37, 191; c) S. Horike, S. Shimomura, S. Kitagawa, *Nat. Chem.,* **2009**, *1*, 695.

[2] O. K. Farha, I. Eryazici, N. C. Jeong, B. G. Hauser, C. E. Wilmer, A. A. Sarjeant, R. Q. Snurr, S. T. Nguyen, A. Ö. Yazaydın, J. T. Hupp, *J. Am. Chem. Soc.,* **2012**, *134*, 15016.

[3] a) L. J. Murray, M. Dinca, J. R. Long, *Chem. Soc. Rev.,* **2009**, *38*, 1294; b) M. Eddaoudi, J. Kim, N. Rosi, D. Vodak, J. Wachter, M. O'Keeffe, O. M. Yaghi, *Science,* **2002**, *295*, 469; c) M. P. Suh, H. J. Park, T. K. Prasad, D.-W. Lim, *Chem. Rev.,* **2012**, *112*, 782; d) J. J. Gassensmith, H. Furukawa, R. A. Smaldone, R. S. Forgan, Y. Y. Botros, O. M. Yaghi, J. F. Stoddart, *J. Am. Chem. Soc.,* **2011**, *133*, 15312. e) N. L. Rosi, J. Eckert, M. Eddaoudi, D. T. Vodak, J. Kim, M. O'Keeffe, O. M. Yaghi, *Science*, **2003**, *300*, 1127.

[4] a) J.-R. Li, R. J. Kuppler, H.-C. Zhou, *Chem. Soc. Rev.,* **2009**, *38*, 1477; b) Z. Zhang, Y. Zhao, Q. Gong, Z. Li, J. Li, *Chem. Commun.,* **2013**, *49*, 653; c) J.-R. Li, J. Sculley, H.-C. Zhou, *Chem. Rev.,* **2012**, *112*, 869; d) E. D. Bloch, W. L. Queen, R. Krishna, J. M. Zadrozny, C. M. Brown, J. R. Long, *Science*, **2012**, *335*, 1606.

[5] L. E. Kreno, K. Leong, O. K. Farha, M. Allendorf, R. P. Van Duyne, J. T. Hupp, *Chem. Rev.,* **2012**, *112*, 1105.

[6] a) Y. Kobayashi, B. Jacobs, M. D. Allendorf, J. R. Long, *Chem. Mater*., **2010**, *22*, 4120; b) G. Givaja, C. Amo-Ochoa, P.; C. Gomez-Garcia, F. Zamora, *Chem. Soc. Rev*., **2012**, *41*, 115; c) M. Yoon, K. Suh, S. Natarajan, K. Kim, Angew. *Chem., Int. Ed.,* **2013**, *52*, 2688.

[7] a) L. Ma, C. Abney, W. Lin, *Chem. Soc. Rev.,* **2009**, *38*, 1248; b) J. Lee, O. K. Farha, J. Roberts, K. A. Scheidt, S. T. Nguyen, J. T. Hupp, *Chem. Soc. Rev.,* **2009**, *38*, 1450; c) K. Manna, T. Zhang, F. X. Greene, W. Lin, *J. Am. Chem. Soc.,* **2015**, *137*, 2665.

[8] a) R. Ananthoji, J. F. Eubank, F. Nouar, H. Mouttaki, M. Eddaoudi, J. P. Harmon, *J. Mater. Chem.*, **2011**, *21*, 9587; b) R. C. Huxford, K. E. deKrafft, W. S. Boyle, D. Liu, W. Lin, *Chem. Sci.,* **2012**, *3*, 198; c) C. He, K. Lu, D. Liu, W. Lin, *J. Am. Chem. Soc.,* **2014**, *136*, 5181.

[9] O. K. Farha, J.T. Hupp, *Acc. Chem. Res.*, **2010**, *43*, 1166; b) M. O'Keeffe, M.A. Peskov, S.J. Ramsden, and O.M. Yaghi, *Acc. Chem. Res.*, **2008**, *41*, 1782; c) D. Zhao, D.J. Timmons, D.Q. Yuan, and H.C. Zhou, *Acc. Chem. Res.*, **2011**, *44*, 123; d) J.J. Perry, J.A. Perman, M.J. Zaworotko, *Chem. Soc. Rev.*, **2009**, *38*, 1400.

[10] H. X. Deng, S. Grunder, K. E. Cordova, C. Valente, H. Furukawa, M. Hmadeh, F. Gándara, A. C. Whalley, Z. Liu, S. Asahina, H. Kazumori, M. O'Keeffe, O. Terasaki, J. F. Stoddart, O. M. Yagh, *Science*, **2012**, *336*, 1018.

[11] S. M. Cohen, *Chem. Rev.,* **2012**, *112*, 970.

[12] a) O. K. Farha, K. L. Mulfort, J. T. Hupp, *Inorg. Chem.,* **2008**, *47*, 10223; (c) J. S. Seo, D. Whang, H. Lee, S. I. Jun, J. Oh, Y. J. Jeon, K. Kim, *Nature*, **2000**, *404*, 982.

[13] Y.-H. Kiang, G. B. Gardner, S. Lee, Z. Xu, E. B. Lobkovsky, *J. Am. Chem. Soc.,* **1999**, *121*, 8204.

[14] a) S. Takaishi, E. J. DeMarco, M. J. Pellin, O. K. Farha, J. T. Hupp, *Chem. Sci.,* **2013**, *4*, 1509; b) T. Li, M. T. Kozlowski, E. A. Doud, M. N. Blakely, N. L. Rosi, *J. Am. Chem. Soc.,* **2013**, *135*, 11688; c) P. Deria, J. E. Mondloch, E. Tylianakis, P. Ghosh, W. Bury, R. Q. Snurr, J. T. Hupp, O. K. Farha, *J. Am. Chem. Soc.*, **2013**, *135*, 16801; d) P. Deria, W. Bury, J. T. Hupp, O. K. Farha, *Chem. Commun.,* **2014**, *50*, 1965.

[15] a) A. K. Chaudhari, S. S. Nagarkar, B. Joarder, S. Mukherjee, and S. K. Ghosh, *Inorg. Chem.*, **2013**, *52*, 12784; b) R. K. Deshpande, G. I. N. Waterhouse, G. B. Jameson, S. G. Telfer, *Chem. Commun.*, **2012**, *48*, 1574; c) D. J. Lun, G. I. N. Waterhouse, S. G. Telfer, *Chem. Soc.*, **2011**, *133*, 5806.

[16] V. N. Vukotic (2014) *Mechanically Interlocked Linkers for Dynamic Metal-Organic Frameworks* (Doctoral thesis). University of Windsor, Windsor, Ontario, Canada.

[17] a) J. E. Mondloch, W. Bury, D. Fairen-Jimenez, S. Kwon, E. J. DeMarco, M. H. Weston, A. A. Sarjeant, S. T. Nguyen, P. C. Stair, R. Q. Snurr, O. K. Farha, J. T. Hupp, *J. Am. Chem. Soc.,* **2013**, *135*, 10294; b) H.-L. Jiang, D. Feng, T.-F. Liu, J.-R. Li, H.-C. Zhou, *J. Am. Chem. Soc.,* **2012**, *134*, 14690.

[18] J. H. Cavka, S. Jakobsen, U. Olsbye, N. Guillou, C. Lamberti, S. Bordiga, K. P. Lillerud, *J. Am. Chem. Soc.*, **2008**, *130*, 13850.

[19] H. Wu, T. Yildirim, W. J. Zhou, *Phys. Chem. Lett.,* **2013**, *4*, 925.

[20] a) P. Vandersluis, A. L. Spek, *Acta Crystallogr.,* **1990**, *A46*, 194; b) Spek, A. L. *Acta Crystallogr.,* **2009**, *D65*, 148.

[21] P. Deria, D. A Gomez-Gualdron, W. Bury, H. T. Schaef, T. C. Wang, P. K. Thallapally, A. A. Sarjeant, Randall Q. Snurr, Joseph T. Hupp, and Omar K. Farha, *J. Am. Chem. Soc.*, **2015**, *137*, 13183.

[22] a) M. J. Katz, Z. J. Brown, Y. J. Colón, P. W. Siu, K. A. Scheidt, R. Q. Snurr, J. T. Hupp, O. K. Farha, *Chem. Commun.,* **2013**, *49*, 9449; b) D. J. Clingerman, W. Morris, J. E. Mondloch, R. D. Kennedy, A. A. Sarjeant, C. Stern, J. T. Hupp, O. K. Farhaab, C. A. Mirkin, *Chem. Commun.,* **2015**, *51*, 6521.

CHAPTER 7

7. 1 Summary and Future Work

Chapter 2 described the use of rigid, Y-shaped 2,4,5-triphenylimidazolium axles for the formation of [2]pseudorotaxanes with the [24]crown-8 ether wheels **24C8** and **DB24C8** and a comparison of these new systems with the previously reported T-shaped systems containing 2,4,7-triphenylbenzimidazolium axles. Although the T-shaped axle produced [2]pseudorotaxanes that are more favorable, it is important to note that the Y shaped axle significantly enhanced the association constant when compared to those found for simple imidazolium or benzimidazolium derivatives.

This work was followed up by a more comprehensive study in **Chapter 3**, in which rigid bistable molecular shuttles were synthesized by combining T-shaped benzimidazolium and Y-shaped imidazolium recognition sites. Combining T-shaped and Y-shaped components results in a linear axle containing two non-equivalent recognition sites with different binding strengths for a single 24-membered crown ether (**24C8** or **DB24C8**) wheel. ^{1}H NMR studies of the neutral form of the molecular shuttles, [**2**⊂**DB24C8**] and [**2**⊂**24C8**], demonstrated that the macrocyclic wheel undergoes rapid translation along the axle and it was determined that the interactions of electron-rich crown ethers with the neutral Y-shaped imidazole recognition site are preferred over those of the T-shaped benzimidazole site. Protonation of the neutral species produced [**2**-H_2⊂**DB24C8**]$^{2+}$ and [**2**-H_2⊂**24C8**]$^{2+}$ which show significant ion-dipole and π-stacking interactions (for **DB24C8**) and strong hydrogen bonding between the recognition sites and wheel. Thus, the charged systems undergo much slower shuttling due to an increased barrier to the translational motion. For these systems, the preference for a particular co-conformation (Y versus T) is dependent on the polarity of solvent. In particular, for less polar solvents (*e.g.* CD_2Cl_2), the wheel resides at the T-shaped

benzimidazolium site. The fact that the position of the macrocycle can be controlled by acid-base chemistry allowed us to produce a new acid-base driven MIM switch.

The ultimate goal for these Y-shaped templating motifs with rigid cores is to develop versions that can be used as efficient MIM linkers for MOF construction. In **chapter 4**, we show that this could be achieved by a combination of the Y-shaped axle with an isophthalate coordinating group to create a MIM linker with an imidazole recognition site followed by clipping of a [24]crown-6 ether (**24C6**) around the axle using ring-closing metathesis (Grubbs I). Then, this MIM linker was used to prepare a robust Zn-based MOF, **UWDM-5**. Using VT ^{2}H SSNMR it was observed that the macrocyclic ring of the MIM undergoes conformational changes and rotational motion about the MOF as the temperature is increased. At lower temperature, the overall motion of the ring is affected by the larger size and higher charge of the imidazolium site compared to those of previously studied aniline axles (**UWDM-1**, **UWDM-2**, and **UWDM-3**). However, these differences disappear at higher temperatures. The development of such a unique material and demonstration of its internal dynamics in the solid state is promising for the incorporation of more complex MIM systems into MOFs.

Future work could be directed at studying the motion of different sized macrocyclic rings inside the MOF which would requires the synthesis of MIM linkers with different sized macrocycles and their incorporation into MOF materials. Future work could also be directed at the development of systems in which interlocked macrocyclic components can undergo controlled dynamic motion by other inputs such as photochemical or electrochemical stimulus.

Although, it was indicated that the Y-shaped MIM ligand can undergo rotational motion inside the MOF, it was still of interest to develop other MIM linkers using Y-shaped axle that could be employed in combination with metal ions to develop materials which

exhibit different dynamic behavior. In **Chapter 5**, a new recognition motif was made by combining two Y-shaped axles to create a new MIM linker with a bis(imidazolium) recognition site. The linker was used in combination with Zr(IV) ions to produce a robust MOF material, **UWDM-6**, with mesoporous channels. **UWDM-6** is a prototype Zr-based MOF with **scu** topology in which $Zr_6(\mu_3\text{-}O)_8(H_2O)_8^{8+}$ nodes are linked by the tetracarboxylate linker. The high thermal and chemical stability of **UWDM-6** allowed post-synthetic modification (PSM) of the material with acid and Li^+ ions. VT ^2H SSNMR experiments were used to characterize the dynamic properties of the macrocyclic ring in the neutral and charged and Li-doped version of **UWDM-6**. VT ^2H SSNMR specra show that Li-doping does not significantly change the energy barrier to rotation, especially at higher temperatures. Whereas, SSNMR spectra of protonated **UWDM-6** are slightly different from **UWDM-6**. The onset temperatures are lower for protonated **UWDM-6,** however the description of the motion is the same. Although, it appears that the thermal energy required to induce conformational changes and partial rotation of the wheel is lower inside the protonated MOF, more studies are required to understand the motion behaviour of the macrocyclic wheel inside the MOF.

Future work will focus on the design of other MIM systems that can be used in combination with Zr nodes to create highly stable materials which show a high degree of porosity. For example, a methodology based on systematic extension of organic linker **6** between metal nodes, is an approach for the development of Zr-MOFs with higher porosity than the prototypical structure, **UWDM-6**.

Future work could also be directed at the development of other molecular machinery using MIM systems inside a MOF that respond to external stimuli such as light to create materials capable of dynamic motion and ultimately develope functional molecular machines that can be controlled inside a crystalline solid-state material.

Post-synthetic modification (PSM) is an approach for manipulating the porosity in MOFs. Studies shows post synthetic ring removal from rotaxane-based MOFs could lead to MOFs with higher porosity. However, it should be noted that for this PSM method to be effective without damaging the MOF skeleton, MOFs with high chemical and thermal stability are needed. With the goal of performing this type of PSM on a MOF, **Chapter 6** outlines preparation of an 8-connected Zr-based MOF (**UWCM-1**) using a rotaxane linker which is formed through clipping of a 24-membered polyether-based macrocycle around a tetracarboxylic linker. **UWCM-1** has a structure similar to **UWDM-6** which shows some degree of flexibility; whereas combination of $ZrCl_4$ and the naked linker produced a rigid material (**UWCM-2**) but its structure could not be determined due to lack of X-ray quality single crystals of suitable size. The macrocycle can be thought of as a protecting group which improves the solubility of the linker and adds steric bulk around the linker which leads different MOF structure. Furthermore, interlocking the macrocycle around the axle together with chemical and thermal stability of Zr nodes provided the opportunity for the PSM of **UWCM-1** with Hoveyda-Grubbs II catalyst, which removed the protecting macrocycle. Interestingly, during PSM, the material undergoes a topological transformation which leads to a more rigid structure analogous to **UWCM-2**. This topological change is the result of conformational changes in the linker which occurs due to ring removal. This evidence indicated that **UWCM-1** and **UWCM-2** possess similar 8-connected Zr nodes with the formula of $[Zr_6(\mu_3\text{-}O)_8(OH)_8]^{-8}$ but adopt different topologies.

Future work will focus on improving the activation method of the materials and performing gas absorption measurements of **UWCM-1** before and after post-synthetic ring removal as well as **UWCM-1**.

APPENDIX

A1. Copyright Permissions

JOHN WILEY AND SONS LICENSE TERMS AND CONDITIONS

Aug 10, 2016

This Agreement between Nasim Farahani ("You") and John Wiley and Sons ("John Wiley and Sons") consists of your license details and the terms and conditions provided by John Wiley and Sons and Copyright Clearance Center.

License Number	3925691250890
License date	Aug 10, 2016
Licensed Content Publisher	John Wiley and Sons
Licensed Content Publication	ChemPhysChem
Licensed Content Title	Rigid, Bistable Molecular Shuttles Combining T-shaped Benzimidazolium and Y-shaped Imidazolium Recognition Sites
Licensed Content Author	Nasim Farahani,Kelong Zhu,Stephen J. Loeb
Licensed Content Date	Mar 22, 2016
Licensed Content Pages	6
Type of use	Dissertation/Thesis
Requestor type	Author of this Wiley article
Format	Print and electronic
Portion	Full article
Will you be translating?	No
Title of your thesis / dissertation	Interlocked Molecules and Materials with an Imidazole Core
Expected completion date	Oct 2016
Expected size (number of pages)	250
Requestor Location	
	Attn: Nasim Farahani
Publisher Tax ID	EU826007151
Billing Type	Invoice
Billing Address	
	Attn: Nasim Farahani
Total	0.00 CAD
Terms and Conditions	

TERMS AND CONDITIONS

JOHN WILEY AND SONS LICENSE TERMS AND CONDITIONS

Aug 10, 2016

This Agreement between Nasim Farahani ("You") and John Wiley and Sons ("John Wiley and Sons") consists of your license details and the terms and conditions provided by John Wiley and Sons and Copyright Clearance Center.

License Number	3925691422750
License date	Aug 10, 2016
Licensed Content Publisher	John Wiley and Sons
Licensed Content Publication	CHEMPLUSCHEM
Licensed Content Title	Thermally Driven Dynamics of a Rotaxane Wheel about an Imidazolium Axle inside a Metal–Organic Framework
Licensed Content Author	Nasim Farahani,Kelong Zhu,Christopher A. O\'Keefe,Robert W. Schurko,Stephen J. Loeb
Licensed Content Date	May 25, 2016
Licensed Content Pages	6
Type of use	Dissertation/Thesis
Requestor type	Author of this Wiley article
Format	Print and electronic
Portion	Full article
Will you be translating?	No
Title of your thesis / dissertation	Interlocked Molecules and Materials with an Imidazole Core
Expected completion date	Oct 2016
Expected size (number of pages)	250
Requestor Location	
	Attn: Nasim Farahani
Publisher Tax ID	EU826007151
Billing Type	Invoice
Billing Address	
	Attn: Nasim Farahani
Total	0.00 CAD
Terms and Conditions	

TERMS AND CONDITIONS

8/10/2016 Rightslink® by Copyright Clearance Center

Copyright Clearance Center RightsLink® Home Account Info Help Live Chat

ACS Publications Most Trusted. Most Cited. Most Read.

Title: Development of Pseudorotaxanes and Rotaxanes: From Synthesis to Stimuli-Responsive Motions to Applications

Author: Min Xue, Yong Yang, Xiaodong Chi, et al

Publication: Chemical Reviews

Publisher: American Chemical Society

Date: Aug 1, 2015

Copyright © 2015, American Chemical Society

Logged in as: Nasim Farahani LOGOUT

PERMISSION/LICENSE IS GRANTED FOR YOUR ORDER AT NO CHARGE

This type of permission/license, instead of the standard Terms & Conditions, is sent to you because no fee is being charged for your order. Please note the following:

- Permission is granted for your request in both print and electronic formats, and translations.
- If figures and/or tables were requested, they may be adapted or used in part.
- Please print this page for your records and send a copy of it to your publisher/graduate school.
- Appropriate credit for the requested material should be given as follows: "Reprinted (adapted) with permission from (COMPLETE REFERENCE CITATION). Copyright (YEAR) American Chemical Society." Insert appropriate information in place of the capitalized words.
- One-time permission is granted only for the use specified in your request. No additional uses are granted (such as derivative works or other editions). For any other uses, please submit a new request.

If credit is given to another source for the material you requested, permission must be obtained from that source.

BACK CLOSE WINDOW

Copyright © 2016 Copyright Clearance Center, Inc. All Rights Reserved. Privacy statement, Terms and Conditions. Comments? We would like to hear from you. E-mail us at customercare@copyright.com

https://s100.copyright.com/AppDispatchServlet#formTop 1/1

NATURE PUBLISHING GROUP LICENSE TERMS AND CONDITIONS

Aug 10, 2016

This Agreement between Nasim Farahani ("You") and Nature Publishing Group ("Nature Publishing Group") consists of your license details and the terms and conditions provided by Nature Publishing Group and Copyright Clearance Center.

License Number	3925701449727
License date	Aug 10, 2016
Licensed Content Publisher	Nature Publishing Group
Licensed Content Publication	Nature Materials
Licensed Content Title	Macroscopic transport by synthetic molecular machines
Licensed Content Author	José Berná,David A. Leigh,Monika Lubomska,Sandra M. Mendoza,Emilio M. Pérez et al.
Licensed Content Date	Sep 1, 2005
Licensed Content Volume Number	4
Licensed Content Issue Number	9
Type of Use	reuse in a dissertation / thesis
Requestor type	academic/educational
Format	print and electronic
Portion	figures/tables/illustrations
Number of figures/tables/illustrations	1
High-res required	no
Figures	Figure 7
Author of this NPG article	no
Your reference number	
Title of your thesis / dissertation	Interlocked Molecules and Materials with an Imidazole Core
Expected completion date	Oct 2016
Estimated size (number of pages)	250
Requestor Location	
	Attn: Nasim Farahani
Billing Type	Invoice
Billing Address	

SPRINGER LICENSE
TERMS AND CONDITIONS

Aug 10, 2016

This Agreement between Nasim Farahani ("You") and Springer ("Springer") consists of your license details and the terms and conditions provided by Springer and Copyright Clearance Center.

License Number	3925700854220
License date	Aug 10, 2016
Licensed Content Publisher	Springer
Licensed Content Publication	Springer eBook
Licensed Content Title	Organizing Mechanically Interlocked Molecules to Function Inside Metal-Organic Frameworks
Licensed Content Author	Kelong Zhu
Licensed Content Date	Jan 1, 2014
Type of Use	Thesis/Dissertation
Portion	Figures/tables/illustrations
Number of figures/tables/illustrations	2
Author of this Springer article	No
Order reference number	
Original figure numbers	Figures 5 and 6
Title of your thesis / dissertation	Interlocked Molecules and Materials with an Imidazole Core
Expected completion date	Oct 2016
Estimated size(pages)	250
Requestor Location	
	Attn: Nasim Farahani
Billing Type	Invoice
Billing Address	
	Attn: Nasim Farahani
Total	0.00 USD
Terms and Conditions	

Introduction
The publisher for this copyrighted material is Springer. By clicking "accept" in connection

NATURE PUBLISHING GROUP LICENSE TERMS AND CONDITIONS

Aug 10, 2016

This Agreement between Nasim Farahani ("You") and Nature Publishing Group ("Nature Publishing Group") consists of your license details and the terms and conditions provided by Nature Publishing Group and Copyright Clearance Center.

License Number	3925700531254
License date	Aug 10, 2016
Licensed Content Publisher	Nature Publishing Group
Licensed Content Publication	Nature Chemistry
Licensed Content Title	Metal–organic frameworks with dynamic interlocked components
Licensed Content Author	V. Nicholas Vukotic, Kristopher J. Harris, Kelong Zhu, Robert W. Schurko, Stephen J. Loeb
Licensed Content Date	May 13, 2012
Licensed Content Volume Number	4
Licensed Content Issue Number	6
Type of Use	reuse in a dissertation / thesis
Requestor type	academic/educational
Format	print and electronic
Portion	figures/tables/illustrations
Number of figures/tables/illustrations	2
High-res required	no
Figures	Figure 3 and 5
Author of this NPG article	no
Your reference number	
Title of your thesis / dissertation	Interlocked Molecules and Materials with an Imidazole Core
Expected completion date	Oct 2016
Estimated size (number of pages)	250
Requestor Location	Canada Attn: Nasim Farahani
Billing Type	Invoice
Billing Address	

NATURE PUBLISHING GROUP LICENSE TERMS AND CONDITIONS

Aug 10, 2016

This Agreement between Nasim Farahani ("You") and Nature Publishing Group ("Nature Publishing Group") consists of your license details and the terms and conditions provided by Nature Publishing Group and Copyright Clearance Center.

License Number	3925700426753
License date	Aug 10, 2016
Licensed Content Publisher	Nature Publishing Group
Licensed Content Publication	Nature Chemistry
Licensed Content Title	A molecular shuttle that operates inside a metal–organic framework
Licensed Content Author	Kelong Zhu, Christopher A. O'Keefe, V. Nicholas Vukotic, Robert W. Schurko, Stephen J. Loeb
Licensed Content Date	May 4, 2015
Licensed Content Volume Number	7
Licensed Content Issue Number	6
Type of Use	reuse in a dissertation / thesis
Requestor type	academic/educational
Format	print and electronic
Portion	figures/tables/illustrations
Number of figures/tables/illustrations	1
High-res required	no
Figures	Figure 4
Author of this NPG article	no
Your reference number	
Title of your thesis / dissertation	Interlocked Molecules and Materials with an Imidazole Core
Expected completion date	Oct 2016
Estimated size (number of pages)	250
Requestor Location	Canada Attn: Nasim Farahani
Billing Type	Invoice
Billing Address	

VITA AUCTORIS

NAME: Nasim Farahani

PLACE OF BIRTH: Tehran, IRAN

YEAR OF BIRTH: 1985

EDUCATION:

- University of Tehran, B.Sc.-Applied Chemistry, Tehran, IRAN, 2007
- Sharif University of Technology, M.Sc.-Inorganic Chemistry, Tehran, IRAN, 2010
- University of Windsor, Ph.D.-Chemistry, Windsor, Canada, 2016